DUBLIN CITY UNIVERSITY

Ollscoil Chathair Bhaile Átha Cliath

Some Novel Electrochemical Detection Systems for Flowing Solution Analysis

By

Michael James Mc Grath, B.Sc.

A thesis submitted for the degree

of

Doctor of Philosophy

Supervised by Prof. Malcolm R. Smyth and Dr. Dermot Diamond

Dublin City University September 1995

Declaration

I hereby certify that this material, which I now submit for assessment on the programme of study leading to the award of Doctor of Philosophy, is entirely my own work and has not been taken from the work of others save and to the extent that such work has been cited and acknowledged within the text of my work.

Signed: Michael James McGrath

Michael James Mc Grath

Date: 18/9/95

For my parents and family

"Everything should be made as simple as possible, but not simpler"

Albert Einstein

Acknowledgements

I would firstly like to thank my supervisors Prof. Malcolm Smyth and Dr. Dermot Diamond for their guidance, advice and patience over the last three years. I am very grateful to them for providing me with the opportunity to carry out research towards a Ph.D. degree.

I also wish to thank Prof. Ari Ivaska for allowing me to work in his laboratories at Åbo Akademi University, Turku, Finland. A special word of thanks to Mr Tauno Ahlfors for his assistance in the construction of the fountain cell. A big thank you to the other members of the group for making me feel so welcome and for giving me a "taste" of Finnish culture.

I am very grateful to Prof. Craig Lunte at the University of Kansas for giving me the opportunity to work in his laboratory. To my co-worker Sangryoul Park a particular word of thank for this inspiration and dedication. To the other members of the Lunte group for their friendliness and assistance during the course of my visit. To Kieran for being the "local Irish support group" and for all the great "chats".

A big word of thanks also to the chemistry postgraduates, in particular Malcolm's research group: Brian, Siobhan, Enda, Gemma, Caroline, Declan, Michaela, Bumni, Bin and to the recently deceased member of our group, Sean. Special thanks to my co-workers at DCU; Tang Fang, for his excellent engineering skills, friendliness and wonderful disposition, and to Dr Emmanuel Iwuoha for his helpful assistance. Thanks to the "38 Dean Swift household:" Mick T, "Ted", Brian, Joe, Spencer, Enda, Mick O'B and Shane for their "stimulating" and "informative" conversations over the last few years. And thanks also to the technical staff for all their practical assistance.

Finally, a final word of thanks to my parents and family for all their love and support, which made this all possible.

TABLE OF CONTENTS

ABSTRACT

Some Novel Electrochemical Detection Systems for Flowing Solution Analysis

Michael James Mc Grath

The developments in modern electrochemical instrumentation and their impact on electrochemical techniques are reviewed in Chapter 1. New potentiostat designs are discussed, particularly multichannel potentiostats for use with arrays of working electrodes. The fundamentals of flow cell design for electrochemical detection systems are also examined. Finally the recent applications of electrochemical detection with LC, FIA and CE are reviewed.

Chapter 2 describes the design and development of a 4-channel computer-controlled potentiostat (expandable to 16 channels) for use with an amperometric array in flowing injection analysis. Control of the purpose instrumentation was effected with a 486-33 MHz personal computer and Analog Devices RTI-815 and RTI-817 data acquisition\control cards which were responsible for hardware control functions and data acquisition via digital and analog control lines. The control software was developed using Microsoft QuickBASIC. The instrumentation developed was used with both linear and radial flow cell configurations which were constructed "in-house". The design was based on the utilisation of common reference and counter electrodes to reduce the complexity of the electrode arrangement. A variety of applications were demonstrated for the system, these included the determination of metal ions in solution and the use of dual sensors for the measurement of glucose in the presence of common clinical interferences.

The design and application of a fountain type flow cell for use with sequential injection analysis (SIA) is discussed in Chapter 3. The unique flow characteristics of the fountain cell make it suitable for use with planar detectors such as glassy carbon electrodes, particularly arrays of these electrodes spaced at equi-distances from the

inlet. The flow characteristics of the fountain cell were analysed with two different electrode array configurations. The development of an on-line polymerisation procedure for pyrrole using the fountain cell is also discussed.

The development an electrochemical detection system for use with capillary electrophoresis (CE) is described in Chapter 4. The system was based on the use of an end column decoupler to separate the working electrode from the high voltages required for separations. Both amperometric and voltammetric detection was implemented with the system using carbon fiber microelectrodes. Dynamic background subtraction was utilised to improve the signal to noise ratio. A number of the parameters affecting voltammetric detection were investigated. The system was applied to the determination of phenolic acid mixtures following separation by CE.

CHAPTER 1

MODERN ELECTROCHEMICAL INSTRUMENTATION AND TECHNIQUES

1.1 Introduction

Analytical techniques based on electrochemical principles make up one of the three major divisions of instrumental analytical chemistry. Each basic electrical measurement of current, resistance and voltage has been used alone or in combination for analytical purposes. If these electrical properties are measured as a function of time, many additional electroanalytical methods of analysis are possible. The individual techniques are best recognised by their excitation response characteristics. An example of one such technique is voltammetry [1-2]. Historically, voltammetry developed from the discovery of polarography by the Czechoslovakian chemist Jaroslav Heyrovsky [3] in the early 1920's. Polarography, which is still the most widely used of all the voltammetric methods, differs from the others in the respect that a dropping mercury electrode is used as the working electrode [4].

Prior to 1960, electrochemical instrumentation consisted mainly of wheatstone bridges, motor driven potentiometers, vacuum tubes and analog meters. Rapid advances in microelectronics, and particular the introduction of the modern op-amp in the 1970's, have led to major changes in the design and development of electroanalytical instrumentation. Miniature, low-cost integrated circuits can now perform many functions that previously required very large cumbersome instruments [5]. The introduction in 1968 of a modern multipurpose voltammetric instrument

(PAR 170) by EG&G Princeton Applied Research Corporation stimulated a broader use of electrochemistry by non-specialists. This was quickly followed by the smaller, less expensive PAR 174 which became the standard for routine polarography and voltammetry [6].

The availability of relatively inexpensive processors and personal computers (PC's) since the mid 1970's has had a dramatic impact on the way electrochemical experiments are performed. It is now possible with modern PC based instrumentation to carry out a variety of electrochemical techniques [7]. Computer controlled instruments offer greater flexibility and sophistication in the execution of a great variety of modes over older autonomous potentiostats.

1.2 Electrochemical Techniques

1.2.1 Amperometry

Amperometry is that class of electroanalytical measurements in which the applied potential is held constant and the current that flows is a function of analyte concentration. Provided that all the substance present is allowed to react at the working electrode and that the electrode reaction proceeds at 100% current efficiency, the electrical charge passed, Q, is related to the amount of the electroactive substance, N, according to Faraday's law:

$$Q = nFN \tag{1.1}$$

where Q is the number of coulombs (a unit of charge) used in converting N moles of material, n is the number of electrons (lost or gained in the transfer process per molecule) and F is the Faraday's constant, i.e. 96,485 coulombs/mole of electrons.

Differentiation of equation 1.1 with respect to time yields the current, which is the measure of the rate at which material is converted.

$$\frac{dQ}{dt} = i = nF\frac{dN}{dt} \tag{1.2}$$

Equation 1.2 therefore relates a measurable quantity, the current, to the fundamental redox process occurring in the cell.

The choice of potential for amperometric detection influences both sensitivity and selectivity of analysis. Optimum sensitivity for a particular analyte is achieved by holding the potential in the limiting current region of the hydrodynamic voltammogram for the analyte in question. Amperometric sensors of themselves have only limited selectivity. This selectivity is provided by the adjustment of the potential at which the working electrode is held. The working electrode can be operated at a potential which is either significantly lower or higher than the oxidation or reduction potential of the interfering species. Many amperometric measurements are therefore based on a trade off between selectivity and sensitivity [8, 9].

1.2.2 The Current Follower

The chief electrochemical variables such as current and voltage are all analog quantities; therefore the circuits required for electrochemical measurements are concerned with the accurate and reliable measurement of these quantities in the analog domain. The circuit elements best suited to these jobs are operational amplifiers (op-amps). One important circuit for the measurement of current based on the op-amp is the current follower. In Figure 1.1., an unknown current source i_{in} is connected directly to the inverting input of an op-amp configured as a current follower. The

output voltage v_o generates the comparison current i_f through the resistor R_f. The subscript f is used for signals and components in the feedback loop. The inverting input is used for the feedback current because it provides the proper corrective direction at the output if i_{in} increases. The current in the feedback loop i_f increases such as to maintain point s at virtual ground.

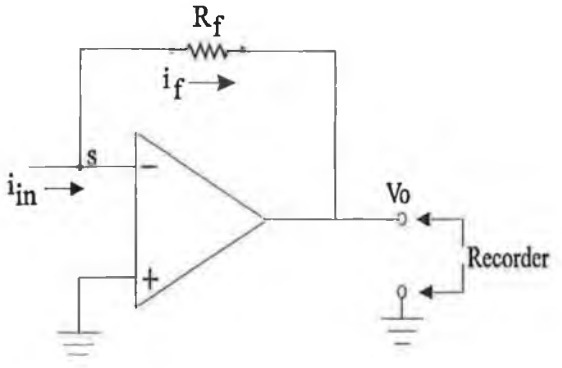

Figure 1.1. The current follower

An approximate analysis can again be made by assuming the potential difference between the inputs of the op-amp is approximately zero as long as v_o is not in limit. Since the non-inverting input (+) is connected to ground, the voltage at the inverting input is at 0 volts. The voltage v_o appears across R_f and $i_f \approx -v_o/R_f$ from Ohm's law. The bias current i_b for the op-amp is generally very small because of the high impedance inputs of the op-amp and the virtual ground at point s. The summing of the currents at point s yields $i_{in} = i_f + i_b$. Because i_b is negligible compared to i_f consequently the currents i_{in} and i_f are essential equal. That is, all the current to point s from the signal source appears in the feedback path through R_f. Substitution of i_{in} for i_f in the equation $i_f \approx -v_o/R_f$ yields:

$$v_o \approx -i_{in}R_f \qquad (1.3)$$

Thus i_f follows i_{in} and produces an output voltage proportional to i_{in}. If a value of 1 MΩ were chosen for R_f, the output voltage would be one volt per microamp of input current.

The current follower circuit is in many ways analogous to the voltage follower. The output voltage produced is the same as the one that would occur if R_f were simply a load resistor across the current source i_{in}. However, the current follower presents a nearly ideal load to the current source and supports a variety of readout devices.

The limitations in the application of the current follower are in the exact relation between v_o and i_{in}:

$$v_o = -R_f(i_{in} - i_b)\left(\frac{A}{1+A}\right) \qquad \text{or} \qquad v_o = -i_{in}R_f + i_bR_f - \frac{v_o}{A} \qquad (1.4)$$

From either form of the equation it can be seen that when A (amplification) is very large and i_b is much less than i_{in}, the output voltage v_o is proportional to i_{in} as expected from equation 1.3. The range of currents that can be measured by the current follower and readout is limited on the low end by the input bias current of the op-amp i_b and the high end by the op-amp's output capability. Op-amp input bias currents vary from 10^{-9} to 10^{-15} amps depending on the quality of the op-amps used, making the current follower useful into the picoampere current range. The output current capability of an op-amp is generally 2-100 mA. The op-amp output must be capable of supplying both the feedback current i_f and the readout device current [10, 11].

1.2.3 Voltammetry

Voltammetry comprises a group of electroanalytical techniques, e.g. square wave voltammetry [12], normal pulse voltammetry [13] and cyclic voltammetry [14]. These techniques are based on the current-potential relationship in an electrochemical cell,

and in particular with the current-time response of an electrode at a controlled potential. Voltammetry involves the application of a potential to an electrochemical cell, the transport of material to an electrode for electrolysis and the measurement of current from the electrolytic process. The electron transfer reaction can take place at the electrode if the potential is appropriate, its magnitude being determined by the surface concentration of some electroactive species. The current is recorded as a function of applied potential. The voltammetric data provides information on the character of the electroactive substance, through the parameters of its voltammetric wave, primarily the half-wave potential, $E_{1/2}$. The signal-to-noise ratio in voltammetric measurements is limited by the background current, which consists primarily of the double layer charging current. This limitation is significantly reduced when the measurement is made in a non-stationary state (pulse polarisation of the working electrode), with separation of the charging current component from the faradaic one (corresponding to the charge-transfer reaction at the electrode). There are a number of non-stationary voltammetric methods, of which alternating current (AC), square wave, normal pulse and differential pulse voltammetry are the most widely used [9].

Voltammetric experiments may be carried out with or without mechanical stirring. If the solution is stirred, the dominant transport mechanism is convection. In other cases, the cell is protected from mechanical forces that might cause convective motion of the solution. As the electrolysis proceeds, the active species in the vicinity of the electrode are depleted by being reduced or oxidised, creating a concentration gradient between the surface of the electrode and the bulk solution. If the applied potential is small, diffusion remains a minor process; however, as the potential is increased, the

diffusion rate increases, resulting in higher magnitude currents. Therefore the analyte must diffuse at a more rapid rate in order to maintain the current with increasing potential. The concentration gradient, and hence the rate of diffusion, is proportional to the bulk concentration. If the solution is dilute, a potential will eventually be reached at which the rate of diffusion reaches a maximum and all the analyte molecules are reduced or oxidised as fast as they can diffuse to the electrode surface. Hence a limiting current value, i_l, is reached, and further increases in potential will not result in increased current. If the solution is stirred or the electrode is rotated, a sigmoidal plot is normally obtained; that is the limiting current remains constant once it is established. This occurs because the diffusion layer, or the thickness of the concentration gradient across which the analyte must diffuse, remains small and constant, since the analyte is continually brought near to the electrode surface by mass transfer (stirring). But if the electrode is unstirred and in a quiescent solution, the diffusion layer will extend farther out into the solution with time, with the result that the limiting current decreases with time and a "peaked' wave is obtained [15, 16].

Of all the mass transport mechanisms, diffusion and migration are most readily susceptible to detailed theoretical treatment. In the presence of supporting electrolyte, migration becomes of negligible importance. In an unstirred solution, the concentration gradient decreases resulting in a decrease in current.

This is given by the Cottrell equation:

$$I_{\lim} = \frac{nFAD^{1/2}C^*}{(\pi t)^{1/2}} \qquad (1.5)$$

where n is the number of electrons transferred, F is the Faraday constant (96,485 coulomb $mole^{-1}$), A is the area of the electrode (cm^2), D is the diffusion coefficient

(cm^2 s^{-1}), C^* is the bulk concentration of the analyte (mM) and t is the time in seconds. Thus the current drops off as the inverse square root of the time t.

In the case of a well-stirred solution, fresh active material is always available to the electrode, so the current stays at a nearly constant value. The magnitude of the current is proportional to concentration, which diminishes slowly because of the charge transfer reaction [15-17].

1.2.3.1 Hydrodynamic Voltammetry

When voltammetric experiments are carried out in unstirred solutions, the current response is a transient that decays with time. As the current approaches zero, the information available disappears. In order to obtain more information, the redox process must be forced to continue. One possible answer is to provide fresh solution to the electrode by mechanical means.

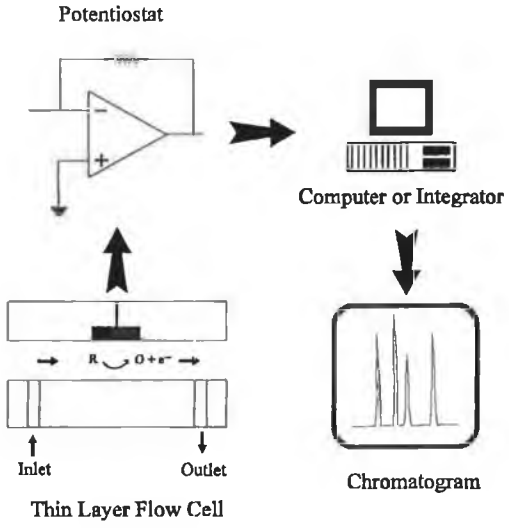

Figure 1.2. Schematic of an electrochemical detection system for LC.

The term "hydrodynamic" is used to describe this procedure, since solution flow is invariably associated with it. Hydrodynamic methods take advantage of enhanced

sensitivity resulting from the enhanced mass transfer of the electroactive substance to the electrode that occurs under hydrodynamic conditions. A steady state is attained rather quickly and measurements can be made with high precision.

One of the fastest growing uses of hydrodynamic voltammetry is electrochemical detection for LC and FIA. A representation of a typical electrochemical detection scheme is presented in Figure 1.2. For these techniques, electrochemical detectors possess advantages of sensitivity and simplicity over many alternative devices. Detectors in such applications must have a small internal volume, since the time needed to replace the volume of the detector with fresh sample determines the limit of resolution for flow systems. Normally the detector volume for monitoring chromatographic peaks must be at least ten times smaller than the volume of the chromatographic peak to ensure satisfactory resolution [1, 9, 17].

LC with electrochemical detection (LC-EC) or FIA-EC is analogous to electrolysis at a fixed point along a flowing stream. The carrier stream passes the solute analytes into an electrochemical cell, normally thin layer (TLC) or wall jet (WJ) type cells, where the flow is constrained to a thin film passing over a planar electrode held at a fixed potential. If the electrode is operated at a potential greater than that required for the electrolysis of the analyte being determined, a measurable charge passes from the electrode to the analyte or vice versa. Under appropriate conditions the resulting current is directly proportional to the concentration of solute passing through the cell [18].

1.3 Flow Cells

Four flow geometries have been described for electrochemical detection [9]. These are:

(i) tubular;

(ii) planar with parallel flow;

(iii) planar with perpendicular flow;

(iv) wall jet (free or confined wall jet).

Of these four geometries, detectors based on the wall jet and thin layer configurations have found the widest range of applications. The thin-layer detector (TLD) is probably most widely used configuration for electrochemical detection in LC. Recently the TLD has also been applied to anodic stripping voltammetry (ASV) [19].

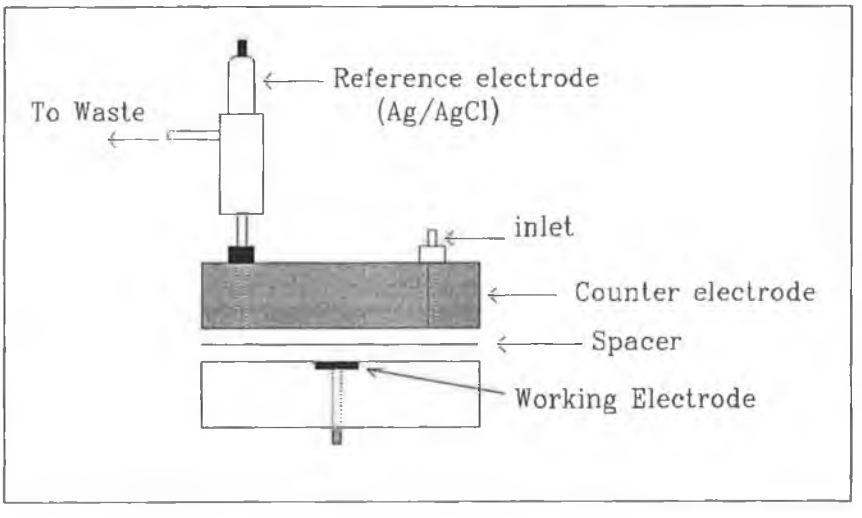

Figure 1.3. Typical thin layer flow cell design.

The response of the TLD is based on a restricted case of the flat plate electrode with parallel flow where development of the boundary layer is constrained by the wall opposite the electrode. The width of the channel between the working electrode and

the opposite wall is dependent on the thickness of the spacer used [20]. The design of a typical thin layer flow cell is shown in Figure 1.3.

For the unrestricted case of a flat-plate electrode with parallel flow, where the solution volume is not constrained and the development of the boundary layer is unrestricted, both the bulk motion and diffusion are involved in the analyte flux to the electrode. For the restricted case of the thin-layer detector, however, only diffusion is of importance in deriving the limiting current.

The principle of the wall jet cell was defined by Glauert who described it as the flow of a jet of fluid that strikes a wall perpendicularly and flows radially over its surface [21]. The critical requirements for the design of a flow-through cell that enables true wall-jet (WJ) behaviour have been defined by Gunasingham and Fleet [22]. Although their limiting-current equation does not include a term to express the separation between the inlet nozzle and disk electrode, the assumption is made that the jet of liquid emerging from the inlet does not break-up before it strikes the electrode disk. In general, the jet has been shown to remain intact for up to 10 mm from the inlet for a Reynolds number of 70. However at a higher Reynolds number the jet can break up and become turbulent much closer to the inlet. Detectors based on the WJ configuration have been widely used in practical applications ranging from LC detection [23-24], ASV [25, 26] and clinical analysis [27].

1.3.1 Flow Cell Requirements

The specific requirements for an electrochemical detector vary with the intended application. However, a number of requirements generally apply [28]:

(i) well defined hydrodynamics;

(ii) low dead volume;

(iii) high mass-transfer rates;

(iv) high signal to noise ratio;

(v) robust, simple, easily maintained design;

(vi) optimised electrode positioning;

(vii) stable reference electrode.

1.3.2 Hydrodynamic Characteristics

In many analytical applications not enough consideration is given to the hydrodynamic behaviour of the flow cell. Normally this is acceptable because it is not necessary to have a cell geometry that is hydrodynamically well defined, provided the flow is reproducible and the detector gives reproducible results. For example, although the wall jet detector (WJD) response can vary between TL and WJ behaviour, depending on the inlet-electrode separation [29], it is reproducible at any fixed separation. For the TLD, the current response depends on the position of the inlet with respect to the working electrode and the degree to which the flow is restricted in the vicinity of the working electrode.

1.3.3 Dead Volume

Dead volume has an important bearing on band spreading and hence on resolution, sensitivity and response time in FIA-EC (flow injection analysis with electrochemical detection) and LC-EC (liquid chromatography with electrochemical detection). Minimisation or avoidance of band spreading in LC-EC detection is of great importance, where there is a need to prevent overlapping adjacent chromatographic peaks.

In the TLD, the geometric volume is purposely constricted to a few microlitres so that maximum coverage of the electrode surface and a high linear flow rate is achieved [30]. In this case, the dead volume is effectively the geometric cell volume. For the WJD, however, the solution from the inlet impinges perpendicularly on the working electrode and spreads radially over its surface. Here, the dead volume is effectively the boundary layer and is independent of the geometric cell volume [20].

1.3.4 Mass Transfer Rate

A high mass transfer rate in a flow cell is normally a desirable feature as it enhances the current response. In flowing systems, the mass transfer rate can be increased by simply increasing the flow rate. A comparison of the response of different detectors has been made by Hanekamp and co-workers [31, 32] on the basis of a generalised equation for the limiting current in terms of the dimensionless Reynolds number Re and Schmidt number, Sc, given by:

$$I=knFDC^{*}(Sc)^{\beta}w(Re)^{\alpha} \qquad (1.6)$$

where k is a constant, n is the number of electrons, F is the Faraday constant (96,485 C mol^{-1}), D is the diffusion coefficient (cm^2 s^{-1}), C^* is the bulk concentration (mol dm^{-3}), Sc is the Schmidt number (dimensionless), w is the electrode diameter (cm), Re is the Reynolds number (dimensionless) and α and β are numerical constants that depend on the particular cell geometry. Although the implication is that the limiting current response increases with Re in practice, if Re is too high, it could lead to break-up of the flow into a turbulent regime.

In FIA-EC and LC-EC analysis, although the solute peak current increases with increasing flow rate, the electrolytic efficiency (defined by the total charge measured)

decreases in response to the decrease in the residence time as the solute band is swept through the detector. On the basis of the work of Hanekamp and co-workers [31, 32], it would appear that the WJD has a greater current sensitivity than the TLD. Equally, however, it is more sensitive to flow fluctuations.

1.4 Electrochemical Instrumentation

1.4.1 Voltammetric Instrumentation

Voltammetry requires a waveform generator to produce an excitation signal, normally a voltage ramp, a potentiostat, a current measuring device and a readout device. Block diagrams for a voltammetric instrument are shown in Figure 1.4.

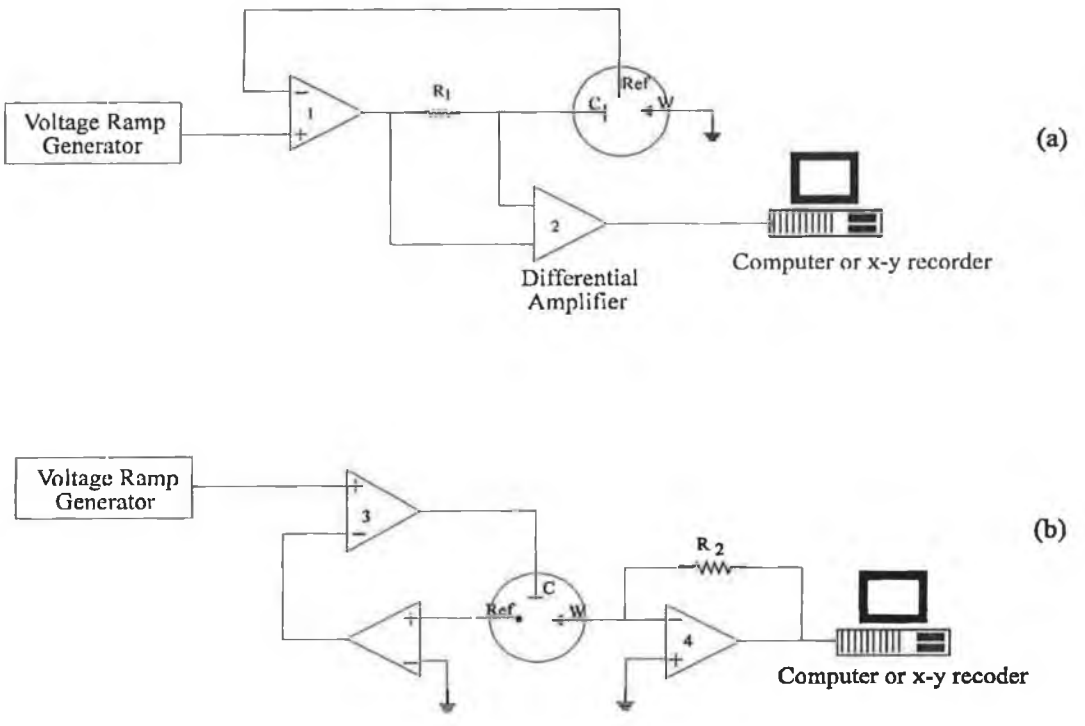

Figure 1.4. Block diagrams for a voltammetric instrument. In (a) the working electrode is directly grounded, thereby reducing electrical noise pick-up. Circuit (b) employs a current-to-voltage converter.

Most modern instrumentation is automatically recording and include ramp generators that are synchronised with an x-y recorder or an analog to digital converter (ADC). The unit marked "ramp generator" consists of either an electronic integrator, or a step function generator that produces a staircase approximation to a ramp. In either case, its output is an increasing voltage, adjustable in both range and slope. The potentiostat applies the potential excitation signal between the working electrode and the reference electrode without allowing charge to pass through the reference electrode (which would change its potential). In circuit (a) the working electrode is directly connected to ground (a lower noise configuration) and the current is measured by the voltage drop across resistor R_1 in series with the counter electrode, as sensed by the differential amp 2. In the alternative circuit (b), the electrode is held at virtual ground by the action of op-amp no.4 but the cell current is forced to flow through resistor R_2 to give to the recorder a proportionate output voltage [17].

Various voltammetric instruments are available from a number of commercial sources ranging in price from £2,000 to £25,000. With computer controlled or processor based voltammetric analysers, it is possible in principle to apply any potential waveform that can be defined mathematically. Such instruments offer various data processing options such as background subtraction, digital filtering, integration, differentiation and multiple voltammogram display. The acquired voltammograms can be displayed on screen, saved to disk or sent to a plotter. Voltammetric analysers with autosamplers are also available which can greatly improve the speed and precision of measurements [5].

1.4.2 The Potentiostat

A characteristic of modern voltammetric instrumentation is potentiostatic control of the working electrode potential accompanied by the measurement of the current at that electrode. The potentiostat must perform these two functions with electrodes of varying conductivity. The potential may be pulsed very rapidly or scanned very slowly, and the resulting cell current may be extremely high or low. The potentiostat has the capability to maintain a set potential to within an accuracy of a few millivolts while only causing a minimal current of the order of a few picoamps to be drawn through the reference electrode. It also has a very rapid response time, typically of the order of a few microseconds, when driving a resistive load [1].

Early designs of direct current (DC) polarographs used a motor driven potentiometer to apply the working potential to a two-electrode cell. By using a large area reference anode such as a mercury pool, the reference electrode potential remained essentially constant while the working electrode was polarised. In this arrangement the polarising potential was applied to the dropping mercury electrode (DME) through the reference electrode and across the cell. The overall cell potential could be defined as:

$$E_{cell} = E_{working} - E_{reference} - iR \qquad (1.7)$$

where the iR term, known as the ohmic drop, is the potential required to overcome the resistance of the experimental system, mainly of the cell. At low current levels in highly conducting media, this system works well. Unfortunately, at higher current levels, it is possible to polarise the reference electrode. A further complication is that in poorly conducting media such as organic solvents, the resistance across the cell is included in the measurements and causes distortion of the voltammogram. The first

solution to this problem was the development of the three electrode manual potentiostat. In this system the cell voltage was applied between the working and reference electrodes, while the true working potential was measured (with a second reference electrode) in a separate circuit with a high impedance voltammeter. This device provided a means for controlling the potential between the electrodes, but had the serious disadvantage that it required constant adjustment of the control voltage during the measurement of a polarogram. A schematic of a typical modern electronic potentiostat is shown in Figure 1.5. Operational amplifier (op-amp) 1 is the control amplifier which supplies the input signal (DC level, voltage ramp etc.) to the cell. Op-amp 2 is a high impedance, unity gain, non-inverting voltage follower, while op-amp 3 is a variable gain current follower which serves to maintain the working electrode

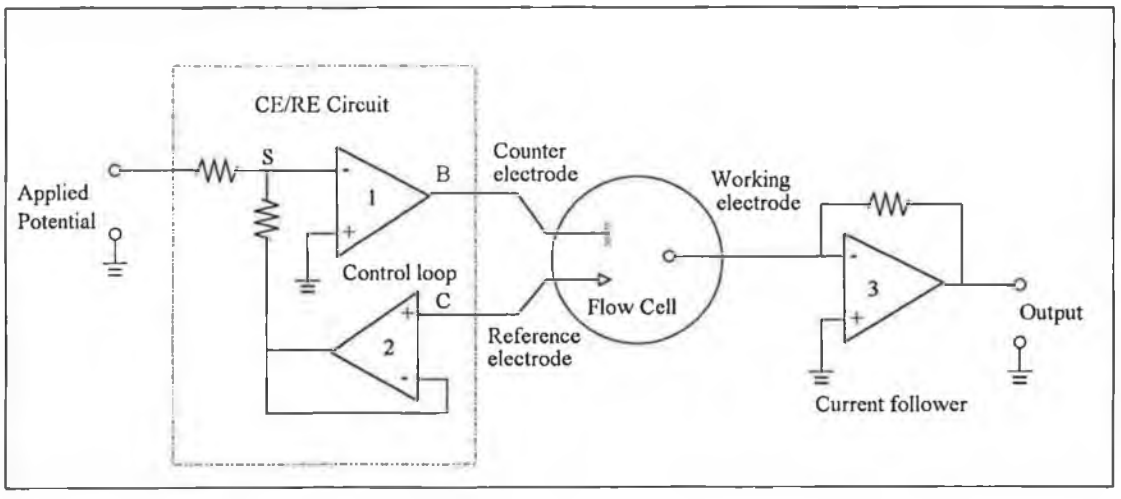

Figure 1.5 Schematic circuit for a three-electrode potentiostat.

at zero volts (virtual ground) and provide an output proportional to the polarographic current. The operation of this circuit can be best visualised realising that an operational amplifier reacts in a manner required to maintain zero potential difference between its inputs. The stable condition for the loop containing op-amps 1 and 2 is

when the output from op-amp 2 is equal in magnitude but opposite in polarity to the sum of the input voltages. This means that the voltage at point S (the summing junction) will always be at zero volts. Thus, the voltage measured at point C should always be the same as that applied to point S, and if momentarily it is not, the voltage at point B will automatically increase to maintain point C equal to point S.

Although the potentiostat must control the potential at the working electrode surface, the potential is actually measured at the reference electrode. The three-electrode potentiostat automatically compensates for the resistance of the solution between the counter and reference electrodes. This makes it possible to use non-aqueous solvents of high resistance and quite dilute aqueous electrolytes. Distortion of the wave shape and slope of the current-voltage signal is much less pronounced, if not entirely eliminated. For extremely small electrodes (ultramicroelectrodes) and extremely small currents, a two-electrode cell often suffices [1, 8, 11].

The operational amplifier (op-amp) circuit is the basic component of most analog signal modifiers. The first op-amp circuits were composed of vacuum tube amplifiers and other necessary elements such as diodes, resistors and capacitors. Discrete transistors later replaced vacuum tubes, and finally entire operational amplifier circuits became available as IC (integrated circuit) chips. About one-third of all IC's are op-amps. More than 2000 types are commercially available. An IC op-amp consumes little power and operates at relatively low voltages (usually 10 to 15 V) with power supplies that need not be highly regulated. The IC op-amps have very low drift with both temperature and time, and can withstand short circuits on the output without damage [33].

1.4.3 The Bi-Potentiostat

The bipotentiostat configuration is utilised for simultaneous control of two working electrodes. Such instruments consist of a conventional potentiostat with a second voltage-control circuit. The basic circuit is outlined in Figure 1.6. One electrode is controlled in the same manner as the signal channel potentiostat. The circuitry responsible for this function is shown in the top half of the figure.

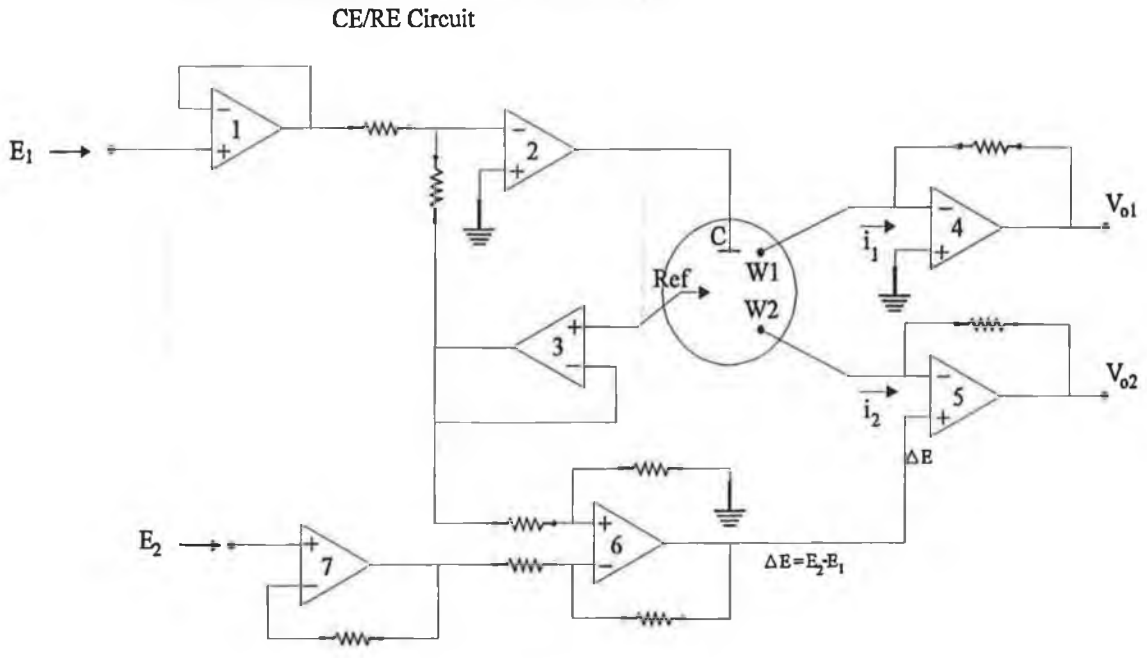

Figure 1.6. Schematic circuit for a bi-potentiostat.

The second electrode is controlled by a current follower (op-amp 5) with a summing point held away from ground by some voltage difference ΔE, because its non-inverting input is away from ground by ΔE. This circuit has the effect of using the first electrode as a reference point for the second. The first electrode can be set at any desired potential, E_1, with respect to the reference, then the second working electrode is offset with respect to the first by $\Delta E = E_2 - E_1$ where E_2 is the potential of the second

electrode with respect to the reference. The counter electrode passes the sum of the current i_1 and i_2. The remaining op-amps (6 and 7) serve as zero-shifting stages. Their function is to supply the desired potential E_2 without concern for the value of E_1. This feature is important when E_1 and E_2 are to be varied independently with time. Op-amps 1-3 are used in the standard feedback loop configuration for the counter and reference electrodes [10, 34, 35].

1.4.4 Multichannel Potentiostats

The construction of electrochemical measurements whereby a number of working electrodes are controlled and monitored simultaneously was the next obvious development of the single channel potentiostat and bipotentiostat. Two main approaches have been adopted in the development of multichannel electrochemical detection systems (more than two independently controlled working electrodes) based on the two types of electrochemical detectors, namely coulometric and amperometric. Of these two approaches, the development of amperometric arrays appears at present to offer the best possibilities in the development of functional array detection systems for LC and FIA.

1.4.4.1 Coulometric Arrays

Coulometric detection is based on the principle of complete oxidation or reduction of an analyte at a large surface area working electrode. The response is therefore mass dependent. Coulometric measurements are advantageous for a number of reasons; namely the measurement is absolute, sensitive, accurate and precise. Provided that all the substance present is allowed to react at the working electrode and that the

electrode reaction proceeds at 100% current efficiency, the electric charge passed Q, is related to the amount of the electroactive substance N, according to Faraday's laws. Coulometric cells can be used to advantage for electrochemical derivative-formation in flowing liquids: a substance that would be difficult to detect is quantitatively oxidised or reduced at a generating electrode with the formation of a suitable product that is then detected electrochemically at an indicator electrode [36, 38]. However, with conventional LC columns, commerical coulometric detectors have limited application, as the requirement of complete electrolysis necessitates a large working electrode area and the mobile phase flow-rate must be very low. It is therefore difficult to maintain a sufficiently small effective volume in the detector and attain flow-rates optimal from the point of view of separation in the column [9].

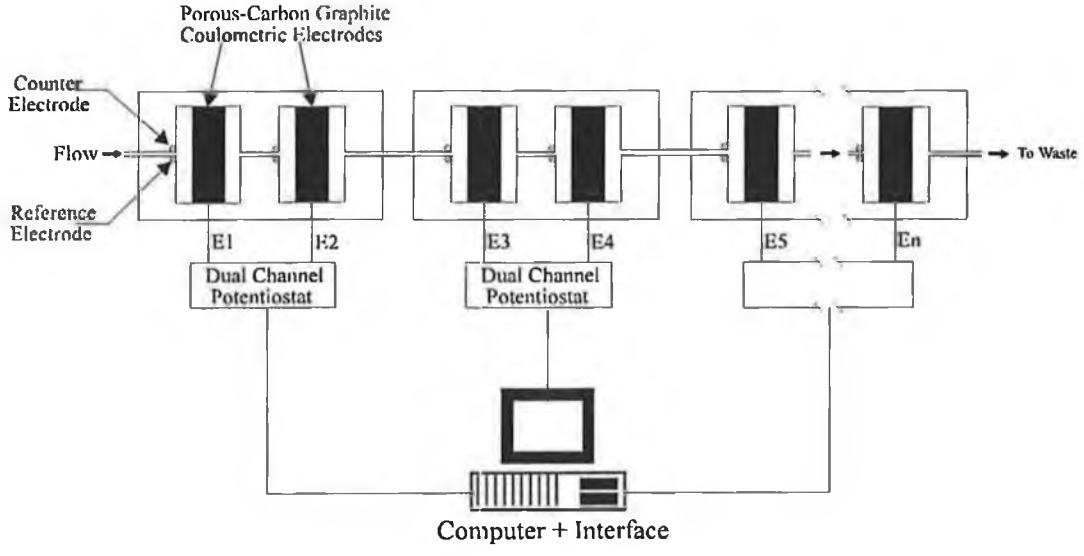

Figure 1.7. Coulometric array configuration

The design of coulometric arrays is based on conventional technology; therefore each working electrode requires its own reference and counter electrodes. A schematic for a coulometric array is presented in Figure 1.7. The detection system consists of a

serial array of coulometric electrodes set at incrementally higher voltages. Compounds are detected at certain electrodes depending on their individual oxidation potentials, and once fully oxidised are 'invisible' to electrodes further up the array. The cells are monitored with banks of single or dual channel low noise potentiostats. As a result these instruments tend to be rather large and cumbersome. A number of publications have described the application of coulometric array detectors to LC systems. Systems containing up to 15 working electrodes have been reported [37]. A coulometric array instrument for applications with LC is commercially available from ESA Analytical Ltd (UK) [38].

1.4.4.2 Multichannel Potentiostats with Amperometric Arrays

The use of amperometric arrays with multichannel potentiostats has been area of promising development over the last number of years. Two principle hardware variations have been used in the design and construction of these systems. One trend has been the use of a configurations based on an extension of the conventional bi-potentiostat. Such a design has been utilised by both Matsue and Fielden in the construction of their multichannel potentiostats for applications with LC and FIA [39, 40]. A schematic of the design utilised by Matsue and co-workers is shown in Figure 1.8.

Their design was based on the use of analog circuits to control functions such as working electrode polarisation and signal amplification. A resistor ladder was used to divide an input voltage into 16 evenly spaced potentials which were applied via a voltage to an microband array.

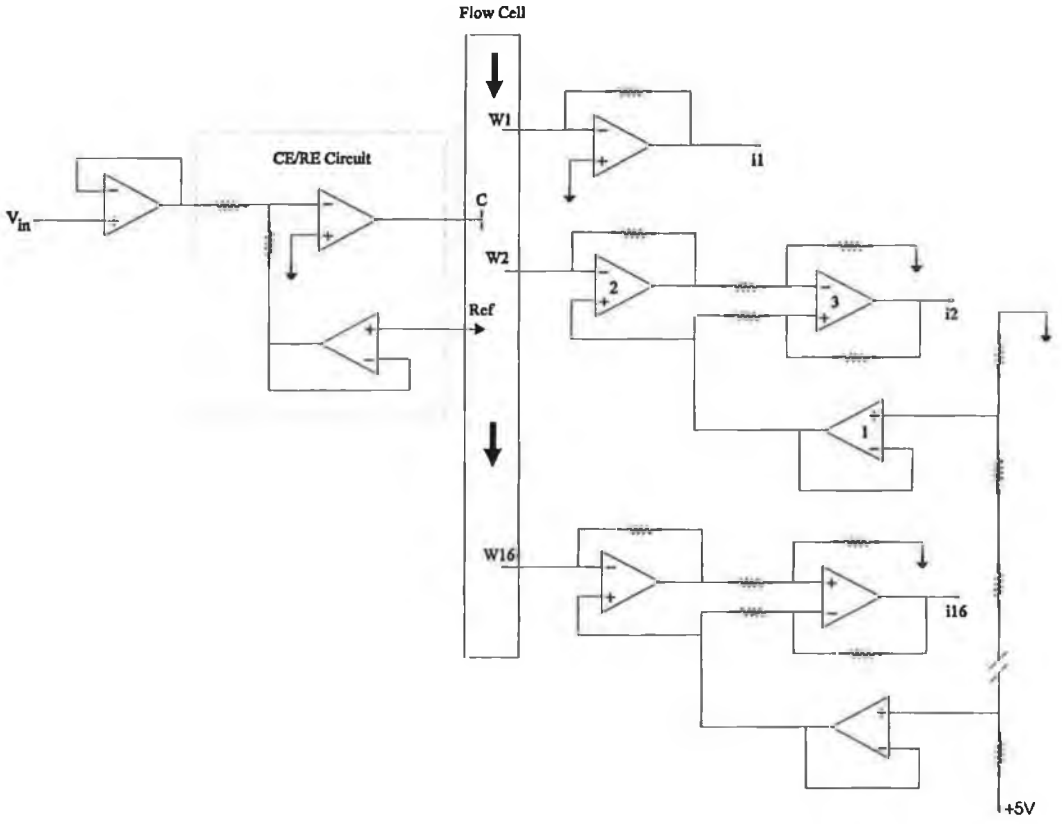

Figure 1.8. Multichannel potentiostat used by Matsue and co-workers (taken from reference [39]).

The array was produced by photolithography. The analog control circuits for each channel, except for channel 1, consisted of a 3 op-amp arrangement. Op-amp 1 was used as a voltage follower, while op-amp 2 served a two-fold purpose; firstly to polarise the working electrode at the input potential, and secondly to monitor, convert and amplify any changes in current to voltage at the electrode surface due to any redox processes taking place.

Op-amp 3 was utilised in a differential configuration to subtract the applied polarisation potential from the signal output from op-amp 2. The signal sampled therefore by the A/D converter was solely from any response at the working electrode. Common reference and counter electrodes were used in a standard feedback loop and

were held at a constant potential. Therefore the difference in potential between the working electrodes and the counter electrode potential was used. The 16 responses from the current-to-voltage converters in the multichannel potentiostat were drawn into two-channel multiplexers, with the resulting two sets of eight signals being digitised successively by an eight-channel analog-to-digital (12-bit) converter system. The instrumentation functions were controlled with via an interface card and PC. No hardware facilities for background current offsetting were incorporated into the design. The necessary background corrections were achieved by subtraction of the background voltammogram obtained prior to sample injection

A variation of this basic design has been used by Fielden and McCreedy when constructing their multi-electrode potentiostat [40]. A schematic of their design is presented in Figure 1.9.

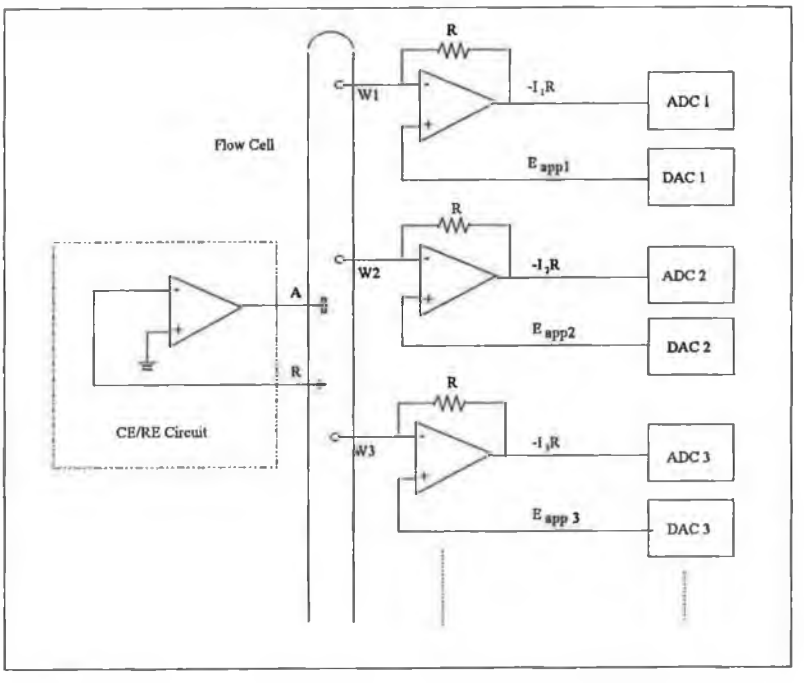

Figure 1.9. Schematic of multi-electrode potentiostat (from Fielden and McCreedy in reference [40]).

Each channel was provided with its own current follower which polarised the working electrode via a 12-bit DAC. Multiplexed analog to digital conversion was used to monitor the outputs of each channel. The potentiostat used a single reference and counter electrode. The reference electrode was maintained at virtual ground by the action of the counter electrode responding to the current demands of the array. Each working electrode was polarised relative to the reference electrode so that the actual applied potential to working electrode is used rather than a difference potential. Fixed value resistors were used with the current followers which limited the operating range of the potentiostat to about three orders of magnitude.

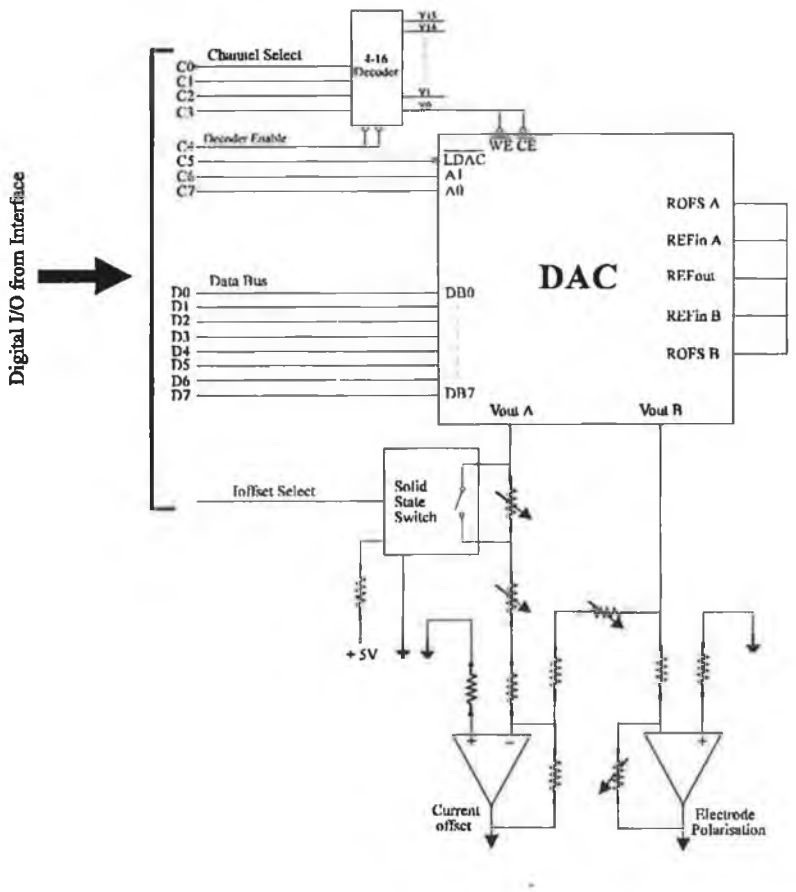

Figure 1.10. DAC control circuit for independent electrode polarisation and current offsetting.

A fundamental feature of a multichannel potentiostat is that each working electrode in the array must function independently, with no electronic cross-talk between the channels. Such a requirement has resulted in the use of dedicated dual channel DAC's for each channel of the potentiostat to control both the electrode polarisation and current offsetting functions. A typical DAC control circuit is shown in Figure 1.10.

The multichannel potentiostat constructed by Hoogvliet et al. [41] was based on the use of a dedicated dual channel DAC (AD 7547) for each channel of the potentiostat. The DAC for each channel was selected via a 4-16 decoder. The DAC's were responsible for background current offsetting (± 0.2 μA, resolution ca. 50 pA) and working electrode polarisation. The principle of maintaining the reference electrode at system ground as described by Fielden et al. [40] was applied. Software selectable sensitivity between 1 mA and 1 nA (7 decades) was available which allowed current measurements in the 1 mA to 1 nA range. An analog low-pass (third order Bessel) filter with a cut-off frequency of 3.2 Hz was incorporated into each channel for noise reduction. An IBM-AT personal computer was used for data acquisition and control of the multipotentiostat via a Burr-Brown PCI-2000 interface. Software for instrumental control, data acquisition, storage, display and data processing was written in Turbo Pascal v 5.0.

1.4.5 Limitations of Potentiostats

The following characteristics are important factors influencing the limitations of modern potentiostats and electrochemical detection systems.

(i) The response time and instability of potentiostats

Amplifier characteristics have an important influence on the accuracy of the potentiostat circuit and its stability. Unfortunately, op-amps are not ideal devices; therefore the output does not respond instantly to any change in response at the inputs. One problem is the dependence of the open loop gain on frequency. A common method of presenting performance characteristics of op-amps is by means of a plot of $\log_{10}$ (gain) vs. $\log_{10}$ (frequency), often referred to as a Bode plot. An example of this type of plot is given in Figure 1.11.

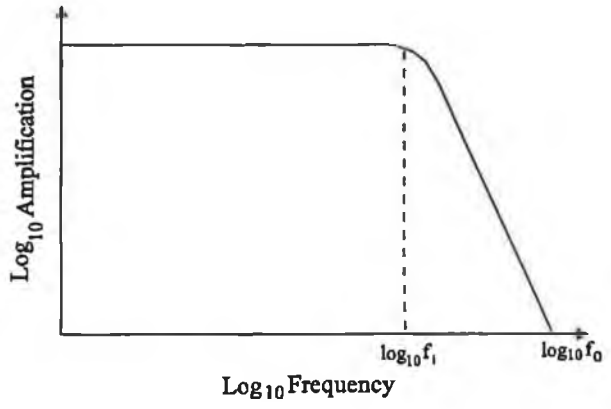

Figure 1.11. Bode plot of $\log_{10}$ frequency vs. $\log_{10}$ amplification for a typical op-amp.

The roll-off frequency (the same as a simple RC low-pass filter) determines the time constant for the potentiostat, τ_1, through the relationship:

$$\tau_1 = \frac{1}{2\pi f_1} \qquad (1.8)$$

where $f_1 = \frac{f_o}{A_s}$, A_s is the static gain and f_o is the frequency of unity gain. From these equations it can be seen that τ_1 can be minimised by using a fast op-amp (high f_o) or by using an op-amp with a small open loop gain. As a large open gain is required for

good accuracy a compromise must be reached between high accuracy and fast response. Careful consideration must be given to the choice of op-amp. Op-amps without internal compensation may afford more satisfactory performance in some situations. The electrochemical cell itself will also have a time constant τ_2 given in the simplest case by R_eC_{dl}, where R_e is the electrolyte resistance between the counter electrode and the working electrode and C_{dl} is the double layer capacitance. R_e can be reduced by avoiding frits, porous plugs, increasing the conductivity of electrolyte or decreasing the electrode separation. C_{dl} can be reduced by using spherical electrodes of small area. It may be possible to effectively eliminate the potentiostat time constant (τ_1) and by careful cell design to minimise τ_2.

The stability of the control circuit relies on negative feedback to the inverting input. A typical equivalent circuit for an electrochemical cell is shown in Figure 1.12.

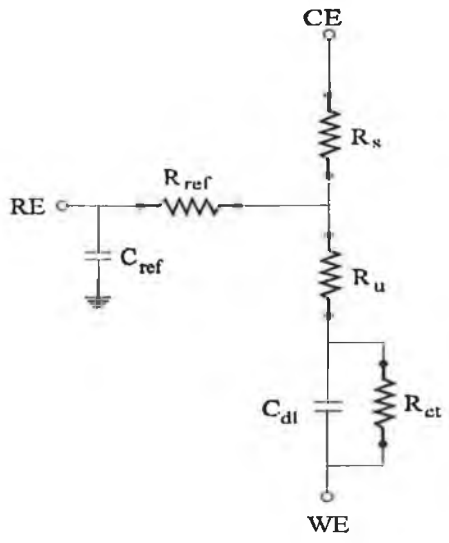

Figure 1.12. Equivalent circuit for an electrochemical cell. R_{ref} is the resistance of the reference electrode and C_{ref} represents the loss to ground in the cell leads. R_s and R_u are the solution and uncompensated resistance respectively, C_{dl} the double layer capacitance of the working electrode and R_{ct} the charging current.

If the response of the potentiostat or the impedance of the cell elements in the feedback loop introduce phase shifts in excess of 180°, then the signal that is fed back no longer limits the gain but will reinforce the output resulting in instability or oscillation of the output. The control op-amp introduces a 90° phase shift for frequencies higher than the roll-off frequency (typically 100 Hz) and an extra 90° can be easily generated in an electrochemical cell.

While little can be done to reduce phase shifts in the cell any reduction in the time constant $R_{ref}\,C_{ref}$ will be advantageous. C_{ref} may be due to excessive capacitance to ground, especially if leads to the cell have grounded shields and are unduly long. A better arrangement uses a driven shield maintained at the reference potential [8, 10, 42].

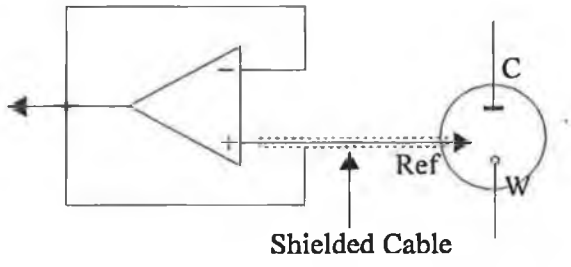

Figure 1.13. Driven shielding

(ii) Output Drive

To avoid non-linear effects, the demands on the potentiostat must not exceed its capabilities in terms of output voltage, current and slew rate. The maximum output voltage is usually limited by the value of the power supply rail to the device. If the output current is not sufficient for the purpose intended, a current amplifier can be used to boost the output up to the required level of magnitude. Non-steady state methods (e.g. linear sweep voltammetry) demand large currents over very short time

periods to change the double layer capacitance which may not be satisfied by some potentiostat designs [10, 42].

(iii) Static accuracy

The accuracy of an op-amp can be described by the equation:

$$\delta V = \frac{Vo}{A} + \frac{E_I}{M} + \text{drift} + \text{noise} \qquad (1.9)$$

where E_I is the input reference potential, A is the amplification, V_o is the voltage output and M is the common mode rejection ratio. For ± 1 mV accuracy both M and A should be of the order of 10^4-10^5 or larger. The static error signal is often referred to as the input offset voltage. The inclusion of small potentiometers in the design of the potentiostat circuit allows balancing (trimming) of this signal. This is, however, limited by the drift of the offset voltage with time, which can be up to 1 mV/day thus limiting the accuracy of any measurements. Chopper stabilised amplifiers can be obtained with a stability of 0.1 μV/day where very high accuracy measurements are required.

(iv) iR Compensation

The usefulness of many electrochemical data depends on the precision and accuracy of potential control. Eliminating the effect of solution resistance in electrochemical measurements is very important and much effort has been spent on this problem. Not all the iR drop is removed by the potentiostatic control. Some fraction, called iR_u (where R_u is the uncompensated solution resistance between the reference and working electrodes), will still be included in the measurement potential. This component may

be significantly large when resistive non-aqueous media are used and can lead to severe distortion of the voltammetric response. Many modern instruments, however, automatically subtract (compensate) the iR_u drop from the potential signal given to the potentiostat via an appropriate positive feedback. A typical circuit for a potentiostat employing positive feedback is shown in Figure 1.14. This circuitry is now widely used because it is compatible with the fastest experimental methods.

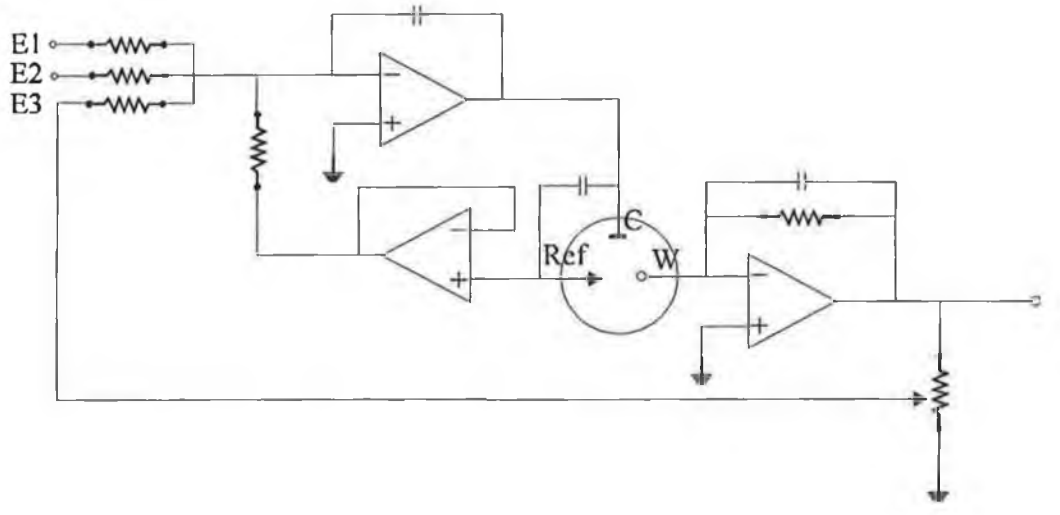

Figure 1.14. Potentiostat with feedback control for the compensation of R_u.

Several other approaches have been taken to overcome this limitation, including improved cell design, numerical data correction after the experiment if R_u is known and electronic iR elimination. Better results can often be obtained by using a combination of these approaches. With the use of electronic methods, careful design of the potentiostat is very helpful. The current interruption potentiostat and the digital potentiostat were designed so that the sensing of the potential between the working electrode and reference electrode is accomplished when no current passes through the electrochemical cell. The potential control is thus free of iR error [43].

(v) Electrode Arrays

Ideal behaviour of a multielectrode detector would include an equivalent response (signal, noise and background) of all channels when the working are electrodes set at the same potential, no cross-talk between the individual channels and signal-to-noise ratios comparable with conventional single-electrode amperometric detectors. Equality of the responses is determined by the hydrodynamic and mass-transfer characteristics of the cell, by electrode and cell geometry, by electrode kinetics and by proper configuration and adjustment of the electronics in the potentiostat. Careful design allows optimisation of all these parameters except that of the electrode response characteristics [41]. A fundamental feature of amperometric array detection systems is the ability to fabricate arrays with near identical surface areas and kinetics. This is impossible to achieve using standard electrode fabrication technology. Arrays which have been constructed using conventional fabrication technology must have their response characteristics normalised to compensate for individual discrepancies using software normalisation procedures. However, these procedures are limited in their effectiveness, and in some cases can add to the differences in response rather than reducing them when large potential windows are used.

A second approach in the fabrication of arrays has been the use of photolithography. Both linear and radial arrays of electrode arrays have been produced using this technique [39, 44]. These arrays generally display a high degree of reproducibility and large numbers of arrays can be produced simultaneously. However these arrays have a limited working life due to poor mechanical characteristics. A limitation of photolithography is the inability to use glass carbon as an electrode material. Glassy carbon is material of choice for most electrochemical experiments. Only metals which

maybe deposited on the copper tracks such as gold and platinum can be used for the working electrodes. Continued development of multiple electrode systems is therefore dependent on the ability to produce stable, reliable and reproducible arrays.

1.5 Electrochemical Detection in Flowing Solutions

Developments in the area of electrochemical detection systems in recent years have focused on a number of areas. Both coulometric and amperometric arrays have been successfully applied to applications with LC and FIA [36, 40]. The use of fast scan techniques such as square wave voltammetry has also emerged in recent years for applications with LC\FIA [45]. These new detection systems all rely heavily on the use of computers for waveform generation and data interpretation. Implementation of these techniques without the use of a computer is practically impossible.

The most common mode of amperometric detection to date has been with a single working electrode maintained at a constant potential. However, this approach gives two dimensional information on the electrochemical properties of the species being detected; namely a particular current value at a fixed potential as a function of time, which gives the user no confirmation as to whether peaks are arising from one or more electroactive species. On the other hand, an extra measurement dimension can provide additional information regarding the number of components contributing to a signal. This has already been very successfully exploited via spectroscopic detectors such as the photodiode array detector [46] and excitation-emission fluorescence detectors [47] in LC. Recently, much attention has been focused on electrochemical flow-through voltammetric detection in order to obtain three-dimensional information (time,

potential and current). This method usually requires a rapid potential scan to detect species flowing in and out of the detector, resulting in increases in the background signal due to charging current and also in distortion of the voltammetric shape. To overcome this problem several techniques have been reported including staircase voltammetry [48], normal pulse voltammetry [49] and differential pulse [25] techniques. However, the detection limits obtained are 2 to 3 orders of magnitude higher than those obtained by conventional amperometric detection systems.

1.5.1 LC with Electrochemical Detection

Liquid chromatography with electrochemical detection has become a popular technique for trace organic analysis because of its ease of use, high sensitivity and excellent selectivity. A wide spectrum of applications with electrochemical detectors have been reported in the literature. These include a variety of compounds at trace levels such as pesticides, aromatic amines, phenolic compounds and neurotransmitters [48, 50-53].

The application of two independently controlled working electrodes in a thin layer flow cell have been reviewed by Roston and Kissinger [54]. These dual electrode arrangements are based on the thin layer single working electrode cells that incorporate downstream reference and counter electrodes. The dual electrode detector offers additional selectivity compared to a single electrode detector. In the first configuration the working electrodes were placed parallel to the flowing stream with each electrode being held at different potentials. The two simultaneous chromatograms could then be ratioed for peak confirmation. The working electrodes were arranged in series in the second configuration. The upstream working electrode generates an electroactive

product which is detected at the second electrode. The series arrangement limits the number of electroactive compounds that can be detected because only those electroactive products that are stable in the time required to reach the working electrode are detected [1, 55].

A dual electrode detector for liquid chromatography, with enhanced capabilities designed to obtained a three-dimensional data array of current responses as a function of both time and potential, has been described by Lunte et al. [56]. By displaying the entire voltammogram it allowed post-run choice of the optimal detection potential with a single fixed potential electrode. Voltammetric detection of 10 to 100 pmol injected of gentisic acid and caffeic acid were possible. The voltammetric data also provide a second method of peak identification for greater certainty in peak assignments. Waveform generation and data acquisition and analysis were controlled by a Zenith 158 personal computer which interfaced with an ADALAB-PC interface card. The utilisation of a dual-electrode detector in a series configuration for the detection of phenolic compounds in commercial beverages and the determination of metabolites of the analgesic acetaminophen in urine was reported by Roston et al. [55]. The upstream working electrode was used to oxidise the compounds of interest which were then detected by reduction at the downstream working electrode. The use of redox cycling allows improvements in selectivity, peak identification and high detection limits at extreme potentials.

The use of a dual electrode arrangement to detect thiols and disulphides has been reported by Allison and Shoup [57]. The thiols and disulphides were determined simultaneously by using thin-layer dual mercury amalgam electrodes in a series configuration coupled to a LC. After chromatographic separation of the sample,

disulphides were first converted to their corresponding thiols at the upstream electrode (-1.0 V vs. Ag/AgCl). Both the thiols and disulphides were then detected as thiols downstream at +0.15 V via their catalytic oxidation of the mercury surface. The application of this method to the determination of phenols in environmental samples which have been chromatographically separated by LC was described by Shoup and Mayer [58].

1.5.2 Scanning Techniques

An increasingly popular voltammetric technique is square wave voltammetry, which combines the advantages of a pulse waveform which minimises interferences from non-faradaic current with a fast scan rate. Standard square waves frequencies are in the region of 200 Hz with a step height of 10 mV resulting in a scan rate of 2 V s^{-1}. The technique demonstrates excellent rejection of background currents. Therefore the square wave net current is insensitive to currents arising from convective mass transport as long as the characteristic time of that transport is large in comparison with the voltammetric pulse width. This is advantageous in LC were the net square wave signal is relatively insensitive to fluctuations in flow rate. An additional of the fast scan voltammetry is the ability to determine changes in the voltammetric response with time non-destructively. This includes the mode of sample presentation as in FIA and LC. Osteryoung and co-workers using square wave voltammetry with LC, were able to obtain three dimensional definition of chromatographic peaks [45]. The unavailability of a stand-alone instrument and the inherent complexity of the technique have hindered the wide spread use of this technique.

The use of fast cyclic voltammetry to perform fast i-E scans with FIA has also been reported in the literature. The information collected by the system could be presented in a number of formats. First, x-y recordings as in cyclic voltammetry could be presented as i-E recordings or derivative recordings; secondly, x-t plots could be recorded. The system has possible applications in both qualitative and quantitative analysis through utilisation of the half-wave potential of the voltammetric process [59].

1.5.3 Multielectrode Techniques

Fabrication of single and multiple electrode arrays by photolithography has been reported in literature for the last number of years. These arrays are often fabricated as interdigitated microelectrode arrays which usually consists of rectangular active elements separated by narrow gaps and with alternating elements held at different potentials. The fabrication of a radial array by photolithography for use in a wall jet flow cell has recently been reported [44]. Early applications of these arrays with single channel potentiostats were reported [60-64]. Matsue and co-workers reported the electrochemical characterisation of two microarray electrodes, an interdigitated microarray electrode (IDAE) and a single potential microarray electrode (SAE), in flowing streams. A comparison between the IDAE and a dual-series rectangular electrode with the same area demonstrated a current amplification of current responses by a factor of 2.8-3.9 due to redox cycling. The application of the IDAE to the selective determination of reversible catecholamines in LC was demonstrated by Matsue et al. [65]. This earlier work was the basis for Matsue's more recent work involving the application of a multichannel potentiostat with an amperometric array to electrochemical detection with LC and FIA.

Wang et al. [66] reported on an amperometric array consisting of 4 chemically modified electrodes in a thin layer flow cell. However, the electrodes were monitored sequentially, rather than simultaneously, as in normal amperometric arrays. Harrington et al. [67] have described a general purpose, multiple working electrode potentiostat, capable of controlling up to 11 working electrodes. The potentiostat was capable of controlling independently the electrode potentials over a continuous range from -2.5 to +2.5 V with current sensitivities in the range 1 mA-100 pA. Low noise performance was achieved through appropriate power isolation and null balancing techniques. For automated data acquisition and control, the multiple electrode potentiostat was interfaced to an Apple IIe microcomputer. All control lines between the microcomputer and the potentiostat were provided by the secondary input/output devices located on the I/O socket of the Apple IIe motherboard. The potentiostat was used with an interdigitated filar microelectrode array for the determination of ferrocene. The instrumentation was designed for either stand alone operation or for computer controlled operation and was capable of implementing either stepped potential or scanned potential programs.

Matsue et al. [39, 68] have utilised their multichannel potentiostat and amperometric array with both FIA and LC to generate 3-dimensional hydrodynamic voltammograms. By applying a stepwise voltage sequence at the working electrode array it was possible to obtain measurements at 80 different potentials, thus improving the resolution of the data obtained. The detection system was applied to the determination of a mixture of several electroactive chemicals, such as ferrocene derivatives, ascorbic acid, uric acid and catecholamines. A detection limit of 1×10^{-8} M for a ferrocene derivative was obtained. It was also possible to determine mixtures of these ferrocene derivatives by

FIA without prior separation. The concentration of each component in the mixed injection was obtained from the magnitude of its diffusion current i_d.

A considerable advance in the development of multichannel potentiostat hardware has been made by Hoogvliet et al. [41]. Their design incorporated independent control of each working electrode through the utilisation of a dual channel DAC (AD 7547) for each working electrode. The instrumentation developed was an improvement over the design reported by Matsue et al. [39, 68] in terms of improved potentiostatic control and current offsetting capabilities, i.e. each working electrode in the array was both polarised and offset ($\pm$ 0.2 μA) for back current independently of each other. Efficient and versatile current setting capabilities are important in high sensitivity situations (1 nA-10 pA) where low level analytical signals are often superimposed on much higher background currents. The potentiostat was used with a radial flow cell design consisting of a 16 carbon paste working electrode array and was applied to the determination of epinephrine with a limit of detection (L.O.D) of 1×10^{-9} LC. While the limit of detection achieved was comparable to a conventional single working electrode systems, the 3-d chromatogram generated by the array is obviously much more comprehensive in terms of information content. The application of the system with biosensor arrays was also discussed.

Fielden et al. [40, 44, 69] have reported the design of an 8-channel amperometric array using a radial flow configuration operating under wall jet conditions, and more recently a radial array produced by photolithography again used in a wall jet configuration. They also described a linear flow cell consisting of two sets of Ø1 mm glassy carbon working electrodes positioned opposite each other and separated by a spacer. However, their hardware did not demonstrate the same degree of instrumental

flexibility as the design reported by Hoogvliet et al. [41]. The hardware design was similar to an extended bi-potentiostat. Control of the instrumentation was effected via a Compac 386/20 PC and software routines written in Turbo Pascal. Their system was applied to the determination of mixtures of metal ions such as Cu(II) and Cd(II) in aqueous solutions using FIA and LC. The signal obtained for the reduction of each metals ion such as Cd(II) was corrected for background contributions by other metal ions present in the sample e.g. Cu(II) when carrying out mixed species determinations, enabling multicomponent determinations to be carried out without prior separation as in FIA.

1.5.4 Capillary Electrophoresis with Electrochemical Detection (CE-EC)

Capillary electrophoresis (CE) has become a powerful analytical method because of the small sample volume and high separation efficiency offered [70]. The detector of choice for CE has been UV which results in relatively high detection limits due to the extremely short pathlengths possible. Efforts to improve the limits of detection for CE have focused on the development of laser induced fluorescence [71, 72] and electrochemical detection [73-77].

The development of electrochemical detection for CE has been difficult in comparison to its implementation in LC and FIA [73]. The main problem is the high potential fields that are used in CE separation. When an electrode was placed in the capillary, noise arising from the high voltage applied across the capillary interfered with detection. The implementation of the decoupler design permitted the first use of on column detection for CE. The decouplers have evolved from the early porous glass

coupler [73] to the cast Nafion type used by Park and co-workers at present [78]. A carbon fiber can be used to detect analytes amperometrically with detection limits in the low nanomolar range. The use of couplers has made electrochemical detection in CE possible by terminating the separation voltage and therefore noise currents, before detection. Some alternative approaches to the coupler have also been utilised which include insertion of the carbon fiber working electrode into a capillary of small internal diameter [79] and chemical etching of the capillary end of a capillary to provide a conical entrance for electrode placement [80].

To date these electrochemical detection schemes have been based on the use of amperometry with a single electrode maintained at a fixed potential. This approach suffers from the drawback of only providing limited information about the electrochemical properties of the analyte being detected. Routine analysis of complex samples with CE-EC is problematic because of the difficulty in assigning absolute peak identities due shifting migration times. However the use of voltammetric detection which can give 3-dimensional definition of the CE peaks can help to overcome. Ewing et al. [81] have described the use scanning electrochemical detection with CE to increase the resolving power for closely eluting solutes. Scan rates in the range 1 to 2.5 V s^{-1} were implemented with 5 μm carbon fibers used in an end-column detection mode. A 5 μm fused silica capillary was used for separation. The detection end of the capillary was etched to a conical shape in order to accommodate the carbon fiber working electrode. The system was applied to the determination of catechols. Linear responses were obtained in the concentration range of 10^{-3} to 10^{-5} M. Detection limits were in the range 2.3 μM to 6.6 μM.

Special consideration must be given to the specifications of the potentiostat required for CE-EC. Arcing between the high voltage end and ground which can occur occasionally results in permanent damage to the potentiostat especially the i-E converter op-amp. BAS now supplies a modified potentiostat which facilitates easy replacement of the damaged op-amps. To date no successful hardware method for the prevention of this type of damage has been developed. The potentiostat must be capable of working at high sensitivities (down to 0.1 pA). Low noise operation of the potentiostat is critical due to the high sensitivity nature of the measurements. Stability of the potentiostat in such high gain situations is vital to the accurate acquisition of the data. The potentiostat must be capable of supplying short high current outputs which are necessary during the electrochemical pretreatment of the carbon fiber working electrode.

1.6 PC and Microprocessor Based Instrumentation

Faced with the desire to join the computer age, many electrochemists have designed and built their own computer-based or microprocessor-based electrochemical systems. Developments in both computer and interface hardware have both contributed to this evolution. The use of the computer strongly affects the ease of instrument operation and the degree of functional adaptability. These systems provide power and flexibility for experimental control of functions such as waveform generation, digital filtering and data acquisition [6, 82].

The computer is both a tool for computation and data analysis. In the role of computation, computers have changed the nature of electrochemistry. They have also made it possible to calculate the response which is expected in complex experiments

situations not amenable to analytical mathematical solutions. Important mathematical techniques in routine use today include digital simulation and numerical integration. In addition, powerful numerical methods are used routinely for analysis of experimental data. The use of a small digital computer to control experiments and acquire data in electrochemistry was described by Lauer as early as early as 1967 [83]. Since that time the reliability of hardware has improved and its cost has dropped dramatically coupled with a dramatic increase in the sophistication of software. However, the principles on which today's computer-based systems are the same. The major difference is that technical elaboration has made it possible to be a user with a smaller investment in knowledge of the system [42].

The application of computers to control electrochemical experiments on-line developed rather slowly, owing to early problems associated with the interfacing and also the high costs. Both of these obstacles have now been largely overcome. It is now possible to purchase PC based systems capable of controlling a wide range of experiments, acquiring and processing data and displaying the results on screen and in hard copy form at an affordable price [42]. The microcomputer based system is particularly well suited to situations where many experiments of the same type will be undertaken with only slight changes in the experimental conditions. It is also useful in studies where a variety of techniques using numerous parameters variations can be quickly and effortless applied from the keyboard of the computer to a sample via the potentiostat. Stored voltammograms can easily be overlaid for comparison purposes or individual features can be selected, magnified and examined in more detailed. Commercial software packages now supply a wide range of analysis tools which are capable of handling must of the common data analysis requirements [5].

Commercial processor-based electrochemical instruments are available in two forms. In the first configuration, a PC is interfaced to the analog instrumentation. In the other approach, the package is integrated in such a way that the processor is dedicated to the electrochemical experiments. Several dedicated, processor-based pulse polarographs have been available since the mid-1970's. The first units were developed by Princeton Applied Research at a time when microprocessors were just beginning to influence all chemical instrumentation [6].

To perform any task, microprocessors must be programmed in a digital environment, using mathematical and logical operations which must be written in machine code. Software or program development at this level is tedious, time consuming and expensive. This therefore hindered the development of electrochemical instruments controlled by such processors. However, in the early 1980's BAS introduced a new class of integrated processor-driven instrumentation based on a concept first developed by Faulkner and co-workers [84] at the University of Illinois. The instrument included some 25 electrochemical techniques. The instrument had automatic R_u built into the hardware. Thus in a single instrument it was possible to implement all the common electrochemical techniques and thus establish quickly the optimum method for required analytical purposes. Data could be digitally smoothed, signal averaged and background subtracted [8].

CHAPTER 2

DESIGN AND DEVELOPMENT OF A COMPUTER-CONTROLLED MULTICHANNEL POTENTIOSTAT FOR APPLICATIONS WITH FLOWING SOLUTION ANALYSIS

2.1 Introduction

In the previous chapter, the background to computer-controlled electrochemical instrumentation and the development of multichannel amperometric detection systems for applications with LC and FIA, was introduced. In this work, a computer-controlled, multichannel potentiostat which can independently control an array of working electrodes. The autonomy of each channel in the potentiostat was achieved by the utilisation of a dual channel DAC (digital to analog converter) (AD7237) (Analog Devices) which was dedicated to electrode polarisation and background current offsetting duties. The design and the development of the analog and digital control circuits for a modular potentiostat capable of controlling up to 16 working electrodes with a common reference/counter electrode is discussed. Control of the purpose built instrumentation was effected via a 486/33MHz personal computer and Analog Devices RTI cards which were responsible for hardware control functions and data acquisition via digital and analog control lines. The control software for the system was developed in Microsoft QuickBasic 4.5 and an Assembly Language Toolbox. The design utilised differs from that used in conventional single channel potentiostats and incorporates many new hardware and software capabilities over work

previously reported in the literature.

2.2 Composition of Multichannel Potentiostat

The computer controlled, modular potentiostat was designed to control independently the potential of 4 working electrodes (WE) (expandable to 16), with common reference (RE) and counter electrodes (CE). A block diagram of the multichannel potentiostat is shown in Figure 2.1.

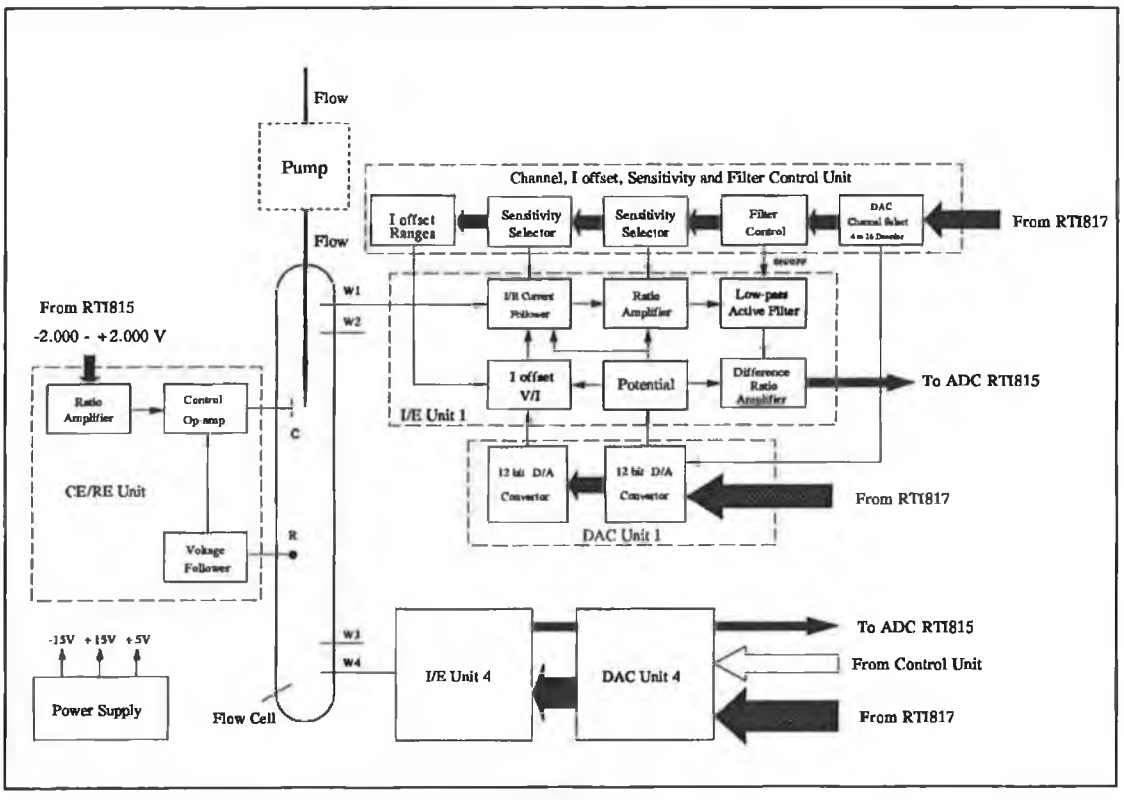

Figure 2.1. Block diagram of the multichannel potentiostat.

The multichannel potentiostat consists of a power supply, a counter electrode/reference electrode (CE/RE) unit, a channel selector, sensitivity selector, current offset extent selector and an analog filter control unit, 4 current to voltage (I/E) converter units and 4 D/A converter units. The digital and analog input/output

(I/O) signals were bussed through the back plane of the PC to the interface boards (RTI-815 and RTI-817 cards) [85, 86].

2.2.1 Counter/Reference Electrode CE/RE Unit

The CE/RE unit is the base circuit of the multichannel potentiostat. This circuit allows for setting a potential between the reference electrode and the working electrode by driving current through the counter electrode sufficient to produce the desired potential difference between the working electrode and reference electrode. The CE/RE unit was based on a quad op-amp (TL074)(SGS-Thompson Microelectronics). The circuit design utilised is shown in Figure 2.2.

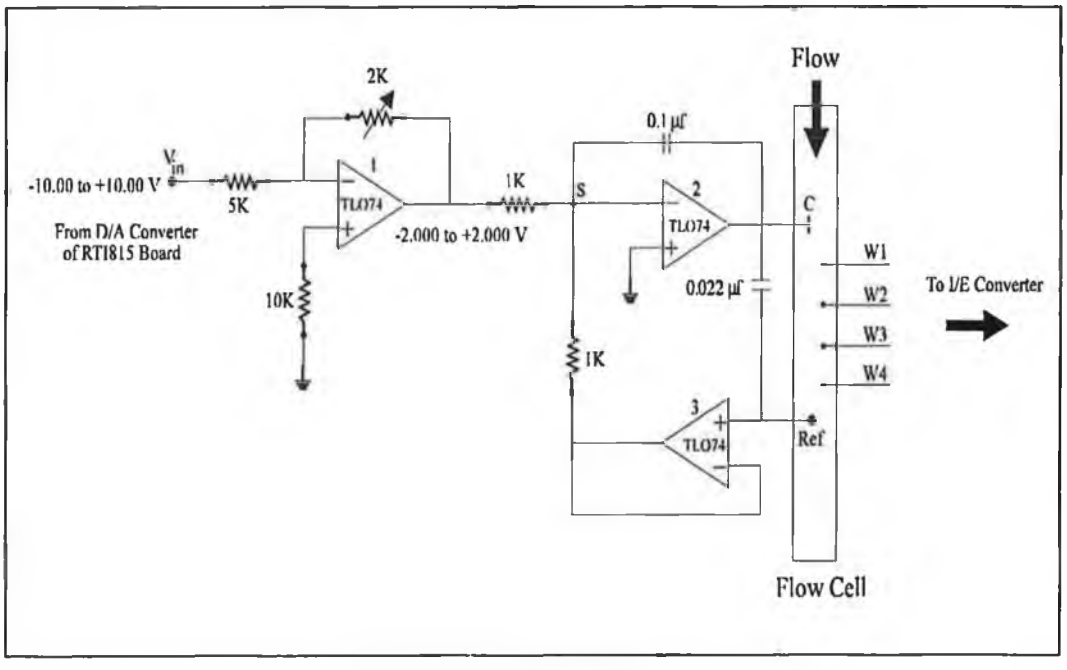

Figure 2.2. Circuit diagram for counter electrode/reference electrode unit.

An input signal in the range ±2.0V (resolution 1 mV) which was controlled by a voltage ratio amplifier (op-amp 1) via the D/A converter of the RTI-815 card was applied to op-amp 2. The default setting was 0.0 V for normal mode operation [40].

Op-amp 3 is a high impedance, unity gain, non-inverting voltage follower. The stable condition for the loop containing op-amps 2 and 3 is when the output from op-amp 3 is equal in magnitude but opposite in polarity to the input voltage of op-amp 2. This means that the voltage at point (s), the summing junction, should always be at zero volts; however, if a change occurs in the junction potential, the output of op-amp 2 will increase to maintain the summing junction at zero volts. The input potential therefore can be accurately maintained between the reference electrode and the working electrode.

2.2.2 Current to Voltage (I/E) Converter Unit

A current to voltage unit consists of a current to voltage converter, 2 sensitivity selectors, an analog filter, a current offset and a differential amplifier. The basic current to voltage converter circuit is a current follower (Figure 2.3). The input is a current, i_{in}, that is obtained from the working electrode. The gain of the circuit is set by the value of the resistor R_f.

$$V_{out} = -i_{in} \times R_f \qquad (2.1)$$

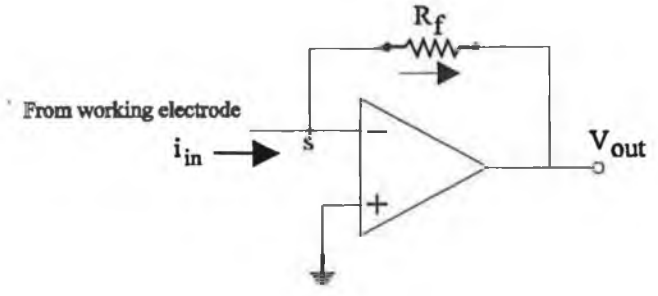

Figure 2.3. Schematic circuit for current to voltage converter

Since the two inputs of an ideal op-amp are always at virtually the same potential, it is intuitive that the non-inverting input (+) is a virtual ground. This feature is important because it allows currents to be converted to equivalent voltages while the current source is maintained at ground potential. This design was utilised when building the potentiostat.

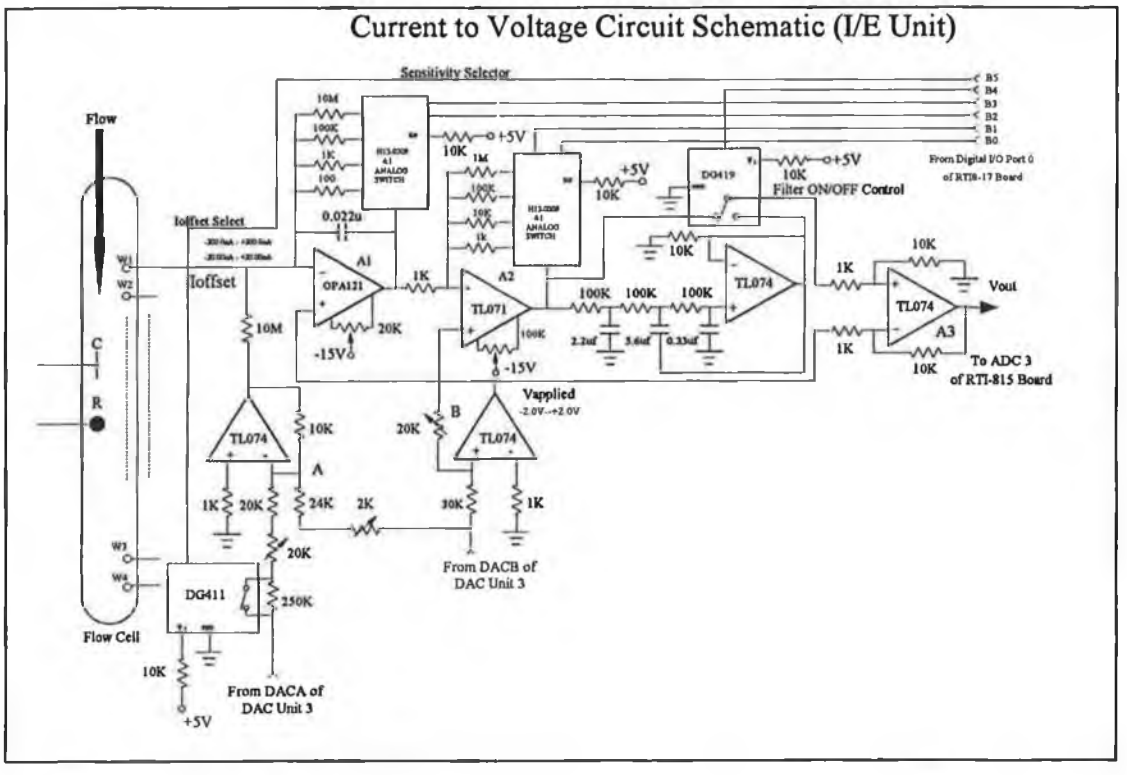

Figure 2.4. Circuit diagram for current to voltage unit

Usually, the maximum close-loop gain of an op-amp is in the range of around 10^8. The signals detected by the multichannel potentiostat discussed in this work are in the current ranges 10^{-11} - 10^{-3} A. If only one op-amp is used, the available gain is not sufficient to meet the necessary amplification requirements; therefore a combination of three op-amps were used to achieve the desired amplification range. The total gain is

therefore:

$$A = A1 \times A2 \times A3 \qquad (2.2)$$

where A1 is the gain of amplifier for current to voltage converter with gain in the range of 10^7 to 10^2, A2 is the gain of voltage ratio amplifier with gain in the range of 10^3 to 10^0 and A3 is the gain of difference amplifier with a gain of 10 (see Figure 2.4) The gain is selected by two analog switches (H13-0509) which are controlled via the computer and the Analog Devices RTI-817 control card, with sensitivities in the range of 1 mA to 10 pA (9 decades).

2.2.3 Current to Voltage Converter Unit Circuit

The current to voltage unit is a major unit of the multichannel potentiostat. It is used to convert a current signal from the working electrode into a voltage signal which is then sent to the computer via the analog to digital conversion interface of the Analog Devices RTI-815 card. The output voltage of the I/E converter unit is ± 5 V full scale. The circuit design utilised is shown in Figure 2.4. Each circuit of the I/E unit contains the following:

1. an I/E converter with a low-noise and low bias current operational amplifier (OPA121) (Burr-Brown) configured as a current follower;
2. a TL071 (Texas Instruments) op-amp functioning as a voltage ratio amplifier;
3. a TL074 (SGS-Thompson Microelectronics) quad op-amp, which was utilised for analog filtering, potential application, current offsetting (V/I converter) and the difference ratio amplifier: the analog low-pass (third-order Bessel) active filter has a cut-off frequency of 1 Hz and can be switched on or off

depending on the signal to noise level;

4. an addressable array of relays which allow current measurements in the 0-1 mA to 0-10 pA range: once selected, however, the chosen sensitivity was identical for each channel;
5. two multi-turn potentiometers which were used in the current follower op-amp (A1) and ratio amplifier (A2) for zero-offset of the output;
6. a calibration circuit with two multi-turn potentiometers into the current offset circuit (A) for accurate setting of the current offset ranges; and
7. a multi-turn potentiometer, which was used in potential circuit (B) for accurate setting of the potential range.

2.2.4 Analog Filtering

A filter is a frequency-selective network that favours certain frequencies of input signals at the discrimination of others. Today, most filters are based on integrated circuitry, particularly the IC op-amp. When op-amps are combined with resistors and capacitors they can accurately simulate the performance of traditional inductance-capacitance filters. Since this new approach usually has gain and needs some supply power, filters built in this way are called *active filters*. While active filters as a concept have been around for quite some time, only recently have reliable, easy-to-use circuits and simple design processes emerged.

The order of a filter governs the strength of its falloff with frequency. The number of energy-storage capacitors in most active filters determines their order. A fifth-order filter usually takes five capacitors, and so on. The higher the order of the filter, the better its performance, the more parts it will take, and the more critical the

restrictions on component and amplifier variations.

For high sensitivity measurements, noise reduction for enhancement of the signal to noise ratio is a vital aspect of the instrumentation function. As the electrochemical signals of interest in our system were low frequency in nature, a third order unity gain analog low-pass filter with a cut-off frequency of 1 Hz was used in the detection circuit for signal to noise ratio enhancement for all measurements. To prevent amplification by the low-pass filter, a third-order low-pass RC active (Bessel) filter of unity gain was used.

2.2.5 D/A Converter and Control Units

A fundamental feature of a multichannel potentiostat is that each working electrode in the array must function independently, with no electronic or chemical cross-talk between the channels. The D/A converter circuit is shown in Figure 2.5.

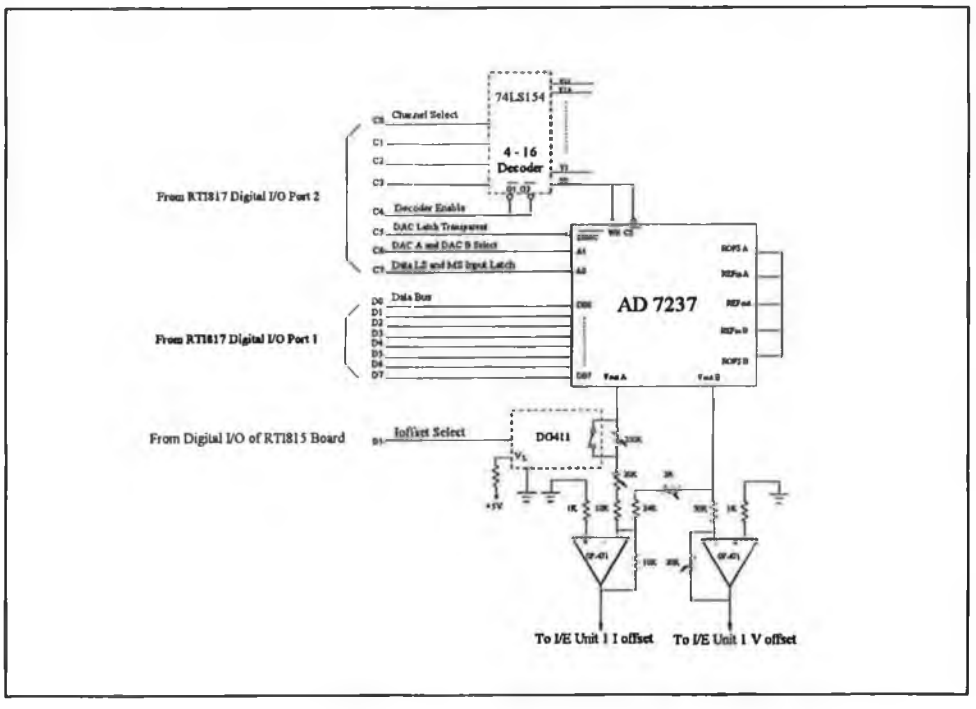

Figure 2.5. Circuit diagram for digital to analog converter unit

In this design, separate digital to analog converters (DAC's) are used to control each working electrode potential and background current offset. Each DAC is a dual channel unit (2 × 12 bits, AD7237). One channel was used to convert digital signals from the computer into an analog polarisation voltage (V_{pol}) versus the reference potential (resolution ca. 1 mV). The other DAC channel was used to control a current offset (I_{offset}).

In order to allow the background current baseline to be set to zero, an independent input current offset facility was used in each channel of the multichannel potentiostat. The background current is produced by a variety of sources such as environmental noise, contributions from the background electrolyte, pump noise and non-zero drift of the detection circuit. The baseline could be corrected automatically or manually set to zero (user defined offset) via the computer. One 12-bit D/A channel converts digital signals from the computer into an analog voltage offset between ± 2.0 V (resolution ≈ 1 mV). This is passed to a V/I converter circuit which transforms the voltage offset signal into a current offset. An analog switch controls and selects the current offsetting facility in the V/I converter circuit. The ranges extend from ± 200.0 nA and ± 20.00 nA, and resolution from ca. 100 pA and 10 pA, respectively. The DAC for each channel was selected via a 4-16 decoder (74LS154)(National Semiconductors). An analog switch (DG411)(Siliconix) was used for selection of the current offset ranges i.e. ± 200.00 nA or ± 20.00 nA.

2.3 RTI Series Data Acquisition/Control Cards

For automated data-acquisition and control, the multichannel potentiostat was

interfaced to a computer. All control lines between the computer and the potentiostat were provided by the Analog Devices RTI-815 and RTI-817 data acquisition\control cards which were located in the I/O bus sockets of the computer motherboard [85, 86].

2.3.1 RTI-815 Board

The RTI-815 is a multifunction analog/digital input/output board that plugs into one of the available long expansion slots of an IBM PC, PC/XT, PC/AT, or equivalent personal computer. The RTI-815 board has capabilities for analog input/output, digital input/output and time-related digital I/O functions.

The RTI-815 interface consists of:

1. 16 digital I/O lines (0 to +5V, TTL compatible);
2. 32 single ended (16 differential) analog input lines, 12-bit resolution, software selectable gain (1, 10, 100, 500), input voltage range (± 5V, ± 10V, 0-10V) jumper selectable, conversion time 25 μs, system through put up to 31.2 kHz;
3. 2 analog out lines (12-bit resolution), ranges 0 to +10V, ± 10 V @ 2 mA.

For effective data validity, measurements from each channel should be as small as possible to reduce the real time differential between the channels which increases with the number of channels. An analog to digital (A/D) conversion time of 25 μs and system throughput of 31.2 kHz is for effective operation of the A/D converter (RTI-815).

Analog input and/or output connections are made to the RTI-815 through the 50-pin

male connector (J2). Digital I/O and counter/timer I/O are connected to the RTI-815 through the 34-pin male connector (J1).

Signals from the four channel potentiostat were acquired via the multiplexed analog inputs of the RTI-815. One analog output was used for counter electrode polarisation, the second could be used for controlling a pump. Digital I/O was used for controlling the sensitivity selection, the potential of the working electrodes, the input current offset, the current offset extent selector and the analog filter. The software-selectable gain of the RTI-card allows for an expansion of the effective sensitivity range (over and above the that offered by the current gain circuitry described earlier) to 100 fA full scale. For synchronisation of data acquisition, potential scan-rate control, and working electrode cycles, the programmable interval counter and timer chip of the computer was used.

2.3.2 RTI-817 Board

The RTI-817 is a 24-channel, TTL compatible (0 to +5V) digital I/O board that plugs into one of the available expansion slots in a PC. The RTI-817 interface provides three 8-channel ports, ports 0, 1 and 2, for digital I/O operations. The channels/ports can be accessed through the J1 connector on the board. Depending on the application, it is possible to address a single channel (bit) of a digital I/O port or all eight channels (byte) of the I/O port. Digital control signals can be sent out indicating the status of a control line or switch or, if the channels are configured as digital input channels, return a digital input value.

2.4 Software

2.4.1 Introduction

Multichannel electrochemical detection is difficult to perform without computerised instrumentation. Therefore, both the control and data acquisition were fully computerised. The software support for both the data-acquisition and hardware control functions was developed "in-house". The software used to control this system was written in QuickBASIC 4.5 (QBasic) with the initial system consisting of a set of system menus which were displayed on the screen. These menus allowed the user to set instrumental working parameters and perform functions such as running the system and plotting the data acquired. The problem with this system was that it was very cryptic and alienating for people who were not familiar with the operation of the system.

In an effort to overcome this problem it was decided to write software with a "Windows" style graphical interface. The new user-computer interface was written using an Assembly Language Toolbox which consisted of a collection of routines in a Quick Library and a stand alone library which could be used in the QBasic environment.

2.4.2 RTI Series Software Drivers

The RTI-800 Series Software package provides a convenient and powerful software interface between the RTI-815 and RTI-817 I/O boards and a computer [87]. The RTI-800 Series software package consists of high-level language libraries, such as the hardware libraries. Each language library consists of a language binding and the

necessary system routines. Bindings handle parameters passing between the detection system program and the hardware libraries. The hardware libraries are board specific (RTI815.LIB, RTI817.LIB) and contain the low-level subroutines that directly perform the I/O functions supported by the RTI-800 Series boards. System routines are hardware independent and include initialisation, program execution delays and logical channel definition clearing.

I/O and system routines are used to access the functions of the RTI-815 and RTI-817 boards. I/O routines are provided for analog I/O, digital I/O, frequency input, event counting and pulse output when these functions are supported by the board.

Each I/O routine has a set-up routine associated with it; system routines do not. A set-up routine defines a record in software, called a *logical channel,* which contains all the information necessary to perform the specified I/O function on a particular RTI board. Once the logical channel is defined, few parameters need to be specified for the I/O function itself. When operations use sequences of physical channels (such as AING), the set-up routine also stores this information in a "channel sequence list" in memory.

The set-up routine must be called before its associated I/O routine or an error will be reported. Up to 256 logical channels can be defined at one time. Once a logical channel is defined, it cannot be redefined unless it is first cleared using the system routine CLCHAN. If appropriate, CLCHAN also removes entries from the channel sequence list. These tasks are also accomplished when the system is initialised.

2.4.3 Data Acquisition and I/O Control Routines

The purpose of an interface is to convert the analog voltage output of an instrument or

sensor to a binary form that can be handled by the digital computer. ADC's are characterised by their resolution, dynamic range and maximum throughput. The resolution of an DAC is defined as the smallest change in an analog signal that can be observed at the digital output. Resolution (R) is determined by the number of bits in the digital signal: 12 bits, 1 part in 4096.

$$R = V_{REF} / 2^n - 1 \qquad (2.3)$$

where n = number of bits.

Thus for an A/D converter with maximum range from -5 V to +5 V DC and 12 bits of output, the smallest change that can be detected in the digital output is

$$10V / (2^{12} - 1) = 2.442 \times 10^{-3} \text{ V}$$

Sampling rates are an important consideration with ADC's. The sampling rate is determined by the experimental requirements and whether the ADC and the computer can accept this rate. The sampling rate can depend both on how much information is required from the analog signal and on what kind of signal processing is planned for the collected data. For theoretical reasons it is necessary to sample a signal with a rate twice as high as the highest frequency component of the signal (Nyquist's Theorem) [1].

The most important characteristics of ADC's are the speed and accuracy of conversion. These parameters are determined by the particular method used to convert the data which can be achieved by a number of methods. Successive approximation is used in the analog to digital converter of RTI-815 card. It has a fixed conversion time that is the same for any value of analog input.

2.4.4 Assembly Language Toolbox Operation

The assembly language toolbox was designed to resemble standard QBasic *Sub Programs* and *Function* procedures. Routines which are required for the program are declared at the beginning of the program. A full set of these routines are provided with the toolbox from which the user can select the ones required for a particular application. Among these routines were ones which could produce vertical and horizontal menus on the screen from which the user could make selections using the mouse or the HotKey facility. HotKey facilities are characters, normally a letter or a number when pressed automatically executes that selection without the user having to press the return key afterwards. These HotKeys are easily recognisable in the menu as they appear highlighted. In the case of selections made using the mouse, this merely involves clicking on the selected choice to execute that particular selection.

2.4.5 Software Design

The menu driven package includes routines which configure the system to the system set-up required by the user, perform data analysis, archive data to and retrieve data from the hard disk, display data in either three dimensional (current vs. time vs. applied potential), or two dimensional formats (current vs. applied potential); or obtain a printout. Both the two and three dimensional display facilities were available in real time during data acquisition. Included in the main menu is a HELP option which allows the user to access help files on system functions and settings.

The program for data-acquisition and system control consists of a series of subprograms which are task specific. These include the system initialisation program, the system main menu program and the display program. A detailed structural layout

for the multichannel potentiostat detection system software is shown in Figure 2.6.

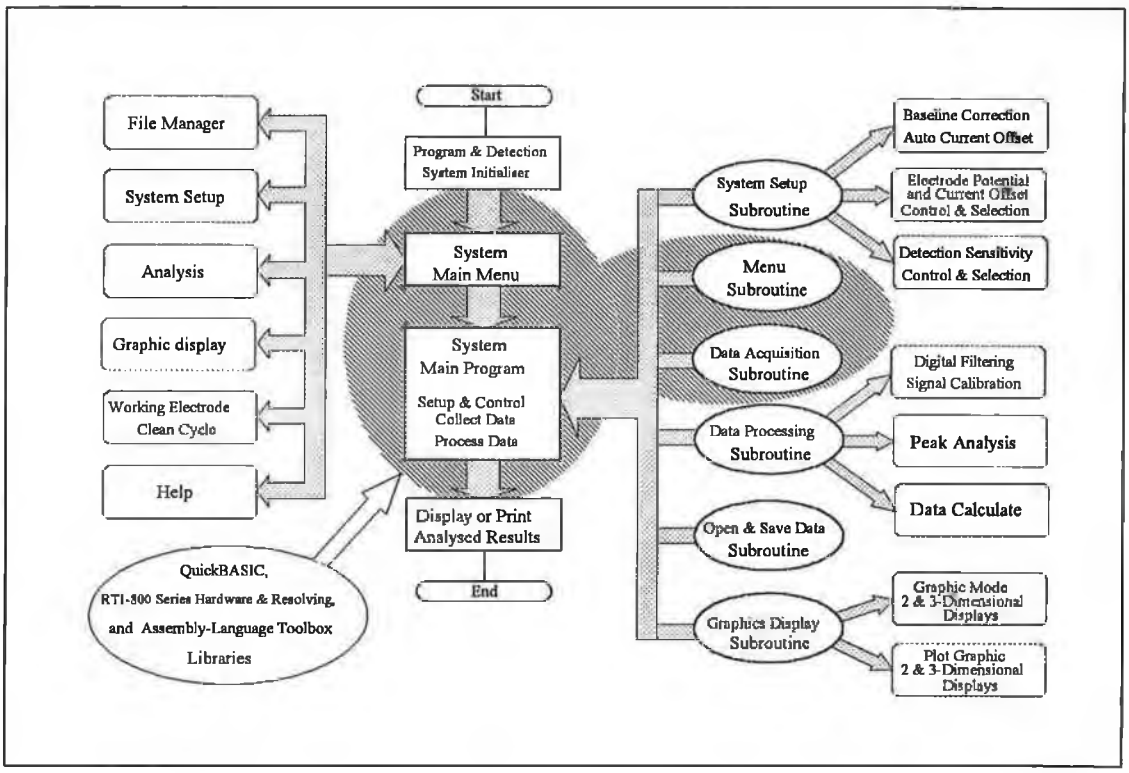

Figure 2.6. Structural layout for multichannel potentiostat detection system software

2.4.5.1 Detection System Program Menu

The main menu of the control program is shown in Figure 2.7. The graphical user interface (GUI) was a windows style environment with a main menu bar which contained a series of sub-menu's. The main menu was presented in a horizontal format using a routine from the Assembly-Language Toolbox called BarMenu, while the vertical menus were presented in a vertical format using routines from the Toolbox known as VerMenus. The menu driven package included routines which are responsible for system settings, data handling and data display. An effort was made to provide flexible, easy to use software. To activate the menu bar, one could use the Mouse or the HotKey to select the desired option.

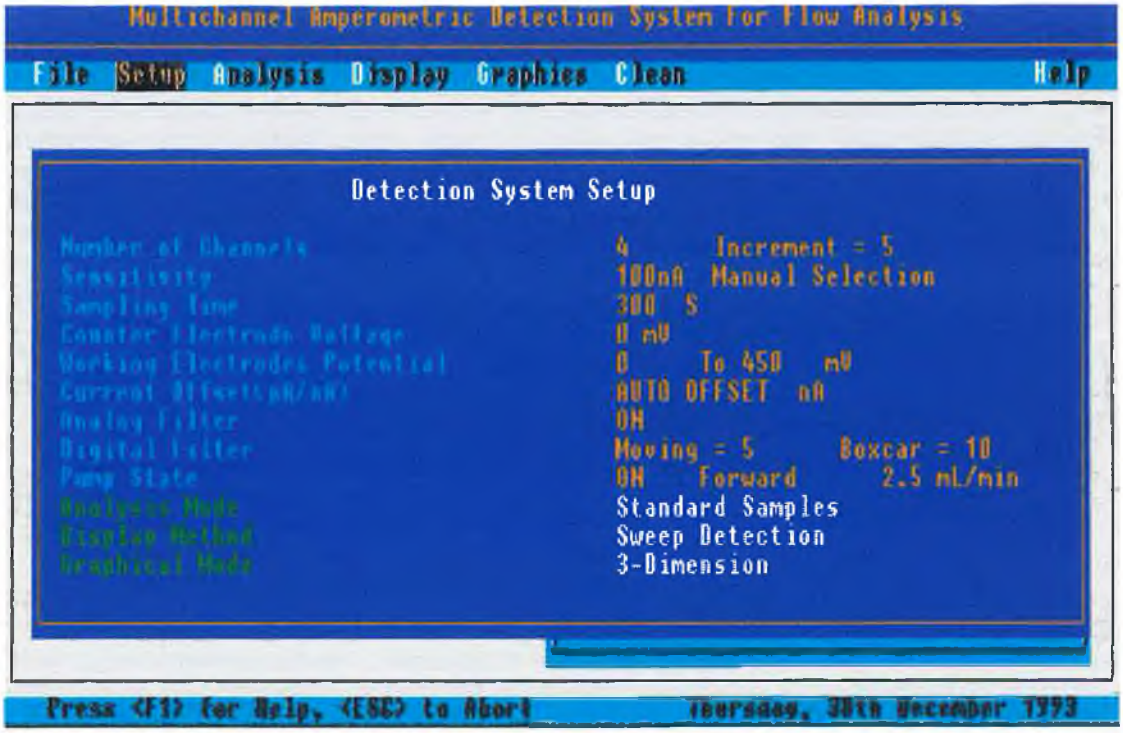

Figure 2.7. The main menu with a Windows style graphical interface.

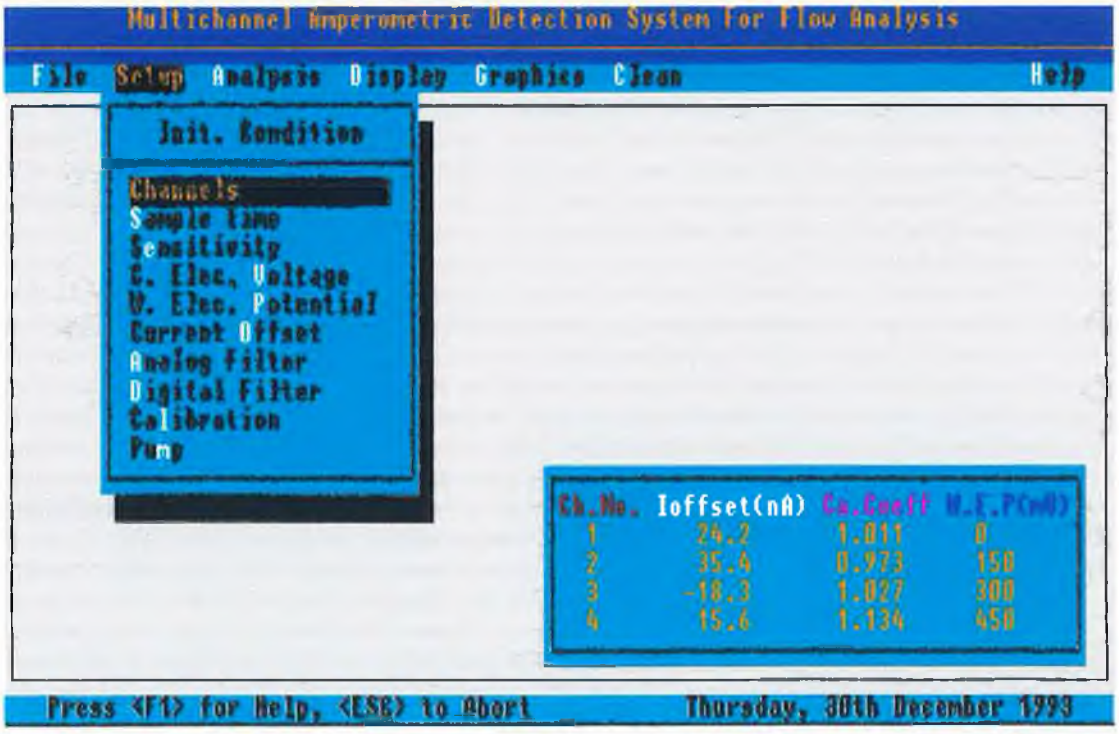

Figure 2.8. The Set-up submenu.

2.4.5.2 Detection System Submenu

The multichannel detection system submenu consists of seven menu bars which control the major system parameters, the system mode and the on-line help facility. The **Set-up** submenu of the multichannel amperometric detection system as it would appear on-screen is shown in Figure 2.8. From the set-up menu the main instrument/parameters are set via the keyboard and mouse. These settings can easily be changed after an analysis run if required.

2.4.6 Graphical Display

The graphical representation includes two-dimensional plots of the currents from 2 or more selected channel vs. potential (2-d voltammogram) and vs. time (3-d voltammogram).

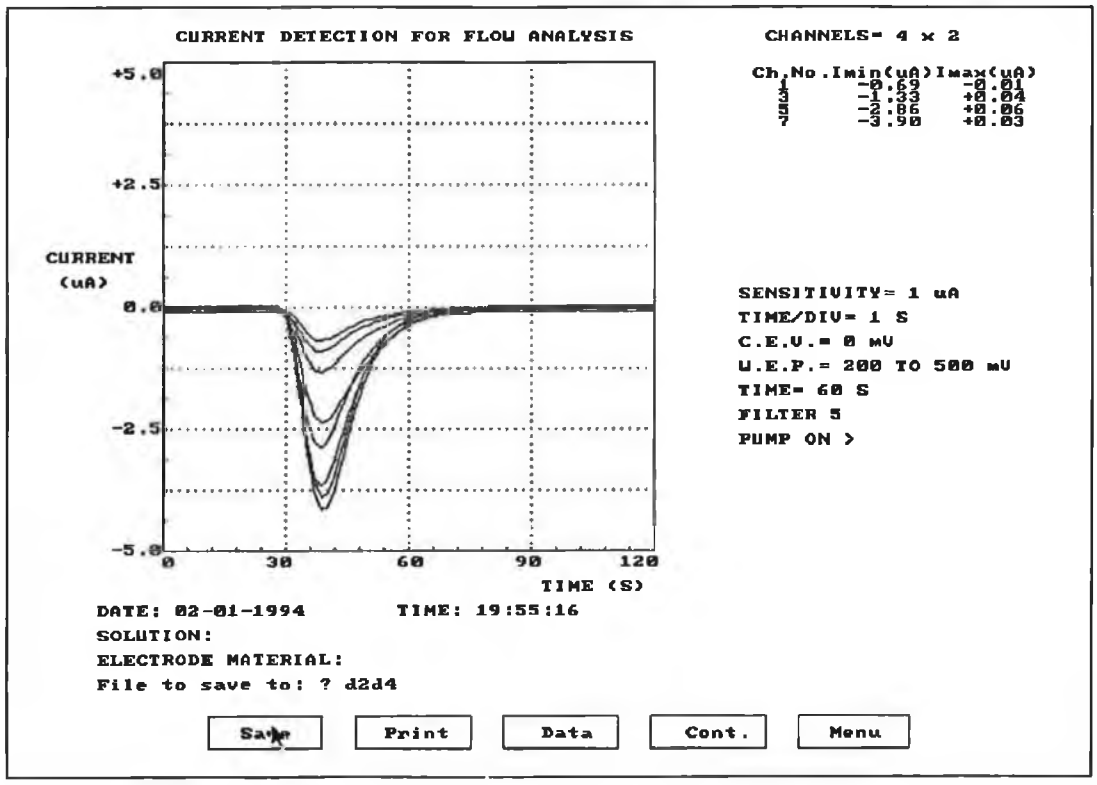

Figure 2.9. On-line display of an injection of uric acid (2×10^{-3} M) in 0.05 M phosphate buffer pH 7.4. using the linear array configuration.

2.4.6.1 Two-dimensional Graphical Display

An example of a 2-D display is presented in Figure 2.9. The 4 electrodes were polarised between + 200 mV and + 500 mV with a current sensitivity setting of 1 μA. A single 42.9 mV step was applied to each electrode to generate an 8 electrode response (4 real, 4 virtual channels). Each channel is represented by a different colour on the display to distinguish clearly between them.

2.4.6.2 Three-dimensional Graphical Display

Figure 2.10 shows the on-line display of a 3-dimensional hydrodynamic voltammogram of hydroquinone (0.1 M) in 0.05 M phosphate buffer pH 7.4. Five sequential voltage steps of 15.8 mV were applied to the working electrode array which were polarised in the range -200 to +100 mV to generate a 20 working electrode (4 real, 16 virtual) response.

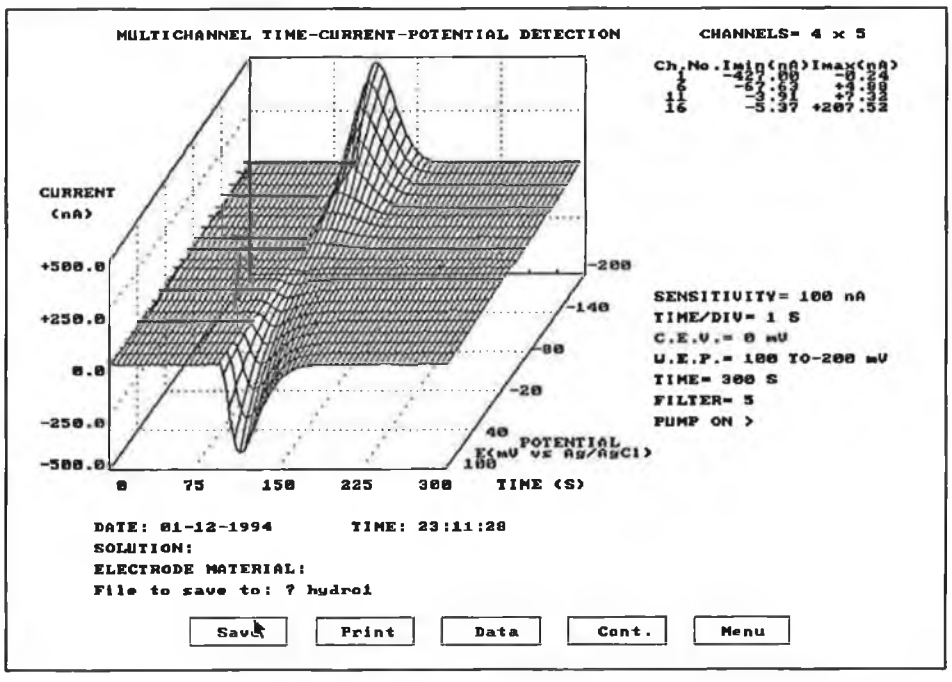

Figure 2.10. On-line display of a 3-dimensional hydrodynamic voltammogram of hydroquinone (0.1 M) in 0.05 M phosphate buffer pH 7.4., obtained using the linear array configuration. Flow rate 0.5 ml/min.

2.4.7 Data Storage

Data is stored in a spreadsheet compatible format (ASCII with "," column delimiter) to facilitate post-run processing with standard applications packages such as Microsoft Excel. The DOS filenames could have up to eight characters plus an optional three-letter extension. The default extension was ".dat".

To save a file:

- From the File menu of the detection system program, the user selects the SAVE command, then the SAVE dialogue box appears;
- In the FILE name box, the user types the required file name. If the user wants to save the file on a different drive or directory, the path must be included as part of the filename.

2.5 Potential Step Sequences

To further improve the voltage resolution of the 3-D voltammogram, a series of potentials steps (up to 5) could be applied to the working electrodes, thus generating a 20-channel response. A 100 ms delay time was utilised before the current was sampled to reduce charging current effects. All potential step sequences were software controlled. The software facilitated the selection of 1-5 potential steps at each working electrode.

2.6 Data Processing

The main objective of data processing is to maximise the information content of an experimental signal. The data processing and representation program were designed to provide digital filtering, baseline correction and calibration of the electrode responses.

A number of digital filters were used and evaluated in terms of their noise reduction capabilities and their effect on signal attenuation. The filters investigated included boxcar averaging and moving point averaging.

2.6.1 Baseline Correction

Due to background noise levels that are produced by inherent cell currents, and non-zero drift by components of the detection circuit, the resultant baseline is non-zero in nature and subsequently produces deviations in the background signal. If the deviation of the baseline is substantial it results in both detection and display overloads. In order to solve this problem an input current offset facility has been incorporated into each channel. Before the signal is passed to the measurement circuit, the baseline of each channel is corrected by the instrumentation control program. The deviation value of the baseline and the required current offset are computed and the desired current offset for each channel is automatically applied via the DAC unit for that channel.

2.6.2 Digital Filtering

The increasing use of computerised instruments has correspondingly increased the importance of software techniques for data acquisition and signal to noise enhancement. Operations such as filtering, linearisation and attenuation, formerly accomplished by hardware devices, are now achieved by software resident in the microcomputer component of the instrument. Software operations offer the advantages of flexibility and diversity. For example, a variety of software filters can be implemented by changing computer algorithms, whereas considerable effort may be required to change hardware filters. Nevertheless, in situations where the computer

cannot execute the required function at a satisfactory rate, implementation with hardware components is necessary.

The minimum hardware units required for software signal-processing functions consists of analog signal conditioning circuits, an analog-to-digital converter and a microcomputer. The rates of sampling the analog data and of the analog-to-digital conversions must be fast enough to provide an adequate frequency range to cover the analog signal and thus ensure minimum loss of information. Although the conversion frequency increases with the sampling rate, the upper frequency limit is determined by the speed of the computer and the memory available for data storage.

Once the data is in digital form, a variety of software enhancement techniques may be used to increase the signal-to-noise ratio. Although these software techniques are readily available and widely used, caution should be exercised in their applications to prevent problems such as undersampling and oversmoothing.

Noise is a central problem in data acquisition and is often difficult to handle. Any electronic system contains (and produces) many types of noise. There are a number of software techniques for the enhancement of the signal to noise ratio. Three of the most commonly used software signal enhancement techniques are boxcar averaging, ensemble averaging and weighted digital filtering.

A number of digital filters were used for noise reduction both on-line and off-line. Boxcar averaging, moving point averaging and a combination of both with variable window sizes were available in real time.

2.6.3 Signal Normalisation

One of the problems arising with these arrays was that all the electrodes gave a slightly different responses under identical conditions; hence it was required to normalise every electrode before starting an analysis run.

Normalisation of the electrode response involved multiplying the response of each channel by a weighting factor to compensate for inherent differences in the working electrode. The software was designed to normalise the array with respect to the array average. Each data point was then multiplied by this factor before it is displayed on screen.

The normalisation software routine was based on the following equation:

$$F(n) = 1 + \frac{R_{AV} - R_{E(n)}}{R_{E(n)}} \qquad (2.4)$$

where $W_{F(n)}$ = weighting factor for each channel, $R_{(av)}$ = averaged array response and $R_{E(n)}$ = individual electrode response.

2.7 Flow Cell Design and Fabrication

2.7.1 Introduction

For optimal amperometric detection, several flow cell parameters are important, such as the cell resistance and capacitance. These are critical to good potential control at any particular electrode and the degree of cross-talk between the working electrodes is important at low analyte concentrations. The signals due to cross talk can be the same order of magnitude as the analytical signal when working at low concentrations. Cross

talk is described as the non-faradaic current occurring at a downstream electrode due to a large current at the upstream electrode. Cross talk can arise in two ways but both are directly related to cell resistance. Cross talk can arise from the iR drop at one electrode affecting the interfacial potential at the other electrode because of the manner in the multichannel potentiostat must implemented. In addition, because of the high resistance of the thin layer cell, a current path from the upstream working electrode to the downstream working electrode can compete with the current path to the counter electrode [88].

When designing and using electrochemical detectors, three principal problems must be solved.

1. The working electrode material must function in a suitable potential range with any residual current and noise being low and constant. The kinetic parameters of the analyte electrode reaction should be favourable and free of interferences from adsorption effects.
2. The measuring cell must be constructed with hydrodynamic conditions permitting sensitive and reproducible measurements.
3. A suitable measuring technique must be chosen from the point of view of sensitivity of measurement, accuracy, reproducibility, selectivity and ease of signal handling.

The design and evaluation of the flow cell utilising an array of independently controlled electrodes in conjunction with amperometry, has been investigated for applications with FIA. Two basic flow cell configurations used in this work were:

- A linear flow cell
- A radial flow cell

2.7.2 Design and Fabrication of Linear Flow Cell

A schematic of the linear flow cell is shown in Figure 2.11. It consists of four main components:

- the cell base (containing the planar electrode array);
- the stainless-steel cell body (counter electrode);
- a thin flow directing spacer (0.18 mm thickness);
- the reference electrode holder.

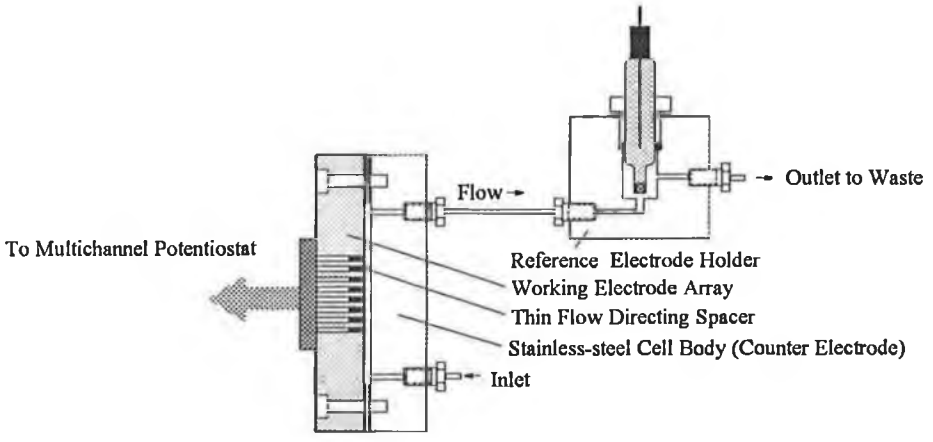

Figure 2.11. Schematic diagram for an assembled linear flow cell.

2.7.2.1 Linear Multi-electrode array

The working electrode array was constructed from glassy carbon rods 5 mm in length (ϕ 1 mm) which were sealed into 1 mm diameter holes in a perspex holder of the required dimensions. The glassy carbon electrodes were sealed in position with silver loaded epoxy (RS). A water-tight seal was effected with polyacrylate glue. An 8 pin chip holder with the legs positioned in the correct spatial arrangement was embedded

in the epoxy to act as a connector for signal wires. The joints were checked with a multimeter to ensure that electrical contact had been established. The analog input lines from the I/E units of the detection system were connected to the chip holder for electrode polarisation and signal measurement. The linear flow cell was used specifically for experiments where redox cycling was required. This technique could be used to generate 3-d voltammograms where both the oxidation and reduction currents were measured.

2.7.2.2 Flow Cell body (Counter electrode)

The main body of each flow cell was fabricated from stainless steel. For the linear flow cell (Figure 2.12), inlet and outlet holes (ϕ 1 mm) were drilled into the stainless steel block with a spatial distance between them slightly larger than the maximum separation of the array. The inlet and outlet holes were drilled 4.5 mm and tapped with an M5 tap which was compatible with standard LC fittings. All surfaces were ground with a horizontal grinder to obtain a high precision finish. Finally, the stainless-steel body was polished with silicon carbide paper (1200 grade) to a final mirror finish. The flow cell surface was checked to ensure planar continuity without which laminar flow conditions may be disrupted.

2.7.2.3 Flow Directing Spacer

A spacer of thickness 0.18 mm shaped from an acetate sheet was placed between the array and the stainless steel body. The flow cell assembly was held together with 4 hexagonal stainless steel screws ensuring correct positioning of the spacer. The stainless steel body of the flow cell acted as the counter electrode and was electrically

isolated from the working electrode array by the spacer.

2.7.3 Reference Electrode Holder

The outlet from the cell was connected to the reference (Ag/AgCl) holder via stainless steel tubing from which the sample stream flowed to waste. A commercial Ag/AgCl reference electrode supplied by EG&G (Princeton Applied Research) was utilised for all experimental procedures. A holder for the electrode was constructed using a flow controller valve. The assembly was connected downstream to the flow cell. One inlet was utilised with the linear flow while two were used with the radial flow cell. The outlet of the assembly was connected to the waste collection vessel with Teflon tubing.

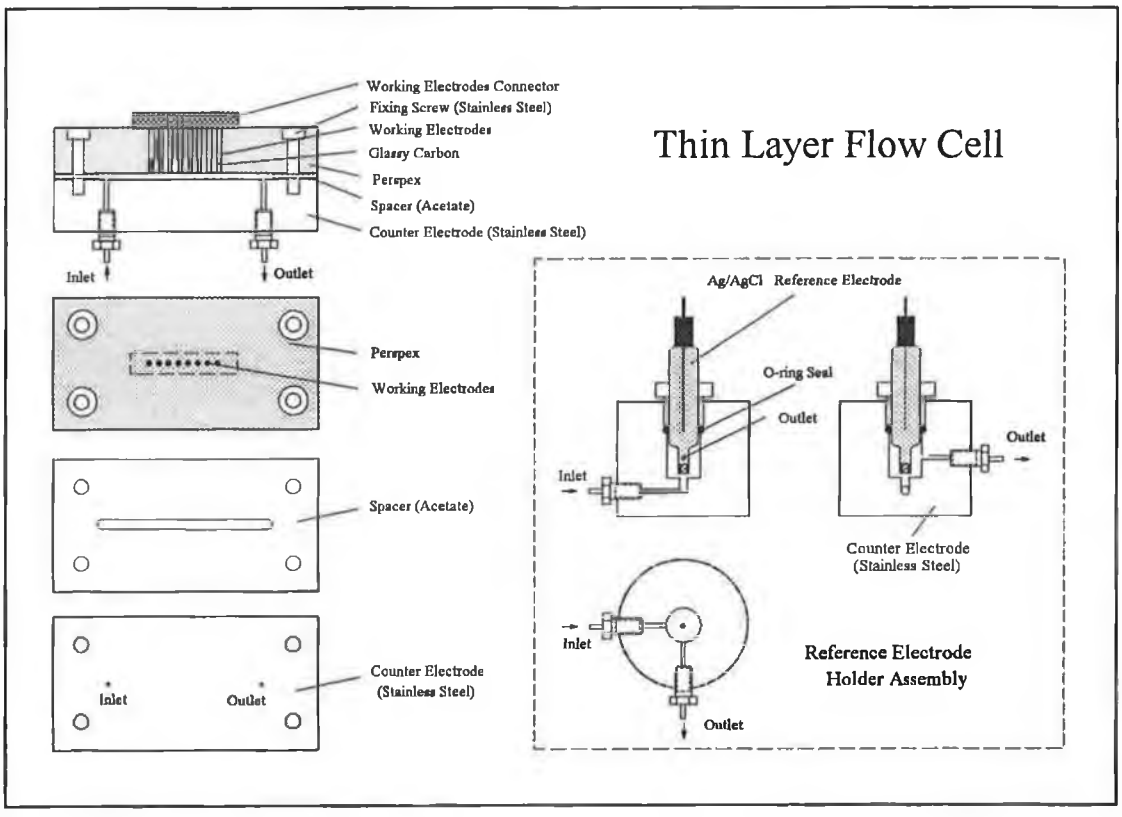

Figure 2.12. Expanded linear flow cell schematic.

2.7.4 Design and Fabrication of Radial Flow Cell

Design details of the radial flow cell are shown Figure 2.13.

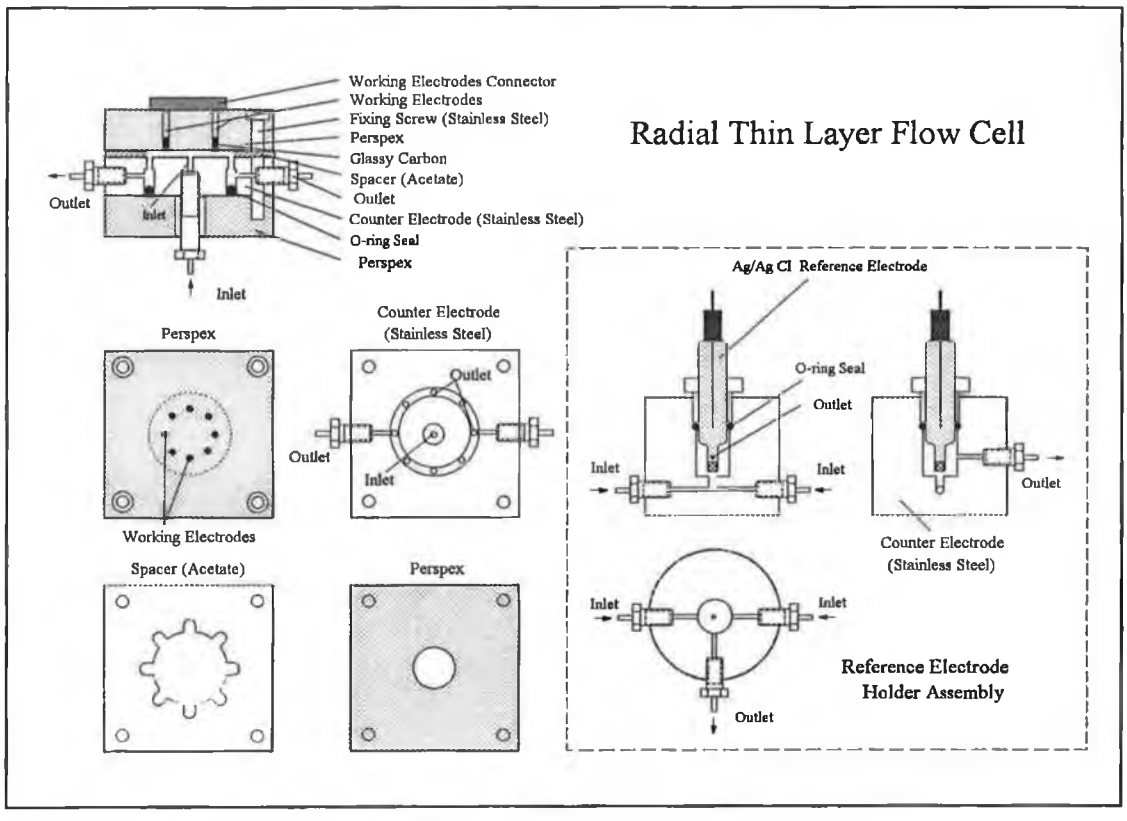

Figure 2.13. Expanded radial flow cell configuration.

2.7.4.1 Production and Assembly

The same method of fabrication as described for the linear flow cell was utilised in the construction of the radial flow cell. The electrodes were placed in a circular configuration of diameter 9 mm. A central inlet of diameter 1 mm was drilled in the stainless steel body. On the reverse side, a trench of outside diameter 17 mm, inside diameter 13 mm and depth 4 mm was machined. Two holes of diameter 1 mm were drilled horizontally into the trench to which the outlets were connected. They in turn

were connected to the reference holder assembly. Outlet holes (total 16) were drilled in a circular fashion into the trench; this allowed provision for a 16 working electrode array where each electrode would have its own outlet. This approach was adopted in an effort to ensure that reproducible laminar flow conditions were achieved at each working electrode. An O-ring seal was pressed into the trench creating a water tight seal and a cavity for fluid collection of suitable dimensions. The assembly was held together as previously described. The cells were placed in a Faraday cage to reduce the effect of noise pick-up from environmental sources. Both the radial and linear arrays consisted of 8 working electrodes, however only 4 electrodes could be used at any given time.

2.7.5 Flow Cell Characterisation

Plots of $\log_{10}$ peak area versus $\log_{10}$ flow rate were used to characterise the flow conditions [40]. According to Fielden and McCreedy peak area can be used instead of charge when characterising flow conditions. An average slope of -0.69 was obtained for the working electrodes of the radial array. This value indicates that thin layer conditions are present in the flow cells in accordance with the classification described by Elbicki [29].

2.8 Experimental

2.8.1 Chemicals

All chemicals used were of analytical grade. Deionised water for the preparation of aqueous solutions was obtained by passing distilled water through a Milli-Q water purification system (Millipore). Ascorbic acid, nitric acid, acetaminophen, D-glucose and potassium dihydrogen orthophosphate were obtained from BDH Chemicals. Potassium hexacyanoferrate(III) was obtained from May and Baker Ltd and dipotassium hydrogen phosphate and potassium chloride from Riedel-de-Haen. Hydroquinone, glutaraldehyde and uric acid were purchased from the Aldrich Chemical Co. Copper(II) nitrate, iron(III) nitrate and copper(II) sulphate pentahydrate were received from Merck. Lead(II) nitrate samples were prepared from a spectroscopic standard supplied by May & Baker. Glucose oxidase (from Aspergillus niger) and albumin (bovine) were purchased from Sigma. All electroactive solutions were freshly prepared each day and degassed for 10 minutes with nitrogen prior to use.

2.8.2 Flow-Injection Analysis System

The FIA system was composed of an ACS Model 351 isocratic pulse-free pump, an injector port with 20µl, 50µl and 100µl fixed sample loops (Rheodyne 7125), PTFE tubing (200 mm x 0.25 mm id) and stainless tubing (0.009" id). The carrier stream was either 0.05 M phosphate buffer, pH 7.4 or 0.1 M KCl. Flow rates in the range 0.2-1.0 ml min^{-1} were used for the flow injection studies.

For biosensor/interference studies the FIA system consisted of the same components listed above, however, the cell used was a commercial dual working electrode thin layer cell (BAS CC-5). The cell assembly was housed in a Faraday cage for noise

reduction purposes. A 0.1 mm Teflon spacer was used throughout. The BAS flow cell contained two glassy carbon working electrodes (diameter 3 mm) embedded in a PEEK plastic block. The carrier stream composed of 0.05 M phosphate buffer, pH 7.4, with hexacyanoferrate(III) at a concentration of 1 mM, was used as the carrier stream. Flow rates in the range 0.3-0.5 ml min^{-1} were used throughout.

2.8.3 Working Electrode Preparation

Newly constructed glassy carbon arrays were initially prepared by polishing with 1200 grade silicon carbide paper. The array was then polished with 6 μm alumina (Metrohm), followed by diamond paste (1 μm) (Kemet) on polishing pads for 3 minutes respectively, before being sonicated in deionised water for 3 minutes to remove any particulate matter. The array was then assembled in the flow cell, and software controlled electrochemical pre-treatment potentials applied. The conditioning program consisted of scanning the potential between ± 1.0 V (vs. Ag/AgCl) for 3 minute periods. The array was electrochemically cleaned as required during normal operation. The array was only polished when a significant reduction in sensitivity was observed.

2.9 Results and Discussion

2.9.1 Linearity

The linearity of the amperometric array was evaluated by injection of standard solutions of potassium hexacyanoferrate(III) in the concentration range 10^{-1}-10^{-7} M (see Figure 2.14). The injections were repeated 5 times at each concentration.

Samples were injected using both flow cell designs. A plot of $\log_{10}$ concentration versus $\log_{10}$ peak height normalised using eqn 2.4 for the radial flow cell yielded a plot with a slope of 0.998 and a correlation coefficient of 0.992. A slope of 0.997 and a correlation coefficient of 0.9985 were obtained for the linear flow cell. The limit of detection was calculated to be 2×10^{-7} M (4 pmoles injected)(S/N=3).

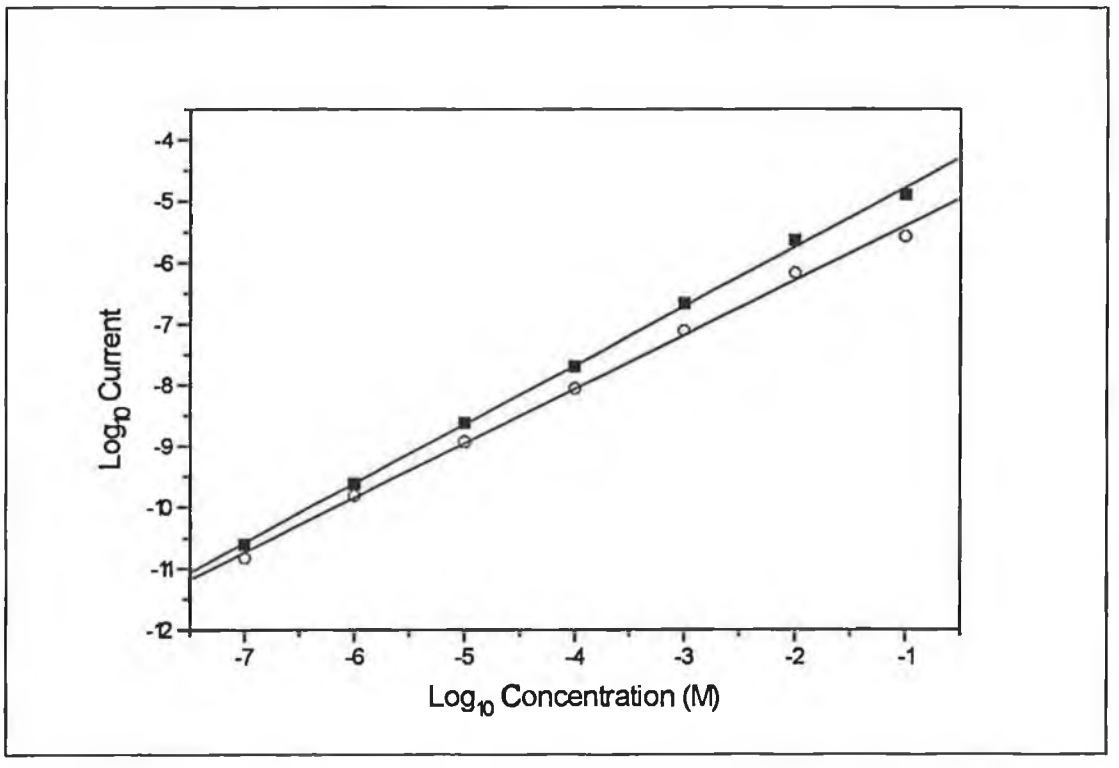

Figure 2.15 Plot of $\log_{10}$ concentration vs. $\log_{10}$ current for both the linear (O) and radial (■) flow cells. Flow rate 0.4 ml/min, carrier stream 0.05 M phosphate buffer (pH 7.4), working electrode potential 0.0 mV vs. Ag/AgCl.

2.9.2 Filters

The effect of analog and digital filtering on the signal were then investigated to evaluate their respective merits and performances. Boxcar averaging and moving point

averaging digital filters were utilised in conjunction with an analog third-order active low-pass Bessel filter which was used on-line. The results obtained are summarised in Table 2.1.

Filter type (no analog filter)	**Relative Standard Deviation (b)**	**Theoretical Prediction (a)**	**Filter type (analog filter)**	**Relative Standard Deviation (b)**	**Theoretical Prediction (a)**
no digital filters	15.6	-	no digital filters	6.4	-
Boxcar Averaging	5.9	4.8	Boxcar Averaging	4.5	2.0
Moving Point Averaging	7.3	7.0	Moving Point Averaging	5.7	2.9
Boxcar Av. & Moving Point Av.	5.4	2.2	Boxcar Av. & Moving Point Av.	2.9	0.9

Table 2.1 The effects of analog and digital filtering on the responses of the radial flow cell, to injections of 4×10^{-6} M potassium hexacyanoferrate(III). The theoretically predicated values are presented also. Flow rate 0.4 ml/min, carrier stream 0.05 M phosphate buffer, pH 7.4.

where, (a) Theoretical Prediction: $\sqrt{n}\left(S/n\right)_0$

$\sqrt{n_1}\sqrt{n_2}\left(n/S\right)_0$

(b) Relative Standard Deviation: $\frac{\overline{SD}}{\overline{X}} \times 100\%$

The most satisfactory results were obtained with a combination of both analog and digital filtering (2.9% RSD). The major problem associated with digital filtering on-line is that of signal attenuation. The effects of the various digital filters are presented in Table 2.2. A combination of boxcar averaging and moving point averaging results in a signal attenuation of 24.4% but conversely results in a 55% reduction in the noise. The improvements in the S/N ratio are not as large as predicted theoretically and therefore would indicate that the noise in the system has a large random characteristic which is difficult to filter out completely. The value of good hardware filtering is also demonstrated. Activation of the hardware filter results in a 59% reduction in the noise level observed in the response signal.

Digital Filter Type	**% Attenuation (Array Average)**
Boxcar Averaging [10]	5.1
Moving Point Averaging [5]	8.1
Boxcar[10] + Moving Point Averaging. [5]	22.4

[ ] number of data points in each window

Table 2.2 The array responses to injections of 4×10^{-6} M potassium hexacyanoferrate(III) without the application of filters were obtained. The effect of two digital filters and their additive effect on signal attenuation were then calculated with respect to the unfiltered responses. The average response of the radial array attenuation are presented.

2.9.3 Array Normalisation Procedure Evaluation

Both the radial and linear arrays were statistically investigated to evaluate both the necessity and effect of an on-line array normalisation procedure. Differences in the responses from the electrodes comprising the array to a single injection of hexacyanoferrate(III) were defined as the inter-electrode %RSD, while the differences at an individual electrode to multiple injections of hexacyanoferrate(III) were defined as the inter-injection %RSD. Standard solutions of potassium hexacyanoferrate in the concentration range 10^{-7}-10^{-1}M were injected 4 times and the resulting data was statistically analysed. Both the inter-electrode and inter-injection %RSD's were compared for array responses with and without normalisation as described in equation 2.4. Sample data analysis tables are shown in Table 2.3 and Table 2.4. This standard format was adopted for all statistical analysis, thus allowing clear comparison between the data sets. The results for the unnormalised radial flow cell data are presented in Figure 2.15. The results indicate that:

- the %RSD between the electrodes in the array is relatively independent of concentration;
- the %RSD between the electrodes is at least 3-4 times that of the RSD for a single electrode subjected to multiple injections (17.7% versus 2.8%)(see Figure 2.15);
- the average %RSD for a single electrode subjected to multiple injections (n=4) shows a clear decrease with concentration from approximately 7% to 2% in contrast to the inter-electrode %RSD which remains constant over the concentration range investigated (10^{-7} M to 10^{-1} M $[Fe(CN)_6]^{3-}$).

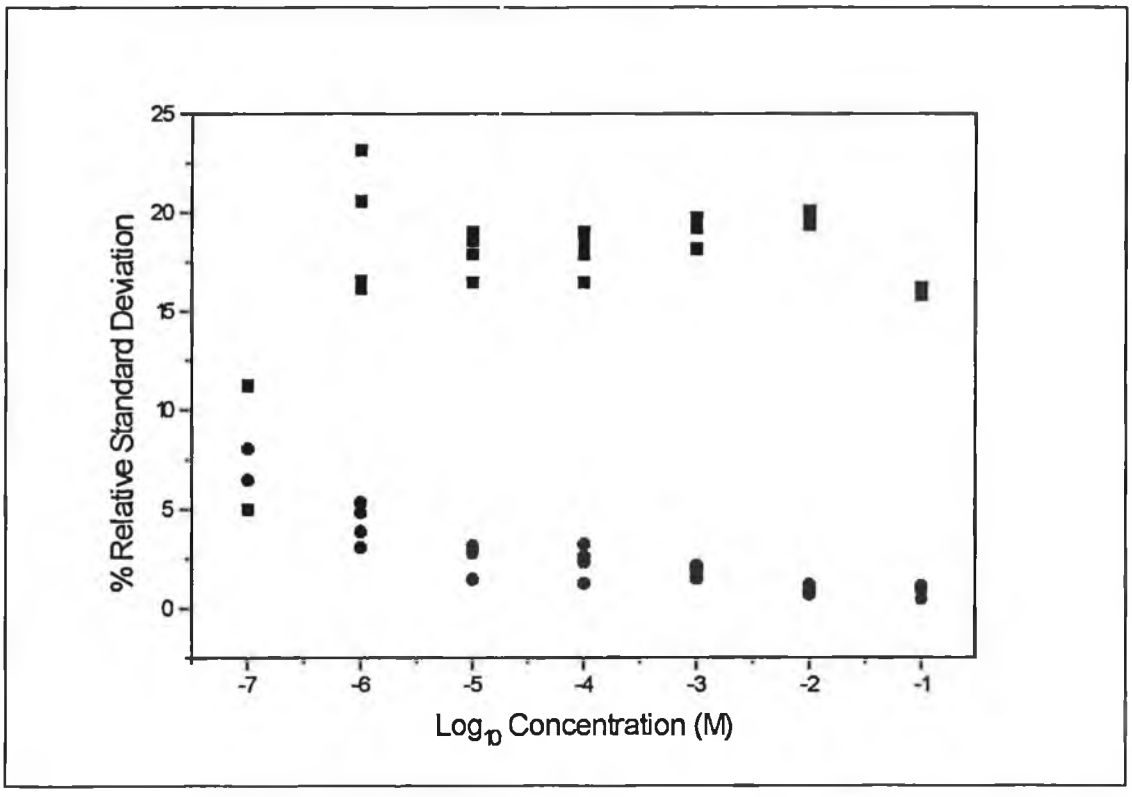

Figure 2.15 Plot of relative standard deviation between the electrodes (■) and at the individual electrodes (•) vs. $\log_{10}$ molar concentration for 4 repetitive injections of potassium hexacyanoferrate(III). The radial electrode responses are presented here without normalisation.

	NO NORMALISATION		RADIAL FLOW CELL				
CONCENTRATION 1E-7 M			CURRENTx 1E-12A				
INJECTION NO.	**1**	**2**	**3**	**4**	**MEAN**	**STDEV**	**%RSD**
1	17.93	23.14	22.43	16.96	20.12	3.12	15.52
2	16.87	25.64	20.23	17.81	20.14	3.93	19.53
3	19.91	21.36	18.97	19.76	20.00	0.99	4.98
4	19.01	22.98	18.99	17.95	19.73	2.22	11.26
MEAN	18.43	23.28	20.16	19.99			
STDEV	1.14	1.53	1.41	1.329			
%RSD	7.15	7.59	8.07	6.50			

CONCENTRATION 1E-6M CURRENTx 1E-12A

INJECTION NO.	E1	E2	E3	E4	MEAN	STDEV	%RSD
1	185	253	191	186	203.75	32.94	16.17
2	194	276	187	168	206.25	47.78	23.17
3	183	247	175	189	198.50	32.84	16.54
4	181	261	180	176	199.50	41.06	20.58
MEAN	185.75	259.25	183.25	179.75			
STDEV	5.74	12.55	7.14	9.61			
%RSD	3.09	4.84	3.89	5.34			

CONCENTRATION 1E-5M CURRENT x 1E-9A

INJECTION NO.	E1	E2	E3	E4	MEAN	STDEV	%RSD
1	1.83	2.66	1.86	1.77	2.03	0.42	20.77
2	1.89	2.49	1.95	1.82	2.04	0.31	15.03
3	1.78	2.58	1.83	1.79	2.00	0.39	19.58
4	1.76	2.62	1.84	1.76	2.00	0.42	20.97
MEAN	1.81	1.81	1.81	1.81			
STDEV	0.06	0.07	0.06	0.03			
%RSD	3.20	2.81	2.93	1.48			

CONCENTRATION 1E-4M CURRENT x 1E-9A

INJECTION NO.	E1	E2	E3	E4	MEAN	STDEV	%RSD
1	19.58	25.91	18.83	17.75	20.52	3.67	17.9
2	18.62	24.32	18.04	17.27	19.57	3.22	16.46
3	18.11	25.22	17.92	17.31	19.64	3.74	19.02
4	18.91	25.45	17.98	17.56	19.98	3.69	18.49
MEAN	18.81	25.23	18.19	17.47	19.92		
STDEV	0.53	0.58	0.37	0.20			
%RSD	3.26	2.65	2.35	1.29			

CONCENTRATION 1E-3M CURRENT x 1E-9A

INJECTION NO.	E1	E2	E3	E4	MEAN	STDEV	%RSD
1	193.82	284.77	211.84	208.10	224.63	40.84	18.18
2	189.45	283.74	203.28	201.10	219.39	43.33	19.75
3	196.3	293.95	213.15	209.97	228.34	44.35	19.42
4	191.8	285.54	207.12	204.30	222.19	42.76	19.24
MEAN	192.84	287.00	208.85	205.87			
STDEV	2.92	4.69	4.53	3.96			
%RSD	1.51	1.64	2.17	1.92			

CONCENTRATION 1E-2M			CURRENT x 1E-6A				
INJECTION NO.	**E1**	**E2**	**E3**	**E4**	**MEAN**	**STDEV**	**%RSD**
1	1.96	3.05	2.32	2.15	2.37	0.48	20.11
2	1.98	3.04	2.35	2.17	2.39	0.46	19.37
3	1.96	3.01	2.35	2.11	2.36	0.46	19.67
4	1.99	3.06	2.31	2.13	2.37	0.48	20.09
MEAN	1.97	3.04	2.33	2.14			
STDEV	0.02	0.02	0.02	0.03			
%RSD	0.76	0.71	0.88	1.21			
CONCENTRATION 1E-1M			CURRENT x 1E-6A				
INJECTION NO.	**E1**	**E2**	**E3**	**E4**	**MEAN**	**STDEV**	**%RSD**
1	8.86	12.82	10.89	9.93	10.63	4.81	15.83
2	8.67	12.68	10.67	9.89	10.48	4.99	16.07
3	8.84	12.79	10.96	9.72	10.58	5.20	16.19
4	8.72	12.75	10.88	9.86	10.55	5.31	16.21
MEAN	8.77	12.76	10.85	9.85			
STDEV	0.09	0.06	0.13	0.09			
%RSD	1.05	0.48	1.15	0.93			

Table 2.3 Statistical analysis of electrode array responses for 4 repetitive injections of potassium hexacyanoferrate(III). Both the inter-electrode and the individual electrode %RSD's are calculated. The data is presented here without normalisation.

	NORMALISED		**RADIAL FLOW CELL**				
CONCENTRATION 1E-7M			CURRENT x1E-12A				
INJECTION NO.	**E1**	**E2**	**E3**	**E4**	**MEAN**	**STDEV**	**%RSD**
1	18.98	20.5	21.19	19.27	19.99	1.04	5.20
2	19.87	23.2	19.81	21.63	21.13	1.62	7.66
3	20.11	21.96	20.16	18.72	20.24	1.33	6.56
4	19.46	20.89	20.19	21.17	20.43	0.77	3.75
MEAN	19.61	21.64	20.34	20.20			
STDEV	0.50	1.21	0.59	1.42			
%RSD	2.53	5.60	2.92	7.03			

CONCENTRATION 1E-6M CURRENT x1E-12A

INJECTION NO.	E1	E2	E3	E4	MEAN	STDEV	%RSD
1	184	196	193	182	188.75	6.80	3.60
2	178	209	186	193	191.50	13.18	6.88
3	187	214	206	188	198.75	13.40	6.74
4	180	197	191	191	189.75	7.09	3.74
MEAN	182.25	204	194	188.5			
STDEV	4.03	8.91	8.52	4.80			
%RSD	2.21	4.37	4.39	2.54			

CONCENTRATION 1E-5M CURRENT x 1E-9

INJECTION NO.	E1	E2	E3	E4	MEAN	STDEV	%RSD
1	1.97	2.02	1.93	1.84	1.94	0.08	3.93
2	1.99	2.01	1.97	1.98	1.9875	0.02	0.86
3	1.91	2.04	1.96	1.89	1.95	0.07	3.43
4	1.92	2.05	1.91	2.01	1.97	0.07	3.47
MEAN	1.95	2.03	1.94	1.93			
STDEV	0.04	0.02	0.03	0.08			
%RSD	1.98	0.90	1.42	4.08			

CONCENTRATION 1E-4M CURRENT x 1E-9A

INJECTION NO.	E1	E2	E3	E4	MEAN	STDEV	%RSD
1	21.68	22.1	21.89	21.61	21.82	0.22	1.01
2	19.84	21.02	19.94	20.03	20.21	0.55	2.71
3	20.32	20.96	19.54	19.76	20.15	0.64	3.15
4	20.29	21.16	19.62	21.96	20.76	1.02	4.91
MEAN	20.53	21.31	20.25	20.84			
STDEV	0.80	0.53	1.11	1.11			
%RSD	3.88	2.50	5.48	5.31			

CONCENTRATION 1E-3M CURRENT x 1E-9A

INJECTION NO.	E1	E2	E3	E4	MEAN	STDEV	%RSD
1	232.78	239.59	240.72	238..01	237.77	3.51	1.48
2	222.06	230.54	226.03	228.09	226.68	3.59	1.58
3	226.34	227.42	228.73	227.84	227.58	0.99	0.44
4	227.45	231.67	236.87	228.74	231.18	4.18	1.81
MEAN	227.16	232.31	233.09	230.67			
STDEV	4.41	5.19	6.86	4.90			
%RSD	1.94	2.23	2.95	2.13			

CONCENTRATION 1E-2M			CURRENT x 1E-6A				
INJECTION NO.	**E1**	**E2**	**E3**	**E4**	**MEAN**	**STDEV**	**%RSD**
1	2.37	2.41	2.41	2.38	2.39	0.02	0.86
2	2.46	2.5	2.51	2.47	2.49	0.02	0.96
3	2.24	2.38	2.38	2.25	2.31	0.08	3.38
4	2.41	2.45	2.52	2.34	2.43	0.08	3.10
MEAN	2.37	2.435	2.455	2.36			
STDEV	0.09	0.05	0.07	0.09			
%RSD	3.97	2.13	2.87	3.87			
CONCENTRATION 1E-1M			CURRENT x1E-6				
INJECTION NO.	**E1**	**E2**	**E3**	**E4**	**MEAN**	**STDEV**	**%RSD**
1	10.57	10.64	10.58	10.81	10.65	0.11	1.04
2	10.54	10.64	10.6	10.68	10.62	0.06	0.56
3	10.54	10.61	10.58	10.65	10.60	0.05	0.44
4	10.55	10.65	10.56	10.69	10.61	0.07	0.65
MEAN	10.55	10.64	10.58	10.71			
STDEV	0.01	0.02	0.02	0.07			
%RSD	0.13	0.16	0.15	0.66			

Table 2.4. Statistical analysis of electrode array responses for 4 repetitive injections of potassium hexacyanoferrate(III). Both the inter-electrode and the individual electrode RSD's were calculated. The data presented here have been normalised.

The normalised responses are shown in Figure 2.16(a) and 2.16(b). The %RSD between the electrodes is considerably reduced from 17.7% to 2.9% and is comparable to the %RSD for a single electrode with multiple injections (2.8%). These results demonstrate that averaging of the array response without normalisation will introduce significant imprecision and error into the results, thus verifying the necessity of applying a normalisation procedure.

Further analysis of the data by two factor ANOVA demonstrated that all the inter-electrode variances differed substantially from the inter-injection variances without normalisation. For the unnormalised data, F-tests show that the variances of the inter-

electrode results are significantly different to the inter-injection results, ranging from 7.66 at 10^{-7}M ($[Fe(CN)_6]^{3-}$) to 1643.68 at 0.1M ($F_{3,9}$ critical = 3.86). The improvement obtained with normalisation was demonstrated by F-tests which are non-significant at concentrations up to 10^{-4} M (ranging from 0.92 to 2.57) above which they are significant but at a level which is greatly reduced (ranging from 5.20 to 15.95) compared to the unnormalised responses. At concentrations of 10^{-3} M and above, the inter-electrode and inter-injection variances begin to diverge again; hence significant F-tests are obtained as a result of limitations in the normalisation procedure.

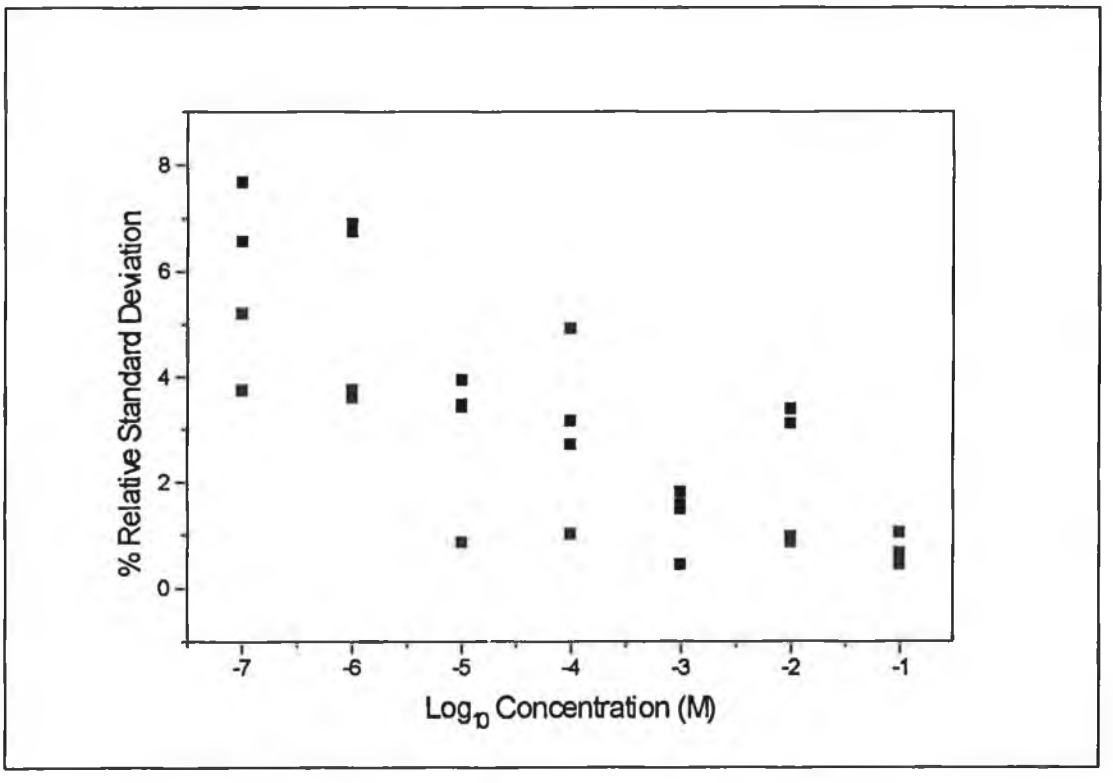

Figure 2.16(a). Plot of the inter-electrode relative standard deviation (■) vs. $\log_{10}$ molar concentration potassium hexacyanoferrate(III) for 4 repetitive injections. The radial flow cell responses have been normalised.

Further refinement of the normalisation procedure is therefore necessary to achieve a situation where none of the F-tests are significant (i.e. no significant difference exists

between the inter-electrode and the inter-injection variances), as otherwise, assembled voltammograms from the combined electrode data would be subject to unacceptable errors.

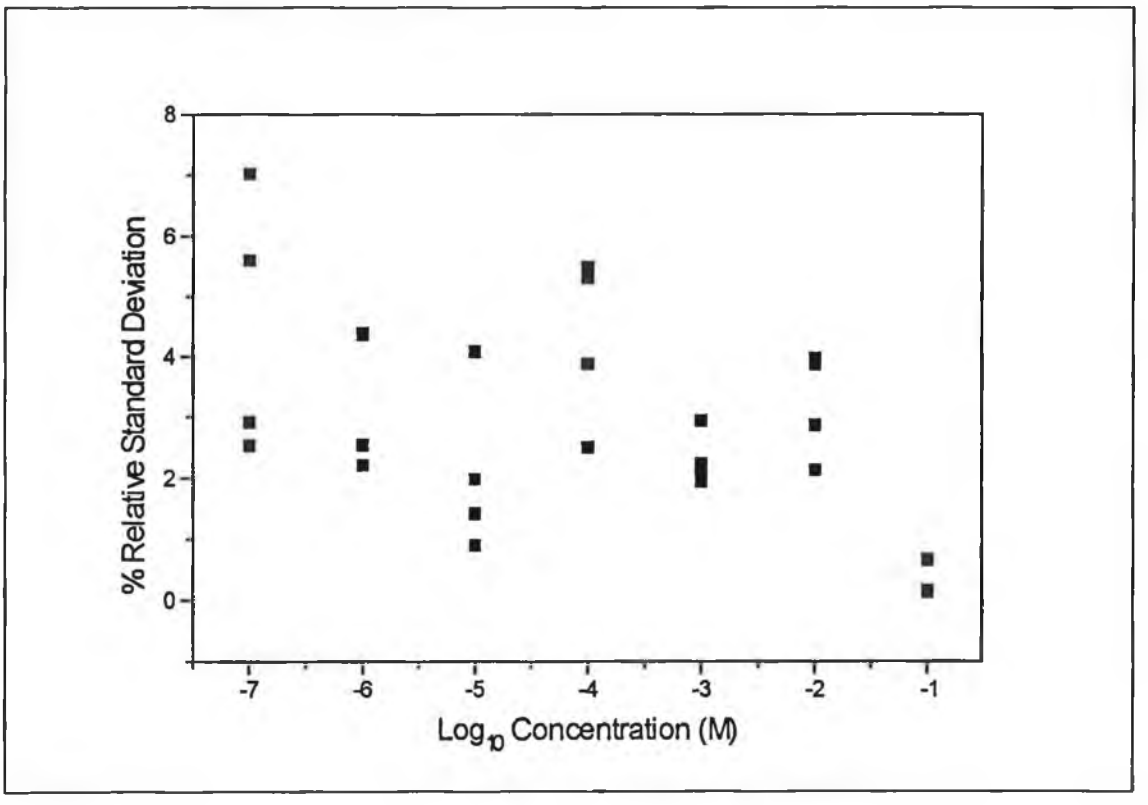

Figure 2.16(b). Plot of relative standard deviation (■) at each individual electrode vs. $\log_{10}$ molar concentration potassium hexacyanoferrate for 4 repetitive injections. The radial array responses have been normalised.

2.9.4 Three-Dimensional Results

Use of multielectrode arrays enables a 3-dimensional plot of the electrochemical response to be obtained, thus enabling features which would normally be hidden in a standard two dimensional display to be identified. This has important applications in chromatography, where the problem of two components eluting at the same time can be difficult to detect. An amperometric array approach offers a possible solution to this problem in a manner similar to that of spectrophotometric diode-array peak purity

elucidation provided there is sufficient resolution (30-50 mV in our experience) between the detection potentials of the co-eluting species. It is also applicable in FIA where simultaneous multicomponent determination without prior separation may be possible. However the situation with amperometric arrays is more complicated, as unlike PDA's, the signal is cumulative as the voltage becomes more extreme.

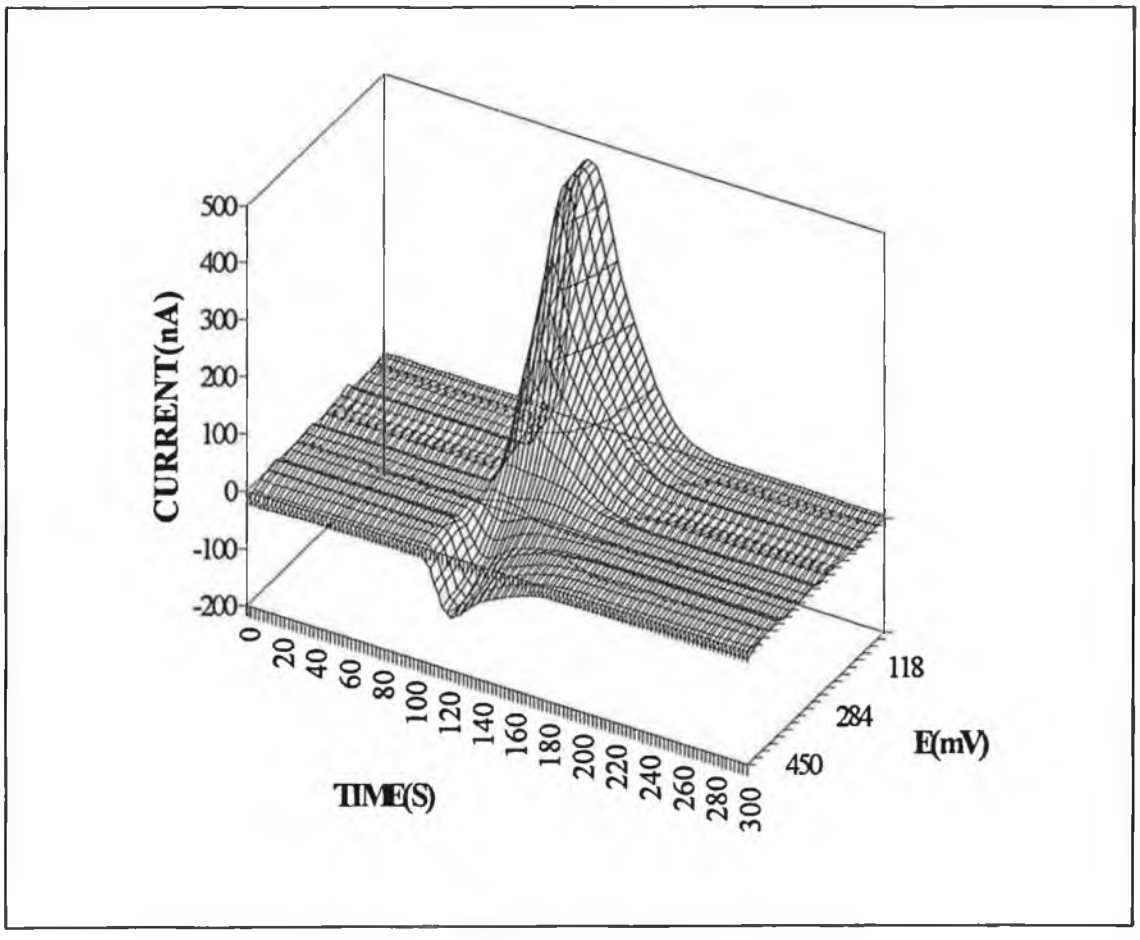

Figure 2.17(a). 3-dimensional post-run presentation (Microsoft Excel) of a potassium hexacyanoferrate(III) (1×10^{-3} M) hydrodynamic voltammogram in 0.05 M phosphate buffer pH 7.4.

Figure 2.17(a) shows the real-time 3-d display generated by the FIA electrochemical array detector (FIA-EA) to an injection of 10^{-4} M potassium hexacyanoferrate(III) (4 electrodes set initially at 0, 120, 240 and 360 mV with each being stepped by 23.68

mV to generate 20 virtual channels covering the range 0 to 450 mV) using the linear flow cell.

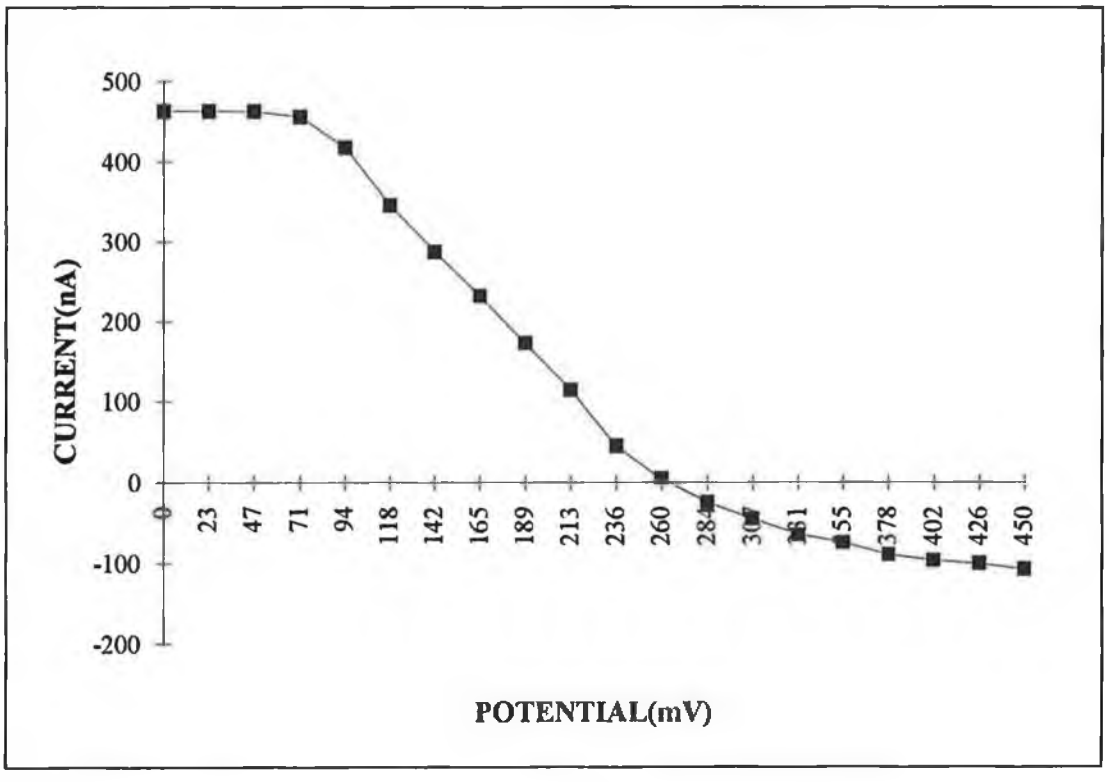

Figure 2.17(b). Hydrodynamic voltammogram of potassium hexacyanoferrate taken from Figure 2.17(a) at 122.5 seconds covering the potential range 0 to 450 mV.

The electrode in closest proximity to the inlet was polarised in the reduction region for potassium hexacyanoferrate(III) i.e. 0 mV. An increasing positive potential was applied at each electrode relative to the previous one in the direction of the outlet. The last electrode was polarised in the plateau region for the oxidation of hexacyanoferrate(III). Both the oxidation and reduction peaks can be clearly seen demonstrating the quasi-reversible nature of the compound. Access to the tabulated data within Microsoft-Excel enables 2-dimensional hydrodynamic voltammograms to be obtained at any desired time during the analysis run (i.e. i, t slices) see Figure

2.17(b). This facility increases the amount of available information for each voltammogram and is important for estimation of the half-wave potential for qualitative work.

The data at time 122.5 seconds were selected as they correspond to both the oxidation and reduction waves being visible on the 3-d display. The reduction wave does not fall as sharply as expected. The elongated nature of the wave probably arises from a combination of factors such as iR drop and slow electrode kinetics coupled with the use of the stepped potential sequence at the electrodes. The halfwave potentials obtained from the hydrodynamic voltammogram in Figure 2.17(b) are comparable to those obtained using an open cell with commercial instrumentation (Bioanalytical Systems CV50W):

- Oxidation halfwave potential: 313 mV : 290 mV (CV50W)
- Reduction halfwave potential: 157 mV : 50 mV (CV50W)

The shifts in potentials are assumed to be a result of the differences in the two techniques.

The highly reversible nature of hydroquinone electrochemistry is shown in Figure 2.18. Oxidation and reduction peaks of almost equal height are obtained. A carrier stream (flow rate 0.4 ml/min) of 0.05 M phosphate buffer (pH 7.4) was used.

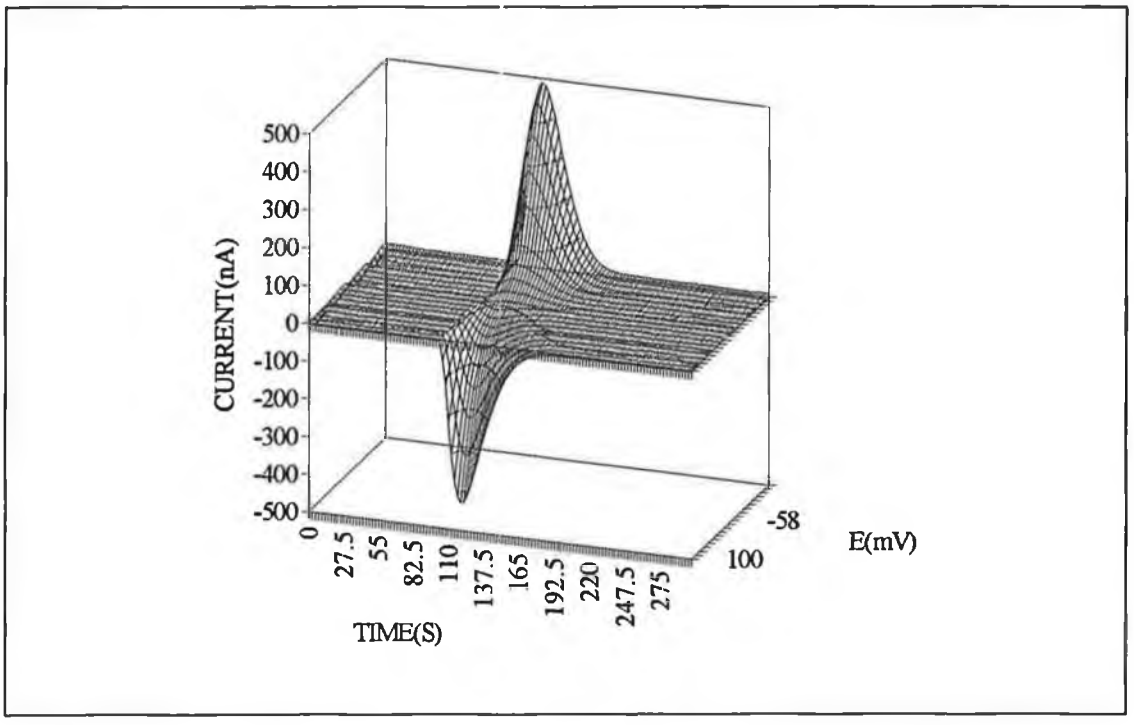

Figure 2.18. 3-dimensional hydrodynamic voltammogram of hydroquinone (0.1 M) in 0.05 M phosphate buffer pH 7.4.

2.9.5 Flow Injection Analysis of Metal Ions

2.9.5.1 Linearity and Reproducibility of Copper Response

The linearity and reproducibility of array responses to injections of Cu(II) ion was investigated. A plot of $\log_{10}$ concentration versus $\log_{10}$ current for Cu(II) ions in the concentration range 500 ppm to 100 ppb was linear with a slope of 0.9904 (see Figure 2.19).

The responses at the individual electrodes to six sequential injections of 10 ppm copper(II) were monitored at a fixed potential of -250 mV to investigate the reproducibility of response. The array responses were normalised using the software normalisation prior to use. The inter-injection %RSD's ranged from 1.07 to 3.05%, while the inter-electrode %RSD's ranged from 0.87 to 2.90%. A summary of the results are presented in Table 2.5.

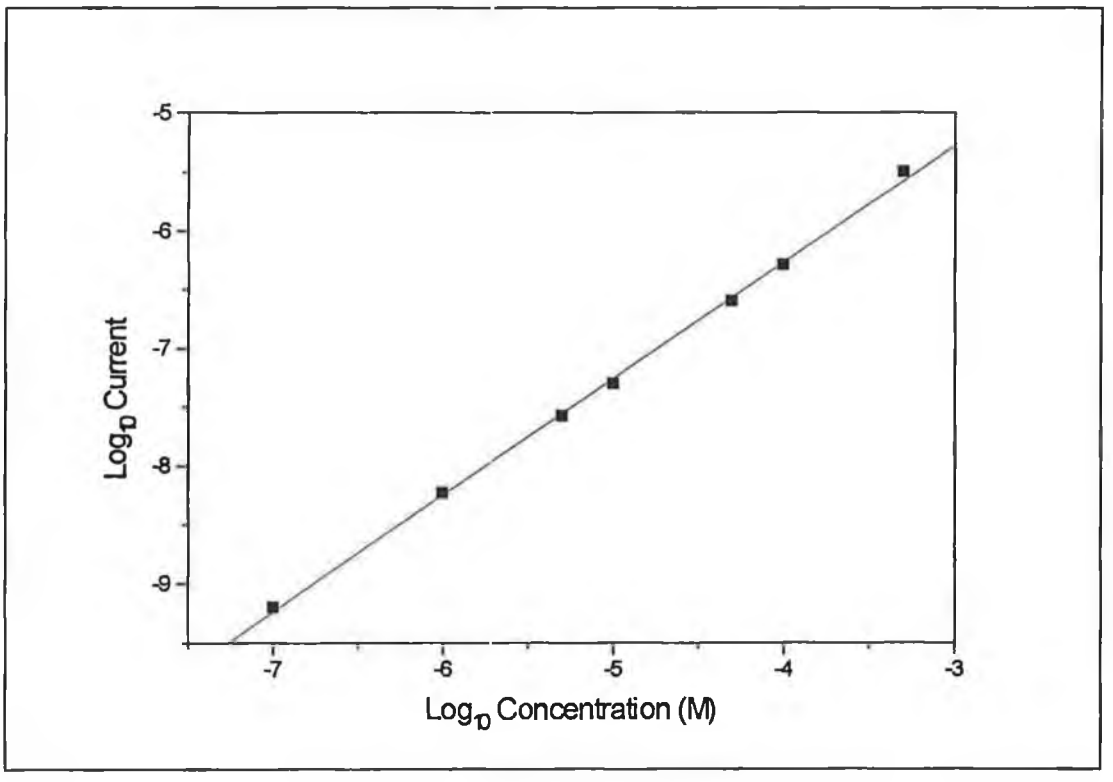

Figure 2.19. Plot $\log_{10}$ molar concentration vs. $\log_{10}$ current for Cu(II) in the concentration range 500 ppm to 100 ppb.

	E 1(uA)	E 2(uA)	E 3(uA)	E 4(uA)	Average	Stdev	%RSD
	96.43	95.43	97.62	94.98	93.08	1.17	1.26
	95.76	92.98	89.43	91.30	92.76	2.69	2.90
	94.08	94.15	93.14	95.14	77.97	0.82	1.05
	93.52	92.76	90.89	95.73	62.57	2.00	3.20
	92.40	93.87	92.85	89.55	55.93	1.85	3.31
	95.60	93.04	91.44	91.78	47.53	1.89	3.97
Average	94.63	93.71	92.56	93.08			
Stdev	1.55	1.01	2.82	2.54			
%RSD	1.63	1.07	3.05	2.73			

Table 2.5 Analysis of array responses to six injections of 10 ppm copper.

2.9.5.2 Copper and Lead Analysis

The array was then applied to the determination of copper(II) and lead(II) ions separately. Concentrations of 200 ppm copper(II) and lead(II) ions were injected and

their voltammograms recorded. A sample 3-dimensional voltammogram of lead(II) is presented in Figure 2.20. The 4 working electrodes of the array were set to initial potentials of -50, -175, -300, -425 respectively. Five potential steps of 25 mV were applied to each electrode to generate a 20 channel response (4 real, 16 virtual) covering the potential range -50 to -550 mV. A 100 ms delay was employed before sampling the current to minimise charging current effects.

The 2-dimensional voltammograms were taken at the current maxima, from which the diffusion current, i_d, and the half-wave potential ($E_{1/2}$) were measured. The half-wave potentials for copper(II) and lead(II) in 0.1 M KCl + 0.5% HNO_3 were found to -140 mV and -410 mV respectively, which were similar to those values obtained using a BAS CV-50W voltammetric analyser in the linear sweep mode ($E_{1/2}$ copper:-95 mV, $E_{1/2}$ lead:-380 mV). The discrepancies observed in the half-wave potentials are probably due to iR drop resulting from differences in cell configurations.

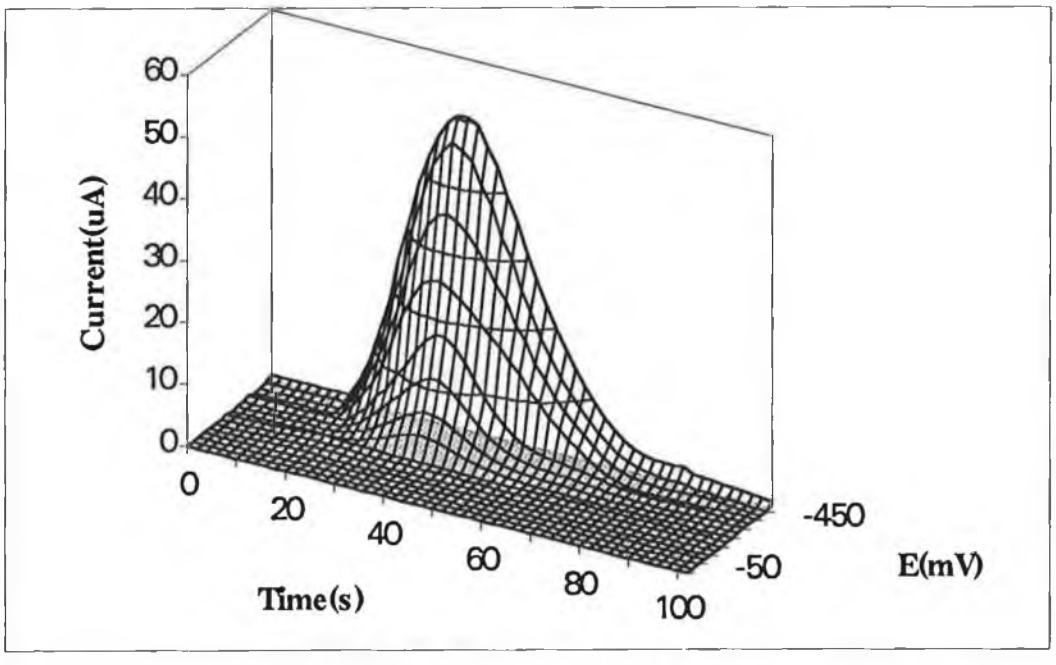

Figure 2.20 3-dimensional voltammogram of 200 ppm lead(II) nitrate. Conditions: mobile phase 0.1 M KCl and 0.5% HNO_3; flow rate 0.5 ml/min.

Relative standard deviations of 5.1% for copper(II) and 2.6% for lead(II) at their half-wave potentials were obtained for repetitive injections of the ions (n=4). The %RSD's for both metals were reduced to less than 2% in the diffusion limited plateau which is more stable than the halfwave potential region.

2-dimensional voltammograms obtained for injections of 100 and 200 ppm lead(II) in 0.1 M KCl and 0.5% nitric acid are shown in Figure 2.21. The voltammograms demonstrate a linear decrease in diffusion current with concentration.

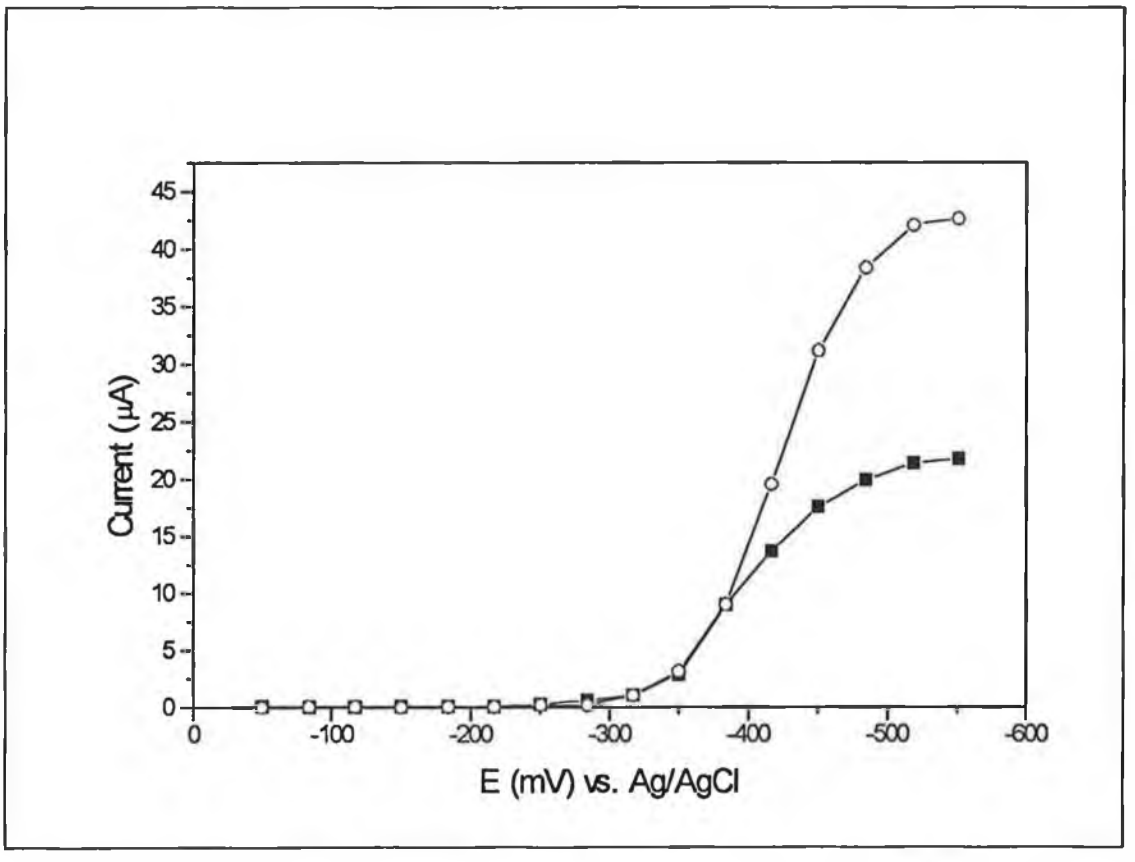

Figure 2.21. 2-dimensional voltammograms of 200 ppm Pb(II) (O) and 100 ppm Pb(II)(■) in 0.1 M KCl and 0.5% nitric acid.

Plots of $\log_{10}$ $[i_d/(i_d-i)]$ versus E (mV) in the concentration range 250 ppm to 50 ppb for both copper(II) and lead(II) yielded linear plots which are presented in Figure 2.22.

These plots indicate that the metals ions are reversibly reducible under these conditions.

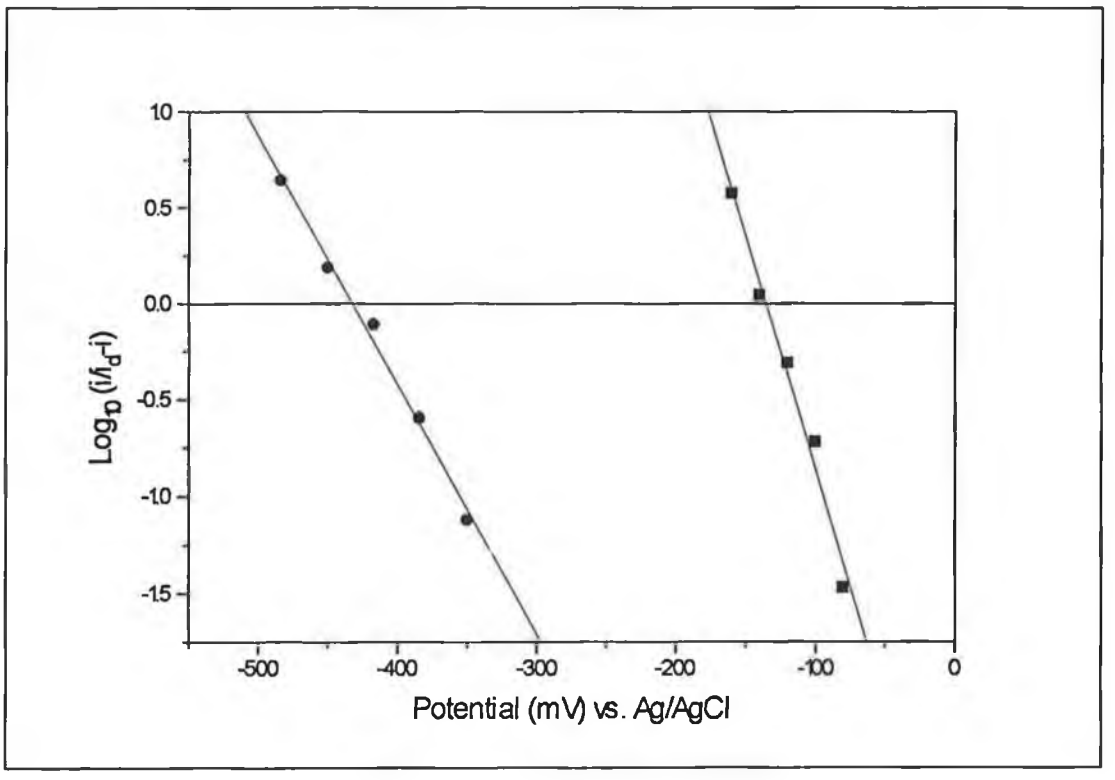

Figure 2.22 Plot of $\log_{10}$ (i/i_d-i) vs. potential (mV) for copper(II) (•) and lead(II) (■).

2.9.5.3 Multicomponent Determinations

FIA requires selectivity in detection, which has led to the use of a number of selective detectors such as ion-selective electrodes, photo-diode arrays and enzyme-based biosensors. Normal fixed potential amperometric detectors generally provide poor selectivity; therefore separation of the individual components is generally required for analysis of mixtures. The use of an amperometric array offers a possible solution to this problem in certain cases, where there is sufficient resolution in the reduction or oxidation potentials of the analytes being determined.

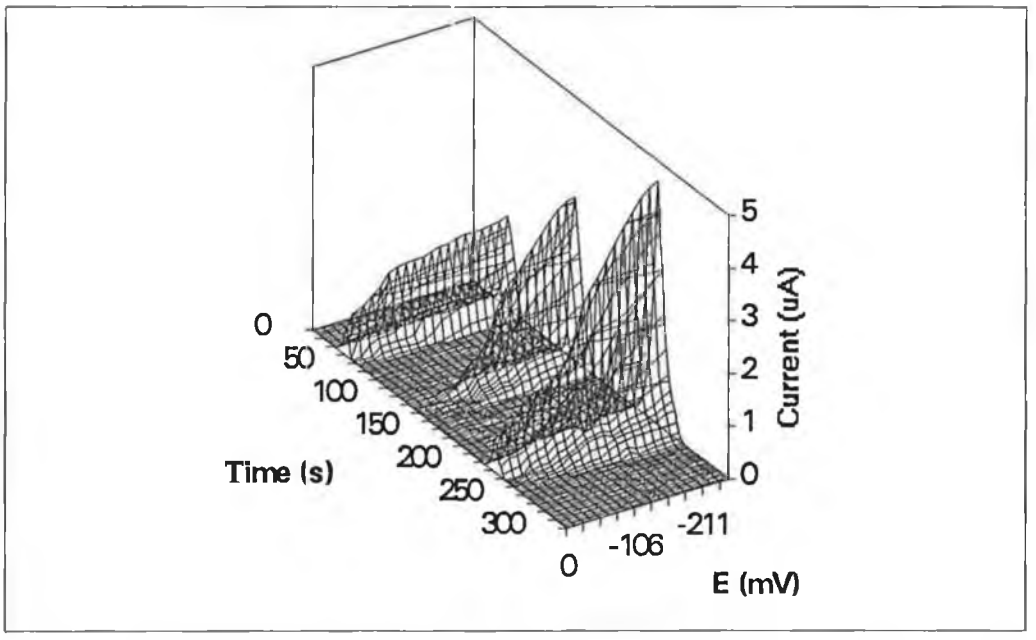

Figure 2.23. 3-dimensional voltammogram of Cu(II), Fe(III) and a mixture of both metal ions at a concentration of 250 ppm. Conditions: mobile phase; 0.05 M phosphate buffer; flow rate 0.5 ml min^{-1}.

Figure 2.23 shows the 3-dimensional voltammograms obtained from injections of 250 ppm Fe(III), 250 ppm Cu(II) and a mixture of both metal ions at a concentration of 250 ppm respectively. The manner in which the Fe(III) and Cu(II) signals are additive to form the mixed injection peak is clearly visible. The three dimensional definition of the peaks allow each peak to be easily identified.

Their respective 2-dimensional voltammograms taken at the current maxima are shown in Figure 2.24. The two electron reduction of copper(II) ions, compared to the single electron reduction of iron(III), are clearly reflected in the magnitude of their respective reductive current responses (i_d for Cu(II) = 3.2μA, i_d for Fe(III) = 1.7μA). The signal resulting from the addition of the individual voltammograms is overlaid with the voltammogram obtained from the mixed injection for comparison purposes.

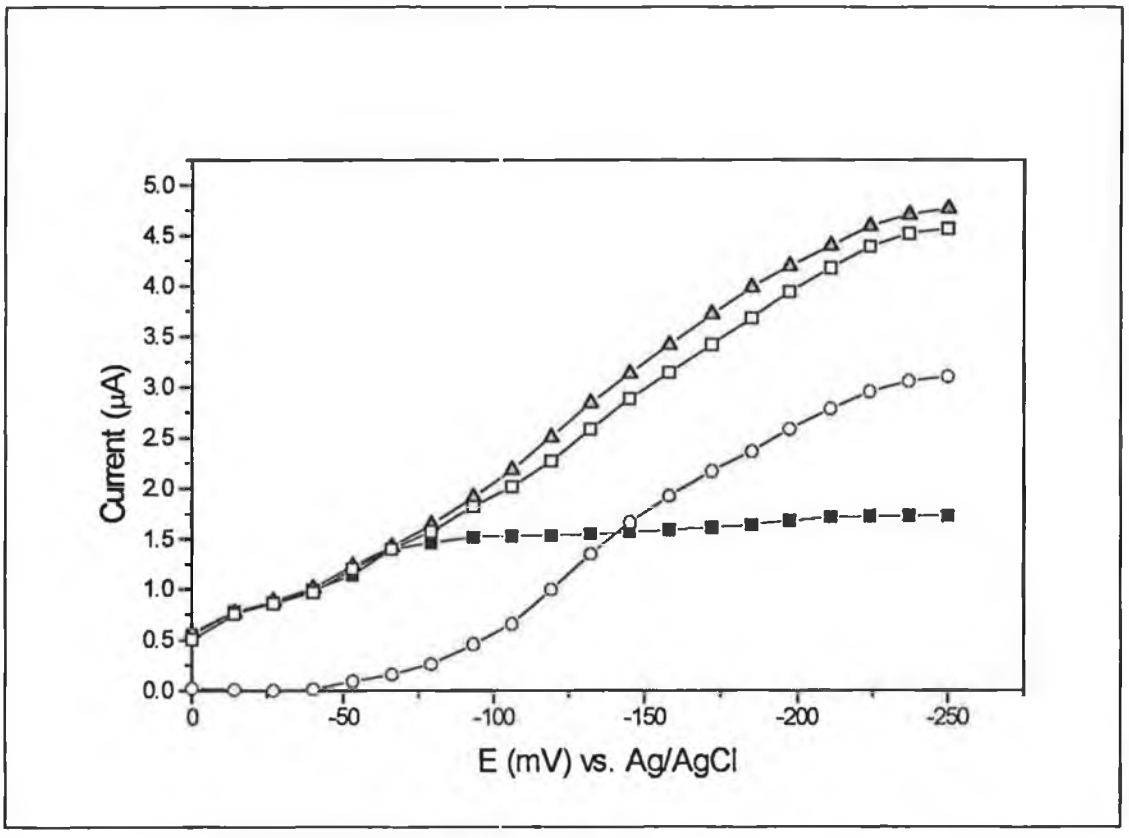

Figure 2.24. Normalised 2-dimensional voltammograms of 250 ppm Fe(III)(■). 250 ppm Cu(II)(○), mixed injection voltammogram (□)(250 ppm of both Fe(III) and Cu (II) and addition of the individual voltammograms of Fe(III) and Cu(II)(▲). Conditions: mobile phase 0.05 M phosphate buffer; flow rate 0.5 ml/min.

From Figure 2.24 it is clear that the individual components are not fully additive between the potential range -65 mV to -250 mV. This probably results from competition between the metal ions for reduction sites on the electrode surfaces. This difference, which remains constant once the half-wave potential of copper(II) is reached, could be compensated for by the inclusion of a weighting factor to adjust the responses appropriately for quantitative analysis.

The results indicate that it is feasible to determine a number of components simultaneously with an amperometric array provided the following criteria are

complied with:

- the reduction or oxidation potentials of the analytes being determined are sufficiently resolved;
- no chemical interference occurs at the electrode surfaces;
- the competitive processes at the working electrode surfaces are predictive (ideally additive).

The 2-dimensional responses obtained in chromatography and FIA can be limited in their information content, thus masking features which could be identified in a 3-D response. Single fixed potential working electrodes are unable to resolve mixtures, while dual electrodes are limited in the extent of their applications. The use of an amperometric array provides a level of information which allows a greater level of confidence in peak assignments and assessment of peak purity.

2.9.6 Biosensor/Interference Studies

2.9.6.1 Introduction

In this work differential measurements were used to normalise a glucose sensor responses for interference effects as outlined by Janata [89]. Two identical sensors were prepared with the glucose oxidase being omitted from one of them. The sensor then acts as a reference device responding only to electro-active species present in the sample. This signal were then be subtracted from the total signal obtained at the enzyme sensor to normalise its response, provided the signals are additive. This regime of interference compensation has been applied to the determination of glucose with acetaminophen and uric acid present as interferences using FIA. Cyclic voltammetry (CV) was used to investigate the addition effect of the interference signal

on the total analyte signal. The sensor design was based on the use of glutaraldehyde to immobilise glucose oxidase onto a glassy carbon electrode. Sensors based on the use of glutaraldehyde are particularly susceptible to interferences effects because of their inability to reject charged molecules and therefore was used for this study. The computer controlled multichannel potentiostat was used for potential application and current measurement duties.

2.9.6.2 Electrode Preparation

The working electrodes were first polished with 6 μm alumina (BAS) and then polished on a second moist polishing pad without alumina followed by sonication in deionised water for 3 minutes to remove any particulate matter before modification. 0.002 g of albumin was dissolved in 100 μl of phosphate buffer, pH 7.4 together with 0.001 g of glucose oxidase. 20 μl of this solution was mixed with 10 μl of a 1% glutaraldehyde solution. 2 μl of this solution was then applied to the electrode surface and dried carefully with an air gun before insertion into the flow cell. The "blank electrodes" were prepared in an identical fashion but with the exclusion of glucose oxidase and were designated the name "reference" sensors. The sensors were polarised at +700 mV vs. Ag/AgCl reference electrode for all measurements. Newly prepared sensors were allowed to equilibrate for 30 minutes prior the injection of samples. Sensors for the CV studies were prepared in an identical manner to the sensors used during FIA measurements.

2.9.6.3 Instrumentation

The computer controlled multichannel potentiostat was used to polarise and monitor

both the glucose and reference sensors Display of the sensor responses were available on-line. The responses from the glucose sensor and the reference sensor were displayed with different colours to distinguish clearly between them. A 5-moving point averaging filter was used on-line to reduce noise. The current off-setting capability of the potentiostat was used to the set the sensor backgrounds to zero. The acquired data was saved in ASCII format for post-run data analysis in Microsoft Excel. A BAS CV-50W voltammetric analyser was used for all CV measurements.

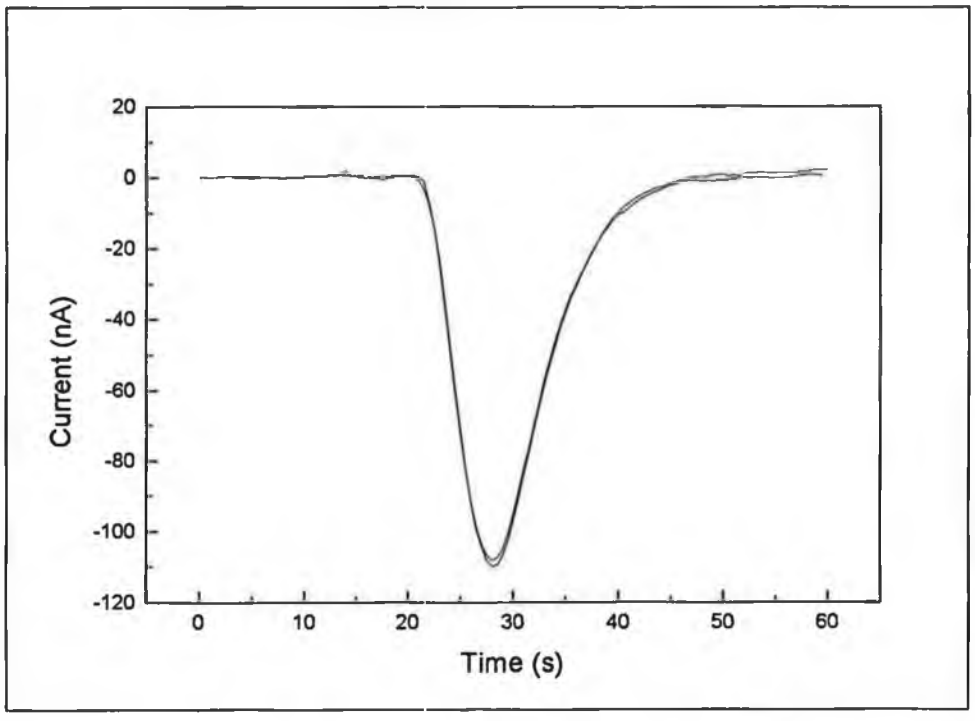

Figure 2.25(a). Normalised FIA responses to an injection of 1×10^{-5} M acetaminophen at both the glucose and reference sensor.

2.9.7.4 FIA Studies

In general, the time needed for a peak to appear and return to the original baseline in FIA was less than 30 seconds. The peak current (I_p) was reached in under 10 seconds for all sensors fabricated irrespective of the sample injected. Figure 2.25(a) shows

both sensor responses to an injection of 1×10^{-5} M acetaminophen. These responses have been normalised using the software normalisation procedure. The software normalisation procedure is necessary to compensate for differences in electrode surfaces such as film thickness and surface area.

The sensor responses to an injection of 1×10^{-5} M uric acid are shown in Figure 2.25(b) without normalisation. The differences in the sensor responses are clearly visible and would introduce a significant element of error into the measurements without correction.

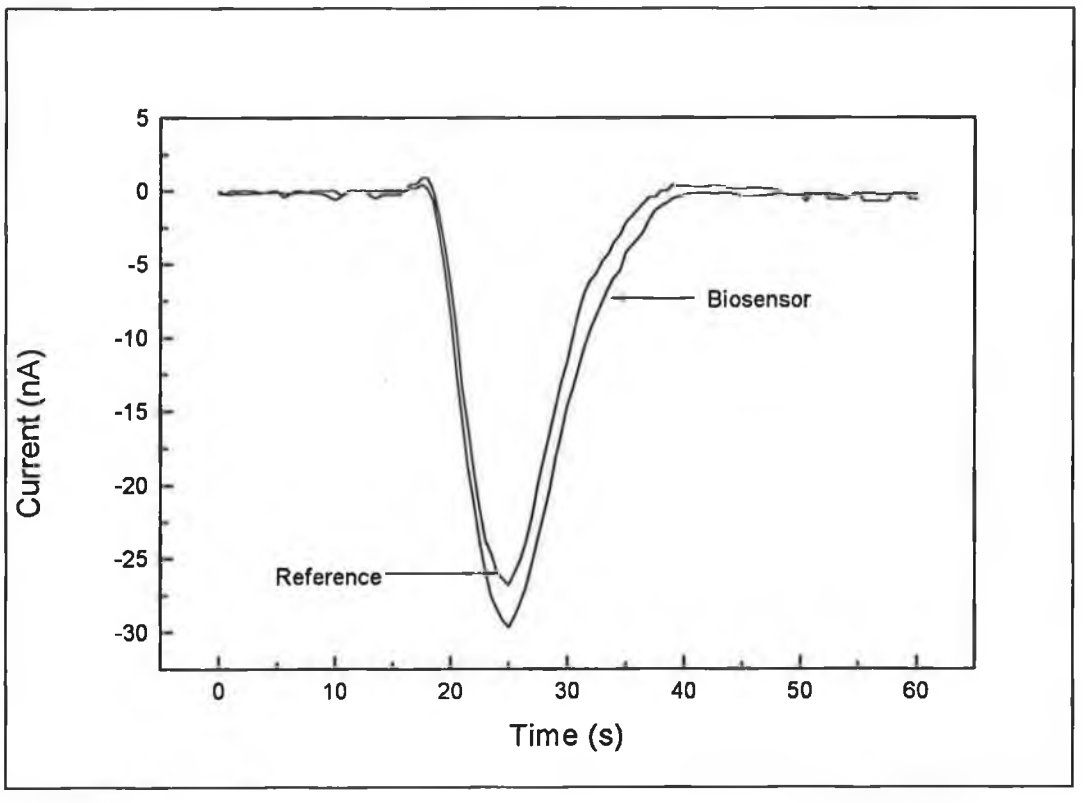

Figure 2.25(b). FIA responses to an injection of 1×10^{-5} M uric acid at both the glucose and reference sensors without normalisation.

The responses of both sensors to an injection of 10 mM glucose are presented in Figure 2.26. The reference sensor demonstrates no visible response to glucose as

expected. The biosensor response was approximately 45 nA in magnitude; however, the magnitude of this response did vary with different sensors. 0.05 M phosphate buffer, pH 7.4 and 1 mM hexacyanoferrate(III) (present as a mediator) was used as the carrier stream for all FIA measurements. The reproducibility of the biosensor response was investigated with repetitive injections of 10 mM glucose. The %RSD was calculated at 3.6% for 5 repetitive injections.

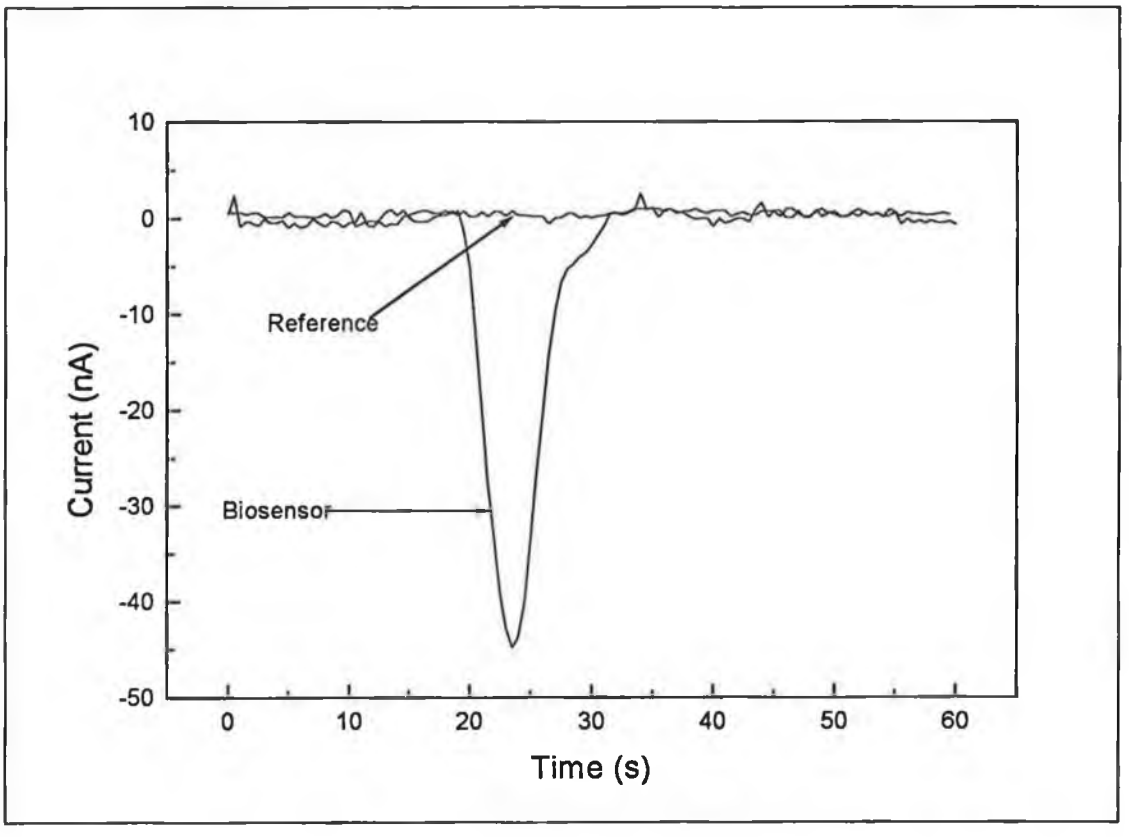

Figure 2.26. Responses to an injection of 10 mM glucose at the glucose and reference sensors. Conditions: flow rate: 0.3 ml min^{-1}, carrier stream 0.05 M phosphate buffer pH 7.4 and 1 mM hexacyanoferrate(III).

The effect of the common clinical interference acetaminophen at a concentration of 1×10^{-5} M on the biosensor responses to injections of 10 mM glucose was then examined. Figures 2.27(a) and (b) demonstrate the principle of the differential measurements

utilised in this study. The sensor responses to injections of 1×10^{-5} M acetaminophen were normalised prior to use. The responses of the sensors to an injection of 10 mM glucose and 1×10^{-5} M acetaminophen are presented in Figure 2.27(a). The biosensor response to a separate injection of 10 mM glucose is also included.

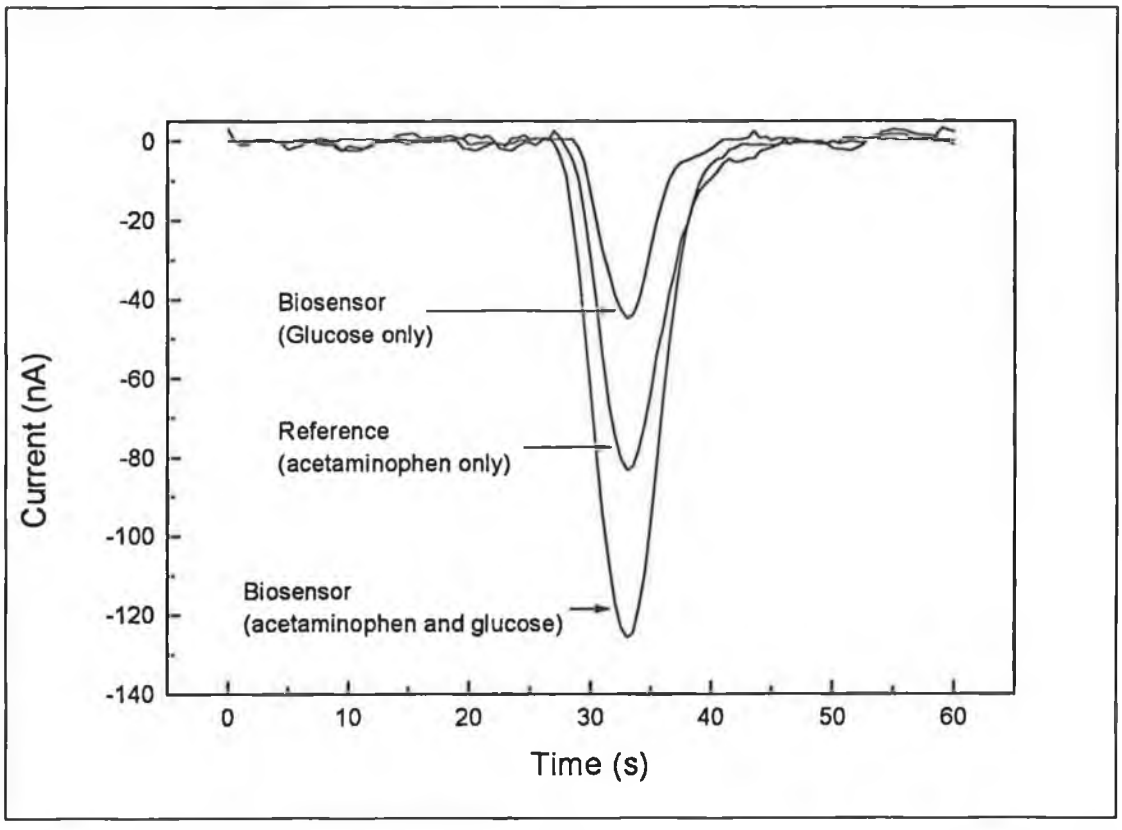

Figure 2.27(a). FIA responses to an injection of 10 mM glucose + 1×10^{-5} M acetaminophen for the glucose sensor and the reference sensor. The biosensor response to a separate injection of 10 mM glucose is also included. Conditions: flow rate 0.3 ml min^{-1}, carrier stream 0.05 M phosphate buffer, pH 7.4 and 1 mM hexacyanoferrate(III), electrode polarisation +700 mV versus Ag/AgCl reference electrode.

The biosensor signal comprises of the additive effect of both the glucose and acetaminophen signals. Therefore the reference signal can be subtracted from the

biosensor signal to give a corrected measurement of the glucose concentration which is free from interference contributions. The corrected glucose signal is presented together with the biosensor response to a separate injection of 10 mM glucose in Figure 2.27(b). Close agreement in the magnitude of the signals was obtained.

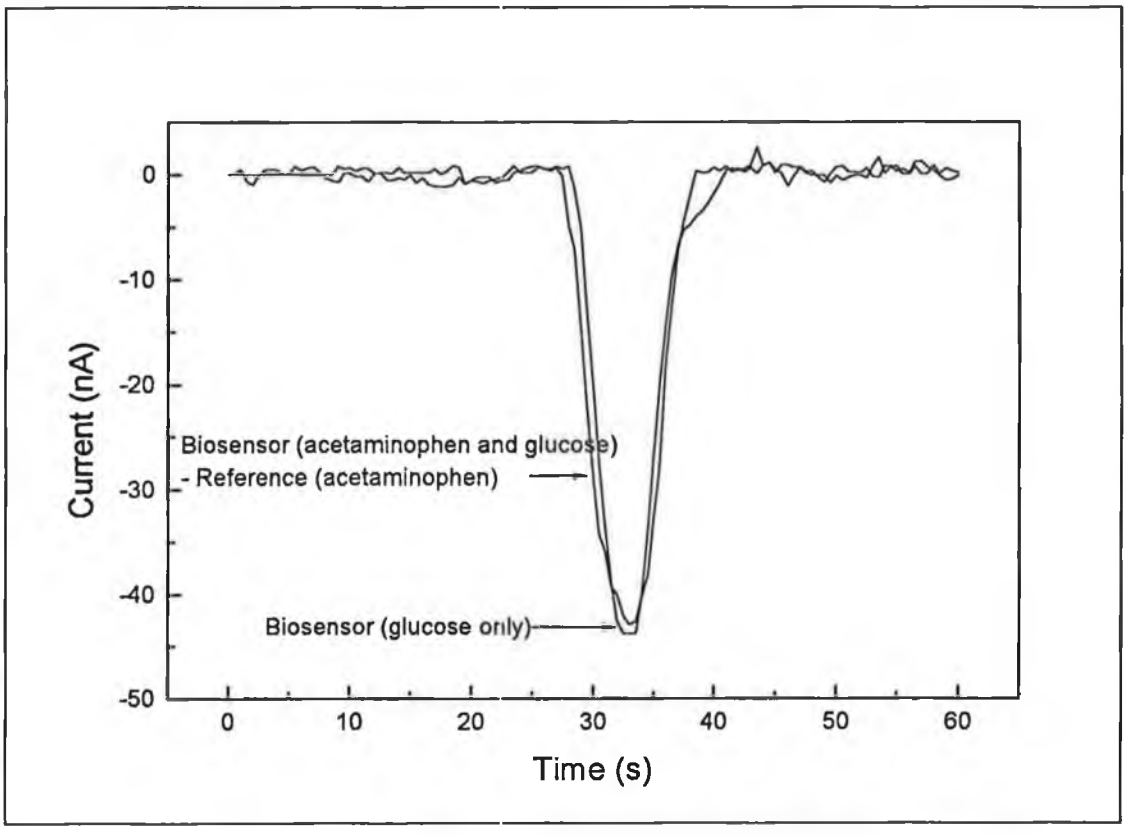

Figure 2.27(b) The corrected biosensor response for an injection of 10 mM glucose with 1×10^{-5} acetaminophen obtained by the subtraction of the reference signal from the biosensor response (presented in Figure 2.27(a)). The biosensor response to a separate injection of 10 mM glucose is presented for comparison purposes.

The reproducibility of the reference sensor response to acetaminophen was investigated by successive injections of 1×10^{-5} M acetaminophen. A %RSD of 3.0% was obtained for 5 repetitive injections. A high degree of reproducibility in the

reference sensor response to acetaminophen is required to prevent the introduction of error when subtracting this response from the biosensor response.

2.9.6.5 Cyclic Voltammetry Studies

Cyclic voltammetry was used to verify the results obtained in the FIA measurements. The measurements were carried out in 0.05 M phosphate buffer under batch conditions, pH 7.4 and hexacyanoferrate(III) at a concentration of 1 mM. No distinct peaks were observed in

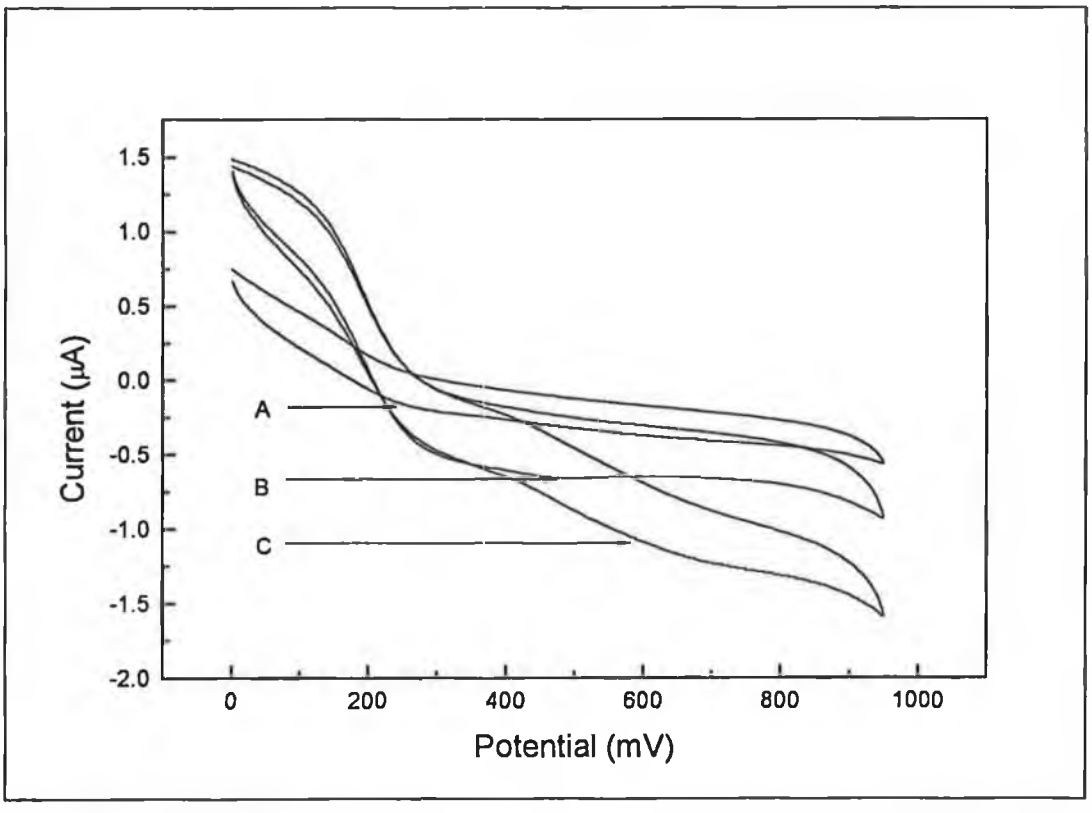

Figure 2.28 Cyclic voltammograms of (A) 10 mM glucose, (B) 1×10^{-5} M acetaminophen and (C) a mixture of 10 mM glucose and 1×10^{-5} M acetaminophen at a glucose biosensor. All scans were carried out in 0.05 M phosphate buffer pH 7.4 and 1 mM hexacyanoferrate(III). Conditions: scan rate 20 mV s^{-1}, potential range 0 to +950 mV.

the CV behaviour. New sensors were prepared for each CV measurement to prevent sample carry-over effects. At $E_{700\ mV}$ the response due to GOx/10 mM glucose reaction was found to be 412 nA in magnitude. The corresponding response for acetaminophen at $E_{700\ mV}$ was 665 nA. The CV behaviour of the glucose and acetaminophen mixture exhibits a current of 1230 at $E_{700\ mV}$ (see Figure 2.28) which is a difference of 153 nA from the sum of the individual currents i.e. 1077 nA.

The discrepancies obtained are probably due to differences in the thickness of the differnt sensor membranes. The CV measurements indicate that the current responses are probably additive under these conditions, which is in agreement with the FIA responses presented in Figure 2.27(a). These observations are also in accordance with those of Male and Loung [89]. Single interferent signals of either acetaminophen or uric acid were found to be additive to the glucose signal at a glucose biosensor.

2.9.6.6 Kinetic Parameters

Figure 2.29 shows the calibration plot of the average sensor responses to injections of glucose in the concentration range 0.4-20.0 mM glucose. Both K'_m and I_{max} were estimated using Michaelis-Menten kinetics. An average K'_m of 3.4 mM and an I_{max} of 660 nA cm^{-2} were obtained. The ratio of $I_{max}\backslash K'_m$ can be used as a measure of catalytic efficiency or sensitivity of the sensor for glucose [90]. The average $I_{max}\backslash K'_m$ of the sensor was calculated to be 195 nA cm^{-2} mM^{-1}.

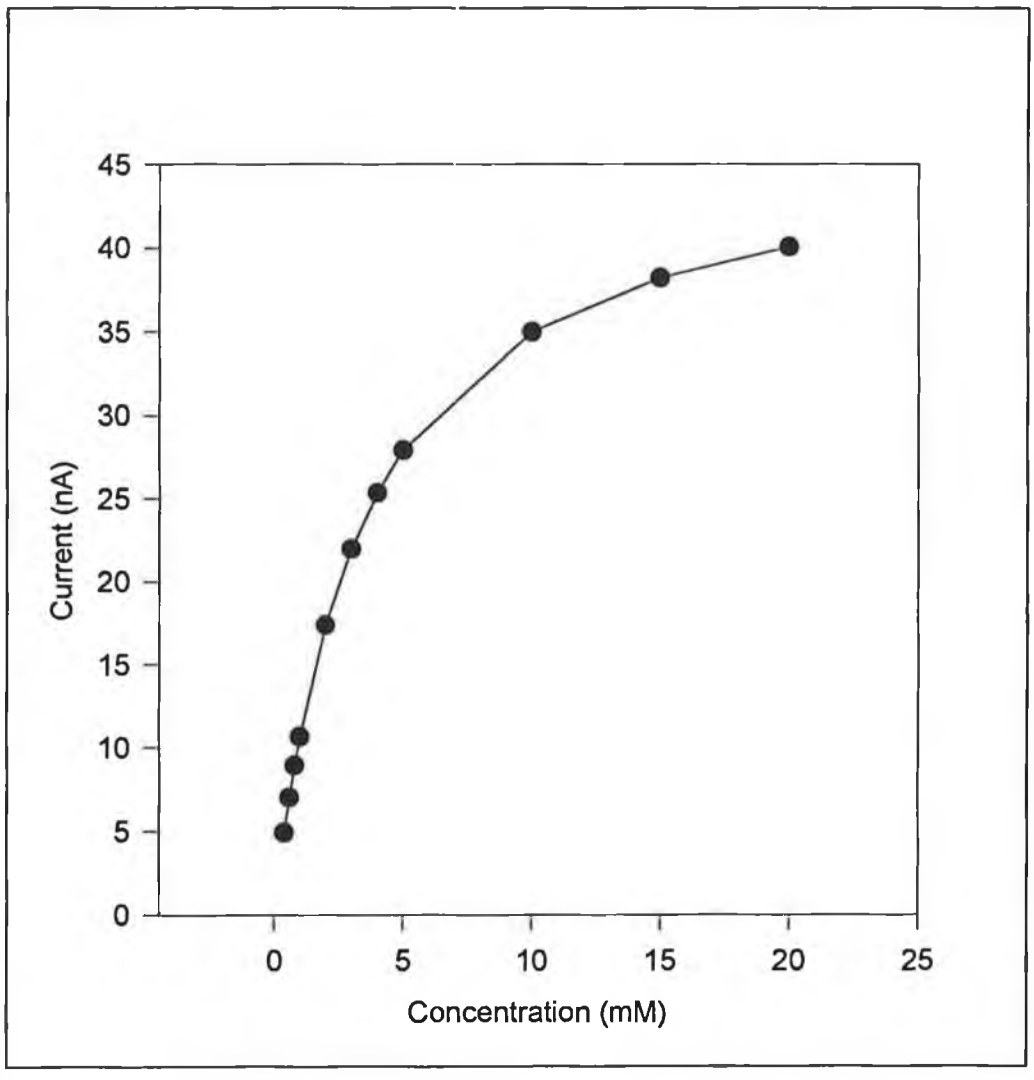

Figure 2.29. Plot of concentration (mM) versus current for injections of glucose in the concentration range 0.4-20 mM. Conditions: flow rate 0.3 ml min^{-1}, mobile phase; 0.05 M phosphate buffer, pH 7.4 and 1 mM hexacyanoferrate(III), electrode polarisation; +700 mV versus Ag/AgCl reference electrode.

2.9.6.7 Conclusion

The principle used in this study can easily be extended to other biosensor-interference systems. The possible general applicability of the system could neglect the necessity of developing individual interference compensation regimes for individual sensor systems.

However, this type of post-run interference compensation is difficult without the use a computer controlled multichannel potentiostat. The use of a computerised instrumentation facilitates easy manipulation of the compensation parameters. A high degree of flexibility is required to accommodate the inherent variations involved in the fabrication of biosensors. Differences in sensor background currents are accommodated by the background offsetting capability of the potentiostat (±200.0 nA). Accurate measurement of both the analyte of interest and the interferences is possible due to the simultaneously measurement of both signals in a parallel flow geometry. Modification of the software would allow flexibility in adaptation of the system to other determinations where interferences are present. Development of a miniature stand-alone instrument is the next step in making the applicability of this type of measurement a feasible option in many biosensor-interference systems. Further work in this area could lead to the development of sensing systems that can cope with the problems of "real world" measurements. Extension of the system to accommodate multiple sensors or the implementation of sensor redundancy schemes to increase the reliability of the analysis system is also possible.

CHAPTER 3

DESIGN, EVALUATION AND APPLICATION OF A FOUNTAIN TYPE FLOW CELL WITH SEQUENTIAL INJECTION ANALYSIS

3.1 Introduction

A variety of flow cell geometries have been described for electrochemical detection as outlined in Chapter 1. Desirable fluid-flow properties in a flow cell are low or controlled dispersion, low dead volume and minimal transitions from one flow cross section to another [92-95]. These parameters are particularly critical in flow cells used for optical detection. Dispersion is a problem in stop-flow measurements because of the difficulty in stopping reproducibly the same part of the sample zone in the detector [93]. Pavan et al. have described the wide variety of analysis based on stopped-flow and injection optosensing; however, they reported that an ideal flow cell capable of accommodating all of these techniques has not been designed [95].

Scudder et al. have reported on the design of a novel flow cell geometry called the fountain cell [96]. The cell was developed for use as a fluorescence microscopy chamber to study living cells. In their design the fluid entered via a central inlet and was directed normal to a flat optical surface. The resulting fountain-like flow pattern was forced into a space between the optical surface and a parallel rear plate. The fluid finally collected in a ring-shaped well which was at all points equidistant from the point of inlet.

The fountain cell was reported to demonstrate characteristics which indicated possible

suitability to electrochemical detection at an enhanced level of performance over some of the standard cell geometries. The fluid element forms a thin flat volume which can be physically matched to planar detectors. This was a useful characteristic in its application with amperometric arrays. A final advantage of the fountain cell was that it gives a smooth flow transition from the inlet tubing to the detection region with minimal unswept volume and no wall effects. The absence of wall effects preserves the shape of the injection zone. This is a desirable feature in anodic stripping voltammetry (ASV) where flow reversal of the sample plug over the surface of the working electrode can be used to enhance sensitivity. A schematic diagram of the fountain cell is shown in Figure 3.1.

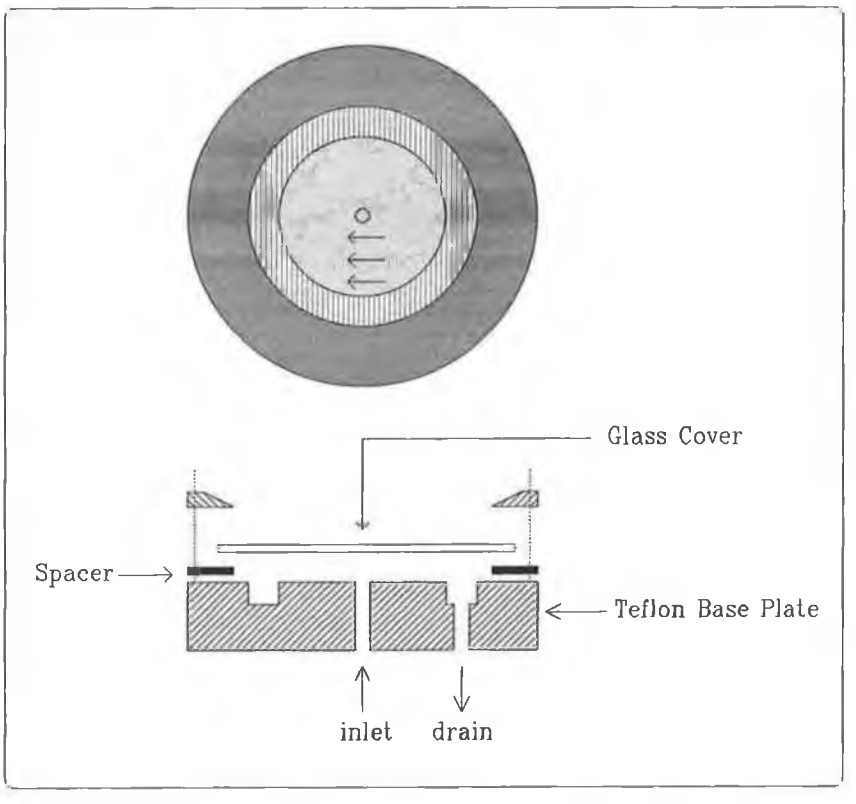

Figure 3.1. Fountain cell schematic (taken from Scudder et al. [96])

The principle of sequential injection analysis (SIA) was first introduced by Ruzicka and Marshall [96]. They described how the relatively constant flow as used in FIA can be replaced by a sinusoidal flow with a synchronised injection. The standard peristaltic pump can be replaced with a cam-driven syringe based pump. The system they described is outlined in Figure 3.2.

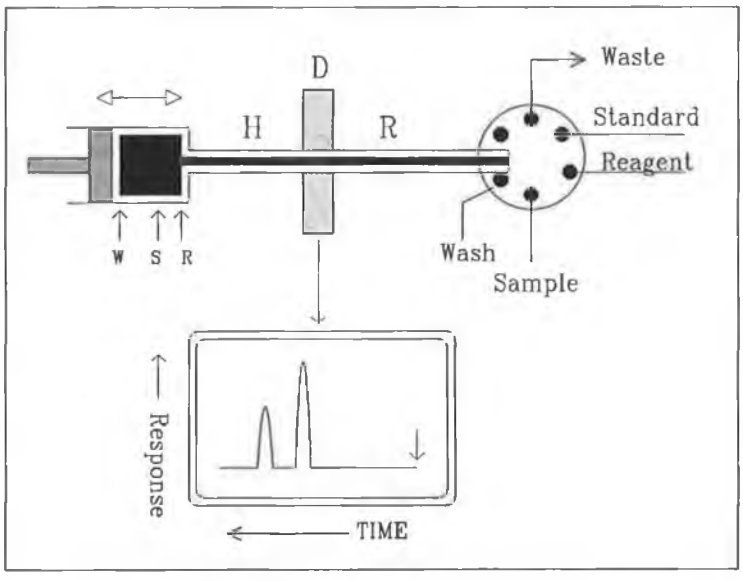

Figure 3.2. Principle of sequential injection analysis (taken from Ruzicka and Marshall [97])

Their description of the principle of SIA was as follows: each measurement cycle begins by aspirating a wash solution (S), reagent injection (R) and measurement during a backward movement of a piston type pump. In this way, well defined zones are injected sequentially into a conduit which serves as a reactor (R), flow-through detector (D) and holding reservoir. Mutual dispersion of the injected zones is achieved through the programmed movement of the zones towards the detector. The measurement cycle is terminated when the flow is reversed and the mutually dispersed zones are propelled back through the system and finally to waste. SIA has one

considerable advantage over FIA, which is a considerably reduced consumption of solvent, usually of the order of 1/10 less. The system was applied to the determination of pH using an optrode sensor which measured changes in the absorbance of the pH indicator bromothymol blue.

The use of a peristaltic pump to replace to a syringe pump has also been reported [98]. The reproducibility of both types of pump were examined by aspirating first 250 μl of 0.01 M sodium tetraborate buffer and then different volumes of 2.56×10^{-4} M Bromothymol Blue. The flow was then reversed and both the dye and the buffer segments were flushed through the detector while the absorbance was continuously monitored. The performance of the peristaltic pump relative to that of the syringe pump was found to be satisfactory with a RSD of 1-2%. The authors also discussed the advantages of the peristaltic pump over the piston pump for sequential analysis. They concluded that the main advantages were as follows:

(i) wash aspiration is unnecessary therefore a shorter sampling cycling can be used;

(ii) simpler system design and operation is possible;

(ii) wide availability of peristaltic pumps.

A schematic for a SIA system utilising a peristaltic pump is shown in Figure 3.3.

3.2 Fountain Cell Design

Schematic diagrams of the fountain cell components are presented in Figures 3.4 to 3.8. The diagrams are drawn on a 1.1 scale. The cell is composed of the following principle parts:

- working electrode assembly (labelled part A);
- working electrode assembly II (labelled part A.2);

- counter electrode assembly (labelled part B);
- reference electrode and waste collection assembly (labelled part C);

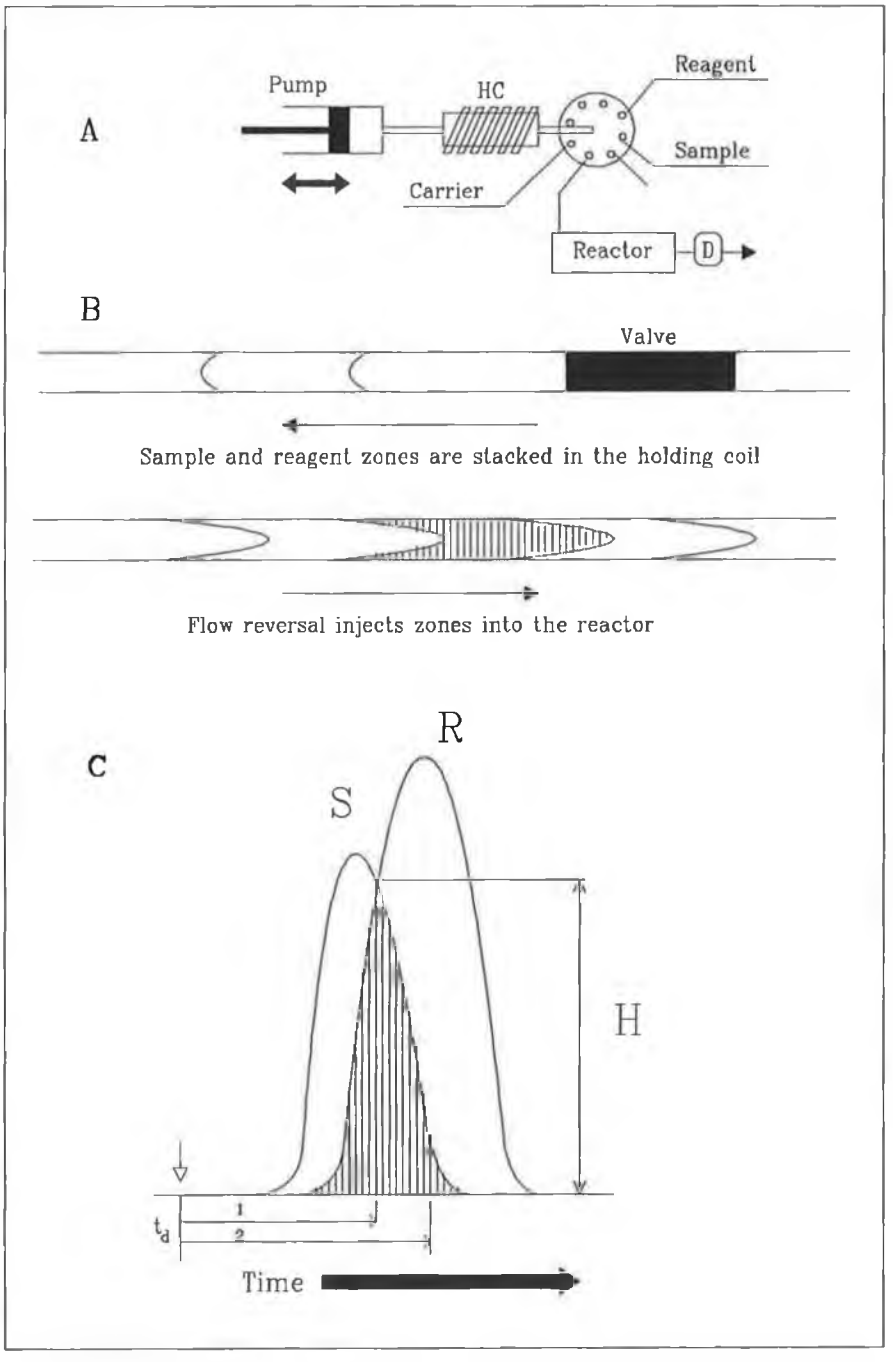

Figure 3.3 Principle of sequential injection analysis. (A) system schematic; (B) structure of stacked and injected zones; (C) concentration profiles as observed by the detector. HC, Holding coil; D, detector; S, sample; R, reagent; H, peak height; I, point of injection (taken from Ruzicka [99]).

3.2.1 Fabrication of Working Electrode Assemblies

These assemblies consisted of 44.0 × 44.0 × 8.5 mm perspex blocks into which ø2 × 6 mm long glassy carbon rods were sealed. For assembly A the glassy carbon rods were positioned 5 mm from the centre point in the block in a cross like geometry (4 electrodes). The electrodes in the array designated A.2 were positioned in a linear arrangement in geometric alignment with the inlet. Electrical connections to the electrodes were established via silver wires which were pressed fitted to the sides of the carbon rods (see Figure 3.4). The silver wires were then soldered to 2 mm brass pins which served as the connection points for the potentiostat. The electrodes were sealed in position with methylacrylate glue to ensure a water tight seal. Newly constructed arrays were firstly polished with 400 grade silica carbide paper and then sequentially with 600, 1000 and 1200 grade paper. The electrodes were finally polished to a mirror finish with 0.30 μm alumina and 0.05 μm alumina. The arrays were polished with both 0.3 μm and 0.05 μm alumina prior to each experiment and washed with deionised water to remove any particulate matter.

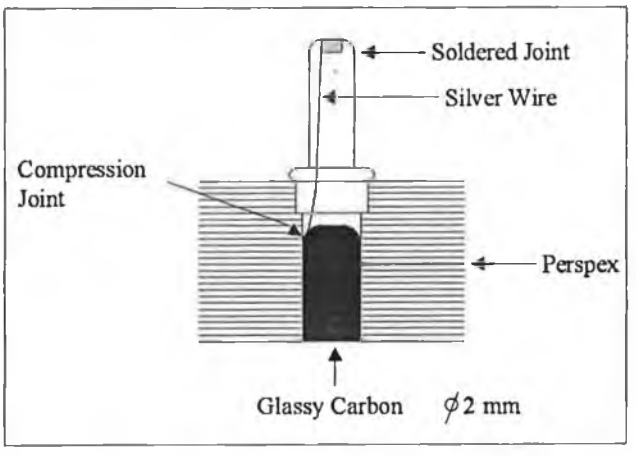

Figure 3.4 Working electrode assembly details.

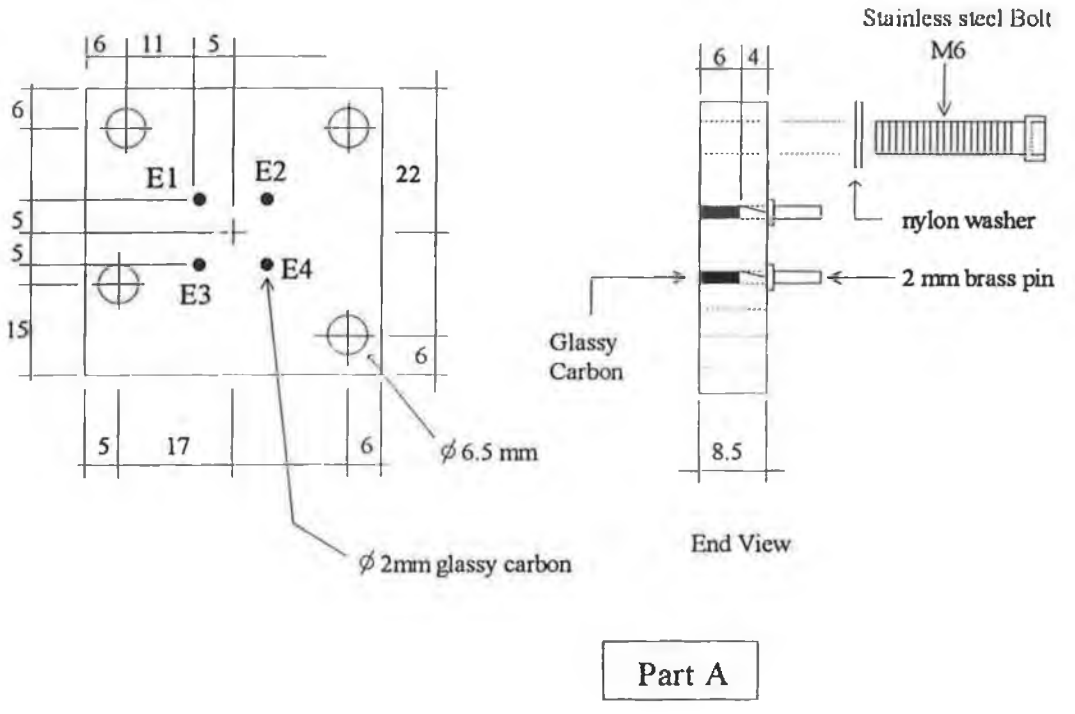

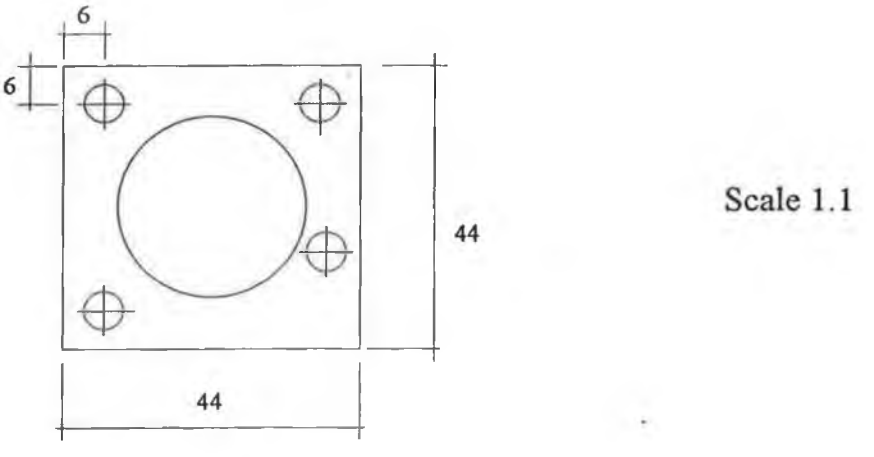

Teflon Spacers- 0.1, 0.25, 0.5 mm thickness

Figure 3.5. Working electrode assembly

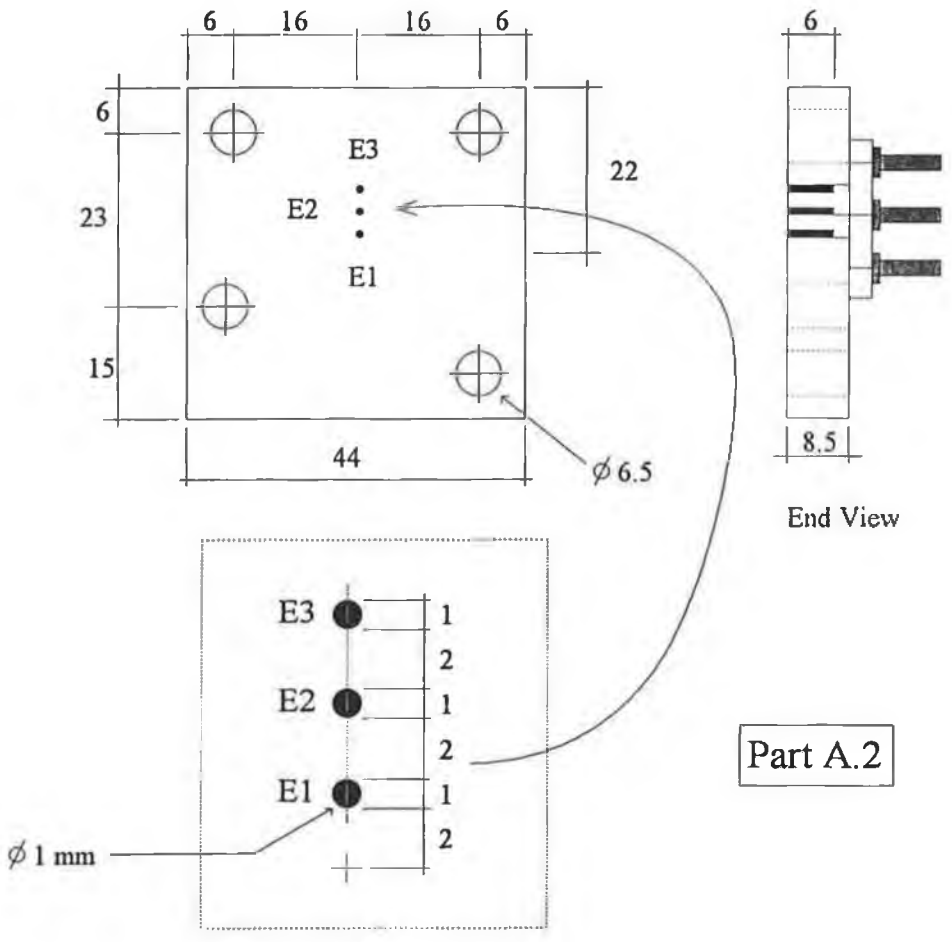

Figure 3.6. Working electrode assembly 2.

3.2.2 Counter Electrode Assembly

The counter electrode assembly was fabricated as shown in Figure 3.7. A ø2 mm pin screwed into the side of the assembly was used to attach the counter electrode cable. The face of the assembly containing the well was polished to a mirror finish to ensure a smooth fluid flow with silica carbide paste and then finally with silica carbide paper (400 grade) to the required finish. Seven M4 stainless steel bolts were used holding the plate in position with the reference electrode and waste collection assembly. The heads of the bolts were counter-sunk to ensure a water-tight seal with the Teflon spacer and working electrode assembly.

3.2.3 Reference Electrode and Waste Collection Assembly

Fabrication of this section of the flow cell was as outlined in Figure 3.8. M4 and M6 helicores were fitted to all holes to hold the assembly bolts. O-ring seals were fitted into the waste collection trench to reduce the volume without which an insufficient volume would have been maintained in the trench to cover the reference electrode. A special "key" was fabricated which allowed easy removal of the FIA connections from their recessed positions.

A view of the assembled flow cell is presented in Figure 3.9. The cell was held in a retort stand via the clamp arm during measurements.

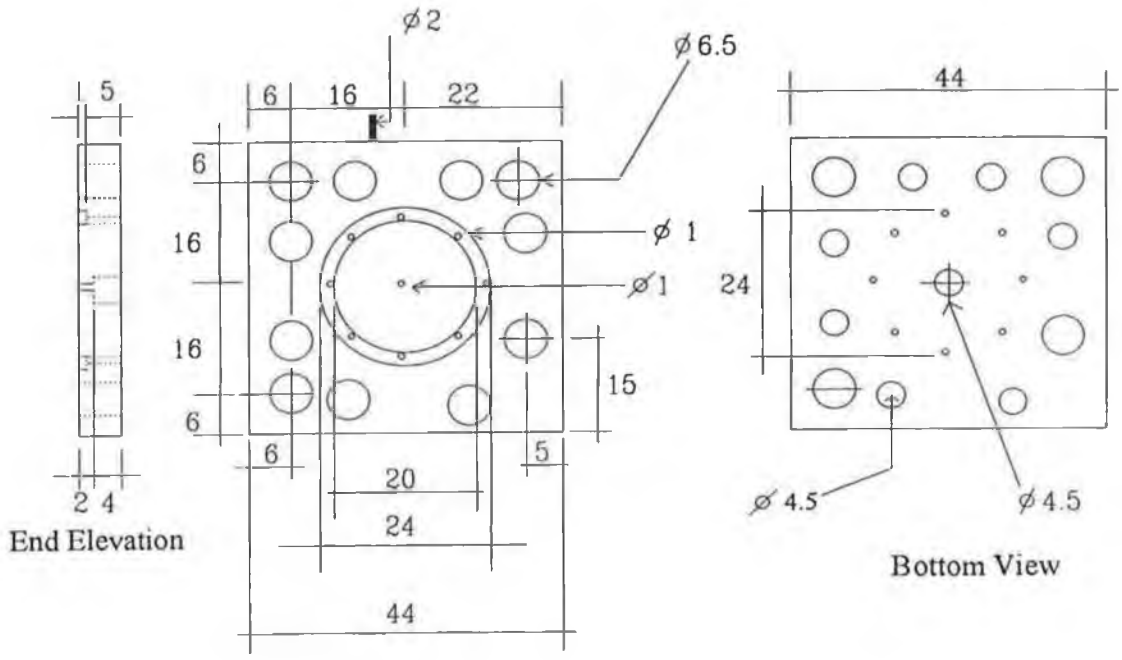

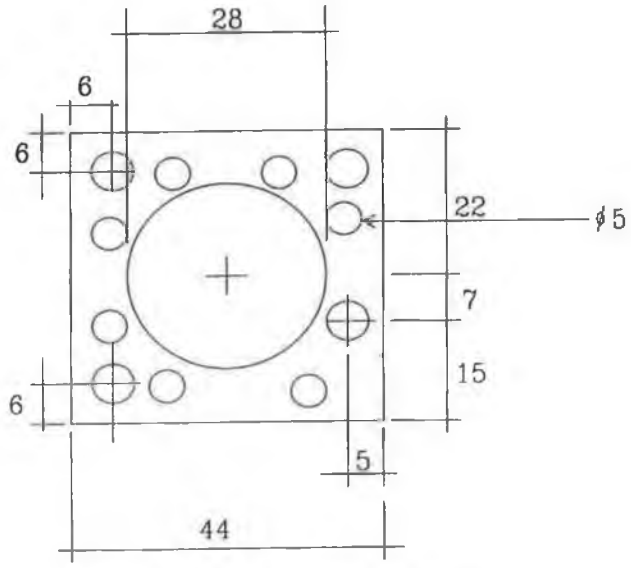

Figure 3.7. Counter electrode assembly.

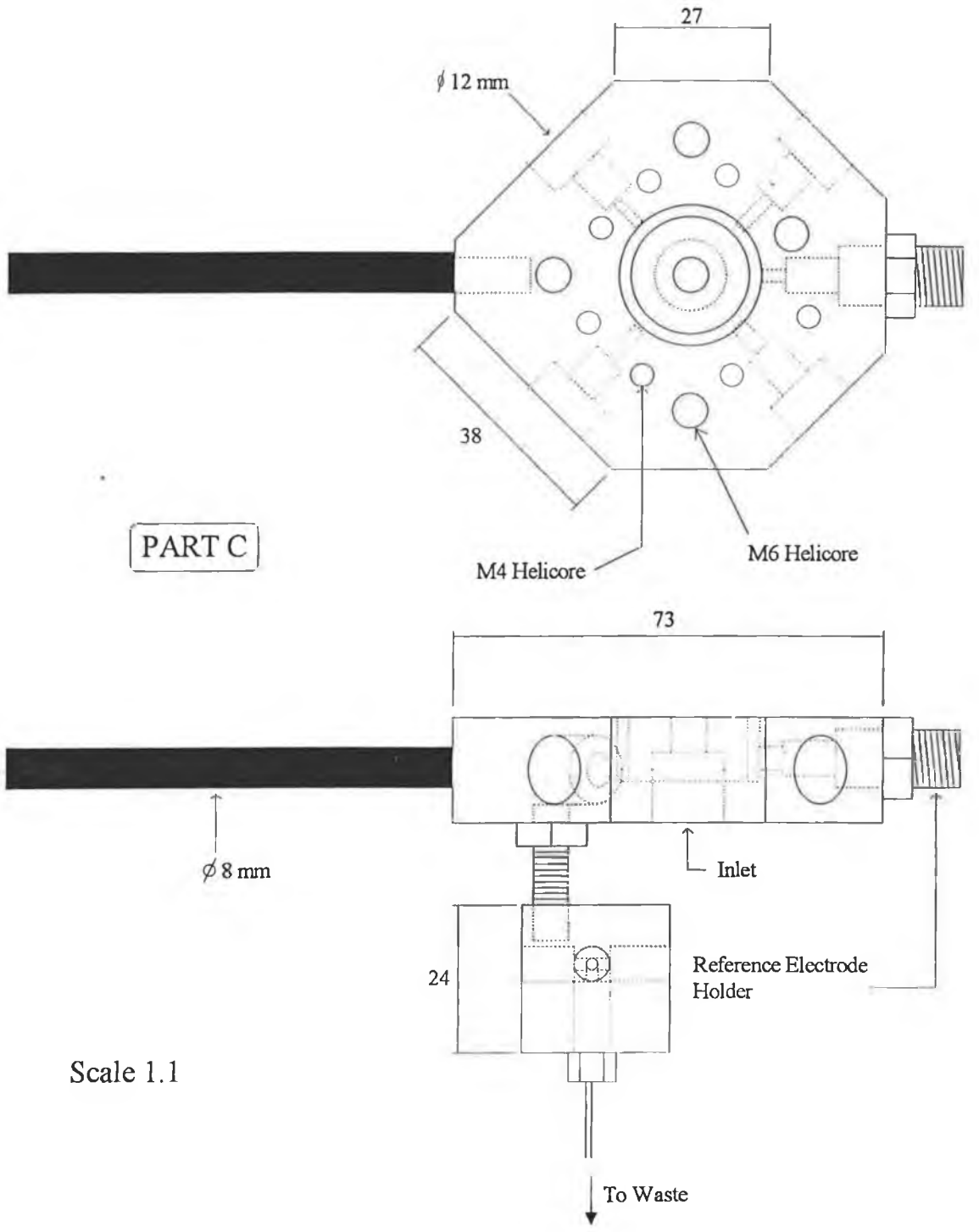

Figure 3.8. Reference electrode and waste collection assembly.

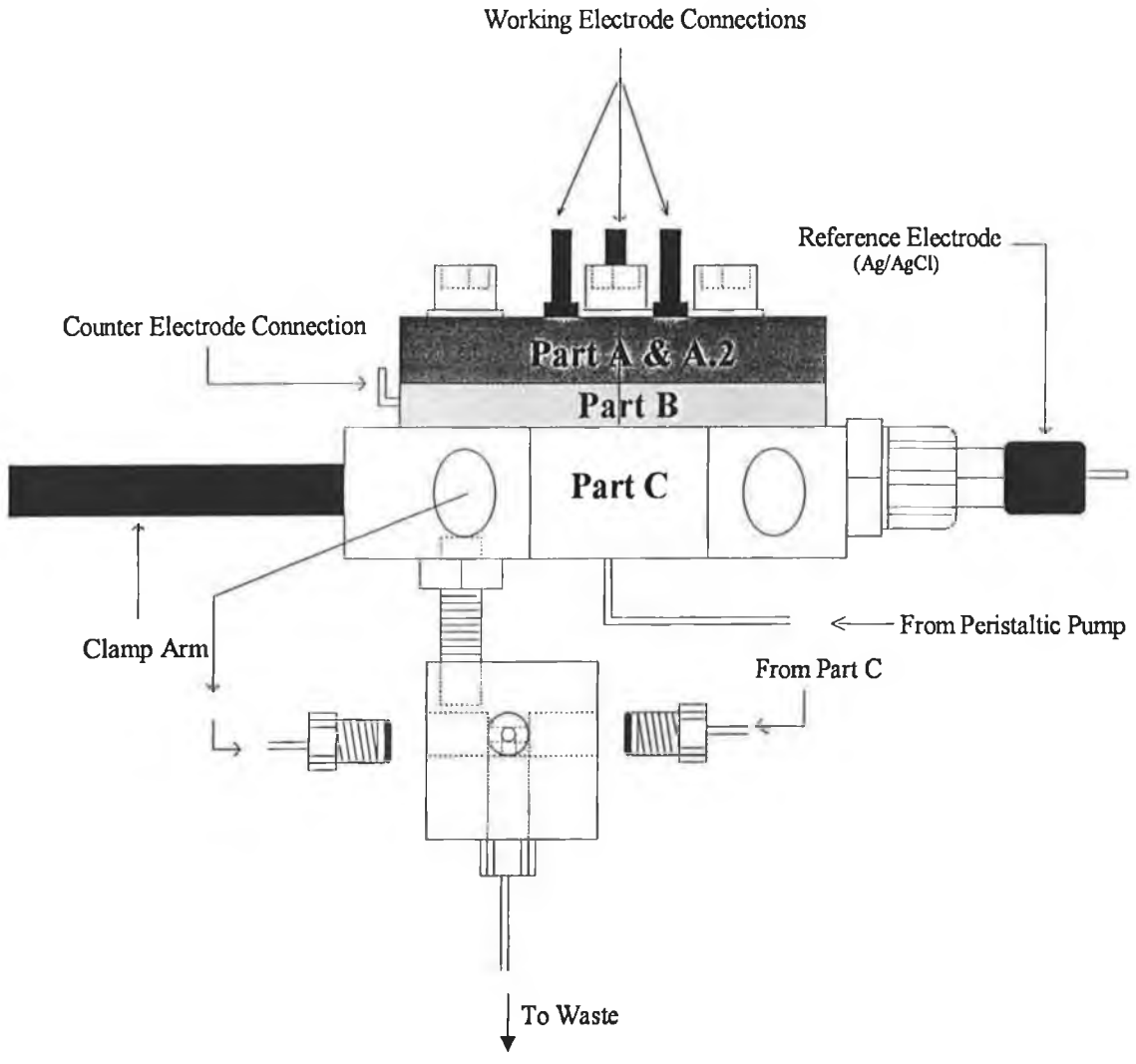

Figure 3.9. Assembled fountain cell.

3.3 Cell Volume and Dead Volume

The total cell volume was calculated to be 247.9 µl with a 0.25 mm spacer. This consisted of a trench volume of 171.0 µl and an electrode area volume of 76.9 µl. In normal thin layer flow cells the dead volume of the flow cell can be defined as the geometric cell volume [30-32]. However, in the case of the fountain cell, this is

probably not applicable as the carrier stream retained in the trench no longer has any direct bearing on the flow behaviour at the electrodes. Therefore the dead volume of the cell can be defined as the volume of liquid in contact with the electrode array which is 76.9 μl. This dead volume is probably satisfactory for FIA and SFA techniques but may need to be reduced for applications with chromatography which requires cells with smaller dead volumes to prevent peak overlap and band broadening.

3.4 Experimental

3.4.1 Chemicals

Potassium hexocyanoferrate(II), anhydrous sodium acetate, sodium chloride, pyrrole and glycine were all purchased from Merck GmbH, Germany. All chemicals used were of analytical grade. Deionised water used for the preparation of aqueous solutions was obtained by passing denionised water through a Milli-Q water purification system (Millipore). Electroactive solutions were prepared fresh each day prior to use and degassed with argon prior to use.

3.4 2 Sequential Injection Analysis System

The layout of the of the SIA system incorporating the fountain cell is shown in Figure 3.10. This system configuration was used for all the evaluation studies. All components in the system were under computer controlled except for the potentiostat which functioned independently and required manual setting. The SFA system consisted of a peristaltic pump (Alitea, Sweden), an 8-channel multi-port valve

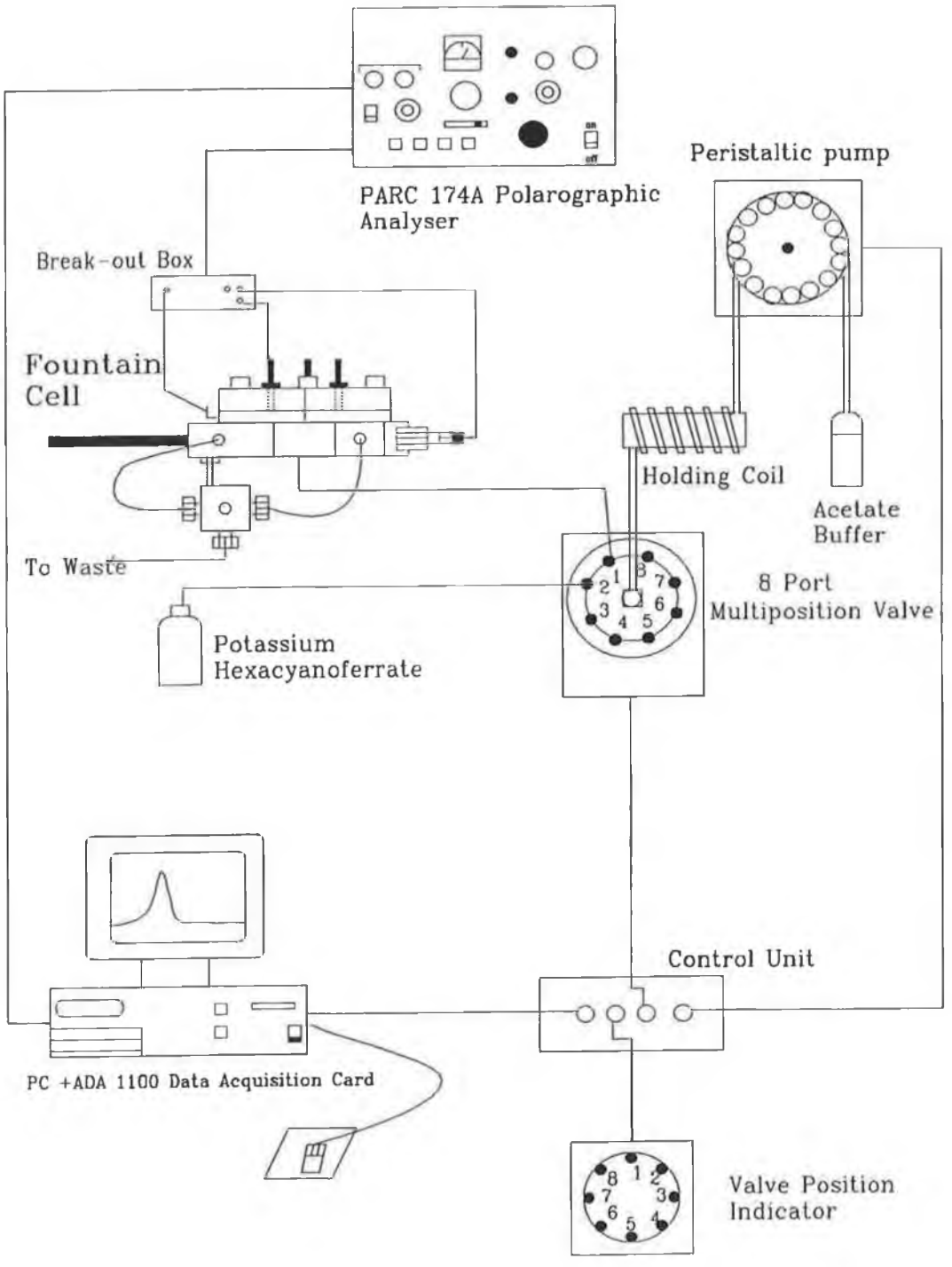

Figure 3.10. Schematic of SFA with the fountain cell.

(Pharmacia, LKB, Sweden), a pump and valve control unit (constructed "in house") and a valve position indicator unit (constructed "in-house"). A single channel PARC 174A potentiostat (EG&G) was used for electrode polarisation and current monitoring duties. The carrier stream was 1.0 M sodium acetate buffer for the characterisation studies. A 0.1 M sodium chloride for all polymerisation studies.

3.4.3 ADA 1100 Data Acquisition\Control Card (Real Time Devices)

An ADA-1100 card was used for all instrumentation control functions (except control of the 174A polarographic analyser) and data acquisition duties. The base address for the card was 300

Hex. A sampling rate of 5 points per second was normally used for most experiments. The ADA interface consists of:

1. 8 single-ended analog inputs with an input impedance of > 10 MΩ. The inputs were configured to bipolar operation ± 10 V;
2. 24 digital I/O lines which were TTL/CMOS compatible. The A/D conversion was successive approximation with 12 bit resolution and a system throughput of up to 38 KHz;
3. 2 analog outputs (12-bit resolution).

A FIA LAB software package, β release (Alitea, USA), was used for control of the instrumentation and data acquisition. The software package was written specifically for the I/O cards from Real Time Devices, Inc. Hardware operations were listed in event tables. The instructions in these event tables were executed sequentially. A typical event table is shown in Table 3.1. The time required for the data acquisition

step (event no.3) was dependent on the flow rate used. Typically a data acquisition time of 80 s was utilised with a pump flow rate of 20% (0.6 ml/min), 60 s with flow rate of 40% (1.2 ml/min) and so forth with higher flow rates.

Event No.	Time (s)	Duration (s)	Pump Speed %	Valve Position	Potential (mV)	Data Acquisition	Title
1	0.00	20.00	60	1	+300.0	off	clean
2	20.00	8.00	-30	2	+300.0	off	sample
3	28.00	45.00	30	1	+300.0	on	analyse
4	73.00	20.00	30	1	+300.0	off	clean

Table 3.1 Typical event table for SIA system operation. A negative sign (-) in the pump speed indicates operation of the pump in the reverse direction. The PARC 174 A was used throughout for potential application.

3.5 Results and Discussion

3.5.1 Reproducibility of Response

The reproducibility of response at electrode 1 (see Figure 3.5) to 8 injections of 10 mM potassium hexacyanoferrate(II) was investigated. A %RSD of 0.89% was calculated for 8 repetitive injections. The responses obtained are shown in Figure 3.11. A high degree of reproducibility in both the peak shape and response magnitude were obtained. This would indicate both reproducible flow conditions and dispersion characteristics are experienced at one electrode.

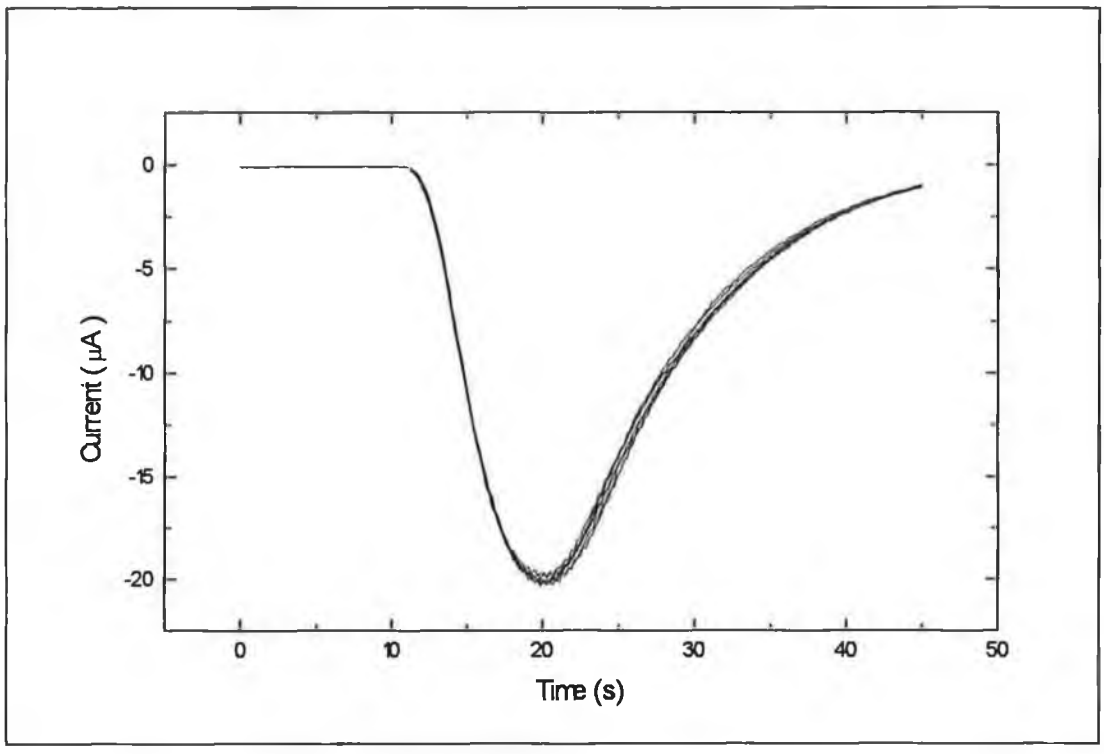

Figure 3.11 Responses obtained to 8 injections of 0.01 M potassium hexacyanoferrate(II) at electrode 1. Mobile phase 1.0 M sodium acetate buffer, flow rate 0.9 ml/min, sample volume 160 μl, potential +300 mV vs. Ag/AgCl.

The reproducibility of response of the each electrode in the array was then investigated. The responses at each electrode to 8 injections of 0.2 mM hexacyanoferrate(II) were monitored; a summary of the results obtained are presented in Table 3.2. The responses of electrodes 1-3 are presented because of an excessively large background observed at electrode 4. This was probably due to poor sealing of the electrode into the perspex block which may have allowed accumulation of fluid around the electrode body. The reproducibility of response at each electrode was found to be high; however, the inter-electrode response time reproducibility was poor. The %RSD in the response time of the individual electrodes was calculated to be 13.6%.

Electrode No.	%RSD n = 8	Average Response Time (s)
1	1.8	23.7
2	2.2	27.1
3	2.0	19.1

Table 3.2. Reproducibility of electrode responses to 8 injections of 0.2 mM hexacyanoferrate(II).

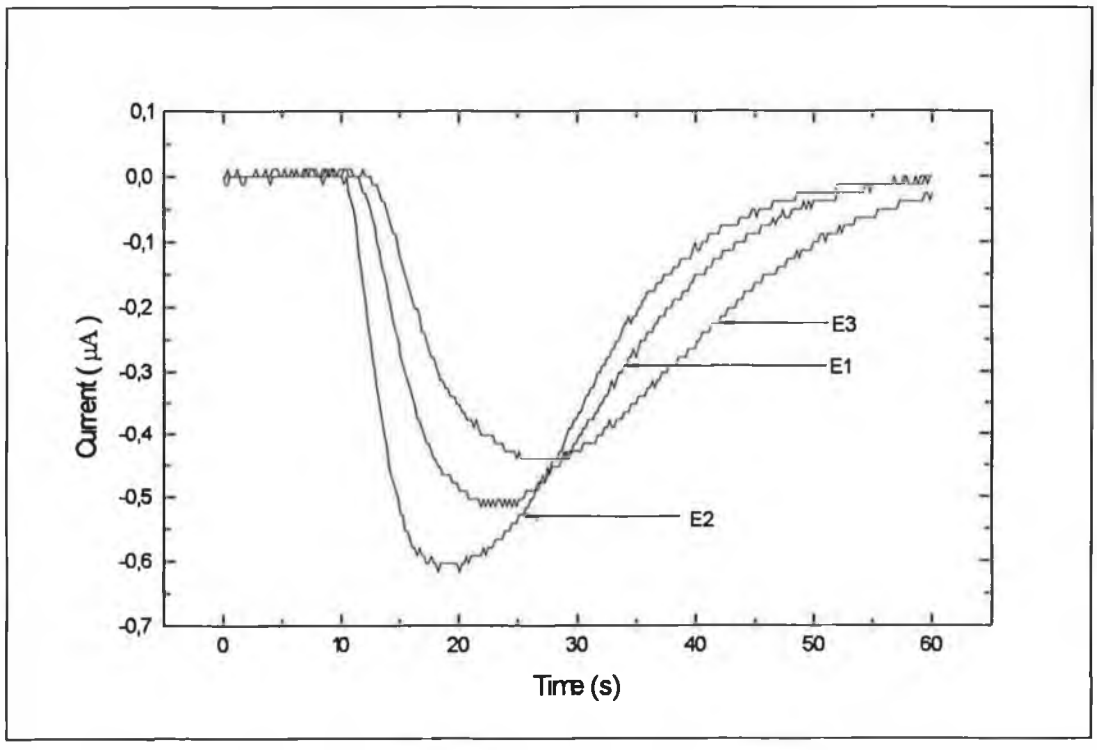

Figure 3.12. Average responses at electrodes 1, 2, and 3 to 8 injections of 0.2 mM hexacyanoferrate(II). Flow rate 0.9 ml/min, potential +300 mV vs. Ag/AgCl.

The average response from each electrode is presented in Figure 3.12. It is clear from Figure 3.12 that significant differences existed between both the peak shapes and magnitudes of response at each electrode. The two main reasons for these differences

were concluded to be:

1. non-ideal electrode behaviour;
2. non-ideal flow behaviour.

These conclusions resulted in further investigations of how changes both in the flow rate and the cell volume parameters affected the response characteristics of each electrode in the array.

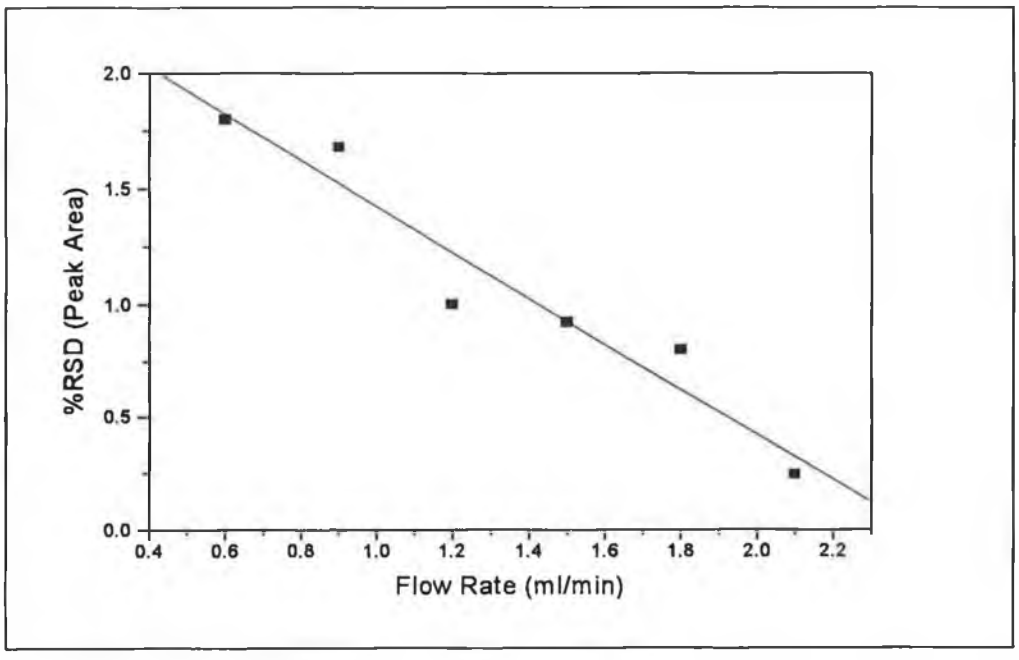

Figure 3.13. Plot of flow rate vs. relative standard deviation of peak area for 3 injections of hexacyanoferrate(II) at flow rates in the range 0.6-2.1 ml/min at electrode 3.

A plot of flow rate vs. %RSD (peak area) is shown in Figure 3.13. The data set was taken at electrode 3. The plot indicates that the %RSD decreases with flow rate. It is unclear whether this decrease in %RSD is linear or non-linear in nature. A linear regression coefficient of 0.966 was obtained for the plot.

The effect of flow rate on the reproducibility of response time was also investigated. A summary of the results obtained are presented in Table 3.3. The results indicate that the %RSD decreases with flow rate with the lowest %RSD's being observed in the range 1.5 to 2.1 ml/min.

Flow Rate (ml/min)	%RSD
0.6	1.95
0.9	1.70
1.2	1.03
1.5	0.67
1.8	0.01
2.1	0.89

Table 3.3. The effect of flow rate on the reproducibility of response time.

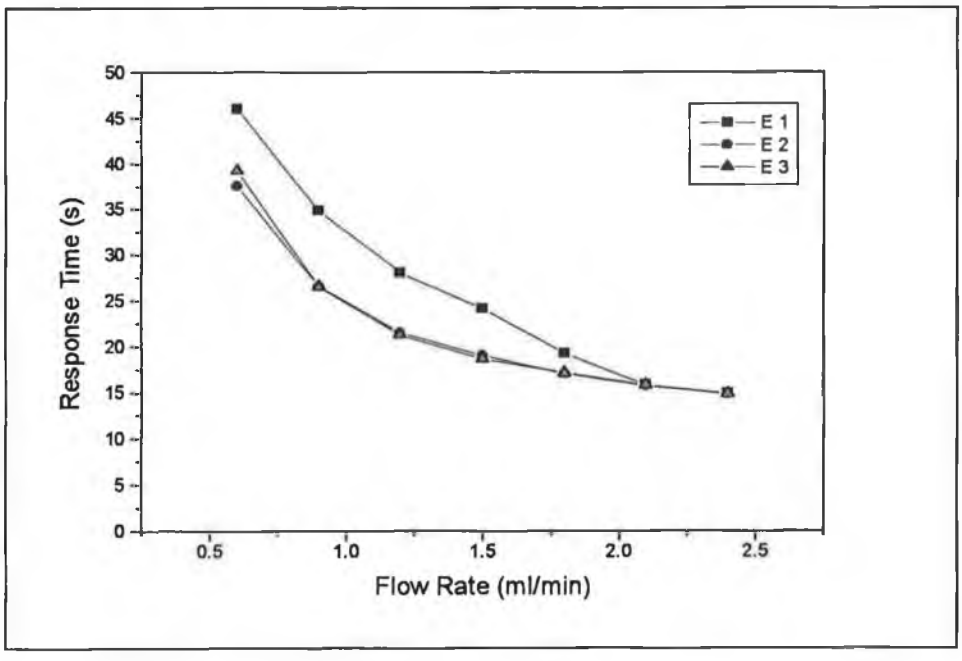

Figure 3.14. Plot of flow rate vs. response time at E1, E2 and E3 for a 0.5 mm Teflon spacer.

From plots of flow rate vs. response time using spacers of 0.1, 0.25 and 0.5 mm thickness, the best correlation between the electrode response times and the flow rate was obtained with a spacer of 0.5 mm (see Figure 3.14). It is believed that the sample plug can develop geometrically more evenly in all directions with the 0.5 mm spacer and consequently the plug reaches the electrodes at approximately the same time.

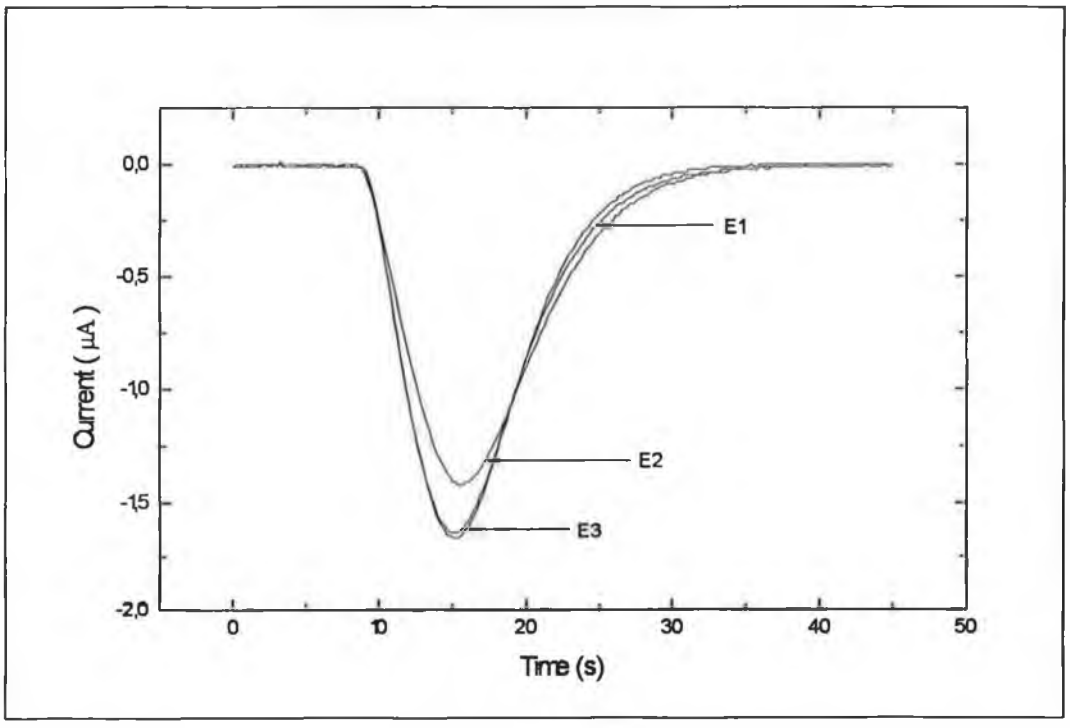

Figure 3.15. Responses to injections of 1 mM hexacyanoferrate(II) at E1, E2, E3, flow rate 2.1 ml/min, spacer thickness 0.5 mm.

The responses in Figure 3.15 demonstrate the improvement in both the reproducibility of the peak shape and the response magnitude as compared to those presented in Figure 3.12. Closer approximation to true fountain cell behaviour may account for the improved response characteristics observed in Figure 3.15. The differences in the responses are probably due to differences in the electrode kinetics with a minimal contribution from the flow conditions.

3.5.2 Flow Cell Characterisation

In characterisation of electrode systems in a flow stream, a plot of $\log_{10}$ charge (Q) (for these experiments Q = peak area) vs. $\log_{10}$ flow rate (U) should yield straight line data within experimental limits. The slopes for such plots should identify the type of flow behaviour. These will not necessarily be exact slopes, but lie in certain ranges. It is generally accepted that such an experiment will yield slopes as follows for given flow behaviour types [29, 40]:

- wall jet; -0.23 to -0.33
- planar; -0.48 to -0.58
- plate (thin layer); -0.65 to -0.74

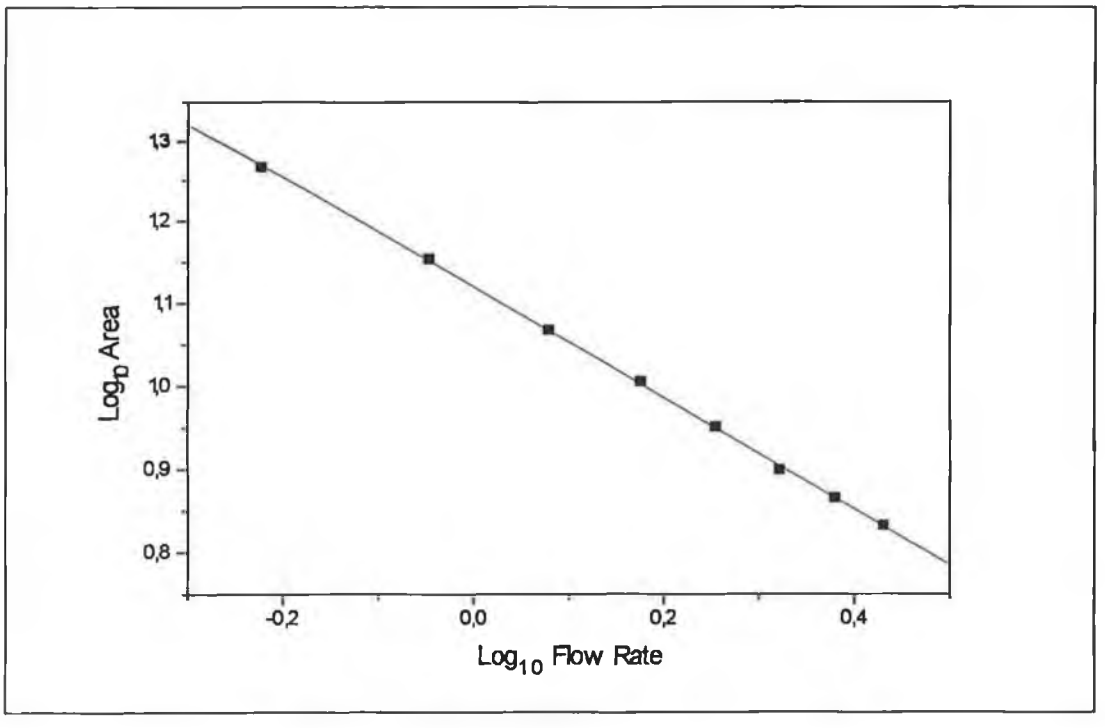

Figure 3.16 Plot of $\log_{10}$ flow rate versus $\log_{10}$ area for injections of 10 mM hexacyanoferrate(II) at electrode 3 with a spacer thickness of 0.25 mm.

A plot of $\log_{10}$ flow rate versus $\log_{10}$ area for electrode 3 to injections of 10 mM hexacyanoferrate(II) yielded a plot with a slope of -0.666 (see Figure 3.16). This indicates that thin layer flow conditions were observed at this electrode under these conditions. The effect of spacer thickness on the flow characteristics of the cell were then investigated. Plots of $\log_{10}$ flow rate versus $\log_{10}$ area were prepared for each electrode with spacer thickness of 0.1, 0.25, 0.5 mm (see Figure 3.17 (a), (b) and (c)).

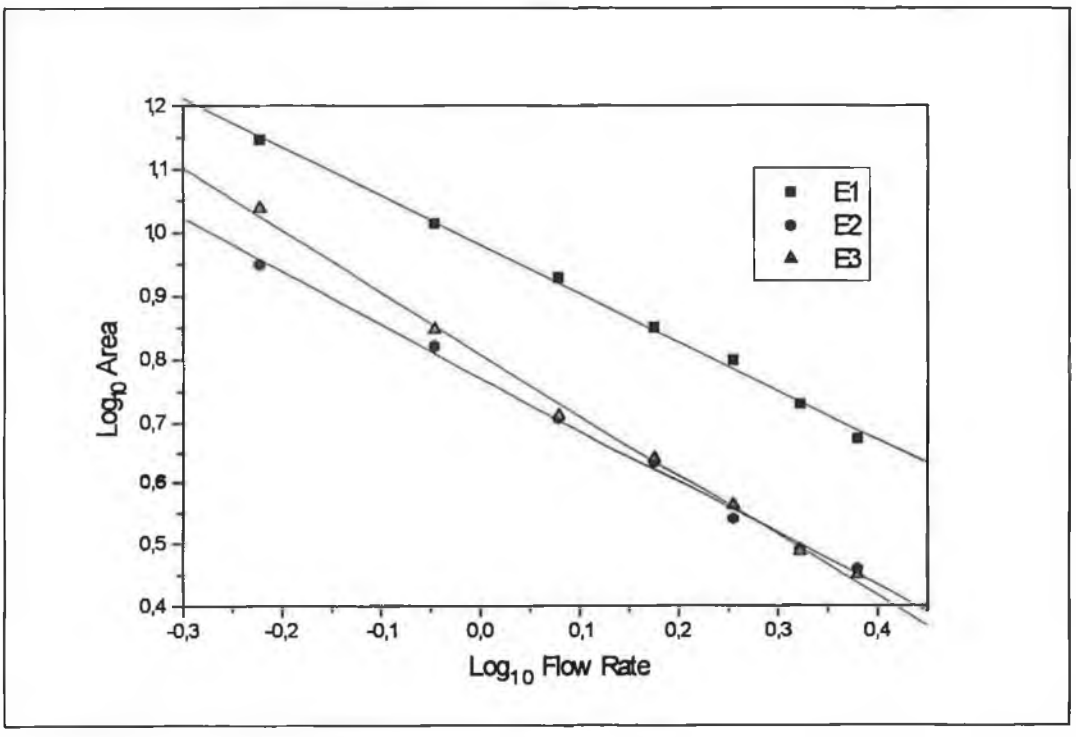

Figure 3.17(a) Plot of $\log_{10}$ flow rate versus $\log_{10}$ area for a 0.1 mm spacer at electrodes 1, 2 and 3.

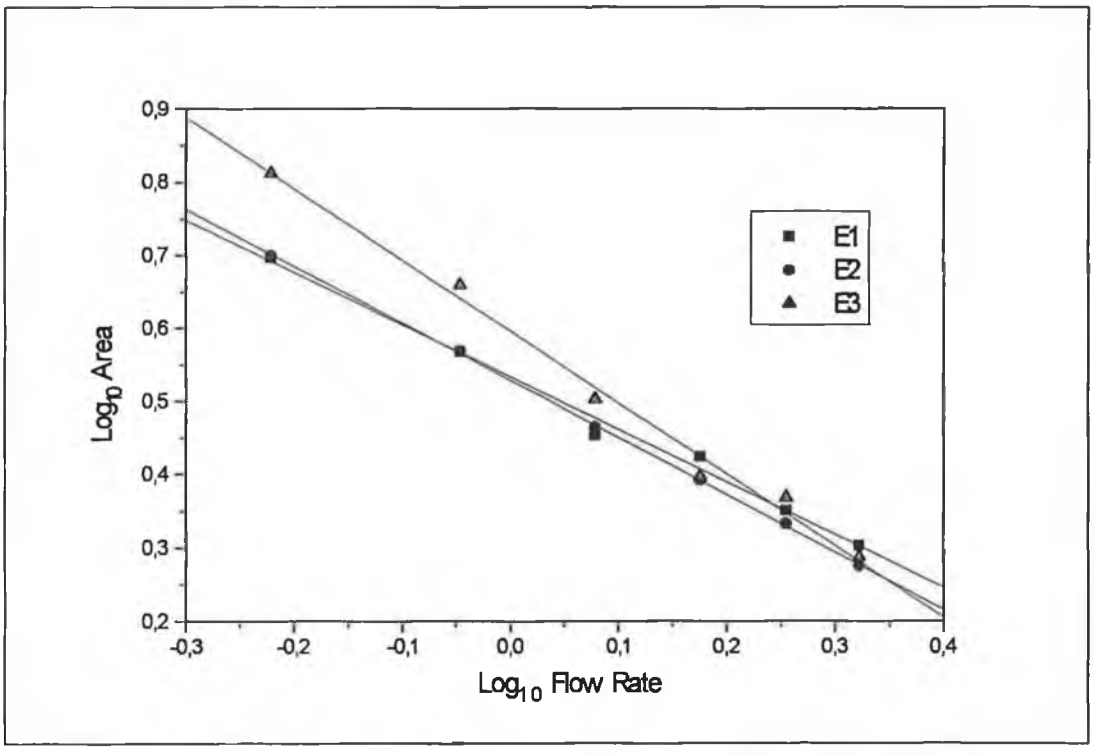

Figure 3.17(b) Plot of $\log_{10}$ flow rate versus $\log_{10}$ area for a 0.25 mm spacer at electrodes 1, 2 and 3.

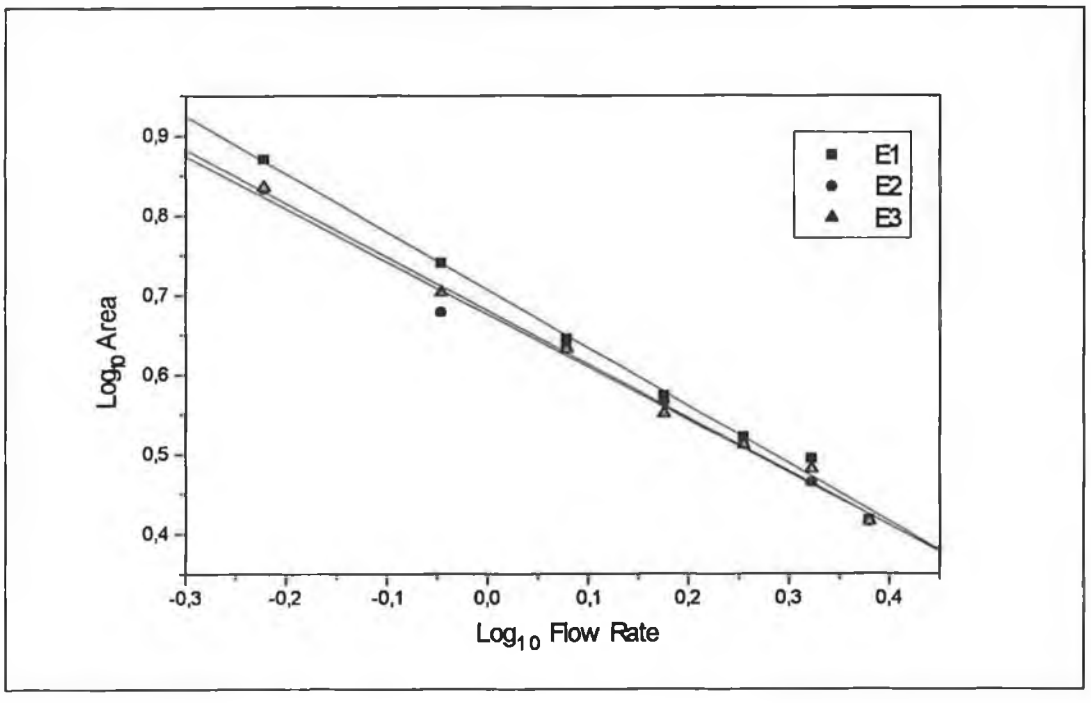

Figure 3.17(c) Plot of $\log_{10}$ flow rate versus $\log_{10}$ area for a 0.5 mm spacer at electrodes 1, 2 and 3.

A summary of the experimental slopes obtained together with the theoretical slopes are presented in Table 3.4.

Spacer Thickness (mm)	Electrode No.	Linear Regression Coefficient (R)	Theoretical Slope	Experimental Slope
0.10	1	0.9984	-2/3	-0.74
	2	0.9980	-2/3	-0.80
	3	0.9984	-2/3	-0.95
0.25	1	0.9998	-2/3	-0.72
	2	0.9953	-2/3	-0.78
	3	0.9960	-2/3	-0.97
0.50	1	0.9976	-2/3	-0.73
	2	0.9950	-2/3	-0.69
	3	0.9974	-2/3	-0.68

Table 3.4 A summary of the data obtained from plots of $\log_{10}$ flow vs. $\log_{10}$ area for the individual electrodes in the array.

The results indicate again that the spacer thickness plays a significant role in influencing the flow characteristics at the electrode array. The most uniform behaviour is obtained with a spacer of 0.5 mm thickness. All electrodes were observed to demonstrate thin layer characteristics with this spacer. It is believed that with the other spacers the sample plug is constricted in it's development. As a result the sample plug

is detected faster on one side of the cell than the other. A deeper well may help to improve the situation by ensuring a more even development of the sample plug in all directions or a reduced number of outlet holes.

3.5.3 Linear Electrode Configuration

The response characteristics of a linear electrode arrangement (labelled part A.2, see Figure 3.6) were investigated. The response obtained at each of the electrodes at a flow rate of 1.2 ml/min with spacers of 0.1, 0.25 and 0.5 mm are presented in Figure 3.18(a), (b), (c).

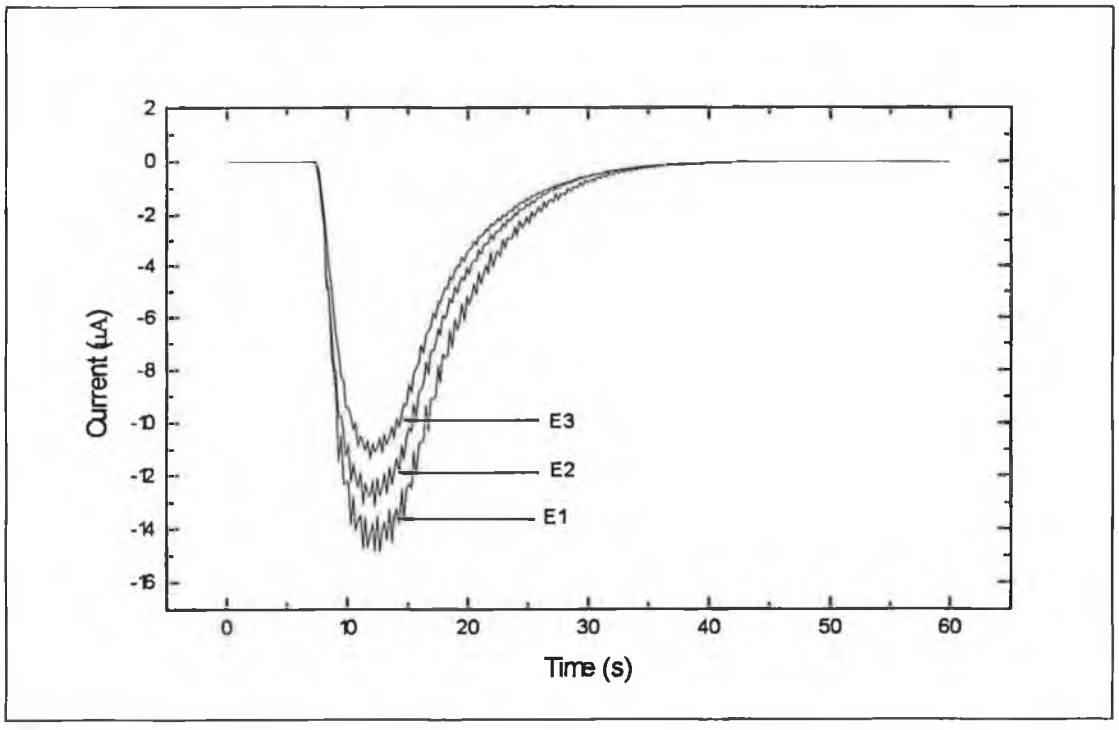

Figure 3.18(a) Responses obtained with the linear electrode configuration to injections of 10 mM hexacyanoferrate(II) using a spacer thickness of 0.1 mm and a flow rate of 1.2 ml/min.

The results indicate that diffusion of the sample plug was reduced with a spacer of 0.1

mm. The results with 0.1 and 0.25 mm spacers also indicate that the sample plug becomes narrower as it moves away from the inlet, which is an expected feature with fountain cell behaviour. The results obtained with a 0.5 mm spacer do not indicate this behaviour leading to the conclusion that diffusion of the sample plug was a significant process. The noise observed in the responses is probably due to pulse noise from the peristaltic pump. The reduced responses observed at electrodes 2 and 3 result from a number of factors. The velocity of the sample plug increases as it moves away from the inlet. Therefore the sample plug moves more rapidly over electrode 3 than over electrode 1 which has significant effect on the response. Secondly as the sample plug becomes narrower the amount of analyte that can be reduced or oxidised as the sample plug passes over the electrode is also diminished. There is also some contribution from diffusional processes.

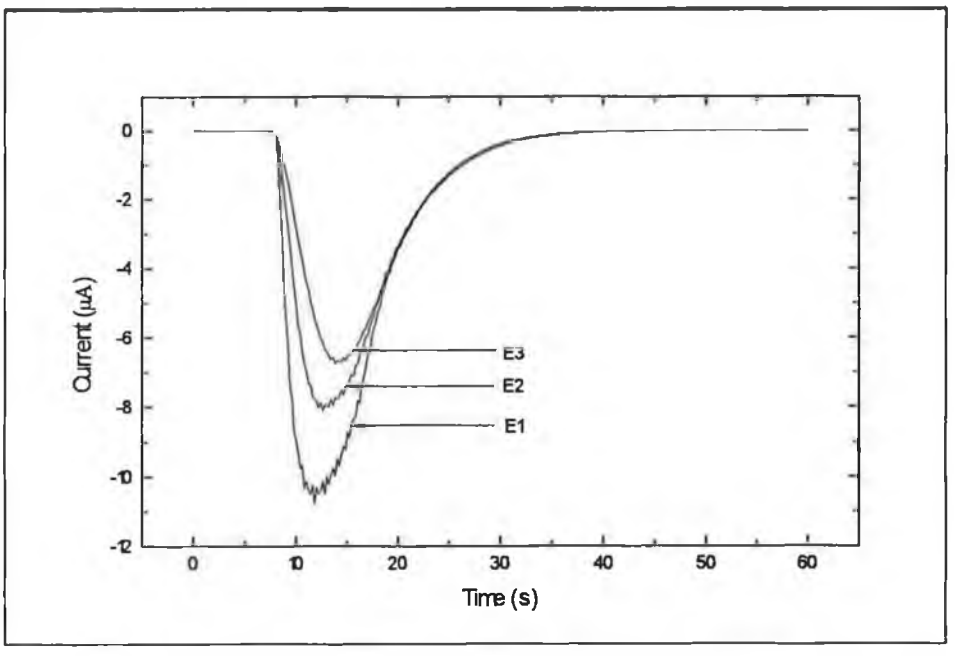

Figure 3.18(b). Responses obtained to injections of 10 mM hexacyanoferrate(II) at the linear array using a spacer thickness of 0.25 mm and a flow rate of 1.2 ml/min.

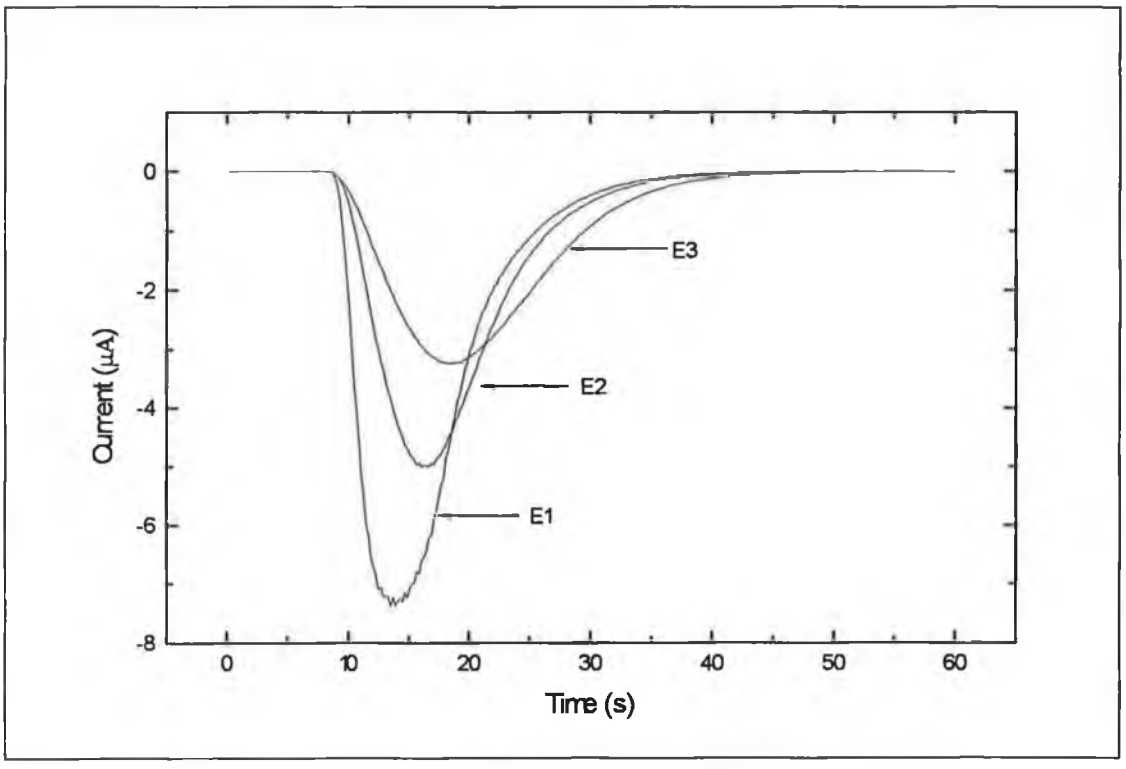

Figure 3.18(c). Responses obtained with the linear array to injections of 10 mM hexacyanoferrate(II) using a spacer of 0.5 mm thickness and a flow rate of 1.2 ml/min.

3.5.3.1 Flow Characterisation

Plots of log flow versus log area were prepared in an effort to establish if the flow behaviour was similar at each electrode. The plots indicate that each electrode experiences a very similar type of flow behaviour (see Figure 3.19). The slopes obtained for the plots were as follows:

E1 $\Rightarrow$ **0.76** (probable thin layer conditions)

E2 $\Rightarrow$ **0.74** (thin layer conditions)

E3 $\Rightarrow$ **0.73** (thin layer conditions)

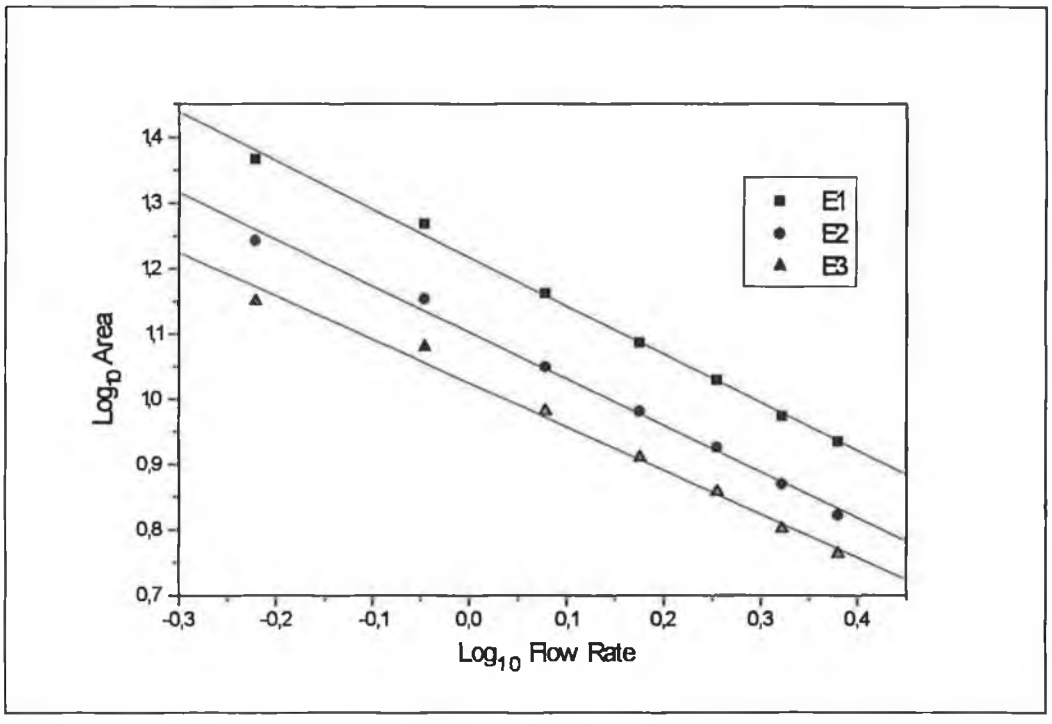

Figure 3.19. Plot $\log_{10}$ flow rate vs. $\log_{10}$ area for injections of 10 mM hexacyanoferrate (II) at electrodes 1, 2 and 3 in the linear electrode configuration.

The reproducibility of response under different flow conditions was also investigated. A summary of the results obtained are presented in Table 3.5. The results demonstrate that the %RSD of the electrode responses show little dependence on flow rate. The higher %RSD at E1 is probably a result of turbulence in the sample plug due to its close proximity to the inlet.

	% RSD		
Flow Rate (ml/min)	E1	E2	E3
0.9	1.2	0.7	0.7
1.8	1.3	0.8	0.8

Table 3.5. The %RSD of response (area) at each electrode at two different flow rates.

3.6 On-line polymerisation

An on-line method for the polymerisation of pyrrole was then developed using the fountain cell and the SFA system. The three different methods utilised were as follows:

1. static polymerisation;
2. stopped-flow polymerisation;
3. continuous-flow polymerisation.

The static polymerisation procedure involved pumping a plug of pyrrole (0.1 M in 0.1 M NaCl) of sufficient volume into the fountain cell, stopping the flow and polymerising at +800 mV for 3 minutes. The pyrrole was then was washed out of the cell to waste. The stop-flow polymerisation involved a similar procedure, however, two 5 second periods of carrier stream flow were utilised. The method used is outlined in Table 3.6

Time (s)	Pump State
60	off
5	on (0.6 ml/min)
60	off
5	on (0.6 ml/min)
50	off

Table 3.6. Event table for the stop-flow polymerisation procedure.

The final method utilised involved continuously flow of 0.1 M pyrrole in a 0.1 M NaCl carrier stream through the flow cell with the electrode held at a constant potential of

+800 mV.

Cyclic voltammograms (CV) for the polymer films obtained using these methods are shown in Figures 3.20-3.22. It was expected that the film thickness obtained with flow through polymerisation methods would be greater than those obtained with static polymerisation due to the increased rate of mass transfer to the electrode surface in a flowing stream. The results obtained indicate the reverse trend as exhibited in the CV's shown in Figures 3.20 to 3.22. This probably due the negative mechanical shearing effect of the flowing stream being dominant over the positive effect of increased mass transfer. It is believed that many of the initial oligomers formed are swept away in the carrier stream thus removing the necessary precursor sites for polymeric film formation.

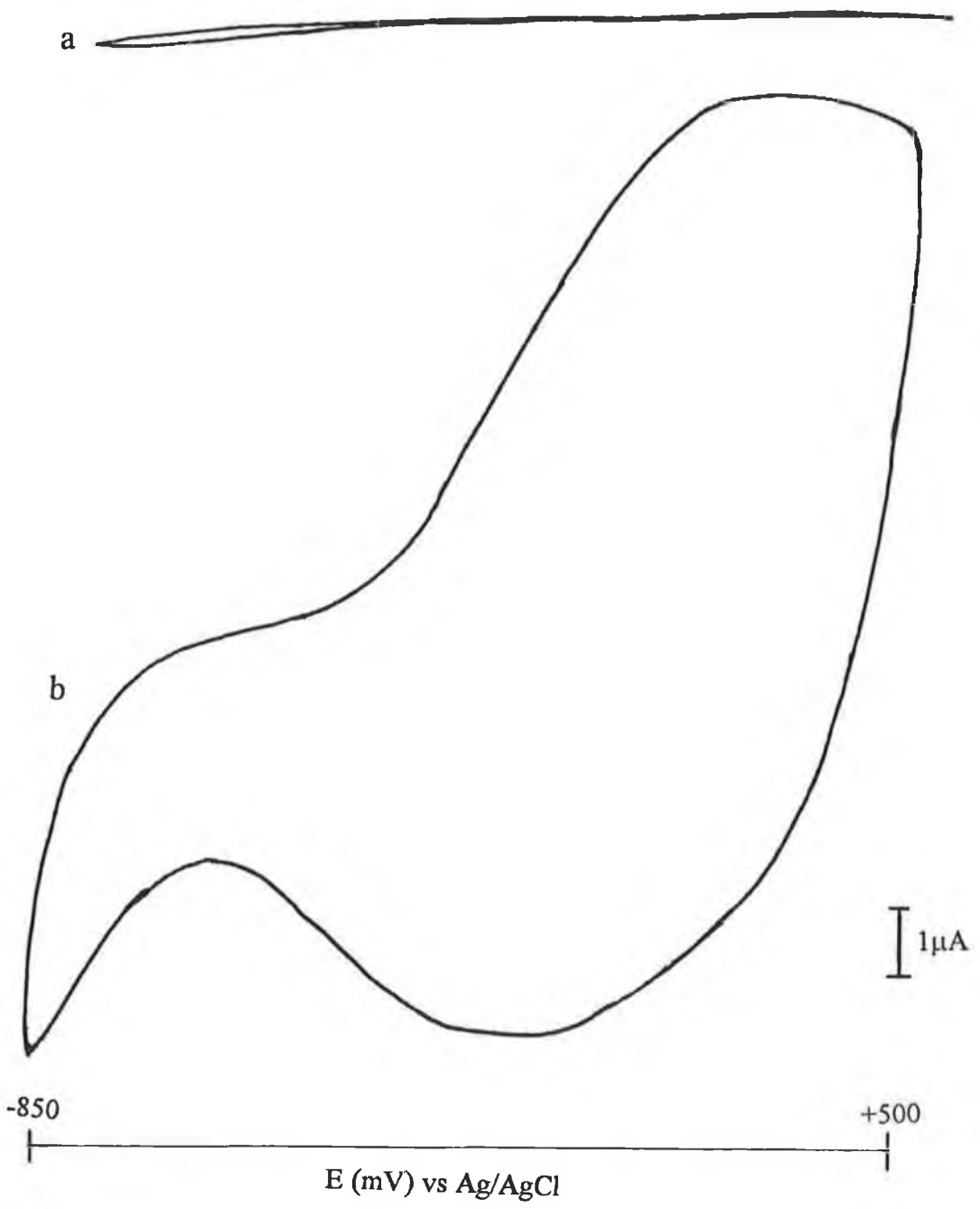

Figure 3.21

(a) Background scan in 0.1 M NaCl prior to polymerisation.

(b) Cyclic voltammogram of polypyrrole coated glassy carbon electrode in 0.1 M NaCl. The pyrrole was polymerised using a static polymerisation procedure in the fountain cell. Conditions: current range; 1 mA, sensitivity X axis; 100 mV/cm, sensitivity Y axis 10 mV/cm, scan rate 50 mV s^{-1}.

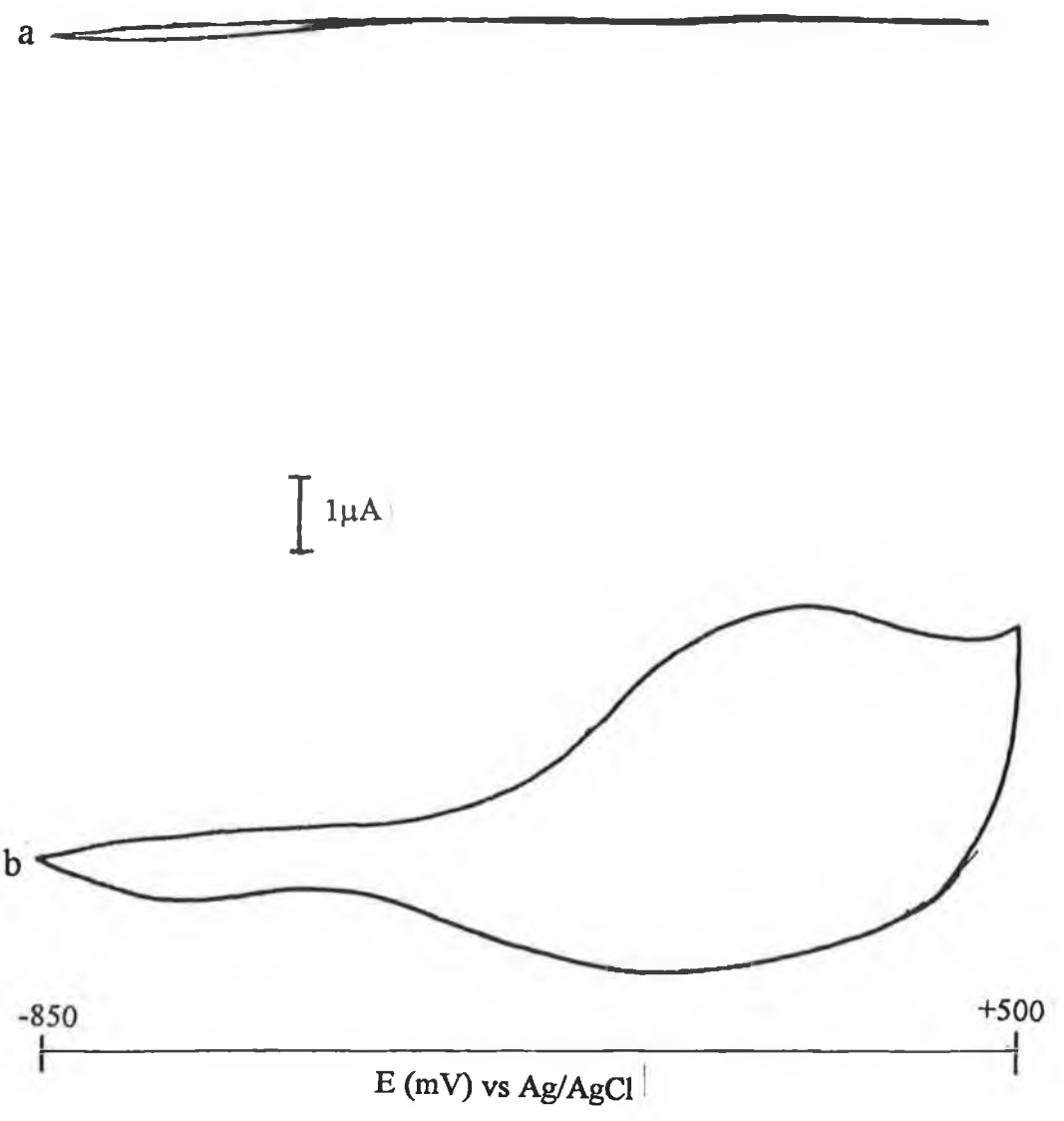

Figure 3.22 (a)

(a) Background scan in 0.1M NaCl prior to polymerisation.

(b) Cyclic voltammogram of polypyrrole-coated glassy carbon electrode in 0.1 M NaCl. The pyrrole was polymerised using a flow rate of 0.3 ml/min. Conditions: current range; 1 mA, sensitivity X axis; 100 mV/cm, sensitivity Y axis 10 mV/cm, scan rate 50 mV s^{-1}.

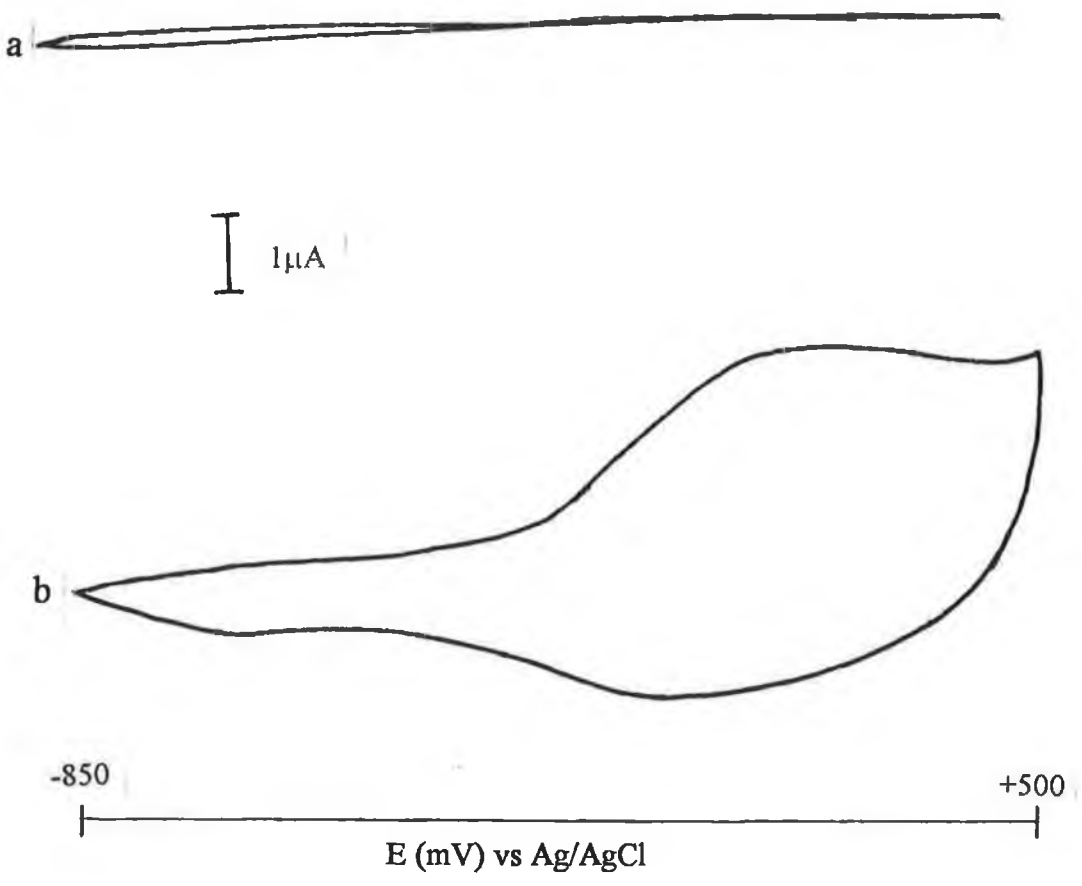

Figure 3.22 (b)

(a) Background scan in 0.1 M NaCl prior to polymerisation.

(b) Cyclic voltammogram of polypyrrole coated glassy carbon electrode in 0.1 M NaCl. The pyrrole was polymerised using a flow rate of 0.6 ml/min. Conditions: current range; 1 mA, sensitivity X axis; 100 mV/cm, sensitivity Y axis 10 mV/cm, scan rate 50 mV s^{-1}.

3.6.1 Anion Detection using a Polypyrrole Coated Electrode.

Using the optimal stop-flow polymerisation procedure, a polypyrrole coated electrode was prepared in the fountain cell. The cyclic voltammogram of the polypyrrole electrode is shown in Figure 3.23. This CV shows the classic redox transitions from the neutral to conducting state at potentials similar to those observed by other workers [100] The CV of the electrode in 0.1 M glycine is also shown in Figure 3.23. The CV indicates the suitability of glycine as a carrier stream for SFA experminents. The electrode was then used to detect chloride anions polarised at potential of +500 mV as described by Ward et al. [101].

The responses of the electrode to 5 injections of 100 ppm of Cl^- using a 0.1 M glycine carrier stream are shown in Figure 3.24. A relative standard deviation of 3.2% was obtained for the 5 injections. However, the response of the electrode was observed to decrease continuously with time, indicating that the doping process in the polypyrrole was irreversible. Optimisation of the polymerisation process would therefore be necessary to produce an electrode possessing the necessary characteristics for use in a flow cell. Once this has been achieved it would then be possible to develop a system consisting of on-line polymerisation as already described and an on-line 5 point standardisation procedure. Standards of the anion to be detected could be placed in series around the multi-port valve allowing on-line standardisation to be carried out. Multi-injections of the standards can be used to increase the accuracy of the calibration curve without a large increase in the analysis time. Also the use of an on-line polymerisation procedure should also increase the reproducibility of the polymerisation process coupled with the highly reproducible flow characteristics of the fountain cell.

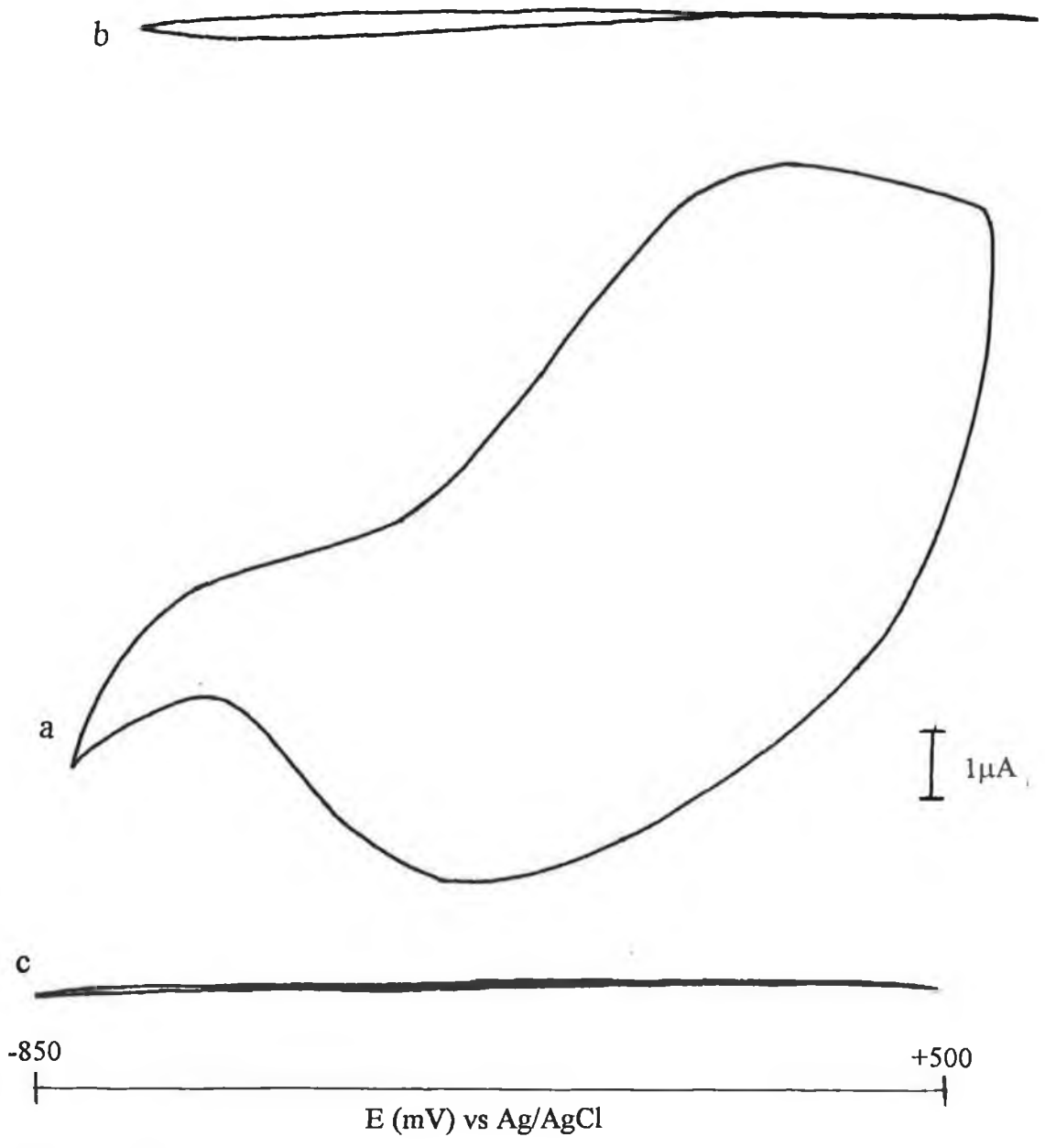

Figure 3.23

(a) Cyclic voltammogram of polypyrrole coated glassy carbon electrode in 0.1 M NaCl. The pyrrole was polymerised using the stop-flow polymerisation procedure.

(b) Background scan in 0.1 M NaCl prior to polymerisation.

(c) Background scan of polypyrrole electrode in 0.1 M glycine. Conditions: current range; 1 mA, sensitivity X axis; 100 mV/cm, sensitivity Y axis 10 mV/cm, scan rate 50 mV s^{-1}.

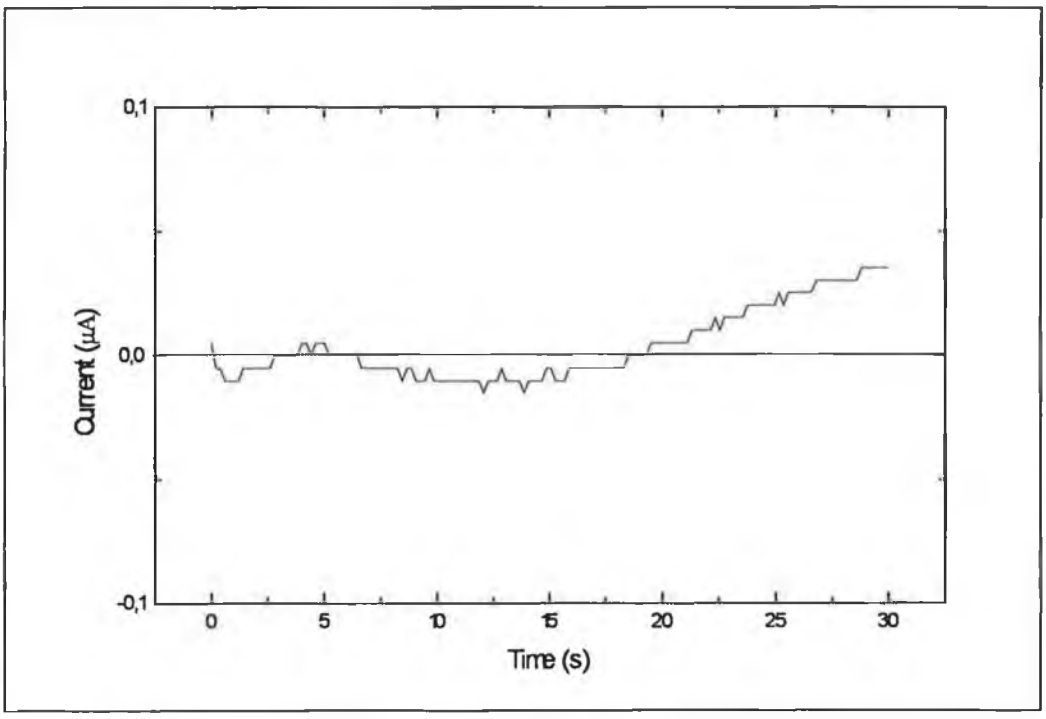

Figure 3.24 (a) Background response of polypyrrole electrode in 0.1 M glycine.

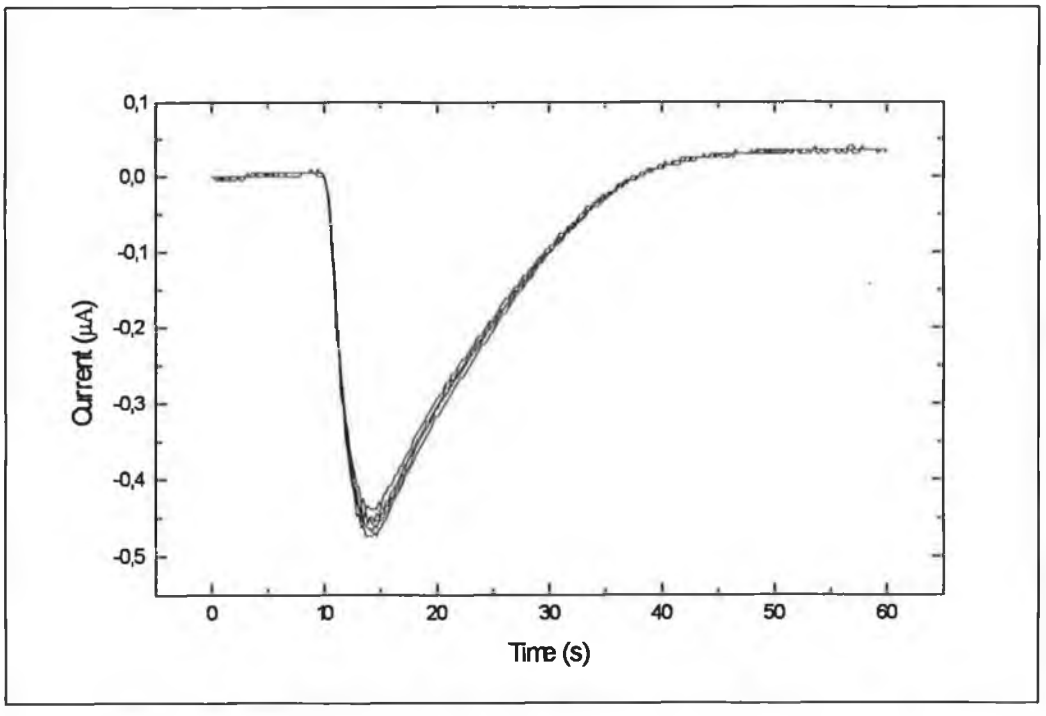

Figure 3.24 (b) Response at polypyrrole electrode to 5 injections of 100 ppm Cl^-. Potential +500 mV, carrier stream 0.1 M glycine.

CHAPTER 4

ELECTROCHEMICAL DETECTION WITH CAPILLARY ELECTROPHORESIS

4.1 Introduction

Capillary electrophoresis (CE) has found widespread application recently due to its excellent separation efficiencies and small sample volumes [70]. The detector of choice for CE has been UV spectrometry which results however in relatively high detection limits. Efforts to improve the limits of detection for CE have focused on the development of laser induced fluorescence [71, 72] and electrochemical detection [73-77]. The development of on-column and end-column electrical decouplers has made the routine implementation of electrochemical detection with CE possible.

To date, these electrochemical detection schemes have been based on the use of amperometry with a single electrode maintained at a constant potential. Routine analysis of complex samples with CE-EC is problematic because of the difficulty in assigning absolute peak identities due to shifting migration times. This problem is particularly acute in complex matrices where the analytes of interest may be at low concentration and a large number of peaks are obtained. However, the use of voltammetric detection can give 3-dimensional definition of the CE peaks. The voltammetric shape of a peak is generally characteristic for a particular compound, and coupled with its migration time, aids in the identification process. In this chapter the application of both amperometric and voltammetric detection with CE is described together, with their application in determining phenolic acids.

4.2 Hardware

Implementation of the voltammetric detection system required the design and construction of some analog circuits. These circuits were used for signal conditioning and activation of the working electrodes. The construction of a differential amplifier circuit for background subtraction of the charging currents was also necessary.

4.2.1 Deglitching and Smoothing Filter

Glitches arise from instabilities when the registers of the DAC are being switched from one state to another. They appear as spikes on the staircase voltage ramp output of the DAC. They are problematic because they result in brief but large changes in the potential of the working electrode, which in turn results in significant changes in the charging current. A variable frequency (10 kHz to 0.01 kHz) low pass filter was incorporated on the output of the DAC to remove any glitching. A schematic of the circuit is shown in Figure 4.1.

4.2.2 Activation Circuit (Potentiostat Modifications)

Modification of the BAS PA-1 potentiostat was necessary for successful implementation of the electrode activation scheme. An additional 2 kΩ feedback resistor was added to the standard PreAmplifier circuit as shown in Figure 4.2. This resistor facilitated the increased current demands placed on the potentiostat during activation of the working electrode. The resistor was controlled via a relay which allowed switching in and out of the resistor as required. Additionally, the deglitching filter was switched off during the activation procedure as shown in Figure 4.2.

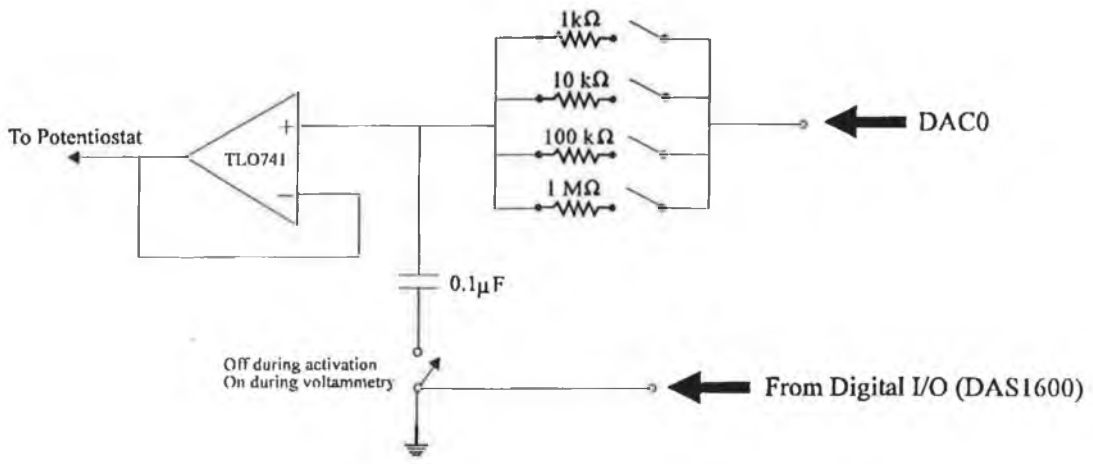

Figure 4.1 Deglitching Filter

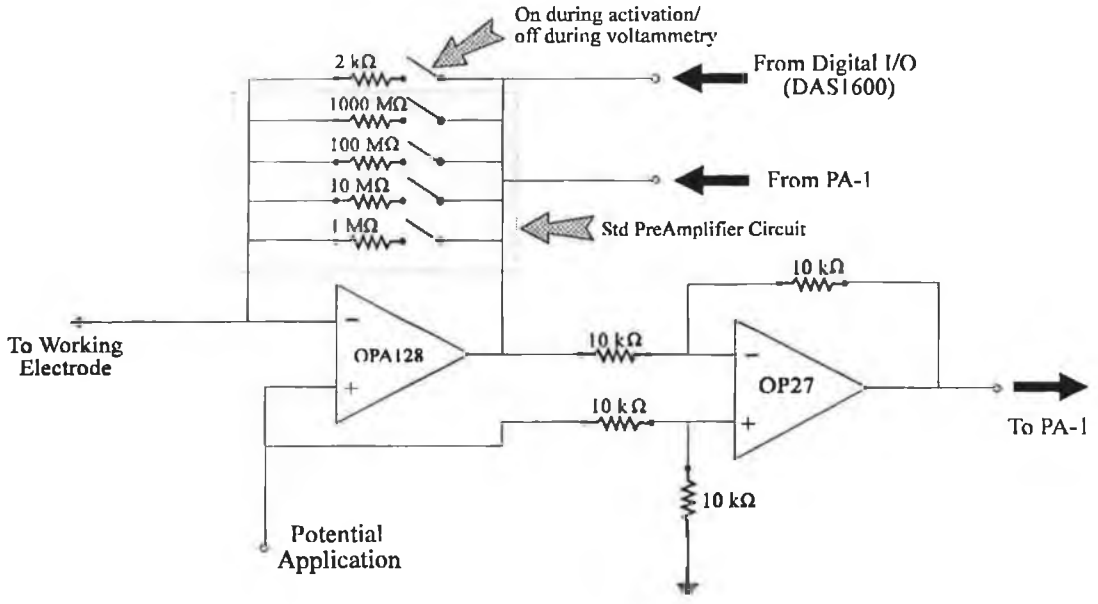

Figure 4.2 Schematic of the modifications to the PreAmplifier circuit of the PA-1 for electrode activation.

4.2.3 Differential Amplifier Circuit

A differential amplifier circuit was constructed for dynamic background subtraction of charging currents from the total current. The circuit utilised is shown in Figure 4.3. The first measurement channel uses one of the differential analog input channels of the DAS1600 board to obtain the difference in signals between PreAmplifier A and

PreAmplifier B, which is then sampled by the ADC of the board (channel 2).

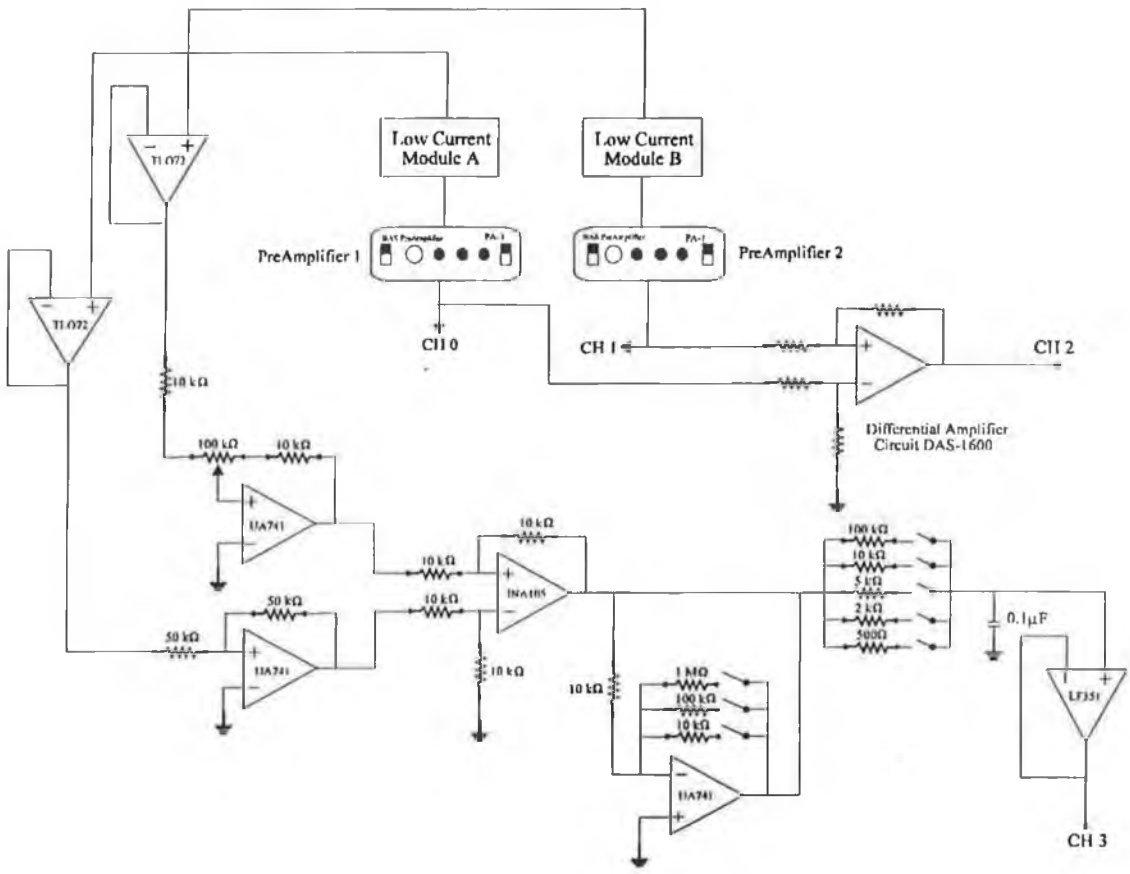

Figure 4.3 Schematic of the differential amplifier circuit used for subtraction of charging currents.

The analog circuit constructed was based on an INA105 instrumentation op-amp (Burr-Brown) configured as a differential amplifier. Unity gain voltage followers (TL072) were provided on the inputs of the differential amplifier. An amplifier with variable gain was included on the non-inverting input of the differential amplifier. The variable gain amplifier was used to compensate for differences in the two working electrodes which minimises the output of the differential amplifier. The output of the differential amplifier was filtered by a series of user selectable low pass filters in the range 100 Hz to 20 kHz before being inputted to the analog inputs of the DAS1600

(channel 3). An additional amplifier circuit providing gains of 1, 10 and 100 was included for high sensitivity situations.

4.2.4 CIO-DAS1600 Data Acquisition\Control Card

The DAS1600 (Computer Boards Inc., MA) is a multi-functional digital and analog I/O board with a base address of 300 HEX. The card consisted of the following features:

- 8 differential analog input channels (jumper selectable);
- two 12 bit digital-to-analog converters;
- 16 bit analog-to-digital converter (successive approximation) at rates up to 100 kHz;
- 8 digital I/O lines;
- 8254 counter/timer chip.

The use of a 16 bit analog to digital converter afforded an increase in resolution of the voltammetric data (1 part in 65,536). The timing functions of the 8254 counter/timer chip were accessed to control synchronisation of data acquisition with application of the potential ramp. The DAS1600 was controlled and monitored by writing to and reading from consecutive 8 bit I/O lines addresses.

4.3 Software

Software for both data acquisition and control of the instrumentation was written in Turbo C (Borland). Through a series of software menus it was possible via the DAS1600 to set and control all the instrument functions and parameters save that of sample introduction. 3-dimensional display of the acquired data was available in real time to the user. Data sets were acquired at 0.5 s intervals. Each data set consisted

usually of 50 data points in the potential axis. Due the large amount of data acquired in a typical analysis run (10 minutes) it was necessary to use a RAM drive for data storage. Data was written to the RAM drive as two minute data blocks. Each block of data consisted of 240 time points with 50 potential points. Data was stored in floating point format which required 4 bytes per point. A typical 10 minutes run was approximately 900 kB in size. Once the analysis run was completed a number of options were available for data handling such as further background subtraction of the data, rescaling of the display, geometric change of the display angle and saving the data to the hard disk. The data was saved in ASCII format to facilitate post-run data analysis in MicroCal Origin (ver. 3.5).

4.4 Experimental

4.4.1 Chemicals

Caffeic, sinapic, ferulic, chlorogenic, vanillic, protocatechuic, gentisic and p-coumaric phenolic acids were all obtained from Sigma (St. Louis, MO). Hydroquinone and catechol were received from Sigma. Nafion perfluorinated ion exchange powder (5% solution) was purchased from Aldrich (Milwaukee, WI). All other chemical were reagent grade or better and used as received.

All stock solutions of the phenolic acids were prepared in 0.1 M perchloric acid and kept refrigerated until use. Prior to use, the phenolic acid stock solutions were diluted to the required concentration with buffer and stabilised with an EDTA/bisulphide solution consisting of 8 mM EDTA and 0.1 mM sodium bisulphate. CE run buffers were prepared by titrating the free acid to the desired pH with solid sodium hydroxide solution. An alkaline-EDTA solution for capillary activation was prepared by titrating

0.5 M disodium EDTA with solid sodium hydroxide to pH 13. All solutions were prepared in deionised water which was obtained by passing distilled water through a Nanopure water purification system (Sybron-Barnsted, Boston, MA) and filtered through a 0.45 μm pore size Acrodisc syringe filter (Fisher, Fair Lawn, NJ) before use.

4.4.2 Working Electrode Construction

The working electrodes for electrochemical measurements were prepared by inserting a 33 μm o.d. carbon fiber (Avco Speciality Products, Lowell, MA) into a 5 cm length of fused-silica capillary of the same type used for the electrophoresis (50 μm i.d.). A schematic of a working electrode is shown in Figure 4.4. The carbon fiber was allowed to extend approximately 25 mm on either side of the capillary. Poly-acrylate glue was applied to either end of the capillary to fix the fiber in position. A standard syringe needle was cut to 30 mm in length while retaining the sharpened tip. At approximately the centre point of the needle, a 5 mm section of the needle was ground away to expose the inter channel. The capillary was inserted through the flat end of the needle until the carbon fiber was visible. Silver loaded epoxy was applied to the fiber to fix it in position and to establish electrical contact.

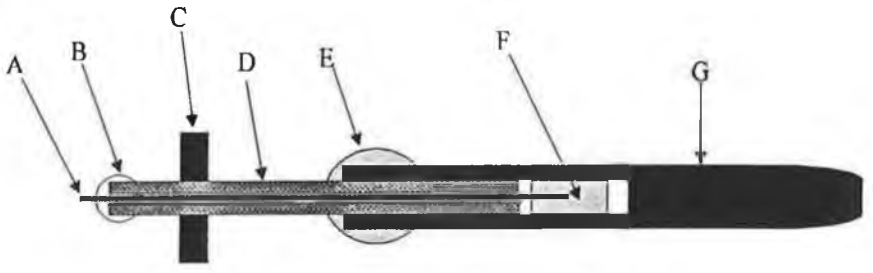

Figure 4.4 Carbon fiber working electrode; (A) 33 μm carbon fiber; (B) silicon glue; (C) septum; (D) fused silica capillary; (E) silicon glue; (F) silver loaded epoxy; (G) needle

Epoxy was applied to the junction between the capillary and the needle barrel, establishing a water tight seal. Silicon glue was then applied to the carbon fiber-capillary junction to effect a water-tight seal. The electrode was allowed to cure for 24 h at room temperature. The exposed carbon fiber was cut to the required length before use.

4.4.3 Construction of End-Column Decoupler

Fused silica capillary (50 μm i.d.) from Polymicro Technologies (Phoenix AZ) were cut to desired lengths. One end of the capillary was ground to a conical shape with alumina paper (1000 grade). This conical shape was used to enlarge the area that contacted the Nafion and also to ensure a smooth angle. This end of the capillary was then glued to a 20 mm × 5 mm piece of epoxy board to improve the rigidity of the capillary. The other end of the capillary was ground sufficiently to facilitate fitting of a Teflon tube, which in turn was connected to a syringe. Both ends of the capillary were sonicated in ethanol. Using the syringe, the capillary was flushed with ethanol to remove any particulate matter and then dried in an argon stream. The capillary was introduced into an electroplating cell via a septum. From the opposite side of the electroplating cell a short piece of capillary (3 cm long and 100 μm i.d.) was introduced. The capillaries were aligned with the spatial distance between the capillaries set at 1 cm. Both capillaries were threaded with a piece of tungsten wire (20 cm long, 47 μm in diameter, California Fine Wire Company, Grover City, CA). The tungsten wire was cleaned by sonication in ethanol before use. The wire was inserted into the 50 μm i.d. capillary to a depth of 10 cm under the microscope. The other end of the tungsten wire was connected to a galvanostat (Model 173

Potentiostat/Galvanostat, Princeton Applied Research, Princeton, NJ). The whole assembly was immersed in an electroplating solution consisting of 1M copper sulphate and 0.5 M sulphuric acid. The exposed portion of the tungsten wire between the two capillaries was plated with copper by applying 5 mA for 10 seconds first and then a small portion (several mm) of the plated wire was inserted into the 50 μm i.d. capillary. While insertion was performed, the plating current was lowered to 0.1 mA. Plating and insertion were repeated until the plated wire completely packed the 50 μm i.d. capillary. At this point the plating current was set to 5 mA and held constant until the required thickness of copper plating was reached (90 μm, total diameter of the plated wire). The 50 μm i.d. capillary was frequently purged with air during this process. Purging was necessary to exclude the bath solution from the inside of the capillary. Immediately after electroplating was finished, the assembly was washed with deionised water and dried. Drops of a 2 to 1 mixture of Nafion (as received) and DMF was cast onto the wire and the 50 μm capillary to construct a Nafion tube around the plated wire. The entire assembly was rotated to ensure a continuously layer of Nafion around the wire and capillary. The final thickness of the Nafion layer was equal to the outside diameter of the capillary (≈360 μm). The decoupler assembly was cured in an oven at 120\°C for 1 h. The area where the capillary and Nafion superimposed was covered with polyacrylate glue and then covered with quick-set epoxy resin. The epoxy was allowed to cure at room temperature for 10-12 hours. The completely cured decoupler assembly was immersed in 0.1 M nitric acid. The copper plating was removed by reverse electrolysis. Once the copper plating was removed the tungsten wire could be easily removed. The decoupler was flushed with deionised water. The Nafion decoupler was cut to a length of 1 mm with a razor blade under a microscope.

Figure 4.5 illustrates the structure of the decoupler. The capillary and decoupler were flushed with 0.5 M EDTA solution (pH 13) for 1 hour to remove any copper remaining in the capillary and the decoupler. The capillary was finally flushed with run buffer to obtain pH equilibrium inside the capillary before use.

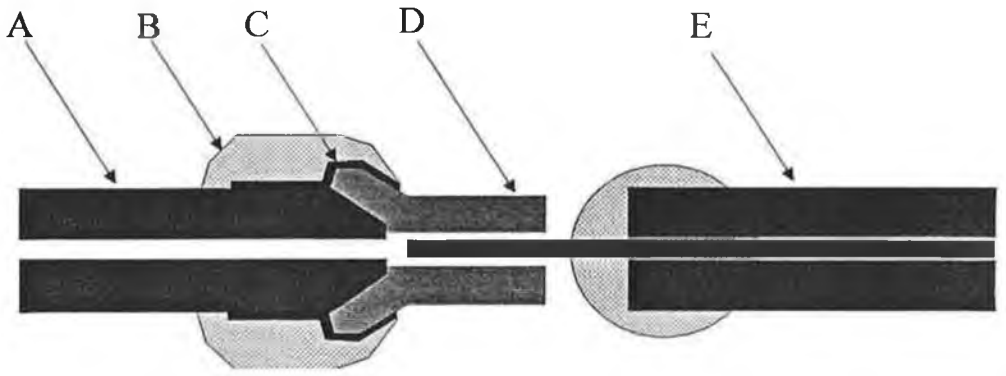

Figure 4.5 End-column decoupler schematic, (A) separation capillary (50 μm i.d.); (B) epoxy; (C) polyacrylate glue; (D) Nafion; (E) carbon fiber (diameter 33 μm).

4.4.4 On-Column Decoupler

Fused-silica capillaries of 50 μm i.d. (Polymicro Technologies, Phoenix, AZ) were cut to the desired lengths. One end of the capillary was ground to a conical shape with 1000 grade silicon carbide paper. After grinding the capillary was flushed with water. The separation capillary was placed on a piece of epoxy board and fixed with epoxy glue. A 10 cm piece of tungsten wire was inserted into the detection capillary which was then held in an electrochemical cell via a septum. The separation capillary was inserted into the electrochemical cell on the opposite side to the detection capillary. The tungsten wire was inserted through the detection capillary and into the separation capillary. The distance between the capillaries was adjusted under a microscope to 1

cm. Electroplating of the tungsten wire and application of the Nafion were carried out as described for the end-column decoupler. Once the Nafion had dried, reverse electrolysis was used to remove the copper plating from the tungsten. The tungsten wire could be easily removed from the capillaries after removal of the copper. If any Nafion solution penetrated into the capillaries and partially blocked liquid flow, it was removed by injecting a small amount of 50% isopropyl alcohol. Finally the joint was flushed with water. The end-column decoupler was then constructed on the end of the detection capillary. The assembly of the on-column and end column decouplers is shown in Figure 4.6.

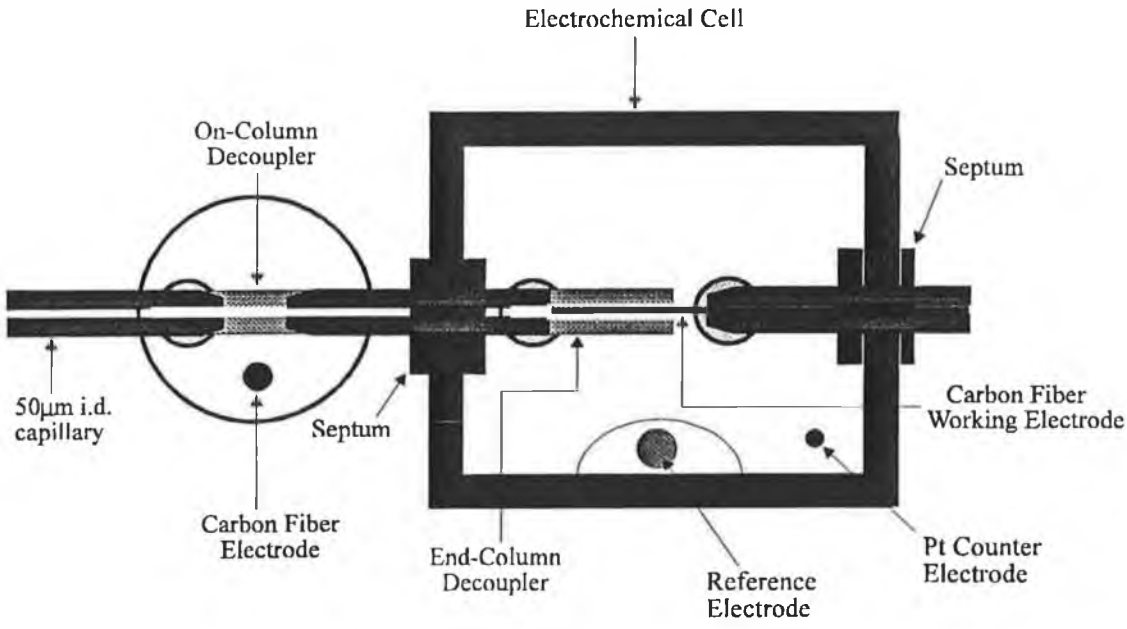

Figure 4.6 Electrochemical cell schematic with on-column and end-column decoupler configuration.

4.4.5 CE-EC System

The CE apparatus consisted of a perspex safety cage fitted with an interlock for operator safety, which housed the anodic high voltage end of the capillary. A high

voltage dc (0-30 kV) power supply (Glassman High Voltage, Whitehouse Station, NJ) was connected to the anodic end of the capillary. The electrochemical cell which was constructed "in house" from a Teflon block, consisted of a cathodic reservoir containing the decouplers with the working electrode, reference electrode (Ag/AgCl) and a platinum counter electrode.

Initially, a separate cell was utilised for background subtraction of the charging current. A carbon fiber electrode was held free standing in the cell together with a Ag/AgCl reference electrode and platinum counter electrode. The cell was filled with 0.1 M phosphate buffer pH 2.5. The pH of this solution approximated that which was experienced by the working electrode in the end-column decoupler. The end-column decoupler was held in 0.1 M HCl. Perfusion of H^+ through the Nafion decoupler which is a cation exchanger, titrated the phosphate run buffer pH 6.0. The electrochemical response of the phenolic acids is increased at lower pH. However this titration process was not sufficiently fast enough; therefore pH mismatching occurred between the local environments of both electrodes. The on-column decoupler was placed in front of the end-column decoupler to ensure a high degree of titration of the phosphate run buffer prior to reaching the end-column decoupler. The electrode for compensation was normally held in the on-column decoupler cell.

As described earlier, a differential amplifier circuit based on an INA105 instrumentation op-amp was used to output the difference signal between the working electrodes to the ADC of the DAS1600 card. For voltammetric studies, the pH of the buffer was adjusted approximately to that experienced by the working electrode in the region of the decoupler. Sets of micro-positioners (Newport) were used for movement of the carbon fiber working electrode in 3 dimensions, which was necessary during

insertion of the working electrode into the end-column decoupler. The interface between the computer and the instrumentation was based on a CIO-DAS1600 data acquisition/control card (ComputerBoards Inc., MA.). Two BAS PA-1 potentiostats were used for current monitoring and potential application duties. Potential ramps were applied to the potentiostats via one of the D/A converters of the DAS1600 control/acquisition card. Scan rates up to 24 V s^{-1} were implemented. On-line box-car digital filtering of the data was also used for noise reduction purposes.

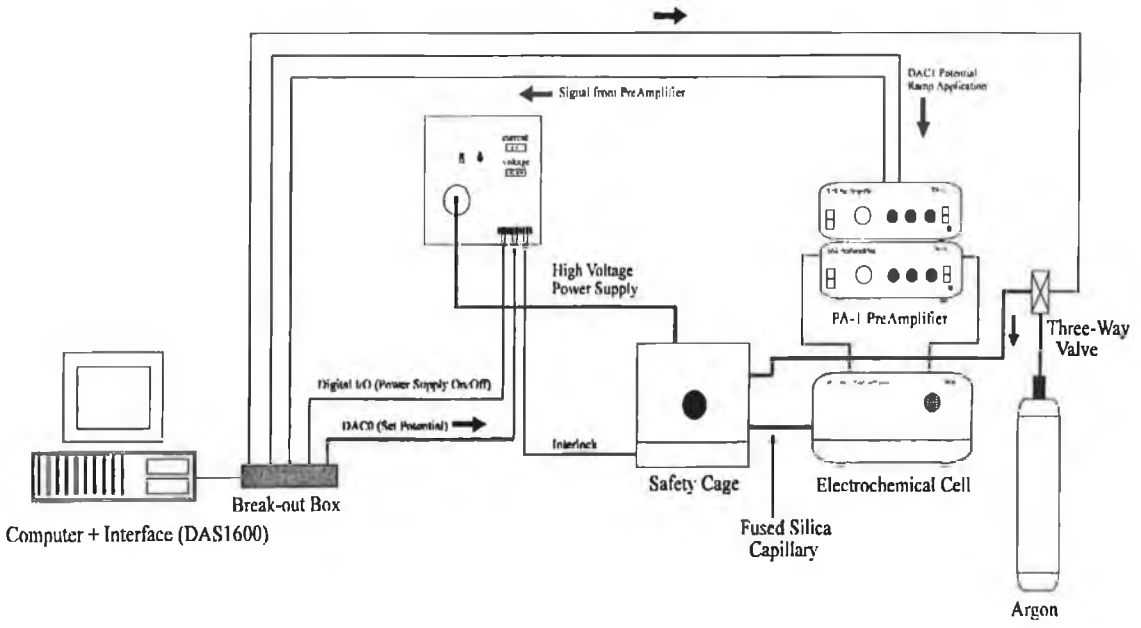

Figure 4.7 Schematic of CE system.

4.4.6 Working Electrode Preparation

A standard activation procedure of the carbon fiber electrode was developed and utilised throughout this study. The procedure consisted of washing new constructed electrodes in deionised water and then scanning (20 mV s^{-1}) them in phosphate buffer pH 6.0 to ensure that the background was sufficiently low (< |5| nA). Electrodes that

did not meet this initial requirement were discarded. The electrode were then sonicated in 5% (v/v) "Micro" cleaning solution (International Products, Trenton, NJ) solution for 1 minute. The background voltammograms were again recorded to ensure that no major change had occurred in the background. Electrodes were then electrochemically activated by the application of a scanning potential ramp between -2000 mV and +2000 mV at 10 kHz for 30 s.

4.4.7 Experimental Conditions

4.4.7.1 Cyclic Voltammetry/FIA Studies

Cyclic voltammetry (CV) studies were carried out in an open cell with a carbon fiber microelectrode (33 μm), a Ag/AgCl reference electrode and a platinum counter electrode. A scan rate of 20 mV s^{-1} was used throughout. Three buffers were used for these investigations: 0.1 M phosphate buffer pH 2.5, 0.1 M acetate buffer pH 4.75 and 0.1 M phosphate buffer pH 6.0.

The physical configuration of the CE system was not changed for the FIA studies. The same three buffer systems that were used in CV studies were used in sequence as carrier streams under 20 psi of argon pressure. A 65 mm long capillary (50 μm) internal diameter was used for all FIA measurements with an end-column decoupler. Standard solutions of phenolic acids (100 μM) were prepared in each of the three buffers as required. Pressure injection for 5 seconds was used throughout for sample introduction. A scan rate of 18 V s^{-1} was used for all measurements with a potential window from + 200 mV to + 1000 mV. The 2-dimensional hydrodynamic voltammograms were extracted at the current maxima and plotted.

4.4.7.2 CE Separation Conditions

Phosphate buffer (25 mM, pH 6.0) was used as the run buffer for the CE-UV studies. The cathodic reservoir was also filled with the same buffer. A separation potential of 30 kV was used throughout. The capillary was 65 cm in length with a 50 μm i.d. The capillary was flushed with EDTA solution (pH 13) prior to use each day.

For amperometric detection, 25 mM phosphate buffer pH was generally used as the run buffer. However, for the analysis of beer samples, a 50 mM phosphate buffer was used. The higher ionic strength was required to achieve good separation of the sample. The cathodic reservoir was filled with 0.1 M perchloric acid. Titration of the phosphate buffer results in higher sensitivities for the phenolic acids at lower pH values. A 65 cm length capillary (i.d. 50 μm) with an end-column decoupler was used for separations. A separation potential of 30 kV was used. The capillary was flushed for 10 minutes with EDTA solution (pH 13) at the start of each day and subsequently for 1 minute before each separation run. The capillary was finally flushed with the run buffer for 1 minute prior to sample introduction. A 3 second electrokinetic injection was used throughout.

4.4.8 Beer Sample Preparation

tC_{18} Sep-pak cartridges (Waters Associate, Milford, MA) were preconditioned by flushing 20 mls of deionised water through the cartridge followed by a mixture of 0.75 ml of methanol and 0.25 ml deionised water and finally a further 20 ml of deionised water. Beer samples (36 ml) were acidified with 4 mls of 0.1 M perchloric acid to pH

2.15. The sample was then applied to the tC_{18} Sep-pak cartridge. The cartridge was then flushed with 2 ml of deionised water. The phenolic acids were eluted with 2 ml of 0.05 M phosphate buffer pH 7.0.

4.5 Results and Discussion

4.5.1 Background Subtraction

Background subtraction is an important tool for increasing the signal to noise ratio of voltammograms. The standard strategy involves collection of the background voltammograms prior to introduction of the sample (usually in the run buffer), saving this signal, and finally subtracting this signal from the sample to achieve the required background correction. The problem with this approach is that it does not accommodate changes in the background which may occur during the analysis run. With dynamic background compensation the system can respond and correct for changes in the background while a sample is being analysed. The system is based on the use of two working electrodes and two potentiostats. One electrode is used as a standard working electrode, while the second electrode is used solely for measurement the charging current and correction of it.

The procedure involves two steps; firstly the differential background between the two electrodes is acquired in the run buffer under standard electrophoretic conditions and stored in memory. The second step involves subtraction of the background signal obtained at the working electrode for compensation from the signal at the real working electrode via the differential amplifier during the analysis run. The previously acquired difference background signal is then digitally subtracted in real time from this signal to

give the final corrected signal. This approach results in a flatter background which allows greater resolution of the faradaic current from the background. This is especially important when analysing analytes at low concentrations. Secondly the system can be operated at high sensitivities even with high backgrounds because of effective background subtraction. At sensitivities of 100 nA full scale or lower, the magnitude of the background signal is such that it overloads the system, making measurement of the faradaic current impossible even when this signal is small. Thus the measurements must be made at reduced sensitivities, and consequently resolution during measurement of the data is lost even with the 16-bit ADC.

Standard background methods can be used to some limited effect; however backgrounds can easily change 50-100 nA between runs; thus losing the faradaic signal at lower sensitivity settings. On the other hand, current scales smaller than the magnitude of the background current can be used if the background current is subtracted with the second electrode prior to analog-to-digital conversion.

The advantage of the dual electrode configuration over a single electrode is demonstrated in Figure 4.8. There is a significant difference in the background of the single electrode (see Figure 4.8 (A)) compared to that of the dual electrode system (see Figure 4.8 (B)).

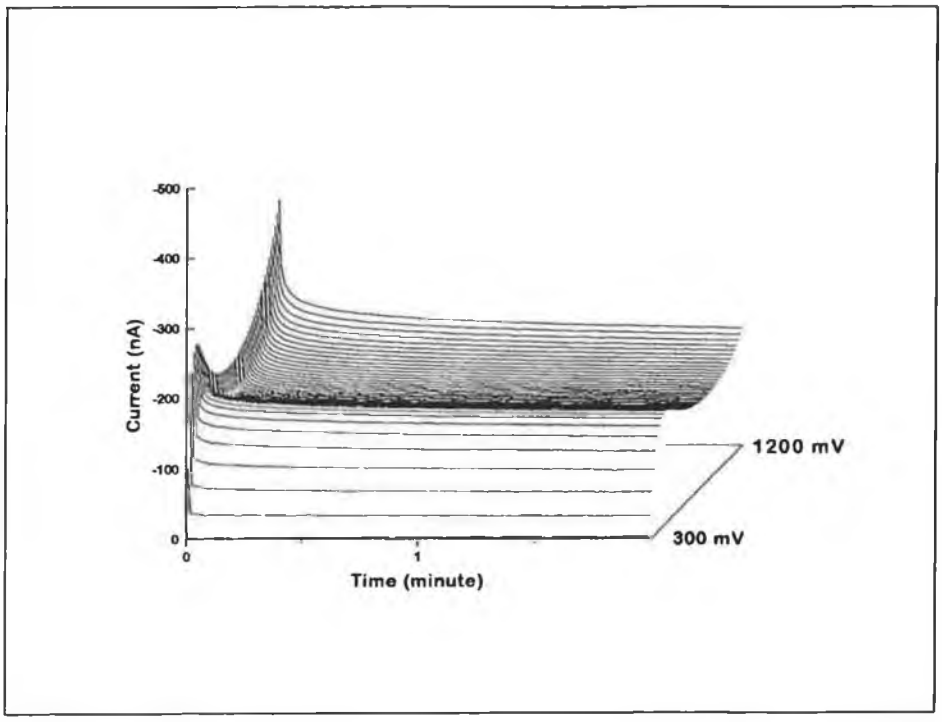

Figure 4.8 (a) Blank with single working electrode. Conditions: Scan rate 16 V s^{-1}, 0.1 M phosphate buffer pH 2.5.

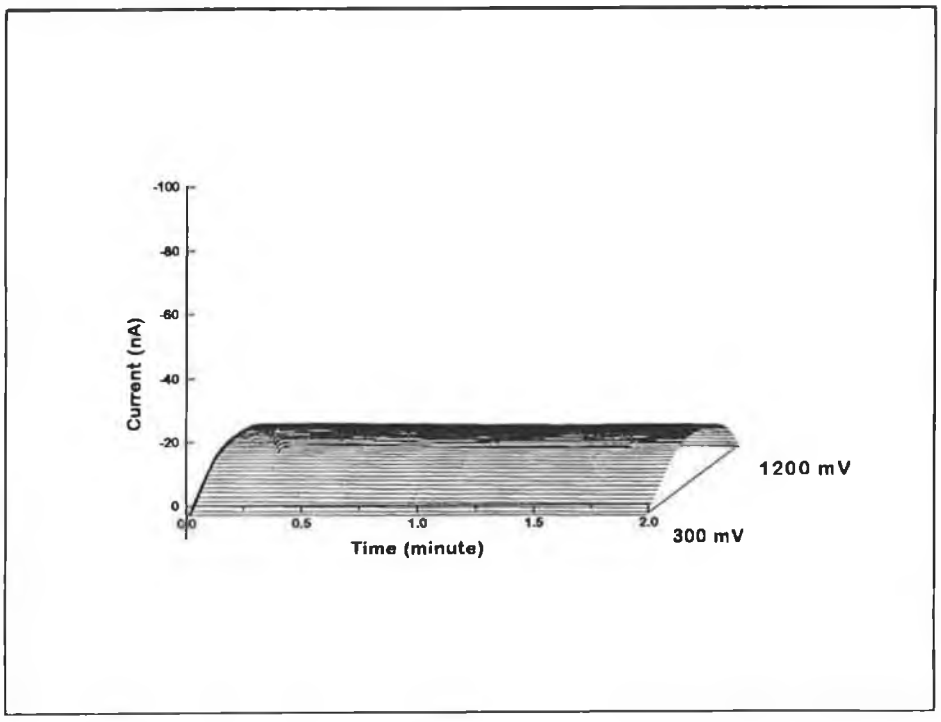

Figure 4.8 (b) Blank with dual electrode system. Scan rate 16 V s^{-1}, 0.1 M phosphate buffer pH 2.5.

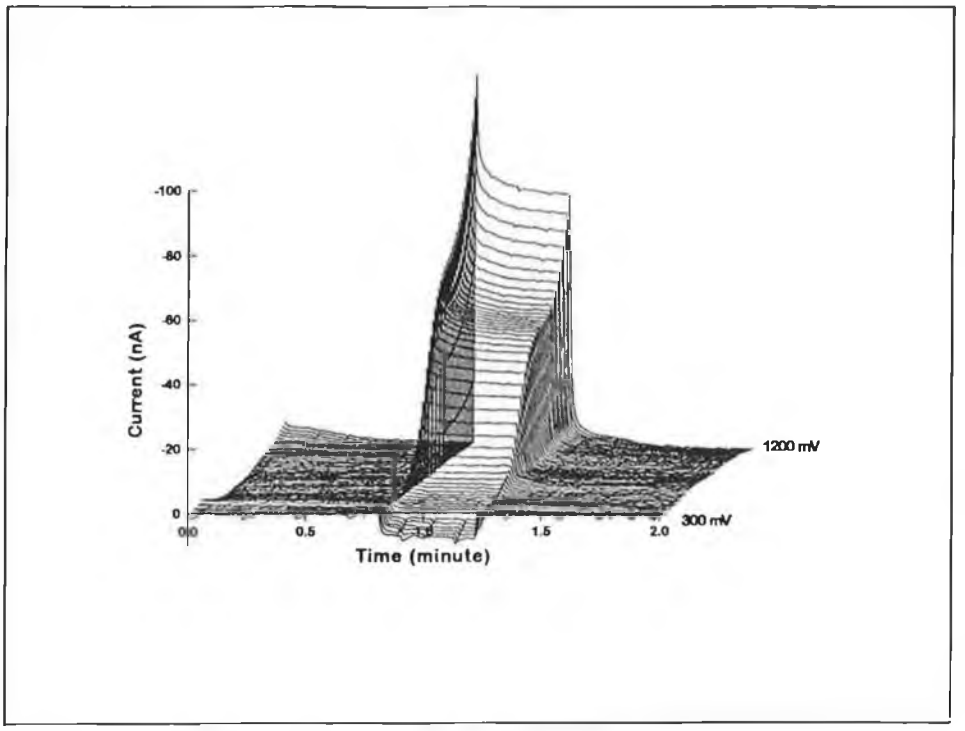

Figure 4.8(c) Voltammogram of 10 μM protocatechuic acid, with background signal subtracted using a single electrode. Scan rate: 16V s^{-1}.

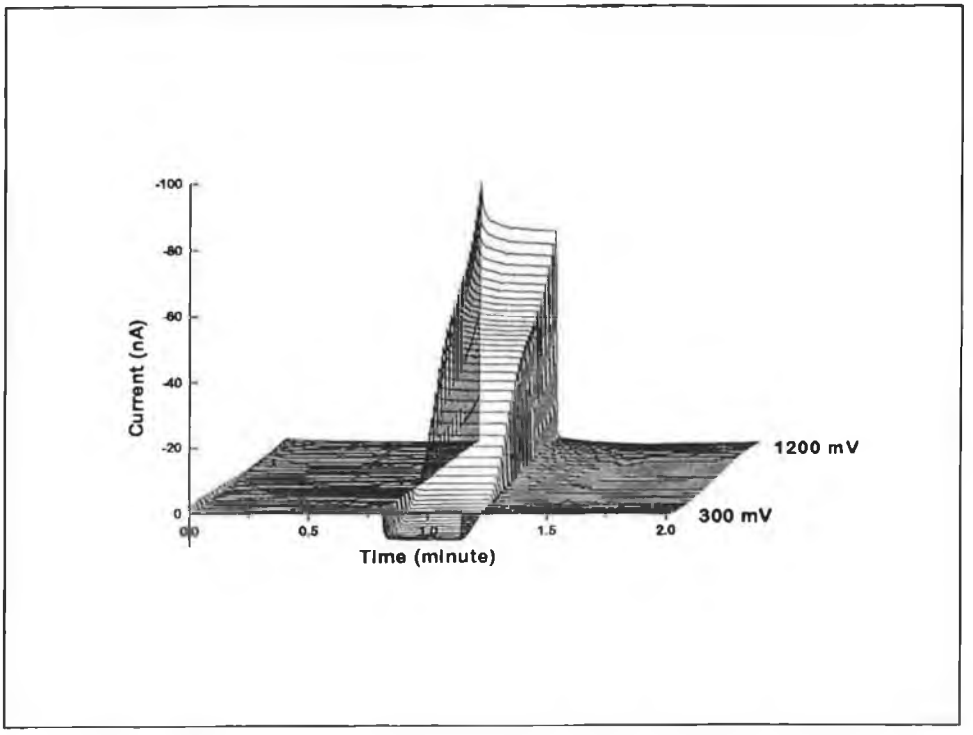

Figure 4.8 (d) Voltammogram of 10 μM protocatechuic acid with background signal subtracted using a dual electrode system. Scan rate: 16V s^{-1}.

The dual electrode system exhibits a much flatter background. These differences are reflected in the background subtracted voltammograms of protocatechuic acid (10 μM) shown in Figures 4.8 (C) and (D). The dual electrode system results in a smoother and flatter baseline compared to that of a single electrode.

The initial voltammetric system was based on the use of an end-column decoupler. It was found however that the end-column decoupler was not satisfactory in terms of its ability to facilitate titration of the run buffer with the electrochemical cell solution (0.1 M HCl). An on-column decoupler was then added approximately 1.5 cm in front of the end-column decoupler. The on-column decoupler was held in 0.1 M HCl. Nafion, which is a cation exchanger, allowed perfusion of H^+ ions through the decoupler titrating the run buffer. The combination of both decouplers allowed titration of the phosphate run buffer pH 6.0 down to pH 2.5, the pH which the working electrode for compensation was exposed to.

4.5.2 Electrode Activation

Preparation of the working electrode plays a vital role in the correct electrochemical behaviour of carbon fiber electrodes. A standard procedure for activation of the carbon microelectrodes was developed to maximise the performance of the electrodes. The activation procedure criteria were based on the requirements that the sensitivity/voltammetric of response of the electrode should be improved without increase of the background current. Secondly the procedure should reproducibly activate the electrode without long term degradation of the electrode performance. Figure 4.9 illustrates how the electrochemical response of the electrode to catechol is enhanced with each step of the activation procedure without significant change in the

background current.

For slow scan work (20 mV/sec), an activation scan rate of 6.25 kHz was found to give the best results, whereas for high speed voltammetry, the activation frequency was increased to 10 kHz. With new electrodes, potential pulses from -2000 mV to +2450 mV were used to achieve optimum activation of the electrode surface. All subsequent activations were carried out using a symmetrical potential waveform of ±2000 mV. This combination was found to maximise sensitivity and maintain longevity of electrode performance. A number of other activation scan rates were additionally examined. However, the 10 kHz scan rate consistently gave rise to the most suitable activation of the electrode without increase of the background current.

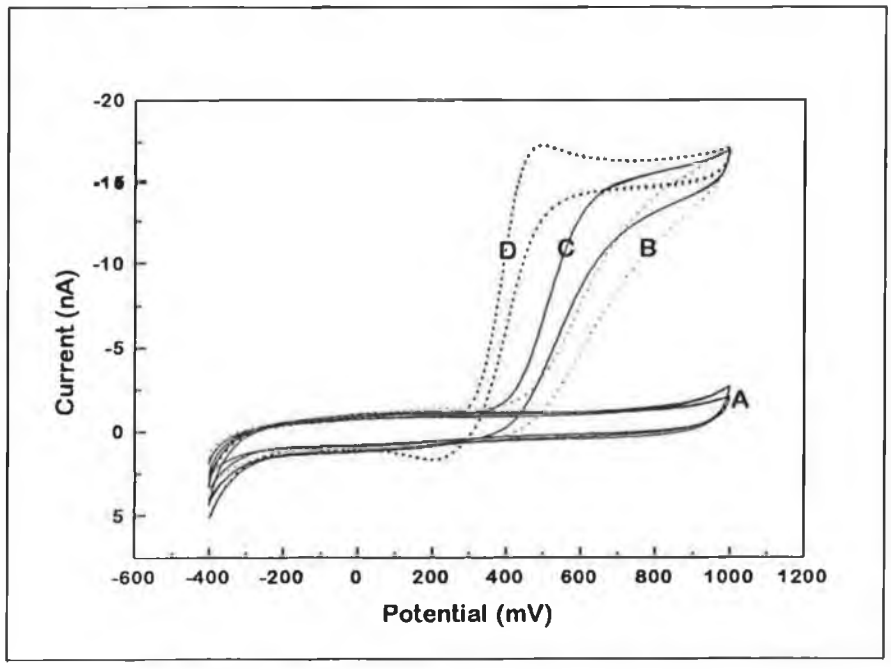

Figure 4.9 Activation of carbon fiber microelectrode. **(A)** Background scan after each step in the activation procedure; **(B)** initial scan of 30 μM catechol with a new electrode; **(C)** Scan of 30 μM catechol after sonication of the electrode in micro cleaning solution; **(D)** scan of 30 μM catechol after electrochemical activation of the electrode. Conditions: 0.1 M phosphate buffer pH 6.0; scan rate: 20 mV s^{-1}.

The effect of activation on the electrochemical behaviour of the carbon fiber electrodes using voltammetric detection is illustrated in Figure 4.9. The differences in backgrounds between the an unactivated (■) and an activated (●) electrode is shown in Figure 4.10 (A).

The scans were carried out in phosphate buffer pH 2.5 with a scan rate of 18 V/sec. The voltammetric responses to protocatechuic acid (100 μM) using the electrode prior to activation and after activation is presented in Figure 4.10 (B). A significant difference in the voltammetric responses is visible, and clearly indicates the necessitate of the activation procedure.

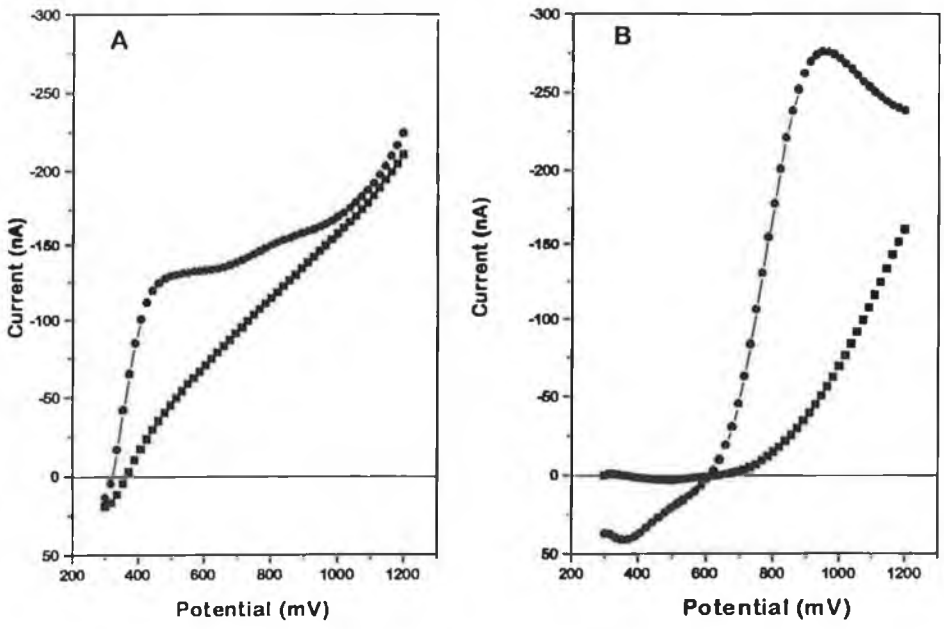

Figure 4.10 Activation of carbon fiber electrode for voltammetry. **(A)** Background with unactivated electrode (■) and an activated electrode (●). **(B)** Voltammetric responses of an unactivated electrode (■) and activated electrode (●) to protocatechuic acid (100 μM). All scans were carried out in open cell. Conditions: scan rate 17.9 V s^{-1}; 0.1 M phosphate buffer pH 2.5.

Careful control of the activation procedure was however required. The effect of over activation is shown in Figure 4.11. Electrodes which had been over-activated were observed to demonstrate "peaking" in their voltammetric waves. Secondly, the halfwave potential was observed to move to less positive potentials. The use of symmetrical activation potentials was found to reduce this problem, as was the use of activation potentials in the range $\leq \pm 2V$.

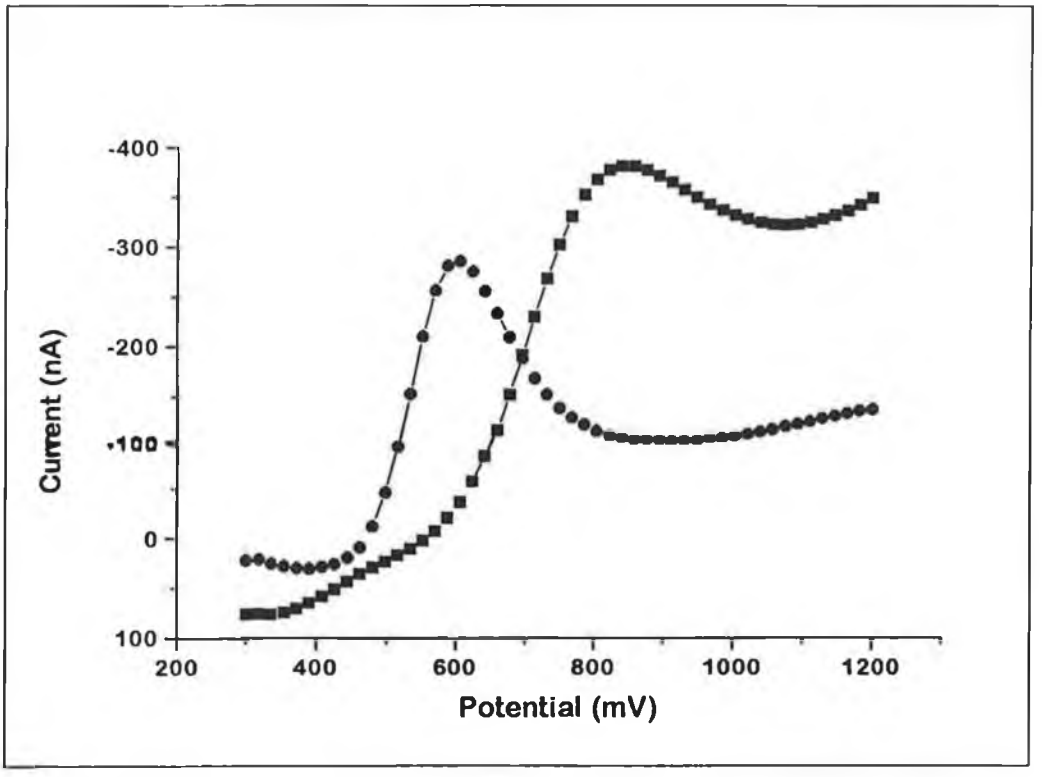

Figure 4.11 The voltammetric response of a normally activated electrode (■) to 100 μM protocatechuic acid as compared to that of an over-activated electrode (●). Conditions: 0.1 M phosphate buffer pH 2.5; scan rate 18.0 V/sec; scan range +300 to +1200 mV.

4.5.3 Scan Range Investigations

The effect of scan range on the voltammetric response of the carbon fiber electrodes

then was investigated. The voltammetric responses to protocatechuic acid (100 μM) using a scan range of +300 to +1200 mV is shown in Figure 4.12 (A).

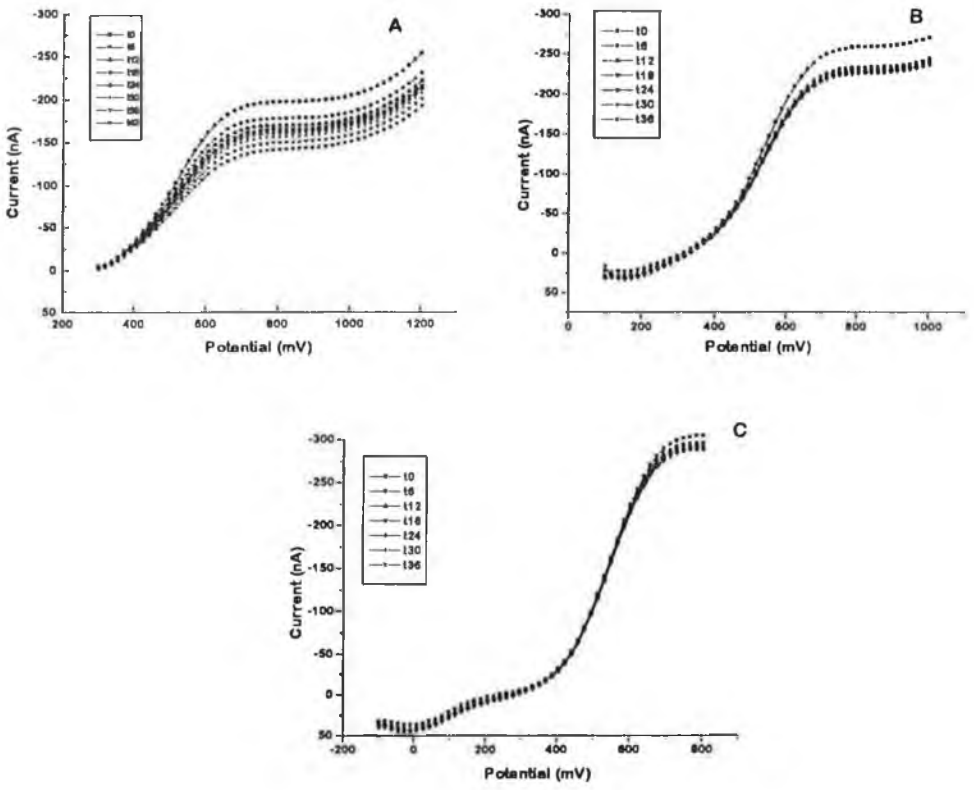

Figure 4.12 **(A)** Voltammetric responses to 100 μM protocatechuic acid using a scan range between +300 and +1200 mV after background subtraction.
(B) Voltammetric responses to 100 μM protocatechuic acid using a scan range between +100 and +1000 mV after background subtraction.
(C) Voltammetric responses to 100 μM protocatechuic acid using a scan range between -100 and +800 mV after background subtraction. Conditions: scan rate; 16 V s^{-1}, 0.1 M phosphate buffer pH 6.0.

The voltammograms were obtained at 6 minute intervals. A clear decrease in the sensitivity of response is observed over time. A similar trend is exhibited in Figure 4.12 (B), with a scan range of +100 to + 1000 mV. The decrease in sensitivity is,

however, not as dramatic over time. Once the scan range is moved into the reductive region, the reproducibility and sensitivity of the voltammetric response in dramatically improved (see Figure 4.12 (C)).

This trend suggests that a surface phenomena is occurring. Scanning down into the reductive potentials may allow reduction of an absorbed oxidative product. A second possibility is that the reductive wave may directly effect the surface activation and in turn increase reproducibility. It appears that for high sensitivity and reproducibility, the scan range must go down into the reductive region for this substance.

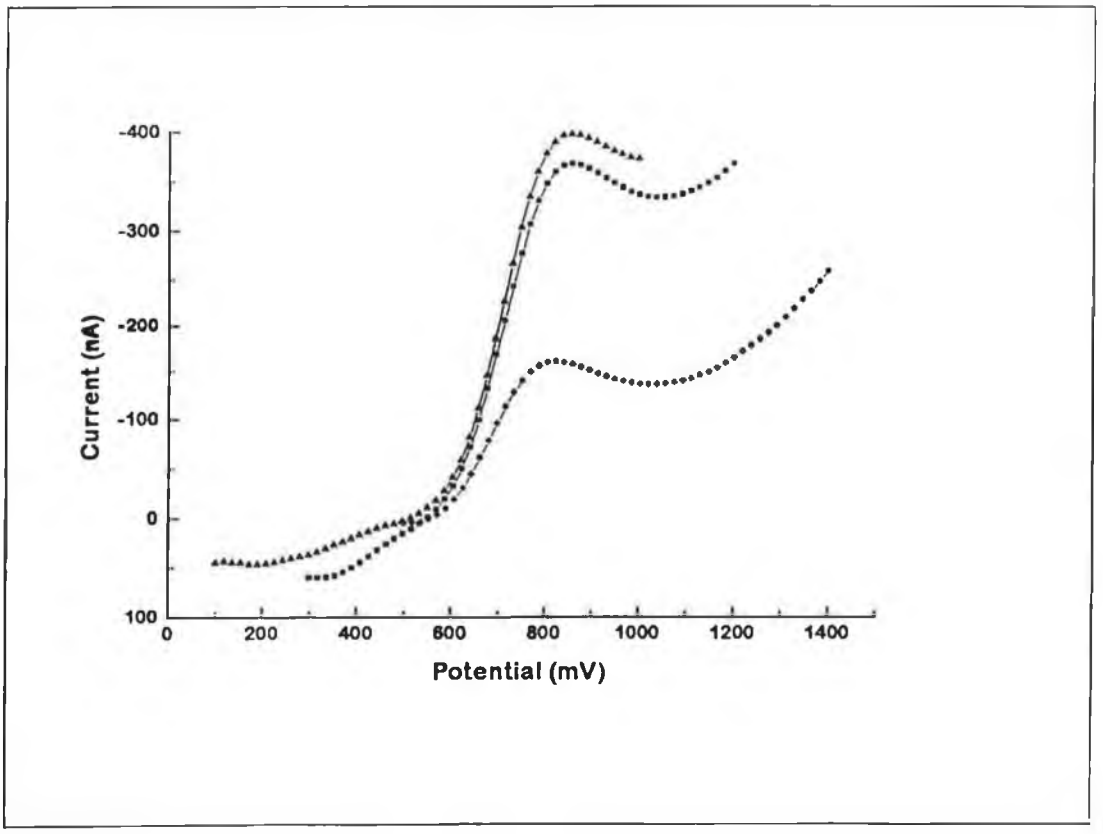

Figure 4.13 Voltammetric responses to 100 μM protocatechuic acid after background subtraction using three different scan ranges in 0.1 M phosphate buffer pH 2.5. (●) +500 mV to +1400 mV, (■) + 300 mV to +1200 mV, (▲) -100 mV to +1000 mV. Scan rate: 16 V/sec.

The effect of scan range at lower pH was also examined. Using three different scan ranges in 0.1 M phosphate buffer pH 2.5, voltammograms of protocatechuic acid (100 μM) were obtained under open cell conditions. The results obtained as shown in Figure 4.13 display a similar trend to that seen in Figure 4.12. The effect of the scan range was concluded to be independent of pH.

4.5.4 Ionic Strength

Ionic strength clearly plays an important role in the minimisation of charging currents effects. It also was found that ionic strength plays an important role in determining the voltammetric response. The voltammograms obtained using phosphate buffers in the concentration range 100 to 5 mM are shown in Figure 4.14.

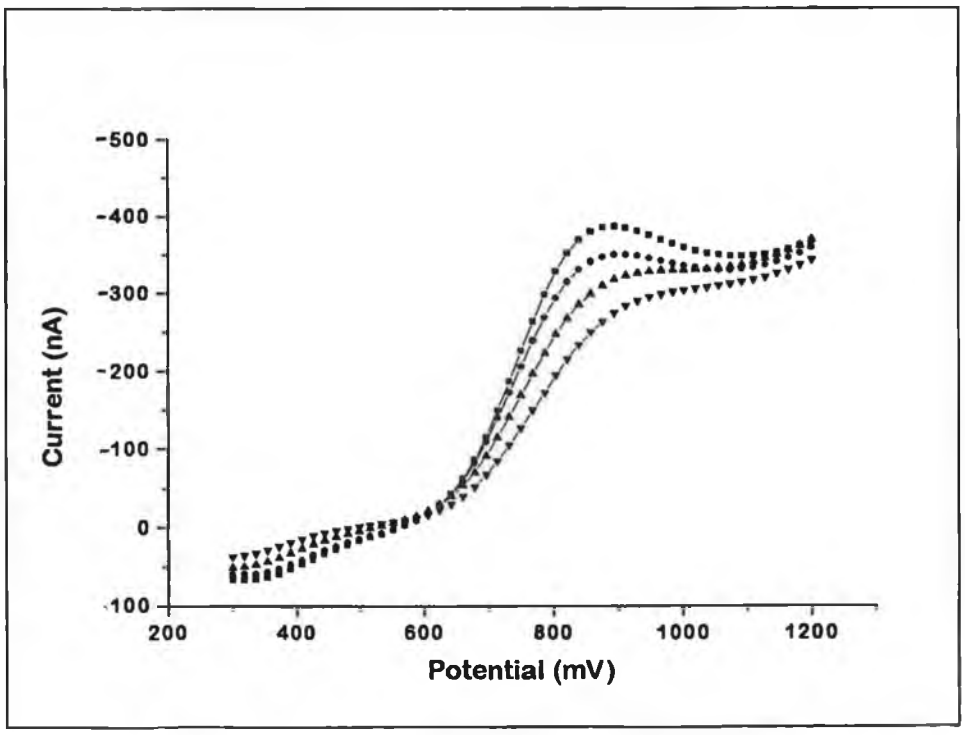

Figure 4.14 Effect of ionic strength on voltammetric response to 100 μM protocatechuic acid. Phosphate buffer pH 2.5, concentration: (■) 100 mM, (●) 50 mM, (▲) 10 mM, (▼) 5 mM.

Both the sharpness of the voltammetric curve and the sensitivity of response was observed to decrease with decreasing ionic strength. As the ionic strength decreases, the conductivity also decreases thus making the iR drop a more important factor. This results in the trend observed in Figure 4.14.

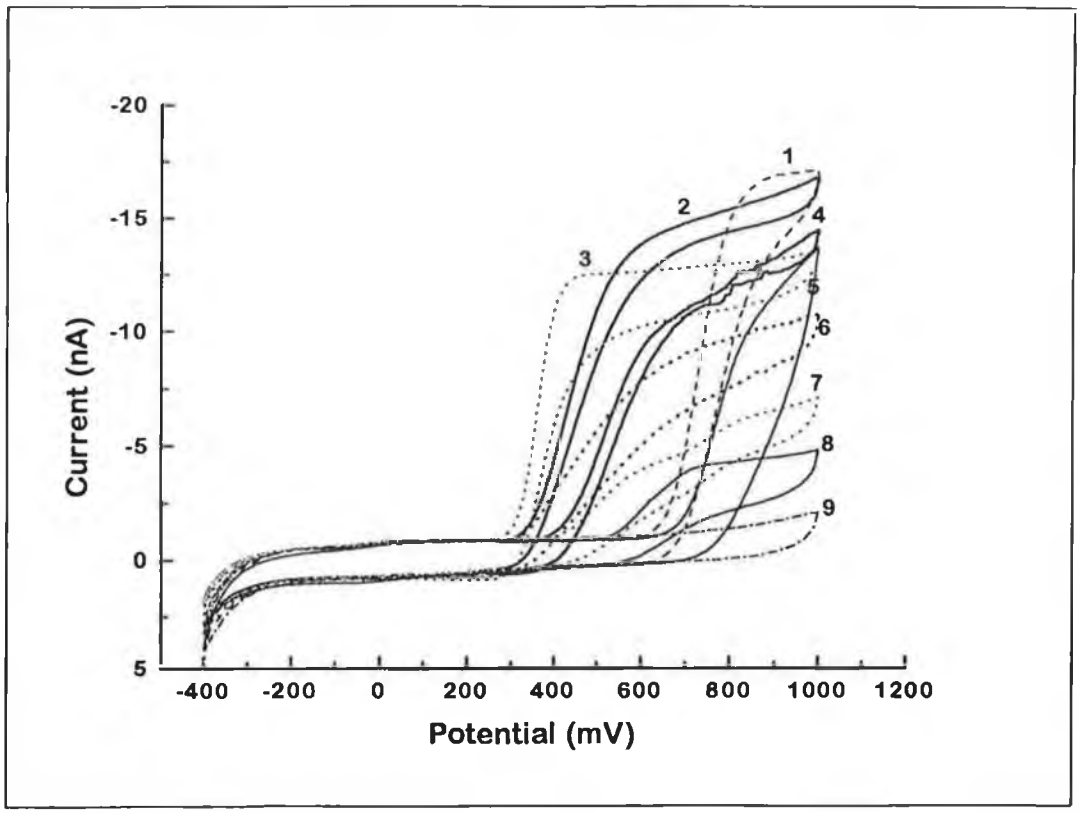

Figure 4.15 Cyclic voltammograms of phenolic acids in phosphate buffer; (1) vanillic acid; (2) gentisic acid; (3) caffeic acid; (4) protocatechuic acid; (5) p-coumaric acid; (6) chlorogenic acid; (7) sinapic acid; (8) ferulic acid; and (9) background. Conditions: scan rate 20 mV/s^{-1}; buffer: 0.1 M phosphate buffer pH 2.5; concentration: 30 μM.

4.5.5 Cyclic Voltammetry and FIA Studies

Slow scan (20 mV/sec) cyclic voltammetry was used for initial investigations of the electrochemical behaviour of the phenolic acids. Scans were carried out in three

different buffer systems. The results clearly indicated the significant effect of pH on the electrochemical behaviour of the phenolic acids. The CV's for the phenolic acids in phosphate buffer pH 2.5 are shown in Figure 4.15. As expected the halfwave potentials of the acids were observed to move to more positive potentials with decreasing pH.

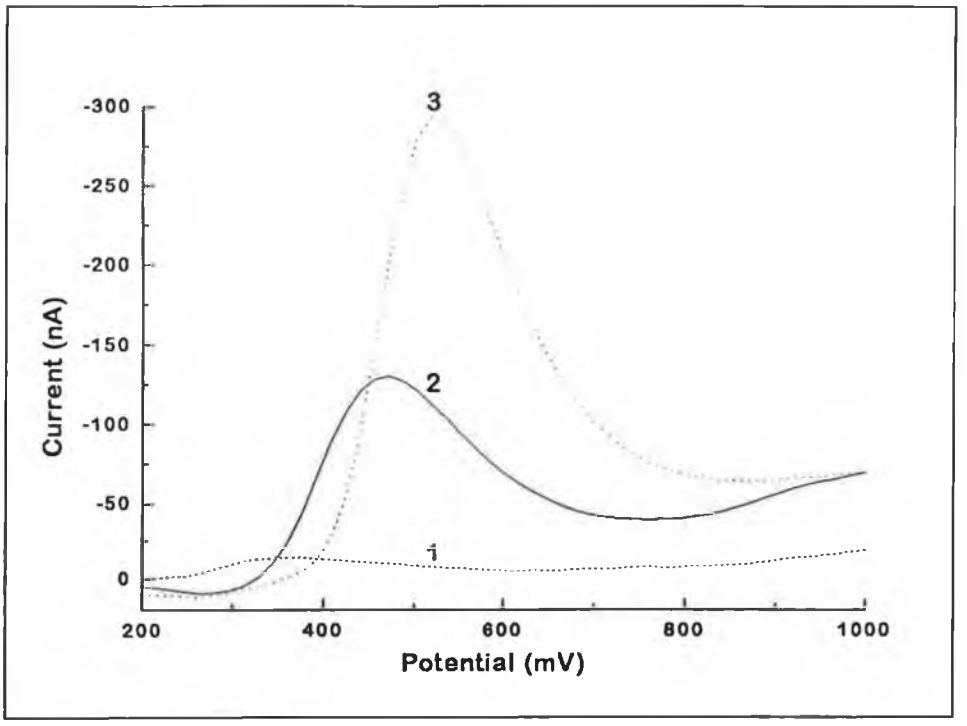

Figure 4.16 Effect of pH on caffeic acid response: (1) 0.1 M phosphate buffer pH 6.0; (2) 0.1 M acetate buffer 4.75; (3) 0.1 M phosphate buffer pH 2.5. Conditions: scan rate: 18 V s^{-1}; concentration: 100 μm; scan range 0 to +1000 mV. Argon pressure: 20 psi.

FIA was used rather than electrophoresis in an effort to minimise the amount of distortion obtained in the voltammetric curves. The results obtained reflected a similar trend to those obtained with the cyclic voltammetry. The halfwave potentials of the phenolic acids were again shifted to more positive potentials with decreasing pH. A dramatic increase in the sensitivity of response was observed with decreasing pH. This

fact was also reflected in the slow scan CV results but at a significantly reduced level.

The 2-dimensional hydrodynamic voltammograms were extracted at the current maxima and plotted. The 2-d hydrodynamic voltammograms for caffeic acid are shown in Figure 4.16. Both the increase in sensitivity and the shift in halfwave potentials with pH are clearly visible. The halfwave potential was 282 mV at pH 6.0, 385 mV at pH 4.75 and 455 mV at pH 2.5.

The hydrodynamic voltammograms of the phenolic acids in phosphate buffer pH 2.5 are presented in Figure 4.17. They were extracted from their respective 3-dimensional voltammograms.

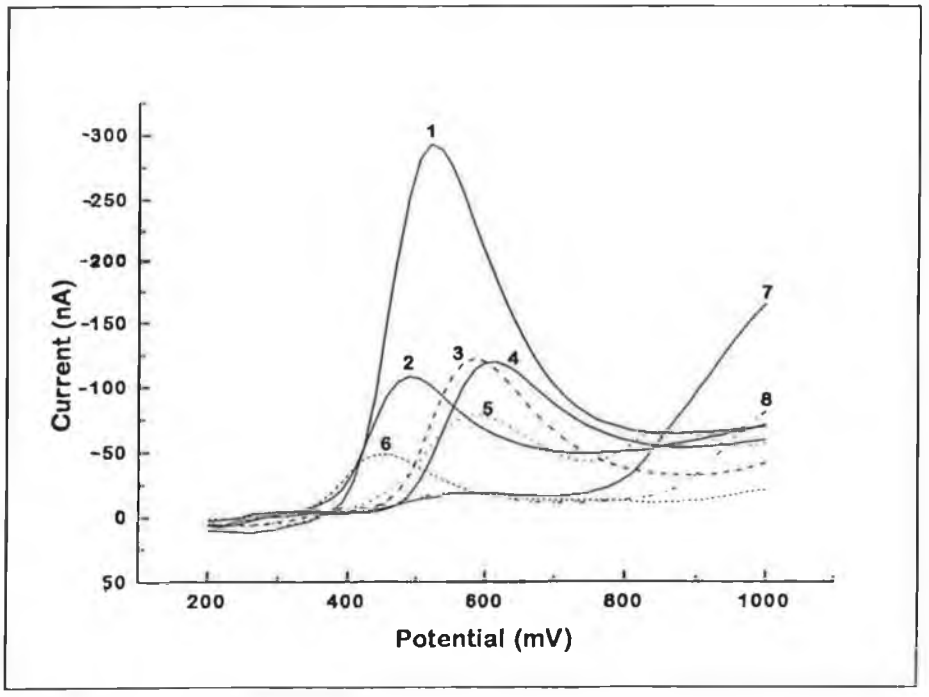

Figure 4.17 The FIA responses of phenolic acids in 0.1 M phosphate buffer pH 2.5. (1) caffeic acid; (2) gentisic acid; (3) chlorogenic acid; (4) protocatechuic acid; (5) ferulic acid; (6) sinapic acid; (7) vanillic acid; and (8) p-coumaric acid. Conditions: scan rate: 18 V/sec; scan range: 200 to +1000 mV; Argon pressure: 20 psi.

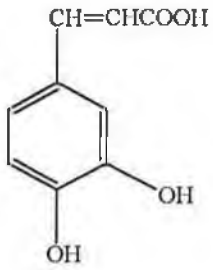

Caffeic Acid

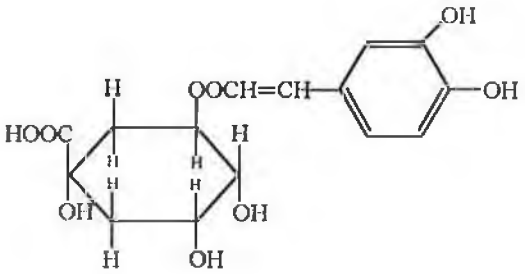

Chlorogenic Acid

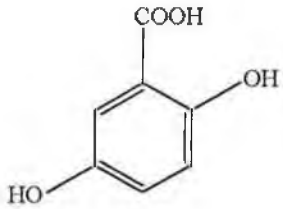

Gentisic Acid

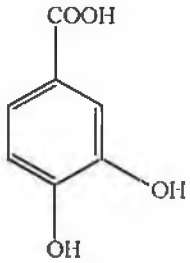

Protocatechuic Acid

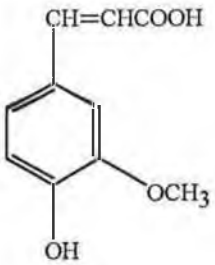

Ferulic Acid

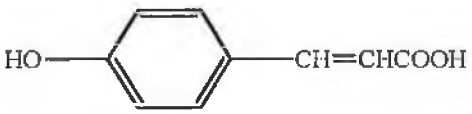

p-Coumaric Acid

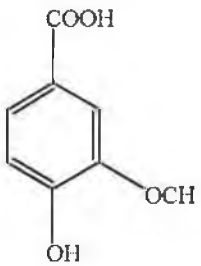

Vanillic Acid

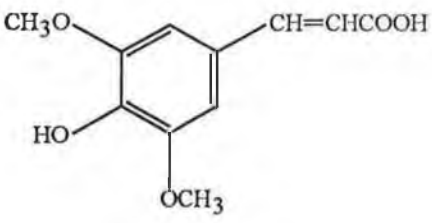

Sinapic Acid

Figure 4.18 Phenolic acid structures.

The di-hydroxyl phenolic acids were found to demonstrate the greatest sensitivity of response due to their n=2 electron reaction. The mono-hydroxyl acids consistently illustrated significantly less sensitivity as compared to the di-hydroxyl acids. The structures of the phenolic acids studied are shown Figure 4.18.

4.5.6 Scan Rate

The scan rate of the potential ramp form is an important parameter in the optimisation of voltammetric detection. The scan rate affects both the sensitivity of response and the magnitude of charging current. Voltammetric detection in CE necessitates the use of high scan rates because of the extremely narrow nature of the CE peaks. Slow scan rates (< 2V/sec) could cause distortion of the peak or miss the peak entirely. The scan rates used in this work ranged from 2 V/sec to 24 V/sec. The optimum scan rates were chosen for their reproducibility of response, minimal background charging currents, minimal distortion of the voltammetric wave and shift in the halfwave potentials. Voltammograms of protocatechuic acid (100 μM) obtained at scan rates in the range 2.0 to 19.0 V/sec are presented in Figure 4.19 (A). The voltammograms presented have been background subtracted. The sensitivity increases as expected with scan rate. The halfwave potentials are also observed to shift to more positive potentials as the scan rate increases. The electrochemical behaviour of the carbon fiber appears to be dependent on the scan rate. As the scan rate increases the electrode appears to lose some of its microelectrode characteristics and starts to exhibit some macroelectrode characteristics. This can be seen in the change from a flat plateau at scan rate 2.0 V/sec to a peak plateau's at higher scan rates as a depletion layer is formed.

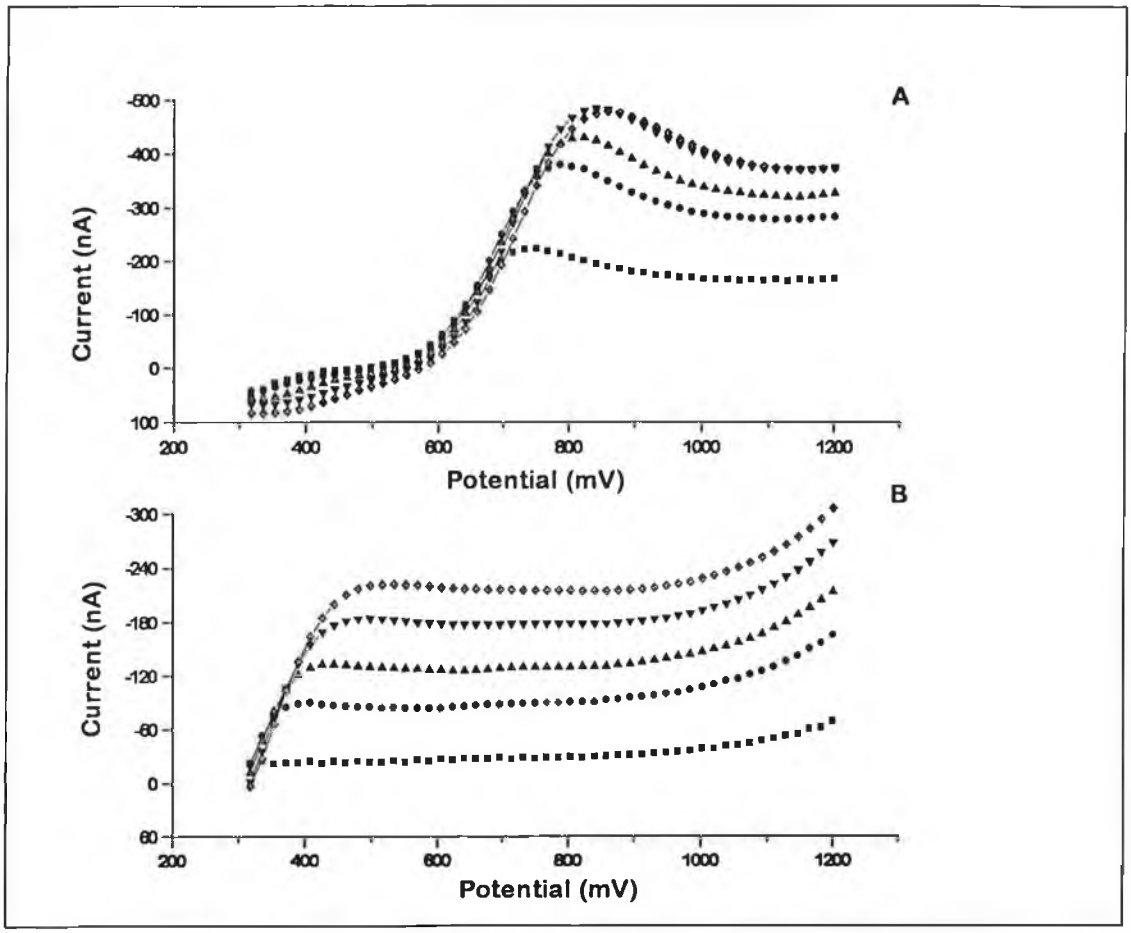

Figure 4.19 (A) Voltammetric curves after background subtraction for 100 μM protocatechuic acid carried out in open cell using scan rates in the range 2.5 V/sec to 19.0 V/sec. (■) 2.5 V/sec, (●) 8.0 V/sec, (▲) 12.0 V/sec, (▼) 16.0 V/sec, (◆) 19.0 V/sec. Electrolyte: 0.1 M phosphate buffer pH 2.5.

(B) Background scans using scan rates in the range 2.5 V/sec to 19.0 V/sec. (■) 2.5 V/sec, (●) 8.0 V/sec, (▲) 12.0 V/sec, (▼) 16.0 V/sec, (◆) 19.0 V/sec. Electrolyte: 0.1 M phosphate buffer pH 2.5.

Plots of the background at the different scan rates are shown in Figure 4.19 (B). Taking the ratio of the voltammogram at their peak currents versus their backgrounds,

it would appear that the lower scan rate would give you a better S/N ratio . As a result of the effective background subtraction regime used in the system it was possible to use higher scan rates, taking advantage of the increased sensitivity without adverse effect on the signal to background ratio.

4.5.7 Determination of Phenolic Acids

4.5.7.1 Sample Preparation

Pre-treatment of the beer samples prior to injection was necessary for two reasons. Firstly the large neutral peak (at 4 minutes) resulted in distortion of the baseline during voltammetric detection (see Figure 4.20 (A)). Secondly the phenolic acids were at low micromolar concentrations and therefore difficult to determine by voltammetry. The phenolic acids were therefore preconcentrated on the Sep-pak cartridge, thus increasing the concentration of analytes. Both C_{18} and tC_{18} Sep-pak cartridges were utilised. It was found that activation of the Sep-pak cartridge was critical. Flushing the cartridge with volumes of methanol greater than 1 ml resulted in difficulty in eluting the phenolic acids with the 0.1 M phosphate buffer pH 6.0.

Initial investigations of the phenolic acids where carried out using a commercial CE system (ISCO, Capillary Electropherograph, Lincoln, NE) with a UV detector. Using a standard solution of the phenolic acids at a concentration of 100 μM, the migration order of the acids was determined by spiking a 20μl aliquot of the standard solution (100 μM) with each phenolic acid individually to a concentration of 500 μM. The migration order obtained is presented in Table 4.1.

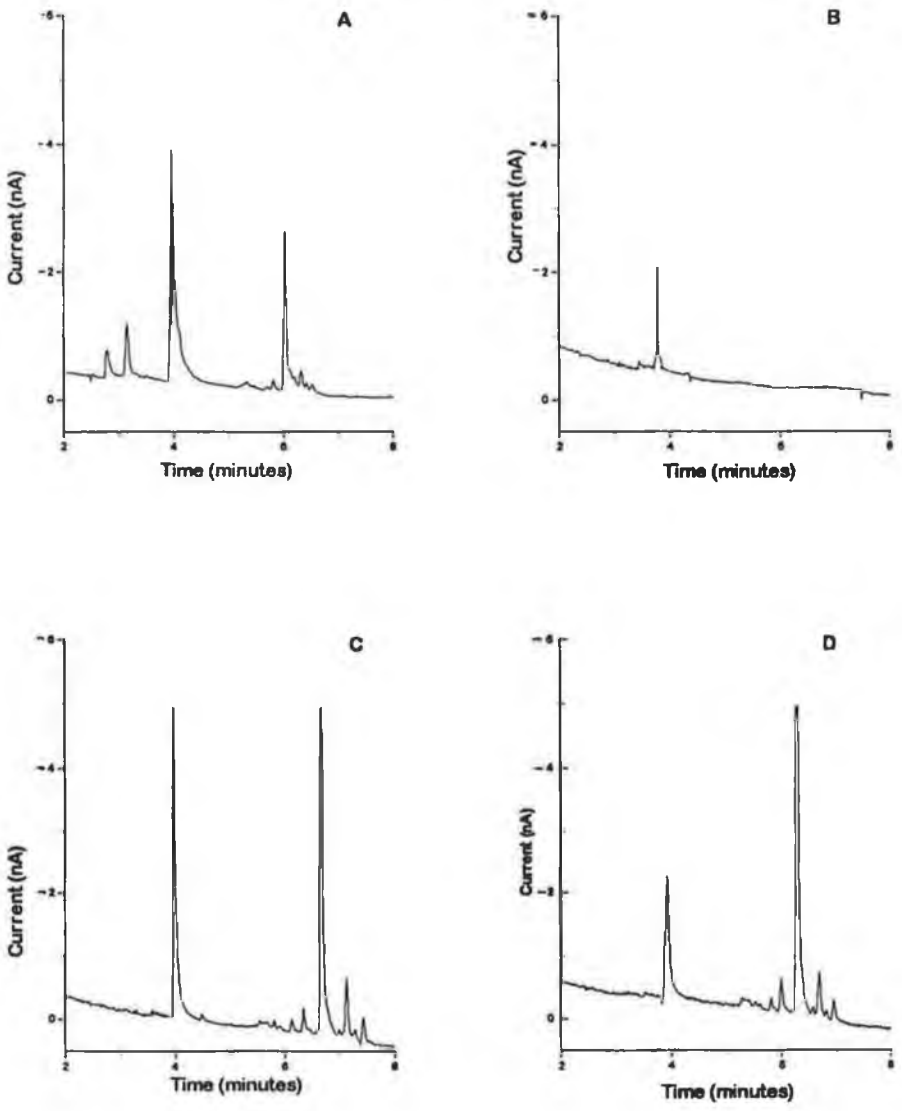

Figure 4.20 (A) Electropherogram of raw beer sample (Budweiser); **(B)** Beer sample (40 mls) after extraction from a C_{18} Sep-pak cartridge; **(C)** Beer sample (20 mls) after extraction from a tC_{18} Sep-pak cartridge;**(D)** Beer sample (40 mls) after extraction from a tC_{18} Sep-pak cartridge; Conditions: 50 mM phosphate buffer pH 6.0; Separation potential 30 kV; Working electrode potential +850 mV.

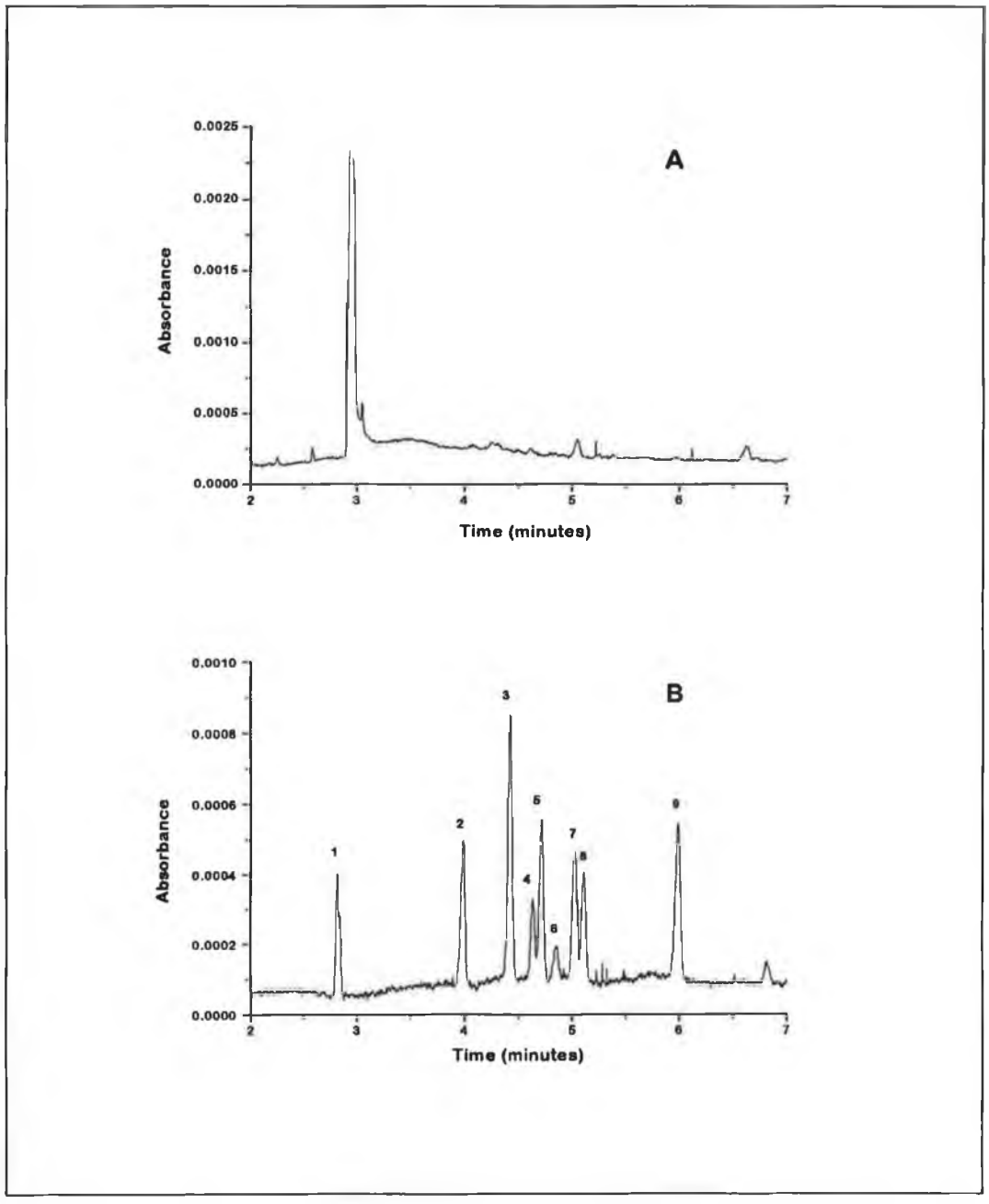

Figure 4.21 (A) Detection of phenolic acids in beer sample by CE-UV. **(B)** 100 μM phenolic standards; (1) catechol; (2) chlorogenic acid; (3) ferulic acid; (4) sinapic acid; (5) caffeic acid; (6) p-coumaric acid; (7) vanillic acid; (8) protocatechuic acid; and (9) gentisic acid.

The migration order of the phenolic acids is generally based on their respective molecular weights. Mobility of ions in fluid solution is governed by their charge/size

ratio. The size of the molecule is based on the molecular weight, the 3-dimensional structure and the degree of solvation (usually hydration). Due to their negatively charged nature of the phenolic acids, they are attracted to the anodic end of the capillary. However, as a result of hydrogen bonding interaction the phenolic acids are swept forward to the cathodic end with the electroosomotic flow. Chlorogenic acid has the highest molecular weight and is therefore eluted first.

This order is followed down to p-coumaric acid and vanillic acid (see Table 4.1). It is believed that the linear structure of the p-coumaric acid allows more hydration than that of vanillic acid. Structural differences between protocatechuic acid and gentisic appear to play an important role in their separation as both compounds have the same molecular weight. Ionic size modifies mobility because of a solute's frictional drag through the supporting electrolyte.

Phenolic Acid	Migration Order	Molecular Weight
Chlorogenic Acid	1	354
Sinapic Acid	2	224
Ferulic Acid	3	194
Caffeic Acid	4	180
p-Coumaric Acid	5	164
Vanillic Acid	6	168
Protocatechuic Acid	7	154
Gentisic Acid	8	154

Table 4.1 Migration order of phenolic acids. Separation conditions: Run buffer; 25 mM phosphate buffer (pH 6.0), Separation potential; 30 kV, Capillary length; 65 cm, Detector wavelength; 220 nm, Injection time, 5secs (vacuum).

The limit of detection for the UV detector was calculated to be in the range 25 to 39 μM (S/N = 3) for the phenolic acids. The beer samples were filtered with a Acrodisc syringe filter prior to injection neat on the CE system. The electropherogram obtained using a detector wavelength of 220 nm is presented in Figure 4.21. Comparing this electropherogram to that obtained for injections of standards it was not possible to identify any peaks corresponding to phenolic acids. Using a detector wavelength of 254 nm yielded a similar result. It was therefore concluded that the phenolic acids where present at concentrations less than the L.O.D. Therefore CE with UV detection is not sufficiently sensitive enough technique for the determination of phenolic acids in beer.

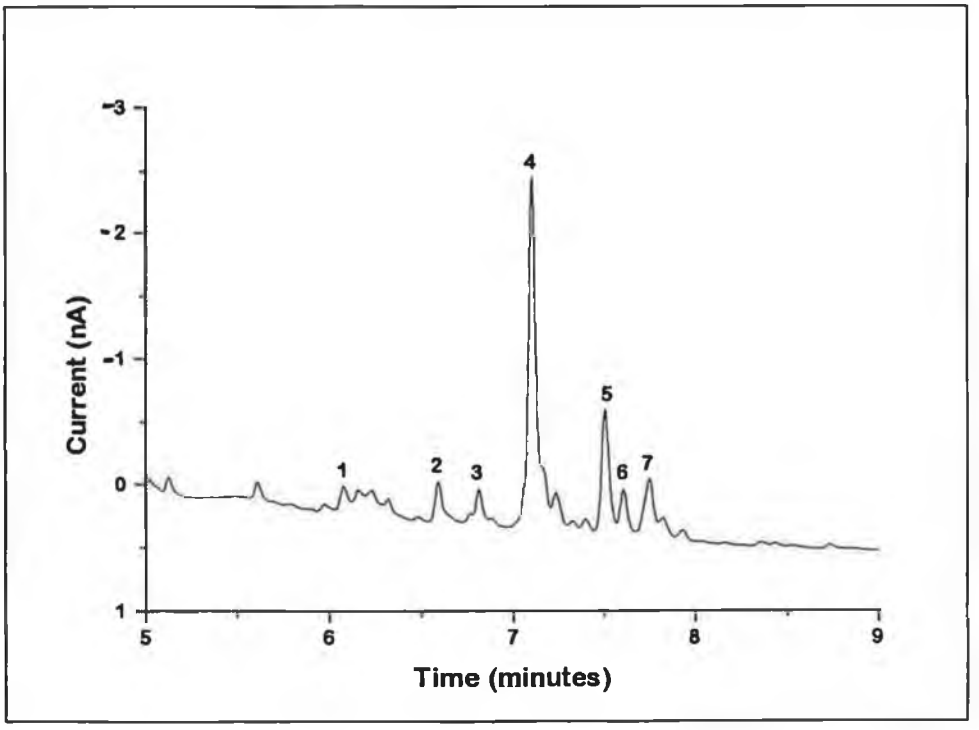

Figure 4.22 Electropherogram of raw beer sample without any sample pre-treatment. (1) chlorogenic acid; (2) ferulic acid; (3) sinapic acid; (4) caffeic acid; (5) p-coumaric acid; (6) vanillic acid; and (7) protocatechuic acid. Conditions: run buffer; 25 mM phosphate buffer pH 6.0, working electrode potential; +1000 mV, separation voltage 30 kV.

CE with amperometric detection was then applied to the determination of the phenolic acids. Amperometric detection is much superior to UV in terms of its detection limits. The electropherogram obtained for an injection of beer is presented in Figure 4.22. Two problems are evident from the electropherogram. Firstly the complex nature of the electropherogram makes assignment of peak identity a difficult task because of shifting migration times coupled with the fact that it is impossible to be 100% confident that a peak is that of the phenolic acid instead of another electroactive compound. Clearly an extra measurement dimension afforded by voltammetry would greatly help the identification process. Secondly the large neutral peak results in distortion of the baseline. Baseline distortion must be minimised for the successful implementation of voltammetric detection.

4.5.8 Voltammetry

Voltammetric experiments were initially carried out with an end-column decoupler configuration only. As previously discussed it was not possible to titrate the run buffer fast enough to achieve the enhancement of sensitivity required with the end-column decoupler. An on-column decoupler was therefore added in front of the end-column to facilitate titration of the run buffer before reaching the end-column decoupler.

Both the separation and voltammetric parameters were examined in terms of the sensitivity of response and peak separation. A scan rate of 18 V/sec was used throughout for these studies. Phosphate run buffers of 5, 10, 25 and 50 mM concentration were used with separation potentials of 20, 25 and 30 kV. The data indicates that sensitivity of response increased with lower ionic strength. This is in direct contradiction with data obtained for open cell studies. No clear explanation has

been developed yet to explain this phenomenon. The sensitivity of response was also observed to increase with increased separation potential. It was concluded that the changes in sensitivity were due to hydrodynamic effects. The electroosmotic flow increased with increased separation potential and decreasing ionic strength. As the electroosmotic flow increases the run time decreases; however the resolution between the peaks is decreased.

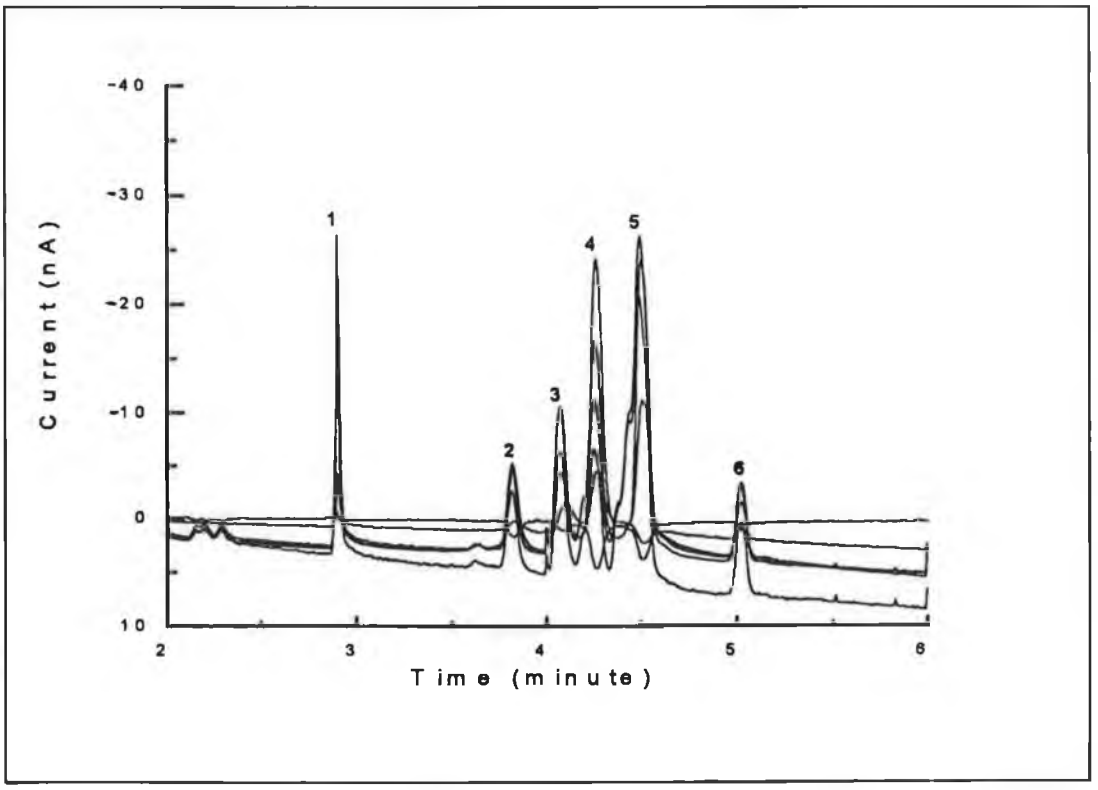

Figure 4.23 Electropherograms of a 10 μM phenolic acid mixture after separation by CE. The electropherograms were extracted from a 3-d voltammogram at a variety of potentials between +300 mV and +1200 mV. Conditions: 5 mM phosphate buffer pH 6.0. Scan rate; 18 V/sec. Injection; electrokinetic-2 seconds. On-column decoupler solution; 0.1 M HCl. Electrochemical cell solution: 0.1 M phosphate buffer pH 2.5.

This fact is reflected in Figure 4.23. Peak 4 is a dual peak composing of ferulic acid

and caffeic acid, peak 5 is triple peak composing p-coumaric acid, vanillic acid and protocatechuic acid. The resolution between the peaks is improved as the separation potential is reduced and the ionic strength of the run buffer is increased. The peaks are completely resolved at a potential of 25 kV and a buffer concentration of 25 mM, as can be seen in Figure 4.24.

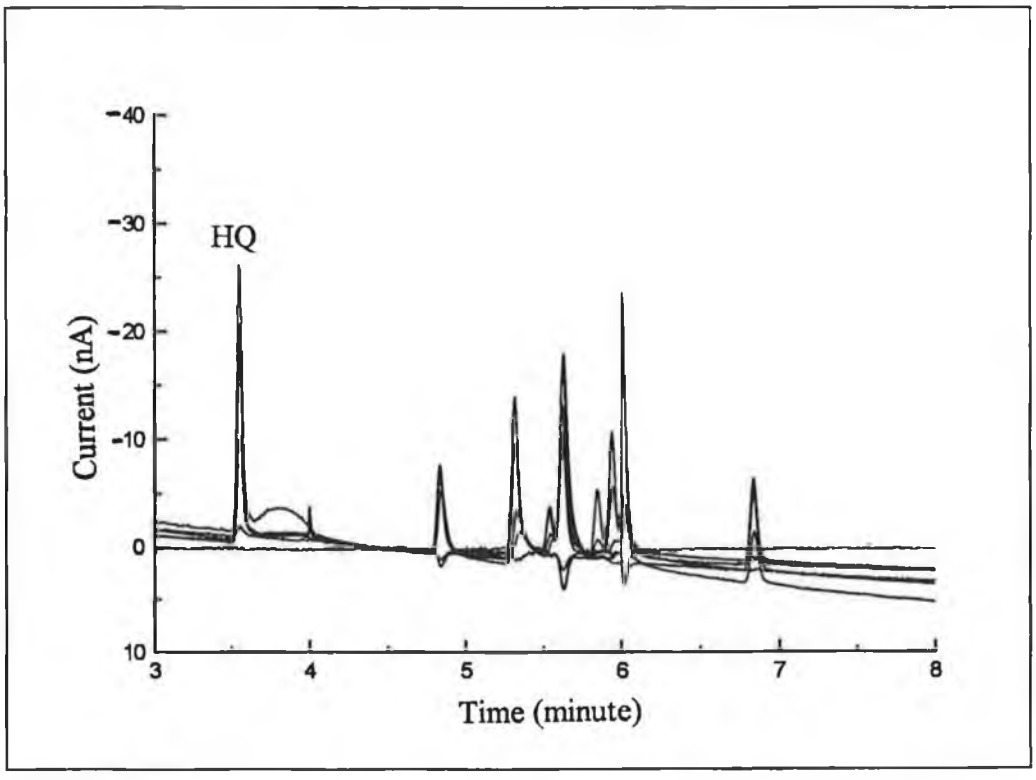

Figure 4.24 Electropherograms of a phenolic acid mixture after separation by CE. The electropherograms were extracted from a 3-d voltammogram a variety of potentials between +300 mV and +1200 mV. Conditions: 25 mM phosphate buffer pH 6.0. Separation potential: 25 kV.

The peaks of the phenolic acids can be seen clearly together with the neutral maker (hydroquinone). The run time is increased by approximately 2 minutes. There is a reduction in sensitivity which is probably due to the thin layer properties of the decoupler which changes with the rate of electroosmotic flow due to hydrodynamic

effects. The hydrodynamic effects may influence the titration of the run buffer which has a direct bearing on the sensitivity of response. It will also have a bearing on the rate of mass transport to the carbon fiber electrode.

Clearly a trade off between sensitivity and resolution must be established. The best resolution was obtained with a 50 mM run buffer and a separation potential of 20 kV. This corresponds to lowest electrosmotic flow under the conditions examined. However, the sensitivity was extremely poor under these set of conditions. Both the ionic strength of the buffer and the separation potential also appear to have some effect on the voltammetry. This effect was not significant as expected.

The hydrodynamic voltammograms taken from their respective 3-dimensional voltammograms are shown in Figure 4.25. The sharpest voltammetric responses were obtained using a separation voltage of 30 kV and a 5 mM phosphate run buffer pH 6.0. (Figure 4.25 (A)). Under these particular conditions good definition of the peak shape is obtained together with a sharp rise in the i-E curve. The i-E curves under these conditions give the closest fit to the theoretical Nernstian response (ΔE = 59.1 mV). Both the sharpness of response and the peak is lost at lower separation potentials (see Figure 4.25 (B)). The results obtained clearly indicate that the separation potential has the most dramatic effect on the i-E curves. The worst responses were again obtained with a separation potential of 20 kV and 50 mM phosphate run buffer.

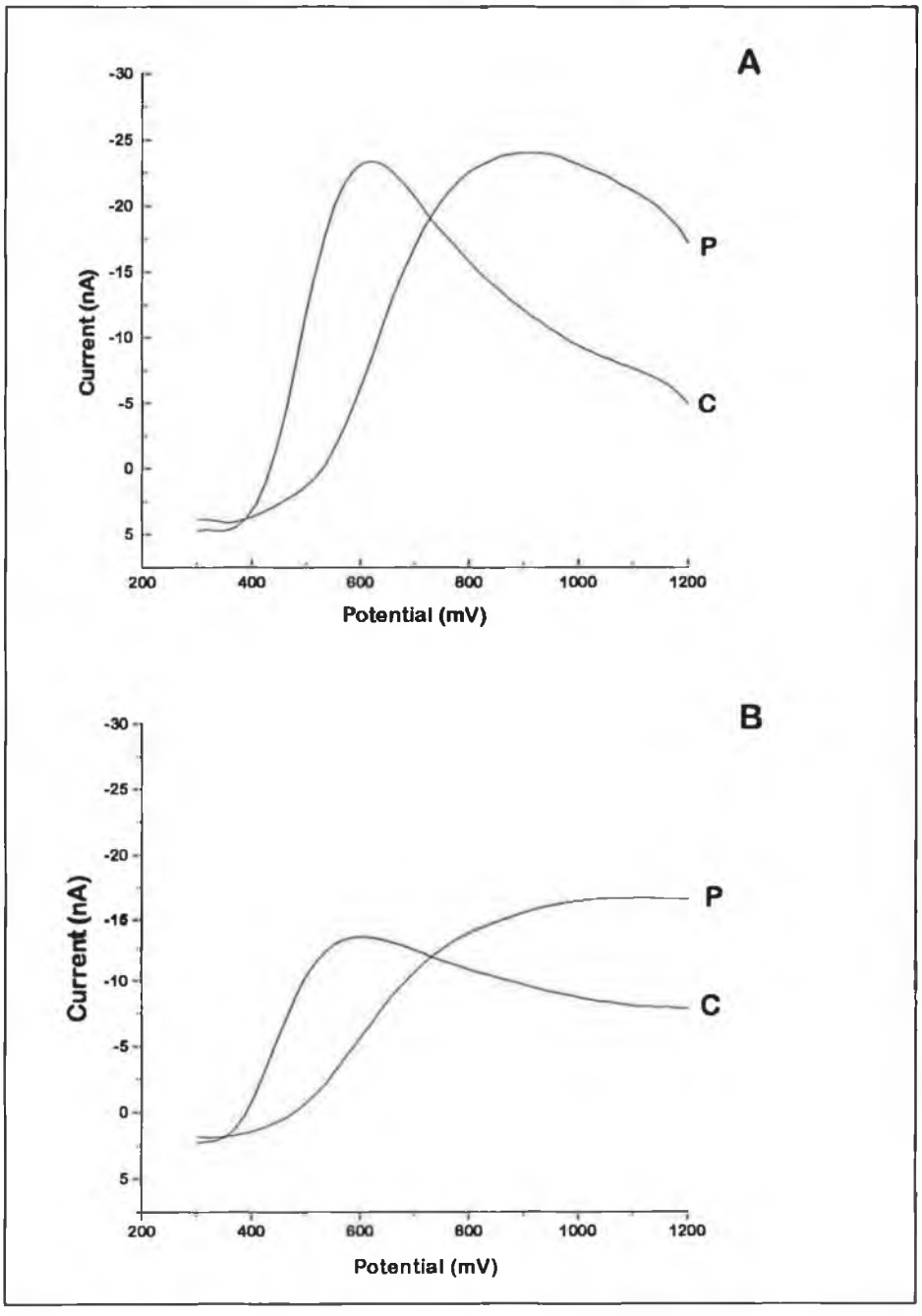

Figure 4.25 (A) Hydrodynamic voltammograms of 10 μM protocatechuic acid (P) and 10 μM caffeic acid (C). Separation potential 30 kV. **(B)** Hydrodynamic voltammograms of 10 μM protocatechuic acid (P) and 10 μM caffeic acid (C). Separation potential 20 kV. Conditions: 5 mM phosphate run buffer pH 6.0. Scan range +300 to +1200 mV. Scan rate 18 V s^{-1}. Injection: electrokinetic-2 secs at 30 kV. On-column decoupler solution: 0.1 M HCl. Electrochemical cell solution: 0.1 M phosphate buffer pH 2.5.

A 3-dimensional voltammogram of a 10 μM standard phenolic acid mixture is shown in Figure 4.26. Good definition of the voltammograms is obtained with the conditions used. The 3-dimensional definition of the voltammograms facilitates ease of peak identification. The information obtained from the peak shape, the halfwave potential and the migration time can be assimilated together when assigning the identity to a peak.

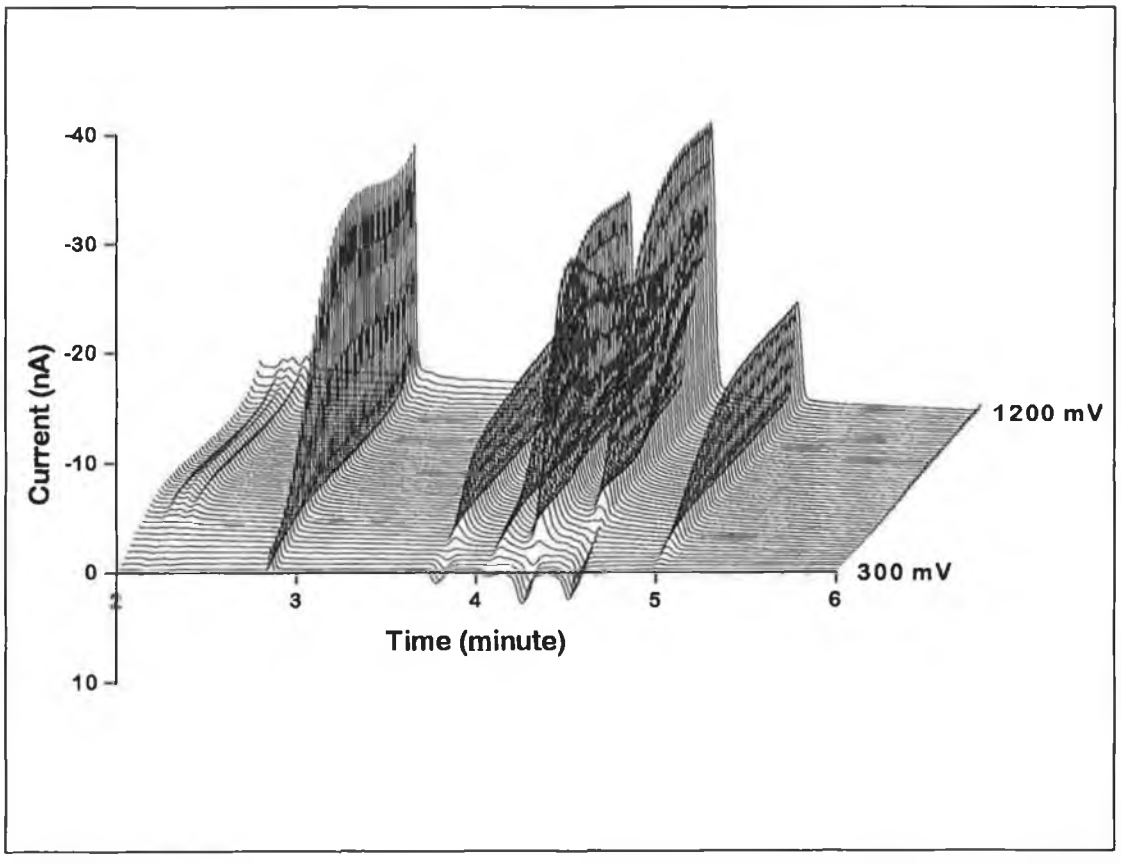

Figure 4.26 3-Dimensional hydrodynamic voltammogram of a 10 μM phenolic acid standard mixture following separation by CE. Conditions: 10 mM phosphate buffer pH 6.0. Scan rate: 18 V s^{-1}. Scan range: +300 to +1200 mV. Separation voltage 30 kV. End-column decoupler reservoir: 0.1 M HCl. Electrochemical cell solution: 0.1 M phosphate buffer pH 2.5. Injection: electrokinetic-2 secs at 30 kV.

The limit of detection for the system is approximately 2-3 μM (S/N = 3) present. This is an improvement over the results reported by Ferris et al. [81]. The voltammograms are also superior in terms of the stability of the baseline and the flatness of the baseline due to the dynamic background subtraction system.

CHAPTER 5

CONCLUSIONS\FUTURE TRENDS

5.1 Conclusions

There is unlikely to be any major revolution in the electrochemical instrumentation and electrochemical detection in the next couple years but rather steady development of the work presented in this thesis. The use of photolithography and related techniques has introduced exciting possibilities into electrochemical instrumentation. The development of disposable electrodes and electrode arrays is now feasible. This may help to remove some of the age old problems of irreproducibility due to surface poisoning that have generally plagued electrochemical measurements. Automation of electrochemical instrumentation will become a practical reality, thus making its application to routine analysis situations easier. Continued evolution in software will make the option of developing one's own software an easier alternative for those who are not computer literate.

In Chapter 2 of this thesis the design, development and application of a multichannel potentiostat was discussed. This potentiostat was used with multiple electrodes or arrays electrodes in both linear or radial configurations. Amperometric arrays can offer a significant improvement in electrochemical detection over single electrodes. With an amperometric array it is possible to achieve the sensitivity of single electrode amperometric measurements while obtaining the same level of information as a voltammetric experiment without the problems of charging current effects. The improvements offered are both in the qualitative and quantitative realms of analysis.

High speed data acquisition, which is equivalent to high scan rates; can be carried out routinely without the undesired charging currents, therefore distortion of the voltammogram can in principle be avoided with multichannel detection. Use of an array should make it possible to implement data redundancy regimes and therefore enhance the reliability and accuracy of the data obtained.

The results obtained highlight the problems of non-ideal behaviour in amperometric arrays. Ideal behaviour of a multielectrode detector would include an equivalent response (signal, noise and background) of all channels when the working electrodes are set at the same potential, no cross-talk between the individual channels, and signal-to-noise ratios comparable with conventional single-electrode amperometric detectors. Equality of the responses is determined by the hydrodynamic and mass-transfer characteristics of the cell, by electrode and cell geometry, by electrode kinetics and by proper configuration and adjustment of the electronics in the potentiostat. The data indicates that significant imprecision and error will be present in the results if normalisation is not utilised.

A fundamental feature of amperometric array detection systems is the ability to fabricate arrays with near identical surface areas and kinetics. This is impossible to achieve with using standard electrode fabrication technology. Arrays which have been constructed using conventional fabrication technology must have their response characteristics normalised to compensate for individual discrepancies in electrode responses. However these procedures are limited in their effectiveness.

A second approach in the fabrication of arrays has been the use of photolithography. The use of this technique to fabricate arrays may play an important role in the future development and application of amperometric arrays. The application of both linear

and radial amperometric arrays has been described in the literature [39, 44]. This technique facilitates the production of electrodes with highly reproducible surface areas. Large numbers of arrays can be produced simultaneously and at relatively low cost. However, these arrays have a limited working life due to poor mechanical characteristics [64]. The continued development of multiple electrode systems is therefore dependent on the ability to produce stable, reliable and reproducible arrays.

The use of amperometric arrays with FIA can allow the determination of multi-components in a single injection without prior separation and has been demonstrated for a mixture of metals ions. This approach can be effective, provided there is sufficient resolution between the halfwave potentials of the analytes being determined and the analytes do interact with each other. This system is probably only effective at determining a limited number of analytes at any given time.

A multichannel potentiostat could also be successfully used with multiple biosensors to determine a number of analytes simultaneously. The determination of glucose in the presence of interferences using two sensors has been demonstrated in Chapter 2. The application presented in this chapter may be expanded to multiple sensor systems. The limitations of the system are determined by the capabilities of the biosensors which at present generally remain poor.

The geometry of a flow cell plays a vital role in electrochemical detection. Flow cell designs based on the thin layer and the wall jet configurations have found the widest applications for electrochemical detection. In Chapter 3, a new cell geometry was introduced for electrochemical detection. The fountain cell possesses flow characteristics which make it suitable for electrochemical detection, especially with multiple electrodes. As the sample plug develops radially from the inlet, each

electrode in the array is exposed to very similar section of the sample plug which is normally difficult to achieve with standard thin layer configurations. This geometry would be ideal with small biosensor arrays which could typically consist of between 2 to 6 sensors coupled to a multichannel potentiostat.

The SFA system described in Chapter 3 has a number of distinct advantages over FIA. Solvent consumption with SFA is significantly lower than that of FIA. Multi-reagent systems are easier to implement. A disadvantage in some cases is the requirement for computer control of the SFA system. An interesting possibility investigated in Chapter 3 was the development of on-line chemical modification of polypyrrole-modified electrodes (CME) in situ. This methodology could easily be extended to other polymer systems or biosensor systems. The various reagents or enzymes were placed at each of the valve ports and aspirated in sequence. The procedure is essentially; automated therefore high reproducibility in the fabrication of the modified electrodes should be possible.

The development of electrochemical detection for CE has been difficult in comparison to its implementation in LC and FIA. The main problem is the high potential fields that are used in CE separation. When an electrode was placed in the capillary, noise arising from the high voltage applied across the capillary interfered with detection. The implementation of the decoupler design permitted the first use of on-column detection for CE. The couplers have evolved from the early porous glass coupler to the cast Nafion type used by Park and co-workers at present [78]. A carbon fiber was used to detect analytes amperometrically with detection limits in the low nanomolar range. The use of couplers has made electrochemical detection in CE possible by terminating the separation voltage, and therefore noise currents, before detection.

Some alternative approaches to the coupler have also been utilised which include insertion of the carbon fiber working electrode into a capillary of small internal diameter, and chemical etching of the capillary end of a capillary to provide a conical entrance for electrode placement.

Special consideration must be given to the specifications of the potentiostat required for CE-EC. Arcing between the high voltage end and ground results in permanent damage to the potentiostat especially the i-E converter. BAS now supplies a modified potentiostat which is modified to allow easy replacement of the damaged op-amps. To date, no successful hardware method of prevention of this type of damage has been developed. In addition the potentiostat must be capable of working at high sensitivities (down to 0.1 pA). Low noise operation of the potentiostat is critical. Stability of the potentiostat in such high gain situations is vital if accurate data are to be obtained. The potentiostat must be capable of supplying short high current outputs which are necessary during the electrochemical pre-treatment of the carbon fiber working electrode.

Routine analysis of complex samples with CE-EC is problematic because of the difficulty in assigning absolute peak identities due to shifting migration times. However, the use of voltammetric detection which can give 3-dimensional definition of the CE peaks helps to overcome this problem, as the voltammetric shape of a peak is generally characteristic for a particular compound. This information, coupled with the halfwave potential of the compound and the migration time, greatly aids in the identification process. The technique is also extremely useful where the problem of co-elution occurs. Contour plots of a peak will normally reveal whether it is homogenous of composed of two or more responses.

There a number of inherent problems associated with the implementation of voltammetric detection with CE. Distortion of the voltammetric response due the electrophoresis current can be particularly acute and difficult to eliminate with traditional decoupler designs. The use of a Nafion end-decoupler provides the required isolation from the electrophoretic current, thus making voltammetric detection feasible. The poor level of sensitivity associated with voltammetric detection is normally a result of severe charging current effects at lower sensitivities. The effects of charging currents were alleviated in the system described by the use of a second potentiostat which was dedicated to dynamic background subtraction of any charging current effects. The use of carbon fiber microelectrode working electrodes (33 μm o.d.) further reduced charging current effects due the smaller working area. Despite the reduction of charging effects, the limit of detection with voltammetric detection is three orders of magnitude higher than that possible with amperometric detection (μM vs. nM). This limiting factor will restrict the general application of voltammetry; however, in specific analysis situations, voltammetric detection will prove a very useful tool.

5.2 Future Trends

The trend in electrochemical instrumentation in recent years has been towards miniaturisation. There has been great interest in the development of entire electroanalytical instruments on single silicon wafers. Construction of an entire CE system with electrochemical detection on silicon appears to offer the most exciting and fruitful prospect at present. These systems offer fast and efficient separations with extremely small reagent consumption. Manz et al. [102] have described the basis for fabrication based on photolithography process. These processes include film

deposition (addition of photosensitive film), etching (removal of the oxide and the photoresist), and bonding (assembly). Using these technologies, a variety of miniaturised analytical systems, including a gas chromatograph, coulometric titrator, oxygen sensor and pH sensor have been fabricated on what is essentially a semiconductor chip [103].

At Ciba-Geigy they have taken the concept of instrument miniaturisation a step further [104]. They propose the development of micro Total Chemical Analysis Systems (μ-TAS). Sampling, sample transport, any necessary chemical reactions, chromatographic or electrophoretic separation and detection can be integrated into one miniature instrument. The major goal with miniaturisation is an improvement of the analytical performance which is characterised by a very significant reduction of the analysis time and cycle times. As an important additional advantage, miniaturisation leads to a drastic reduction of the consumption of sample and mobile phases.

One the major problem associated with miniaturisation of LC and CE has been with reduction in size of the detector. Miniaturisation of optical detectors such as based on UV spectrometry or fluorescence is extremely problematic. On the other hand, electrochemical detectors lend themselves favourably to the reduced scales required. It therefore would appear that electrochemical detection will play an important role in the future development of these systems.

The work in this thesis clearly reflects the trend towards the acquisition of more information [105]. In many cases the standard 2-dimensional response is no longer sufficient to met the requirement of the analytical scientist. The work presented in this thesis offers possibilities for the future development of FIA, LC, SFA and CE in terms of increased information content.

References

1. Willard, H.H., Merritt, L.L., Dean, J .A. and Settle, F.A., *Instrumental Methods of Analysis*, Wadsworth Inc., Belmont, 1988.
2. Skoog, A.D., West, D.M. and Holler, F.J., *Fundamentals of Analytical Chemistry*, Saunders College Publishing, New York, 1988.
3. Heyrovsky, J., *Chem.Listy*, 16 (1922) 256.
4. Bond, A.M., *Modern Polarographic Methods in Analytical Chemistry*, Marcel Dekker Inc., New York, 1980.
5. Wang. J., *Analytical Chemistry*, VCH Publishers Inc., New York. 1994.
6. Osteryoung, J., *Science*, 218 (1982) 261.
7. Kissinger, P.T., *Analyst*, 119 (1994) 874.
8. Kissinger, P.T. and Heineman, W.R., *Laboratory Techniques in Electroanalytical Chemistry,* Marcel Dekker Inc., New York, 1984.
9. Stulik, K. and Pacakova, V., *Electroanalytical Measurements in Flowing Liquids,* Ellis Horwood, New York, 1987.
10. Horowitz, P. and Hill, W., *The Art of Electronics*, Cambridge University Press, New York, 1987.
11. Malmstadt, H.V., Enke, C.E. and Crouch, S.R., *Electronics and Instrumentation for Scientists*, The Benjamin/Cummings Publishing Company Inc., Menlo Park, California, 1981.
12. Osteryoung, J.G. and Osteryoung, R.A., *Anal.Chem.*, 57 (1985) 101A.
13. Blutstein, H., Bond, A.M. and Norris, A., *Anal.Chem.*, 46 (1974) 1754.
14. Nicholson, R.S. and Shain, I., *Anal.Chem.*, 36 (1964) 706.
15. Christian, G.D., *Analytical Science*, New York, Wiley-Interscience, 1986.
16. Plambeck, J.A., *Electroanalysis Chemistry, Basic Princilpes and Applications*, Wiley-Interscience, New York, 1982.
17. Vassos, B.H. and Ewing, G.W., *Electroanalytical Chemistry*, Wiley-Interscience, NewYork, 1983.
18. Bioanalytical Systems, *User Manual Electrochemical Detectors,* West Lafayette, Indiana, 1987.
19. Wise, J.A., Heineman, W.R. and Kissinger, P.T., *Anal.Chim.Acta,* 172 (1985) 1.

20. Weber, S.G., *J.Electroanal.Chem.*, 172 (1983) 1.
21. Glauert, M.B., *J.Fluid.Mech.*, 1 (1956) 625.
22. Gunasingham, H. and Fleet, B., *Anal.Chem.*, 55 (1983) 1409.
23. Gunasingham, H., *Anal.Chim.Acta*, 159 (1984) 139.
24. van der Linden, W.E. and Dieker, J.W., *Anal.Chim.Acta*, 119 (1980) 1.
25. Wang, J. and Dewald, H.D., *Anal.Chem.*, 56 (1984) 156.
26. Wang, J. and Freiha, B.A., *Anal.Chem.*, 57 (1985) 1776.
27. Moody, G.J., Sanghera, G.S. and Thomas, J.D.R., *Analyst*, 111 (1986) 605.
28. Bard, A.J., *Electroanalytical Chemistry*, vol 16, Marcel Dekker Inc., New York, 1989.
29. Elbicki, J.M., Morgan, D.M. and Weber, S.G., *Anal.Chem.*, 56 (1984) 978.
30. Kissinger, P.T., *J.Chem.Educ.*, 60 (1983) 308.
31. Hanekamp, H.B. and van Nieuwkerk, H.J., *Anal.Chim.Acta*, 121 (1980) 13.
32. Hanekamp, H.B. and deJong, H.G., *Anal.Chim.Acta*, 135 (1982) 351.
33. Floyd, T.L., *Electronic Devices*, Merrill, Columbus, 1986.
34. Napp, D.T., Johnson, D.C. and Bruckenstein, S., *Anal.Chem.*, 39 (1967) 481.
35. Bard, A.J. and Faulker, L.R., *Electrochemical Methods, Fundamentals and Applications*, New York, Wiley-Interscience, 1980.
36. Matson, W.R., Gamache, P.G., Beal, M.F. and Bird, E.D., *Life Science*, 41 (1987) 905.
37. Matson, W.R., Langlais, P., Volicer, L., Gamache, P.H., Bird, E. and Mark. K.A., *Clin.Chem.*, 30 (1984) 1477.
38. Svendsen, C.N., *Analyst*, 118 (1993) 123.
39. Matsue, T., Aoki, A., Ando, E. and Uchida, I., *Anal.Chem.*, 62 (1990) 407.
40. Fielden, P.R. and McCreedy, T., *Anal.Chim.Acta*, 273 (1993) 111.
41. Hoogvliet, J.C., Reijn, J.M. and Van Bennekom,W.P., *Anal.Chem.*, 63 (1991) 2418.
42. Southampton Electrochemistry Group, *Instrumental Methods in Electrochemistry*, Ellis Horwood, Chichester, England, 1985.
43. He, P. and Faulkner, L.R., *Anal.Chem.*, 58 (1986) 517.
44. Fielden, P.R., McCreedy, T., Ruck, N. and Vaireanu, D-I., *Analyst*, 119 (1994) 953.

45. Samuelsson, R., O'Dea, J.J. and Osteryoung, J.G., *Anal.Chem.*, 52 (1980) 2215.
46. Saitoh, K. and Suzuki, N., *Anal.Chem.*, 51 (1979) 1683.
47. Hershberger, L.W., Callis, J.B. and Christian, G.D., *Anal.Chem.*, 53 (1981) 971.
48. Owens, D.S., Johnson, C.M., Sturrock, P.E. and Jaramillo, A., *Anal.Chim.Acta*, 197 (1987) 249.
49. Caudill, W.L., Ewing, A.G., Jones, S. and Wightman, R.W., *Anal.Chem.*, 55 (1983) 1877.
50. Anderson, J.L. and Chesney, D.J., *Anal.Chem.*, 52 (1980) 2156.
51. Weisshaar, D.E., Tallman, D.E. and Anderson, J.L., *Anal.Chem.*, 53 (1981) 1809.
52. Anderson, J.L., Weisshaar, D.E. and Tallman, D.E., *Anal.Chem.*, 53 (1981) 906.
53. Radzik, D.M., Brodbelt, J.S. and Kissinger, P.T., *Anal.Chem.*, 56 (1984) 2927.
54. Roston, D.A. and Kissinger, P.T., *Anal.Chem.*, 54 (1982) 429.
55. Roston, D.A., Kissinger, P.T. and Shoup, R.E., *Anal.Chem.*, 54 (1982) 1417A.
56. Lunte, C.E., Wheeler, J.F. and Heineman,W.R., *Anal.Chim.Acta*, 200 (1987) 101.
57. Allison, L.A. and Shoup, R.E., *Anal.Chem.*, 55 (1983) 8.
58. Shoup, R.E. and Mayer, G.S., *Anal.Chem.*, 54 (1982) 1164.
59. Cante, F., Rois, A., Luque De Castro, M.D. and Valcarcel, M., *Anal.Chim.Acta*, 211 (1988) 287.
60. Mortia, M., Longmire, M.L. and Murray, R.W., *Anal.Chem.*, 60 (1988) 2770.
61. Anderson, J.L., Whiten, K.K., Brewester, J.D., Ou, T.Y., and Nonidez, W.K., *Anal.Chem.*, 57 (1985) 1366.
62. DeAbreau, M. and Purdy, W.C., *Anal.Chem.*, 59 (1987) 204.
63. Fosdick, L.E. and Anderson, J.L., *Anal.Chem.*, 58 (1986) 2750.
64. Fosdick, L.E, Anderson, J.L, Baginski, T.A and Jaeger, R.C., *Anal.Chem.*, 58 (1986) 2750.
65. Aoki, A., Matsue, T. and Uchida, I., *Anal.Chem.*, 62 (1990) 2206.
66. Wang, J., Rayson, G.D., Lu, Z. and Wu, H., *Anal.Chem.*, 62 (1990) 1924.
67. Harrington, M.S., Anderson, L.B., Robbins, J.A. and Karweik, D.H., *Rev.Sci.Instrum.*, 60 (1989) 3323.
68. Aoki, A., Matsue, T. and Uchida, I., *Anal.Chem.*, 64 (1992) 44.
69. Bearly, T.H., Doshi, A.K. and Fielden, P.R., *Anal.Proc.*, 26 (1989) 389.

70. Wallingford, R.A., Olenfirowicz, T.M. and Ewing, A.G., *Anal.Chem.*, 61 (1989) 292A.
71. Gozel, P., Gassmann, E., Michelsen, H. and Zare, R.N., *Anal.Chem.*, 59 (1987) 44.
72. Wu, S. and Dovichi, N.J., *J.Chromatogr.*, 480 (1989) 141.
73. Wallingford, R.A. and Ewing, A.G., *Anal.Chem.*, 59 (1987) 1762.
74. Wallingford, R.A. and Ewing, A.G., *Anal.Chem.*, 60 (1988) 258.
75. Wallingford, R.A. and Ewing, A.G., *Anal.Chem.*, 60 (1988) 1972.
76. Wallingford, R.A. and Ewing, A.G., *Anal.Chem.*, 61 (1989) 98.
77. O'Shea, T.J., Greenhagen, R.D., Lunte, S.M., Lunte, C.E., Smyth, M.R., Radzik, D.M. and Watanabe, N.J., *J.Chromatogr.*, 593 (1992) 305.
78. Park, S., Lunte, S.M. and Lunte. C.E., *Anal.Chem.*, 67 (1995) 911.
79. Huang, X., Zare, R.N., Sloss, S. and Ewing. A.G., *Anal.Chem.*, 63 (1991) 189.
80. Sloss, S. and Ewing, A.G., *Anal.Chem.*, 65 (1993) 577.
81. Ferris, S.S., Lou, G. and Ewing, A.G., *J.Microcol.Sep.*, 6 (1994) 263.
82. Enke, C.G., Science, 218 (1982) 785.
83. Lauer, G., Abel, J.P. and Faulkner, L.R., *Anal.Chem.*, 39 (1967) 765.
84. He, P., Avery, J.P. and Faulkner, L.R., *Anal.Chem.*, 54 (1982) 1313A.
85. RTI-800/815 User's Manual, Analog Devices.
86. RTI-817 User's Manual, Analog Devices.
87. Software Manual for RTI-800, 815, 817.
88. Lunte, C.E., Ridgeway, T.H. and Heineman, W.R., *Anal.Chem.*, 59 (1987) 761.
89. Ruzicka, J and Hansen, E.H., *Flow Injection Analysis*, J Wiley & Sons, New York, 1988.
90. Male, K.B and Loung, J.H.T., *Biosensors & Bioelectronics*, 8 (1993) 239.
91. Adeyoju, O., Iwuoha, E.I. and Smyth, M.R., Anal.Proc., 31 (1994) 177.
92. Ruzicka, J. and Hansen, E.H., *Anal.Chim.Acta*, 173 (1985) 3.
93. Jeppensen, M.T. and Hansen, E.H., *Anal.Chim.Acta*, 214 (1988) 147.
94. Ruzicka, J. and Hansen, E.H., *Anal.Chim.Acta*, 214 (1988) 1.
95. Pavon, J.L.P., Gonzalo, E.R., Christian, G.D. and Ruzicka, J., *Anal.Chem.*, 64 (1992) 923.
96. Scudder, K.M., Pollema., Cy.H. and Ruzicka, J., *Anal.Chem.*, 64 (1992) 2567.

97. Ruzicka, J. and Marshall, G.D., *Anal.Chim.Acta*, 237 (1990) 329.

98. Ivaska, A., and Ruzicka, J., *Analyst*, 118 (1993) 885.

99. Ruzicka, J., *Anal.Chim.Acta*, 261 (1992) 3.

100. O'Riordan, D.M.T. and Wallace, G.G., *Anal.Chem.*, 58 (1986) 126.

101. Ward, P. and Smyth, M.R., *Talanta*, 40 (1993) 1131.

102. Manz, A., Harrison, D.J., Verpoorte, E.M.J., Fettinger, J.C., Paulus, H., Ludi, H. and Widmer, H.M., *J.Chromatogr.*, 593 (1992) 253.

103. Harrison, D.J., Manz, A., Fan, Z., Ludi, H. and Widmar, H.M., *Anal.Chem.*, 64 (1992) 1926.

104. Effenhauser, C.S. and Manz, A., *Am.Lab.*, Sept (1994) 15.

105. Willis, B., *Am.Lab.*, Dec (1994) 13.

Appendix

List of Publications

1. Development of a Computer Controlled Multichannel Potentiostat for Applications with Flowing Solution Analysis. Tang Fang, Michael Mc Grath, Dermot Diamond and Malcolm R. Smyth, Anal.Chim.Acta, 305 (1995) 347-358.
2. Application of a Multichannel Potentiostat to Metal Ion Determinations in Flow Injection Analysis. Michael J. Mc Grath, Tang Fang, Dermot Diamond, and Malcolm R. Smyth, Anal.Lett., 28(4) (1995) 685-696.
3. The Use of Differential Measurements with a Glucose Biosensor for Interference Compensation during Glucose Determinations by Flow Injection Analysis. Michael J. Mc Grath, Emmauel Iwuoha, Dermot Diamond and Malcolm R. Smyth, Biosensors and Bioelectronics, 1995 (in press).
4. Design and Application of a Fountain Type Flow Cell for Applications with Sequential Injection Analysis. Michael J. Mc Grath, Ari Ivaska, Dermot Diamond and Malcolm R. Smyth, (in preparation.).
5. Application of Voltammetric Detection with Capillary Electrophoresis for the Determination of Phenolic Acids. Sangryoul Park, Michael J. Mc Grath, Dermot Diamond, Malcolm R. Smyth and Craig E. Lunte, Anal.Chem., (in preparation).
6. Developments in Modern Electrochemical Instrumentation. Michael J. Mc Grath Dermot Diamond, Book Chapter, (in preparation).